Predicting Time-Dependent Deformations in Prestressed Concrete Girders

by

Levent Isbiliroglu

A thesis submitted to the Graduate Faculty of
Auburn University
in partial fulfillment of the
requirements for the Degree of
Master of Science

Auburn, Alabama
December 13, 2014

Keywords: camber, curvature, strain, creep, shrinkage,
time-step analysis

Approved by

Robert W. Barnes, Chair, Associate Professor
Anton K. Schindler, Professor and Director of the Highway Research Center
Justin D. Marshall, Associate Professor

Abstract

A prestressed concrete girder camber prediction program, which utilizes a time-step approach, was improved to a new version including modifications, new features, and the *fib* Model Code 2010 material prediction model. The original version of the software was developed by Claire E. Schrantz in 2008. A few crucial corrections were included by Brandon R. Johnson in 2012.

In the new version, a user is able to obtain predicted strains and stresses at designated depth, define actual and design compressive strengths, import variables from and export output data to a spreadsheet for further analysis. The camber prediction software includes four concrete modulus of elasticity (MOE) development models: two-point MOE model (uses MOE test results from two ages), AASHTO LRFD, ACI 209R-92, and *fib* MC 2010. Creep and shrinkage prediction models include AASHTO LRFD, ACI 209R-92, and *fib* MC 2010.

Experimental data were collected from four previous research projects at Auburn University. This part of the study was used to verify the application's capability of predicting time-dependent strain, curvature, and deflection. Measurements of strain and camber values were obtained from full-scale prestressed girders constructed with vibrated concrete (VC) or self-consolidating concrete (SCC). Camber and strain measurements of nineteen AASHTO BT-54 girders, fourteen AASHTO BT-72 girders, and six AASHTO Type I girders were collected.

Measured camber data from twelve 15 in. deep T-Beams were also used in this study. Compressive strength of the concrete mixtures at 28 days varied between 6300 and 13,600 psi.

Time-dependent properties and deflections were predicted by using the new version of the camber prediction software. The two-point MOE model in combination with various creep and shrinkage prediction models was chosen for predictions. Predictions were compared with the collected data from the fifty one girders to evaluate the accuracy of the creep and shrinkage prediction models.

The comparison of time-dependent responses showed that camber *growth*, which is affected by creep, is overestimated for high-strength girders on average and include both over- and underpredictions for moderate-strength girders. ACI 209 predicts creep most accurately for high-strength girders, and AASHTO LRFD predicts creep most accurately for moderate-strength girders. Shrinkage predictions, which have an effect on prestress losses, are overestimated for high-strength girders and have mixed distribution of estimations for moderate-strength girders.

Acknowledgements

I would like to express my deepest gratitude to my advisor, Dr. Robert W. Barnes, for his guidance, encouragement, and patience. His wholehearted support and valuable advices are greatly appreciated.

I am also thankful to Alabama Department of Transportation providing the financial support for this master's thesis. I would like to extend my thanks to my committee members and Dave Mante for their valuable feedback.

I would also like to give special thanks to my parents, Murat and Sevim Isbiliroglu, and my brother, Yigit Deniz, who have been inspirational in this academic endeavor. Their faith and love have helped me to remain dedicated and motivated. I would also like to thank to my friends from Ankara and Auburn for keeping me uplifted during my stay in Auburn.

Table of Contents

List of Tables

List of Figures

List of Abbreviations

AASHTO	American Association of State Highway and Transportation Officials
ACI	American Concrete Institute
ALDOT	Alabama Department of Transportation
BT-54	Bulb-tee girder 54 in. in height
BT-72	Bulb-tee girder 72 in. in height
PCI	Precast/Prestressed Concrete Institute
SCC	Self-consolidating concrete
UE-StDev	Unbiased estimate of standard deviation
VB	Visual Basic
VC	Vibrated concrete

Chapter 1 Introduction

1.1 Background

Time-dependent deformations of prestressed girders depend on a wide variety of factors. Material and section properties of a prestressed girder, curing conditions, initially applied prestressing force, and environmental conditions are important factors. Engineers are likely to conservatively estimate some of the important elements such as concrete strength, modulus of elasticity, and prestress losses in order to satisfy available code requirements and stay on the safe side.

Some of the current prediction models do not cover high-strength concrete; however, it is commonly used in the precast plants producing prestressed girders. High-strength girders tend to have a greater modulus of elasticity than the moderate-strength girders. High-strength girders may exhibit less creep and shrinkage deformations as well. For design purposes, the actual strength of concrete is assumed to be equal to the specified strength. This conservative practice can result in overestimated camber when actual strengths are greater than specified.

The prediction of time-dependent deflection can be especially important during the planning of construction. Underestimating camber may result in adjusting the deck forms during construction to provide the required deck elevations. Overestimating camber can result in a bridge that sags under superimposed dead load such as the loads due to the deck and the barrier rails. Both cases can bring about construction delays and unexpected cost.

A time-step approach can be implemented to estimate the camber along with the prestress loss. With this method, deformations for each time increment and each specified cross section are determined. The time-step method can also be used to analyze strain and stress development on a girder cross section over time. Including realistic material properties can improve the accuracy of predictions of camber and prestress loss.

1.2 Research Objectives

The objectives of this research project are provided below:

- Enhancement of the performance and the user-friendliness of earlier camber prediction software developed in Visual Basic
- Implementation of *fib* Model Code 2010 into the camber prediction application
- Evaluation of the performance of AASHTO LRFD 2014 , ACI 209, and *fib* Model Code 2010 by comparing them with previously obtained test measurements
- Recommendations to select a material prediction model for predicting time-dependent deformations

1.3 Scope and Approach

Improvements were made to the previous camber prediction software. The source code of the software was rearranged completely to add new prediction models and to import the internal data from and export them to a spreadsheet.

For the data collection, four previous research projects including a total of fifty-one prestress girders were investigated: the Hillabee Creek Bridge Project, the AASHTO Type I Project, the High-Performance Concrete Project, and the T-Beams Project. They were also referenced as Project 1, 2, 3, and 4, respectively. This part of the study was used to verify the application's capability to predict time-dependent strains, curvature, and deflections.

In the camber prediction software, the chosen concrete MOE development model was two-point MOE model. The material prediction models for creep and shrinkage of concrete were composed of AASHTO LRFD 2014, ACI 209, and *fib* Model Code 2010. Projects 1, 2, and 3 were analyzed for bottom-flange strain, midspan curvature, and midspan camber, but Project 4 was analyzed only for midspan camber.

1.4 Organization of Thesis

Chapter 2 reviews the time-dependent deformations of a prestressed girder. The time-dependent deflection methods are discussed briefly, and the incremental time-step method is explained in detail. Also, the parameters influencing the time-dependent deflections are explained.

Chapter 3 outlines the algorithm of the camber prediction software. The modifications made to the previous versions are also explained. Discussions of the new features and prediction models of the software are presented. The new input schema and the output logic are discussed in this chapter.

Chapter 4 is a presentation of the experimental data from the four prestressed girder projects. Temperature corrections for internal strain and camber are also discussed. Selected input variables for the use of the predictions are presented.

Chapter 5 includes the analyses of bottom-flange strains, midspan curvatures and camber deflections. Camber is obtained directly, and loss of prestress force is represented by bottom-flange strains. Predicted bottom-flange strains, curvatures and cambers are compared to actual responses of the four projects. The results are evaluated statistically to make suggestions for selecting a material prediction model.

Chapter 6 presents a summary of the study along with conclusions and recommendations.

Chapter 2 Literature Review

2.1 Introduction

The purpose of this chapter is to review the time-dependent deformations of a prestressed girder and to present the state of the art. This chapter begins with the discussion of what time-dependent deflections are and how they can be predicted. The next section continues with the discussion of the elements influencing the time-dependent deflections.

2.2 Time-Dependent Deflection

2.2.1 Overview

Camber is a time-dependent deflection in the upward direction. Figure 2-1 displays the camber displacement obtained with superposition.

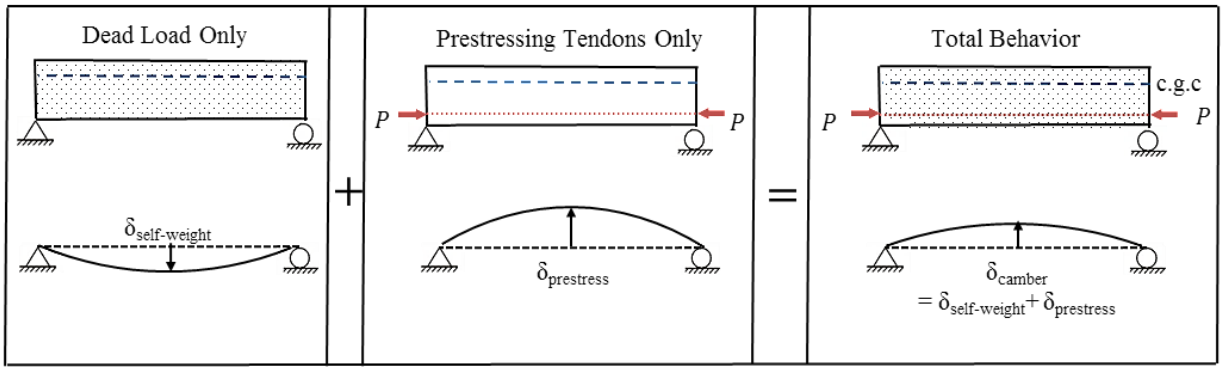

Figure 2-1: Superposition of Displacements due to Self-Weight and Prestressing Force

Self-weight of the concrete causes a beam sagging downward. The eccentric prestress forces result in bending in the upward direction. The superposition of these deflections gives the total response. If it is in the upward direction, then it is called camber.

Camber is the favorable outcome of the effective prestressing force applied eccentrically. The effective prestress is the residual amount after prestress losses. Figure 2-2 demonstrates the key factors affecting the prestress losses and the relation between them. The losses can be event-dependent and broken into two parts: instantaneous (short-term) and time-dependent (long-term). This also explains why the camber does not remain constant under the same loading.

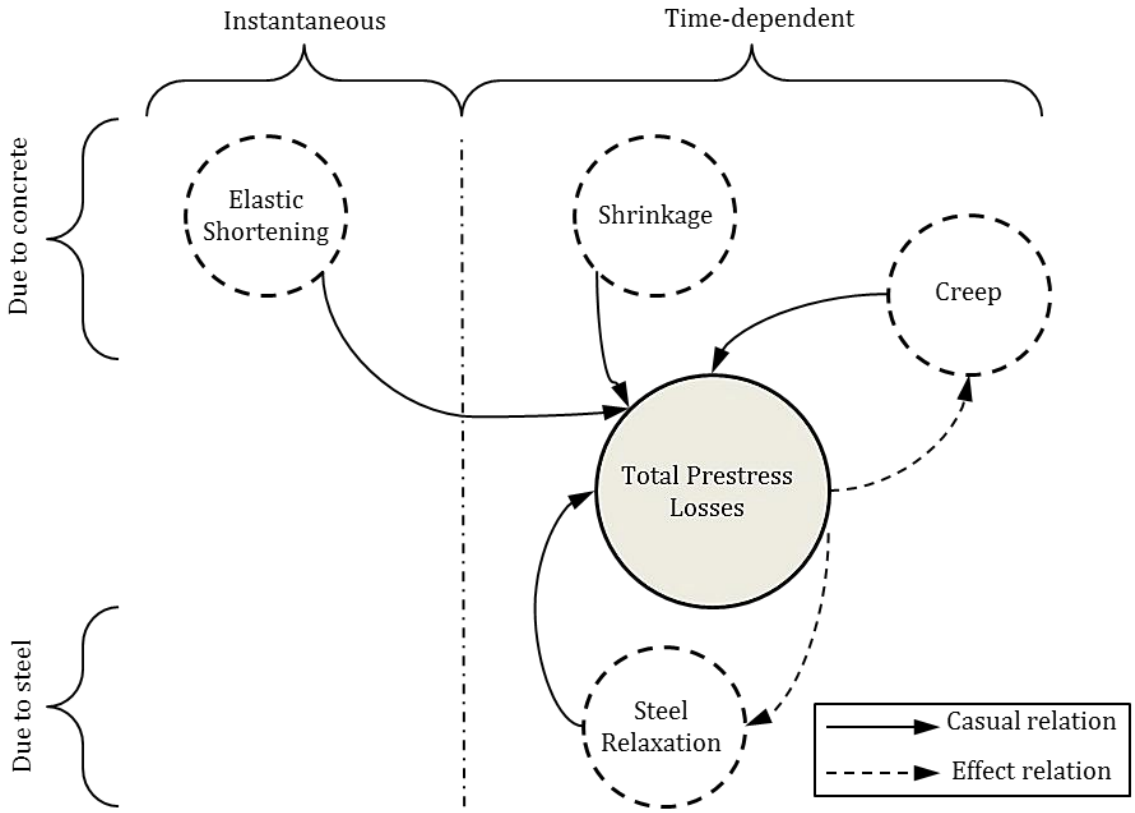

Figure 2-2: Illustration of Prestress Losses for Prestressed Concrete (Adapted from Naaman [2004])

Initial camber—short-term deflection—results as soon as the prestressed strands are released. The short-term deflection can be calculated by using linear-elastic properties and one of the beam deflection methods. Camber growth follows a time-dependent trend because of the maturing concrete properties, the time-dependent deformations of concrete (creep and shrinkage), and the loss of prestress force (steel relaxation).

2.2.2 Methods to Predict Time-Dependent Deflections

The time-dependent deflections can be studied in two main parts, namely, the short-term and the long-term deflections. The short-term deflection (initial camber) can be estimated with classical methods assuming linear-elastic behavior of material. However, the long-term deflections (camber growth) necessitate complex calculations due to the time-dependent behavior. Moreover, estimating long-term performance requires additional parameters such as aging material properties, timing of prestress events, and more properties depend on the chosen creep and shrinkage model (Stallings and Eskildsen 2001).

The methods for calculating the long-term deflections are divided into five more categories by Stallings and Eskildsen (2001). ACI 435R-95 (1995) summarizes the available time-dependent prediction methods, although they ultimately focus on estimating camber. Further time-dependent deformations such as bottom-flange strain and curvature are also needed to compare them with the collected lab and field data.

The first method is the incremental time-step method which is the primary focus of this thesis. This method is outlined by Naaman (2004). The initial strain distributions, curvatures, and prestressing force are required to be calculated first. Creep, shrinkage, and steel relaxation are calculated for each time-step. Later, the incremental prestress losses are computed for each time-step while equilibrium is satisfied. They are repeated for each cross-section and for each time interval. Integrating curvatures over a girder length can finally give the camber development. This method is implemented for this research study, and it is discussed further in the following subsection (Naaman 2004).

The second method is the PCI multiplier method which estimates the long-term deflections using event-specific coefficients. It was first developed by Martin (1977). Concrete

strength at transfer is assumed to be 70% of the 28-day strength, and modulus of elasticity (MOE) at transfer is assumed to be 85% of the final MOE. Short-term deflections are obtained by conventional engineering mechanics. Then, they are multiplied with the multipliers given in Table 2-1. The multipliers for the camber at erection represent girder age between 30 to 60 days (Martin 1977). Further, this method is used in the PCI Design Handbook (2010).

Table 2-1: Long-Term Multipliers (Adapted from Martin [1977])

	Without Composite Topping	With Composite Topping
At erection:		
(1) Deflection (downward) component – apply to the elastic deflection due to the member weight at release of prestress.	1.85	1.85
(2) Camber (upward) component – apply to the elastic camber due to prestress at the time of release of prestress.	1.80	1.80
Final:		
(3) Deflection (downward) component – apply to deflection calculated in (1) above.	2.70	2.40
(4) Camber (upward) component – apply to camber calculated in (2) above.	2.45	2.20
(5) Deflection (downward) – apply to elastic deflection due to super-imposed dead loads only.	3.00	3.00
(6) Deflection (downward) – apply to elastic deflection caused by the composite topping.	--	2.30

The approximate time-step is the third method to calculate camber growth. Deflections affected by creep (self-weight and super-imposed dead load) are summed up with deflections due to live load. Long-term creep coefficient is required for the computations (ACI Committee 435 1995).

The fourth method is the axial strain and curvature method which uses cracked section properties for instantaneous and long-term deflections. Change in deflection is calculated with

strain slope, i.e., curvature. For this method, determination of prestress losses is not required but it uses an aging coefficient that adjusts E_c for each time interval under consideration (ACI Committee 435 1995).

The last method is the prestress loss method. It assumes that sustained dead load does not impose cracking; therefore, non-cracked section is used to find the effects of creep, shrinkage, and relaxation. This method provides stress loss coefficients due to creep, shrinkage, and relaxation. Multiplication factors are applied to the deflections due to initial prestress, member self-weight, super-imposed dead load, and time-dependent prestress losses similar to the PCI multiplier method (ACI Committee 435 1995).

2.2.3 Incremental Time-Step Method

2.2.3.1 Background

An incremental time-step method provides the logic to calculate time-dependent deflections of a prestressed girder. For the purpose of the data comparison, this method is further modified to output other elements along with the camber development.

Short-term values such as initial strain, curvature, stress, and camber are calculated in the beginning. Then, aging concrete material properties (such as concrete MOE), time-dependent deformations (such as creep and shrinkage of concrete), and losses due to steel relaxation are computed for each cross section and each time interval.

Incremental strain and curvature relations are formulated in a way so that they can include the effects of the individual deformations at each time-step while satisfying equilibrium. Linear stress-strain relationships can be used to obtain incremental stresses that accompany these incremental strains and curvatures. Next, total values are computed by adding the incremental

values to the total amount from one previous step. The next step repeats the same procedure but with the updated time-dependent material properties.

2.2.3.2 Principles of Time-Step Method

The overall algorithm is grounded in three principles as stated by Johnson (2012). The first principle is that a plane cross section remains plane and perpendicular to the longitudinal axis. Figure 2.3 shows the infinitesimal element of a beam deformed according to the principle "plane section remains plane". This principle enables the calculation of incremental strains at a distance 'y' from the longitudinal neutral axis as described in Equation 2-1.

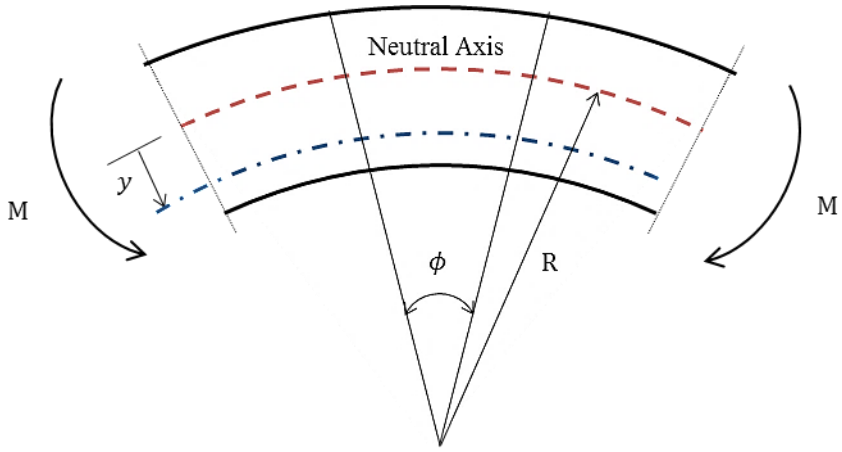

Figure 2-3: Principle of "Plane Section Remains Plane"

$$\Delta\varepsilon = \Delta\varepsilon_{cen} + \Delta\phi \times y \qquad \textit{Equation 2-1}$$

where, $\Delta\varepsilon_{cen}$ = incremental strain at the centroid of a cross section

$\Delta\phi$ = incremental curvature of a cross section

y = distance from the centroid of a cross section

The second principle is that strain change on a concrete section is equal to the sum of the stress-dependent strains and the stress-independent strains such as creep, shrinkage, and thermal

strains. The non-linear material behaviors such as cracking of concrete and yielding of reinforcement steel are not included. This principle is formulated as given in Equation 2-2.

$$\Delta\varepsilon_c = \frac{\Delta f_c}{E_c} + \Delta\varepsilon_{c,cr} + \Delta\varepsilon_{c,sh} + \Delta\varepsilon_{c,T} \qquad \textit{Equation 2-2}$$

where, $\Delta\varepsilon_c$ = change in strain on a cross section of a concrete section

Δf_c = change in stress due to the resultant force on a concrete section

E_c = modulus of elasticity of concrete

$\Delta\varepsilon_{c,cr}$ = change in concrete strain due to creep

$\Delta\varepsilon_{c,sh}$ = change in concrete strain due to shrinkage

$\Delta\varepsilon_{c,T}$ = change in concrete strain due to temperature

The third principle is the equilibrium of applied forces and moments. Figure 2-4 shows the strain (stress-dependent) and stress diagrams of a prestressed concrete section under self-weight and prestress forces. Total change in normal force on a cross section is equal to the change in axial stresses integrated over the cross section within a time step.

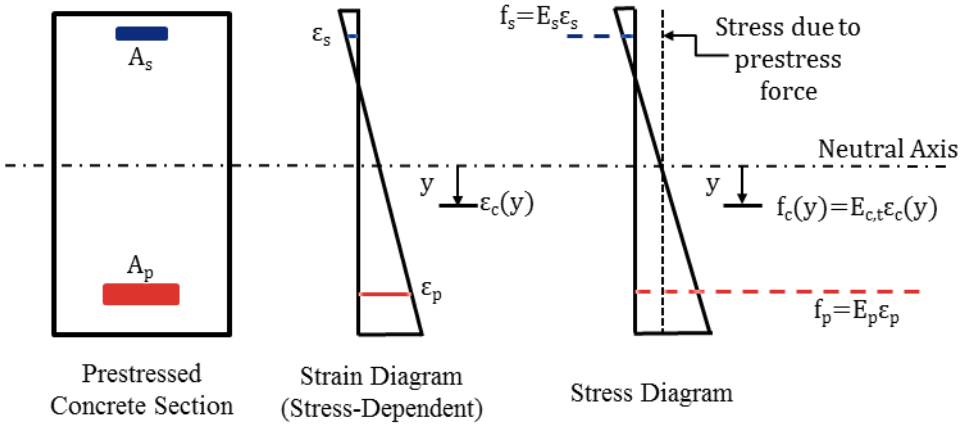

Figure 2-4: Strain and Stress Diagram of a Prestressed Concrete

Incremental forces on the concrete section, the prestressed strands, and the reinforcing bars are formulated together as given in Equation 2-3. The internal stresses over the concrete

section also result in bending moment. Moment and axial force equilibrium must be satisfied for each time step as given in Equation 2-4. The equilibrium relationships below are adapted from Schrantz's research (2002).

$$\Delta N = \int_{A_c} \Delta f_c dA_c + \sum \Delta f_p A_p + \sum \Delta f_s A_s \qquad \textit{Equation 2-3}$$

$$\Delta M = \int_{A_c} \Delta f_c y dA_c + \sum \Delta f_p y_p A_p + \sum \Delta f_s y_s A_s \qquad \textit{Equation 2-4}$$

where, Δf_c = incremental change in concrete stress

A_c = cross-sectional area of concrete

Δf_p = $E_p \Delta \varepsilon_p + \Delta f_{p,r}$ = incremental change in stress in a prestressed steel layer

E_p = modulus of elasticity of prestressing steel

$\Delta \varepsilon_p$ = incremental change in strain in a prestressed steel layer

$\Delta f_{p,r}$ = incremental change in prestress due to relaxation

A_p = cross-sectional area of a prestressed layer

Δf_s = $E_s \Delta \varepsilon_s$ = incremental change in stress in a non-prestressed steel layer

E_s = modulus of elasticity of non-prestressed reinforcing steel

$\Delta \varepsilon_s$ = incremental change in strain in a non-prestressed steel layer

A_s = cross-sectional area of a non-prestressed reinforcing steel layer

ΔN = incremental change in axial force

ΔM = incremental change in bending moment

2.2.3.3 Assumptions

The new features are added within the camber prediction software satisfying the original assumptions listed below:

- The geometry of long and slender beam is assumed for the girders analyzed in the application. It ensures that the principles in Section 2.2.3.2 can be incorporated.
- Linear-elastic material stress response is assumed for stress-dependent strains. Non-linear behavior such as cracking of concrete or yielding of steel is not included. This research study intends to investigate the time-dependent deflections until the erection of a girder. This assumption is reasonable since the prestressed girders are not designed to crack under service loads.
- Self-weight of a girder is uniformly distributed over its length. Unit weight of the plain concrete is increased with an amount of 5 pcf in order to include the approximate weight of steel reinforcement as recommended in AASHTO LRFD.
- The girders are assumed to be simply-supported. This assumption is made according to the storing conditions in the prestressed plants and permits performing determinate structural analysis.
- Perfect bonding between reinforcement and concrete is assumed. It allows the derivation of some compatibility equations.
- Effect of steel transfer length is assumed to be limited to the end segment of each group of bonded strands in the discretized girder.
- Girders are assumed to be symmetric about the midspan.

2.3 Factors Affecting Time-Dependent Deformations

2.3.1 Overview

Aging concrete properties and decreasing prestress forces are the reasons behind the time-dependent trend of the deformations. The bonds holding the cement and aggregates tend to strengthen, as concrete matures. This characteristic signifies the importance of concrete strength and modulus of elasticity development for the time-dependent deflections.

Similarly, losses in prestressed strands drive the time-dependent trend. The amount of prestress losses gives the difference between initial jacking stress and the long-term effective prestress. Prestress losses can be event-dependent such as elastic shortening and time-dependent such as those due to prestressing steel relaxation, creep, and shrinkage. Figure 2-5 demonstrates the losses during the service life of a prestressed girder.

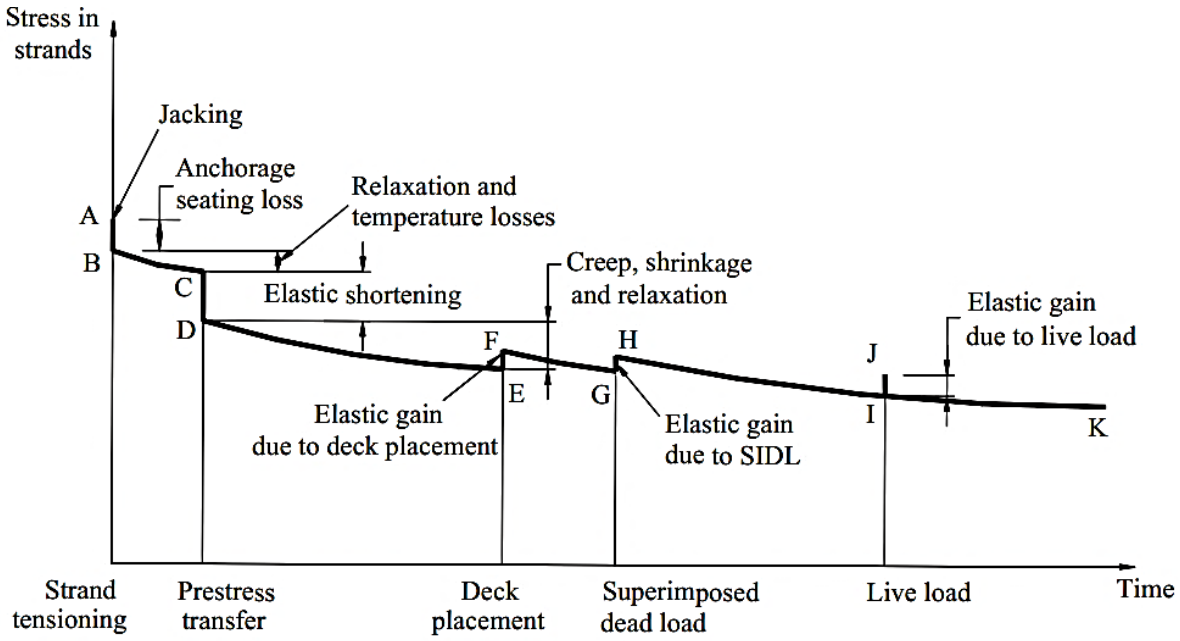

Figure 2-5: Stress vs. Time in a Prestressed Concrete Girder (Tadros et al. 2003)

This study focuses exclusively on the losses up to the deck placement—indicated as erection of girders in the study. The losses from Point B to E are explained in the coming subsections. In the figure, losses due to shrinkage are marked as if they start only after prestress

transfer (Point D); nevertheless, autogenous shrinkage deformations can develop before the prestress transfer depending on the construction practice.

2.3.2 Concrete Strength

Concrete strength depends on type of cement, water-to-cementitious material ratio, admixtures, quality of aggregate, and duration and type of curing. It is a time-dependent material property and liable to increase rapidly at early ages and gradually at later ages. Using high-strength concrete is a usual practice for prestressed girders since they are able to quickly reach the satisfactory strength level required for the release of strands.

ACI Committee 363 (1997) stated that the time-dependent behavior of high-strength concrete needs to be distinguished from the behavior of normal-strength concrete. Actually, high-strength concrete has greater rate of strength development at early ages, and two of the reasons were explained as "(1) an increase in the internal curing temperature in the concrete cylinders due to a higher heat of hydration and (2) shorter distance between hydrated particles in high-strength concrete due to lower water-cement ratio".

Furthermore, error in camber prediction escalates when the actual concrete strength values start to differ considerably from the specified design strength. In fact, O'Neill and French (2012) made a recommendation to Minnesota Department of Transportation (MNDOT) with regard to the design strengths at release. They monitored fourteen girders in order to understand the overestimated camber problems for the bridge girders in Minnesota. They suggested that the concrete strength at release, f'_{ci}, should be multiplied by an overstrength factor of 1.15 since the fabrication plants intend to exceed the design strength, and they want to make the precasting beds ready for the next production as quickly as possible.

Similarly, Hofrichter (2014) studied approximately 1900 girder production cycles for Alabama bridge girders over the last 6 years. This study intended to minimize the chances of camber prediction errors for construction stage and help engineers during the design phase. Hofrichter determined that the specified strengths alone are not good predictors of average concrete strength; accordingly, he recommended the relationship in Equation 2-5 for the use of Alabama Department of Transportation (ALDOT).

$$f_{ci}^{*} = \begin{cases} 7500 \text{ psi}, & \text{for } 4000 \text{ psi} \leq f_{ci}' \leq 7000 \text{ psi} \\ f_{ci}' + 500 \text{ psi}, & \text{for } 7000 \text{ psi} < f_{ci}' \leq 9000 \text{ psi} \end{cases} \qquad \textbf{\textit{Equation 2-5}}$$

where, f_{ci}^{*} = expected concrete strength at release in [psi]

f_{ci}' = specified concrete strength at release in [psi]

Lastly, material testing in the United States is carried out according to ASTM Standard C39 (2009). The 6 in. by 12 in. cylinders are cured under standard laboratory conditions and tested at a specified rate of loading without shock. This standard was used to carry out the material testing in this research.

2.3.3 Concrete Modulus of Elasticity

2.3.3.1 Background

Concrete modulus of elasticity (MOE) describes a portion of the stress-strain relationship. Concrete MOE depends on the type of cement, water-cementitious materials ratio, curing methods, unit weight of concrete and type of aggregate. MOE is linked directly with the time-dependent deflection calculations signifying its importance. This section introduces stress-strain curves and the strength-based MOE prediction models.

Figure 2-6 depicts some of the techniques to determine concrete MOE from stress-strain curve. The initial tangent modulus can be obtained by taking the tangent at the origin. The secant modulus can be determined by connecting the origin with a point on the curve.

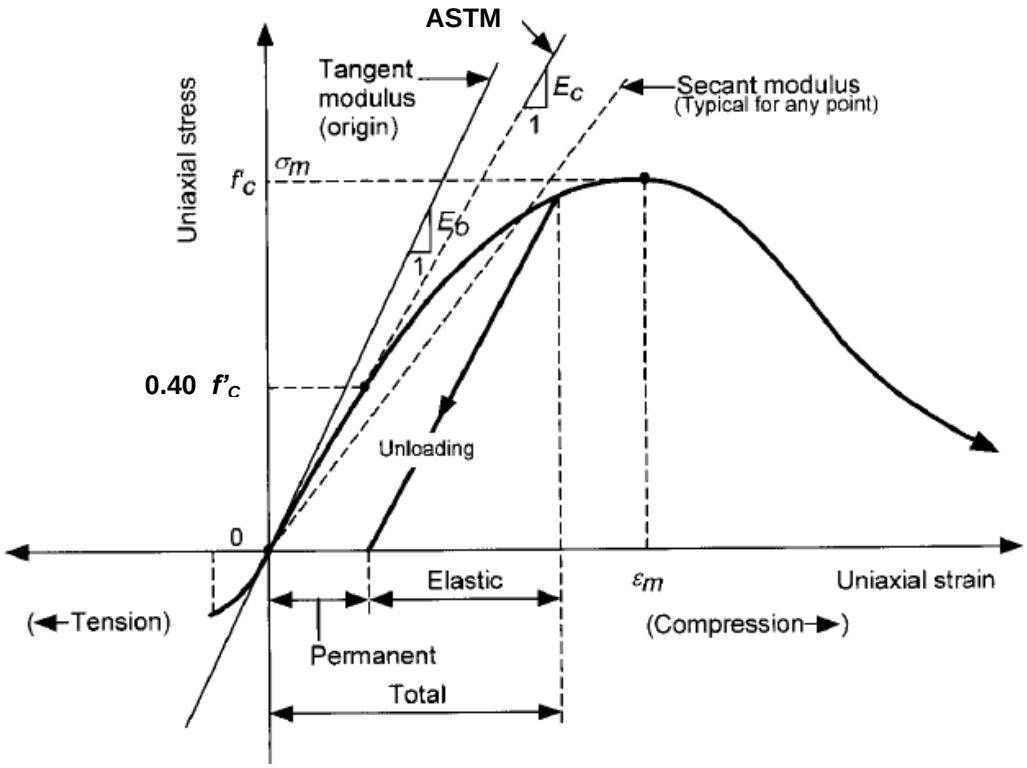

Figure 2-6: Obtaining Modulus of Elasticity from Stress-Strain Curve of Concrete (Adapted from Naaman [2004])

ASTM Standard C469 (2002) declares that the cylinders should be loaded up to 40% of the ultimate load (shown in the figure) and tested twice (at least) after an initial load cycle. The ambient temperature and humidity should be kept constant during the test. It is the governing material testing method in the U.S and necessitates using the testing machine—capable of applying a load at the required rate and of the magnitude—and a standardized compressometer to test the standardized cylinders. The MOE data in this research were obtained based on this method.

The initial portion of stress-strain curve is somewhat linear, and concrete deformations are recoverable. If the applied stress increases beyond the linear part, concrete behaves non-linearly and experiences permanent deformations due to microcracking. Concrete stress-strain trends depend on the age of concrete (Naaman 2004).

Material prediction models such as AASHTO LRFD 2014, ACI 209, and *fib* MC 2010 offer the mathematical relations—strength-based approaches—to obtain MOE development. The MOE development can also be obtained by fitting the measured MOE at two ages into a mathematical model—referred as two-point approach. The latter is used for this thesis research.

Moreover, recent research studies showed that actual MOE can be considerably greater than the code-calculated MOE to take account of the local construction practices. O'Neill and French (2012) evaluated the historical data and the on-going MnDOT practice to estimate E_c. The research revealed that the MOE at transfer should be multiplied by a factor of 1.15 for estimating the 28-day MOE.

Likewise, Hofrichter (2014) suggested modified MOE functions as shown in Equations 2-6 and 2-7 in order to take account of the ALDOT's construction practices. His study was based on the analyzed historical data from the plants where a majority of ALDOT girders are produced.

$$E_{c,t} = 33K_1K_t\omega^{1.5}\sqrt{f^*_{c,t}} \qquad \textbf{\textit{Equation 2-6}}$$

$$E_{c,t} = 33K_1K_t\omega^{1.5}\sqrt{f_{c,t}} \qquad \textbf{\textit{Equation 2-7}}$$

where, $E_{c,t}$ = static modulus of elasticity of the concrete at release or 28 days in [psi]

K_1 = aggregate stiffness factor

= 1.12

K_t = time-dependency factor to account for age of predictions

= 1.04 when predicting release modulus of elasticity (for Equation 2-6)

= 0.96 when predicting 28-day modulus of elasticity (for Equation 2-6)

= 1.02 when predicting release modulus of elasticity (for Equation 2-7)

= 0.99 when predicting 28-day modulus of elasticity (for Equation 2-7)

ω = fresh concrete unit weight at placement in [pcf]

$f^*_{c,t}$ = expected compressive strength of the concrete at the time for which modulus is predicted in [psi]

$f_{c,t}$ = measured compressive strength of the concrete at the time for which modulus is predicted in [psi]

2.3.3.2 ACI 209 MOE Prediction Model

The ACI 209 MOE prediction model is given in Table 2-6. Equations 2-8 and 2-9 show the formulated expression for strength and time development. The coefficients in Table 2-2 are the coefficients, and they are not valid for concrete with Type II and V cement or for blends of portland cement and pozzolanic materials. "Steam" curing is taken to mean accelerated curing, and "moist" curing implies non-accelerated curing. Accelerated curing is the type of curing in which curing temperature is elevated above normal curing temperature due to the exposure of sun, the tarp/enclosure, or the external application of steam or heat.

Table 2-2: The α and β Coefficients

Curing Type	Cement Type	Recommended in ACI 209 (2008)		Used in this research	
		α	β	α	β
Moist	I	4.0	0.85	4.0	0.857
Moist	III	2.3	0.92	2.3	0.918
Steam	I	1.0	0.95	1.0	0.967
Steam	III	0.7	0.98	0.7	0.975

The α coefficients are obtained from ACI 209 (2008), but the β coefficients used in this research are different than ACI 209 because of the inconsistency in 28-day strength. The new β coefficients are derived from Equation 2-9 by equating the 28-day concrete strength.

2.3.3.3 AASHTO LRFD MOE Prediction Model

AASHTO LRFD 2014 uses a similar model with ACI 209 to estimate the 28-day modulus of elasticity. Equation 2-10 in Table 2-6 describes the formulation. Development over time is neither specified nor referred directly in the specification.

2.3.3.4 *fib* Model Code 2010 MOE Prediction Model

The characteristic strength values of different concrete grades are given in Table 2-3. Coefficients that depend on type of cement and aggregate are provided in Tables 2-4 and 2-5, respectively. The cement types according to EN 197-1 (2011) are explained in Appendix I-2. *fib* Model Code 2010 MOE model is given in Equations 2-11a, 2-11b, and 2-12 in Table 2-6. Equation 2-11b should be used when mean compressive strength is available. Otherwise, Equation 2-11a should be used.

Table 2-3: Characteristic Strength Values in [MPa] (Adapted from Model Code [2010])

Concrete Grade	C12	C20	C30	C40	C50	C60	C70	C80	C90	C100	C110	C120
f_{ck}	12	20	30	40	50	60	70	80	90	100	110	120
$f_{ck,cube}$	15	25	37	50	60	75	85	95	105	115	130	140

Table 2-4: Type of Aggregates (Adapted from Model Code [2010])

Types of Aggregate	α_E
Basalt, dense limestone aggregates	1.2
Quartzite aggregates	1.0
Limestone aggregates	0.9
Sandstone aggregates	0.7

Table 2-5: Type of Cement (Adapted from Model Code [2010])

f_{cm}(MPa)	Strength Class of Cement	*s*
≤ 60	32.5 N	0.38
	32.5 R, 42.5 N	0.25
	42.5 R, 52.5 N, 52.5 R	0.20
> 60	All classes	0.20

Table 2-6: Modulus of Elasticity Prediction Models Using Strength-Based Approach

	ACI 209	AASHTO LRFD	*fib* Model Code 2010
Relation	$E_{ct} = g_{ct}\left[w^3\left(f'_c\right)_t\right]^{0.5}$ ***Equation 2-8***	$E_c = 33{,}000K_1 {w_c}^{1.5}\sqrt{f'_c}$ ***Equation 2-10***	$E_{ci} = E_{c0}\alpha_E\left(\frac{f_{ck}+\Delta f}{10}\right)^{1/3}$ or $E_{ci} = E_{c0}\alpha_E\left(\frac{f_{cm}}{10}\right)^{1/3}$ ***Equation 2-11a and 2-11b***
Time Development	$\left(f'_c\right)_t = \left[\frac{t}{(\alpha+\beta t)}\right]\left(f'_c\right)_{28}$ ***Equation 2-9***	Not Available	$E_{ci}(t) = [\beta_{cc}(t)]^{0.5}E_{ci}$ ***Equation 2-12*** $\beta_{cc}(t) = exp\left\{s\left[1-\left[\frac{28}{t}\right]^{0.5}\right]\right\}$ ***Equation 2-13***
Explanation of the Variables	• E_{ct} = modulus of elasticity at a time, t • w = unit weight of concrete in [pcf] • $\left(f'_c\right)_t$ = compressive strength of concrete in [psi] at a time, t • g_{ct} = 33 • $\left(f'_c\right)_{28}$= 28-day specified concrete compressive strength in [psi] • α and β = constants given in Table 2-2	• E_c = modulus of elasticity of concrete in [ksi] • K_1 = correction factor for source of aggregate • w_c = unit weight of concrete in [kcf]	• E_{ci} = modulus of elasticity in [MPa] at 28-day concrete age • Δf = 8 MPa; E_{c0} =21.5×10^3 MPa • f_{ck}= characteristic strength in [MPa] as listed in Table 2-3 • α_E = constant depends on the type of aggregate as tabulated in Table 2-4 • f_{cm}= mean compressive strength in [MPa] at 28-day age measured on cylinders 150/300 mm satisfying ISO 1920-3 • t = concrete age in [days] taking into account of temperature during curing as given below. $t_{0,T} = \sum \Delta t_i exp\left\{13.65 - \frac{4000}{273+T(\Delta t_i)}\right\}$ where, $T(\Delta t_i)$ =temperature in [°C] during the time period Δt_i days • s = coefficient depends on the strength class of cement as tabulated in Table 2-5

2.3.4 Relaxation of Prestressed Strands

Relaxation of prestressed strands occurs due to applied sustained load over a long period of time. Prestressed strands tend to lose prestressed forces gradually under an applied sustained load over a long period of time. Steel relaxation is function of duration of prestressing load, initial prestressing force, yield strength of strands and type of strands.

Naaman (2004) stated that the relaxation losses of prestressing steels can be negligible if stresses are smaller than half of ultimate strength. Also, he points out that the actual relaxation loss will be smaller than the pure relaxation since creep and shrinkage will also act to decrease prestress amount.

Stress-relieved strands and low-relaxation strands are the two types of strands included in the relaxation loss calculations. In order to apply the calculations compatible with the time-step method, Equations 2-14 and 2-15 are modified from Magura et al. (1962). Equation 2-14 is used to calculate the relaxation prior to release, and Equation 2-15 is used to calculate the incremental relaxation over a period of time.

$$f_{p,R,0} = f_{pj} \times \left[\frac{(\log t_{ini})}{K_L}\right] \times \left[\left(\frac{f_{pi}}{f_{py}}\right) - 0.55\right] \qquad \textit{Equation 2-14}$$

$$\Delta f_{p,R} = f_{pi} \times \left[\frac{(\log t_{i+1} - \log t_i)}{K_L}\right] \times \left[\left(\frac{f_{pi}}{f_{py}}\right) - 0.55\right] \qquad \textit{Equation 2-15}$$

where, f_{pj} = jacking stress in [ksi]

t_{ini} = the time between prestress transfer and jacking in [days]

K_L = 10 (stress-relieved); 45 (low-relaxation)

f_{pi} = initial stress in prestressing reinforcement in [ksi] at the beginning of time interval

f_{py} = yield strength of the prestressing reinforcement in [ksi]

t_i = time at the beginning of interval in [days] (relative to jacking)

t_{i+1} = time at the end of interval in [days]

2.3.5 Elastic Shortening

Elastic shortening loss—an instantaneous event—happens once prestressed strands are released on a prestressed concrete girder. Transfer of prestressed force makes reinforcement bars and concrete girder compress until an equilibrium is reached with the tension in the prestressing steel. Perfect bonding between strands and concrete body is assumed to calculate elastic shortening. Transformed-section properties are used, and Equation 2-14 is derived to be compatible with time-step method by Schrantz (2012).

$$\Delta f_{p,ES} = E_p[\Delta\varepsilon_{cen} + \Delta\phi \times y] \qquad \textbf{\textit{Equation 2-16}}$$

where, E_p = modulus of elasticity of prestressing steel in [ksi]

y = distance in [in.] from centroid to the layer considered (downward, +)

$\Delta\varepsilon_{cen} = \frac{-N_o}{E_{ci}A_{tr,initial}}$ = change in strain at the centroid of the cross section

$N_o = \sum E_p\, \varepsilon_{p,initial} A_p$ = axial load on cross section due to prestress transfer in [kips]

$\varepsilon_{p,initial} = \frac{f_{pbt}}{E_p} = \frac{f_{pj} + \Delta f_{p,R}}{E_P}$ = strain at prestressing steel level immediately before prestress transfer

$\Delta\phi = \frac{M_G - M_o}{E_c I_{tr,initial}}$ = change in cross-sectional curvature in [1/in.]

$M_o = \sum N_o\, y_{p,cen}$ = moment on cross section due to prestress transfer in [kip-in.]

M_G = moment due to self-weight (kip*in)

2.3.6 Creep

Creep is "the time-dependent strain in excess of elastic strain induced in concrete subjected to a sustained stress" (Naaman 2004). It is a function of duration and magnitude of the applied load, the mixture proportions, the relative humidity, type of the aggregate, age of the concrete at the time of loading, and the geometry of the member. Ultimate creep coefficient is the maximum possible value which may be attained (theoretically at infinitive).

The creep prediction models according to ACI 209, AASHTO LRFD 2014 and *fib* MC 2010 are tabulated in Table 2-7. The ACI 209 creep prediction model, given in Equations 2-17 and 2-18, can be utilized for normal- and light-weight concrete with Type I or Type III cement. The concrete should also be steam- or moist-cured.

Accelerated curing is the type of curing in which curing temperature is elevated above normal curing temperature due to the exposure of sun, tarp/enclosure, or the external application of steam or heat. Concrete with non-accelerated curing is free of external heating effects and does not experience as much temperature increase as with accelerated curing. Therefore, "steam" curing is taken to mean accelerated curing, and "moist" curing implies non-accelerated curing.

AASHTO LRFD 2014, provided in Equations 2-19 and 2-20, has been suggesting the same creep model since AASHTO LRFD 2005. The creep model is based on NCHRP 496 Report (2003) in which age at loading is expressed in days of accelerated curing. The age at loading, t_i, needs to be divided by 7 days if non-accelerated-cured concrete is used. The concrete maturity, t, is the chronological age relative to the age at loading; in other words, it does not include any curing-type corrections.

The *fib* MC 2010 creep model is given in Equations 2-21 and 2-22. The types of cement according to the European construction practice are given in Appendix I.

Table 2-7: Creep Prediction Models

	ACI 209	AASHTO LRFD 2014	*fib* Model Code 2010
Ultimate	$v_{ult} = 2.35(\gamma_{la}\gamma_{\lambda}\gamma_{vs}\gamma_{\psi}\gamma_{s}\gamma_{a})$ the ultimate shrinkage coefficient ***Equation 2-17***	$\psi(t,t_i) = 1.9k_s k_{hc} k_f k_{ta} t_i^{-0.118}$ the creep coefficient ***Equation 2-19***	$\varphi_0 = \varphi_{RH}\beta(f_{cm})\beta(t_0)$ notional creep coefficient ***Equation 2-21***
Factors	$\gamma_{vs} = \frac{2}{3}[1 + 1.13exp(-0.54 \times V/S)]$ volume-to-surface ratio correction factor	$k_s = 1.45 - 0.13\left(\frac{V}{S}\right) \geq 1.0$ volume-to-surface ratio factor	$\varphi_{RH} = \left[1 + \frac{1 - RH/100}{0.1\sqrt[3]{h}} \times \left(\frac{35}{f_{cm}}\right)^{0.7}\right]\left(\frac{35}{f_{cm}}\right)^{0.2}$
	$\gamma_{\lambda} = 1.27 - 0.0067 \times \lambda$, for $\lambda > 40$ $\gamma_{\lambda} = 1.00$, for $\lambda \leq 40$ relative humidity correction factor	$k_{hc} = 1.56 - 0.008H$ humidity factor for creep	$\beta(f_{cm}) = \frac{16.8}{\sqrt{f_{cm}}}$ coefficient depends on the strength
	$\gamma_{la} = \begin{cases} 1.25(t_{la})^{-0.118}, if\ moist-cured \\ 1.13(t_{la})^{-0.094}, if\ steam-cured \end{cases}$ loading age correction factor applicable, if the loading ages are later than 7 days for moist-cured concrete or later than l-3 days for steam-cured concrete.	$k_f = \frac{5}{1 + f'_{ci}}$ concrete strength factor	$\beta(t_0) = \frac{1}{(0.1 + t_0)^{0.2}}$ coefficient depends on the loading age
	$\gamma_{\psi} = 0.88 + 0.0024\psi$ fine aggregate correction factor		$\beta_H = 1.5h\left[1 + \left(1.2\left(\frac{RH}{100}\right)\right)^{18}\right] + 250\left(\frac{35}{f_{cm}}\right)^{0.5} \leq 1500\left(\frac{35}{f_{cm}}\right)^{0.5}$
	γ_s =0.82 + 0.067 s slump correction factor		$t_0 = t_{0,T}\left[\frac{9}{2 + t_{0,T}^{1.2}} + 1\right]^{\alpha} \geq 0.5\ days$ age of concrete at loading

Table 2-7: (Continued) Creep Prediction Models

	ACI 209	AASHTO LRFD 2014	*fib* Model Code 2010
Factors	$\gamma_a = \max(0.46 + 0.09\alpha, 1.00)$ air content correction factor		$t_{0,T} = \sum \Delta t_i exp\left\{13.65 - \frac{4000}{273 + T(\Delta t_i)}\right\}$ adjusted age of concrete at loading in [days]
Time Development	$v_t = \left[\frac{t^{0.60}}{10 + t^{0.60}}\right] v_{ult}$ time development function ***Equation 2-18***	$k_{td} = \frac{t}{61 - 4f'_{ci} + t}$ time development factor ***Equation 2-20***	$\beta_c(t - t_0) = \left[\frac{(t - t_0)}{\beta_H + (t - t_0)}\right]^{0.5}$ development of creep with time ***Equation 2-22***
Explanation of the Variables	• t_{la} = age at loading in [days] • λ = % relative humidity • V/S = volume to surface ratio in [in.] • ψ = % ratio of fine aggregate to total aggregate by weight • s = slump in [in.] • α = air content in [%] • t = time after loading in [days]	• t_i = age of concrete at time of load application in [days] • V/S = volume-to-surface ratio in [in.] • H = % relative humidity • f'_{ci} = specified compressive strength of concrete at time of prestressing in [ksi]. If concrete age at time of initial loading is unknown at design time, f'_{ci} may be taken as $0.80f_c'$ in [ksi]. • t = maturity of concrete in [days]; relative to time of loading for creep calculations	• f_{cm} = mean compressive strength at 28 days in [MPa] = f'_c + 8 MPa • RH = relative humidity in [%] • h = notational size of member in [mm] = $\frac{2A_c}{u}$ • t_0 = age of concrete at loading in [days] • t = age of concrete in [days] • α = coefficient depends on the type of cement $\alpha = \begin{cases} -1, & for\ 32.5\ N \\ 0, & for\ 32.5\ R, 42.5\ N \\ 1, & for\ 42.5\ R, 52.5\ N, 52.5\ R \end{cases}$ • Δt_i = number of days where a temp. T exists • $T(\Delta t_i)$ = temperature in [°C] during the time period Δt_i

2.3.7 Shrinkage

Autogenous and drying shrinkage are the time-dependent volume reduction of concrete due to the changes in the moisture content. Drying shrinkage occurs due to the evaporated excess water after the end of curing. Autogenous shrinkage occurs due to the hydration of cement. Shrinkage is affected by aggregate type, age at drying, admixtures, water-to-cement ratio, volume-to-surface ratio, amount of reinforcement, and ambient conditions. Ultimate shrinkage is the maximum possible shrinkage strain (ACI Committee 209 1992).

The ACI 209, AASHTO LRFD 2014 and *fib* MC 2010 shrinkage prediction models are given in Table 2-8. The ACI 209 shrinkage prediction model is given in Equations 2-23 and 2-24. One of the time-development functions is given for concrete with 7 days of moist curing (non-accelerated curing), and the other time-development function is provided for 1–3 days of steam curing (accelerated curing).

The AASHTO LRFD 2014 shrinkage model, shown in Equations 2-25 and 2-26 in Table 2-8, has not changed since the AASHTO LRFD 2005.The shrinkage should be increased by 20 percent, if concrete is exposed to drying before five days of curing. The 5-day curing is for non-accelerated curing. The 17-hour (5/7 day) curing is the estimated approximate amount if it is accelerated curing (Schrantz 2012).

The *fib* MC 2010 shrinkage model is given in Equations 2-27, 2-28, and 2-29 in Table 2-8. The explanations and the required coefficients are also provided in the table. The strength class of European cement (required for the coefficients) is provided in Appendix I.

Table 2-8: Shrinkage Prediction Models

	ACI 209	AASHTO LRFD 2014	*fib* Model Code 2010
Ultimate	$\varepsilon_{sh,ult} = \gamma_\lambda \gamma_{vs} \gamma_\psi \gamma_s \gamma_c \gamma_a \gamma_{cp} 780 \times 10^{-6}$ ultimate shrinkage ***Equation 2-23***	$\varepsilon_{sh} = k_s k_{hs} k_f k_{td} 0.48 \times 10^{-3}$ strain due to shrinkage ***Equation 2-25***	$\varepsilon_{cr}(t, t_s) = \varepsilon_{cas}(t) + \varepsilon_{cds}(t, t_s)$ total shrinkage or swelling strains ***Equation 2-27***
Factors	$\gamma_\lambda = \begin{cases} 1.4 - 0.01\lambda, for\ 40 \le \lambda \le 80 \\ 3.0 - 0.03\lambda, for\ 80 < \lambda \le 10 \end{cases}$ humidity correction factor	$k_s = 1.45 - 0.13\left(\frac{V}{S}\right) \ge 1.0$ volume-to-surface ratio factor	$\varepsilon_{cas}(t) = \varepsilon_{cas0}(f_{cm}) * \beta_{as}(t)$ autogenous shrinkage
	$\gamma_{vs} = 1.2\exp(-0.12\frac{V}{S})$ V/S ratio correction factor	$k_{hs} = 2.00 - 0.014H$ humidity factor for shrinkage	$\varepsilon_{cas0}(f_{cm}) = -\alpha_{as}\left[\frac{f_{cm}/10}{6 + f_{cm}/10}\right]^{2.5} \times 10^{-6}$ notional autogenous shrinkage
	$\gamma_\psi = min\begin{cases} 0.30 + 0.014\psi \\ 0.90 + 0.002\psi \end{cases}$ fine aggregate percentage correction factor	$k_f = \frac{5}{1 + f'_{ci}}$ concrete strength factor	$\varepsilon_{cds}(t) = \varepsilon_{cds0}(f_{cm})\beta_{RH}(RH)\beta_{ds}(t - t_s)$ drying shrinkage
	$\gamma_c = 0.75 + 0.0036c$ cement content correction factor	$\varepsilon^*_{sh} = 1.20\varepsilon_{sh}$ Shrinkage should be increased by 20 percent, if concrete is exposed to drying before 5 days of curing have elapsed.	$\varepsilon_{cds0}(f_{cm}) = [(220 + 110\alpha_{ds1})\exp(-\alpha_{ds2} f_{cm})] \times 10^{-6}$ notional drying shrinkage coefficient
	$\gamma_s = 0.89 + 0.041s$ slump correction factor		$\beta_{RH} = \begin{cases} -1.55\left[1 - \left(\frac{RH}{100}\right)^3\right],\ 40\% \le \text{RH} < 99\% \times \beta_{s1} \\ 0.25,\ \text{RH} \ge 99\% \times \beta_{s1} \end{cases}$ the coefficient taking into account of ambient RH
	$\gamma_a = 0.95 + 0.008\alpha$ air content correction factor		

Table 2-8: (Continued) Shrinkage Prediction Models

	ACI 209	AASHTO LRFD 2014	*fib* Model Code 2010
Factors	$\gamma_{cp} = -0.1015 \ln(t) + 1.202$ initial moist curing correction factor (formulated using Table 2.5.3 in ACI 209)		$\beta_{s1} = \left[\frac{35}{f_{cm}}\right]^{0.1} \leq 1.0$
Time Development	$\varepsilon_{sh}(t) =$ $\begin{cases} \left[\frac{t}{35+t}\right]\varepsilon_{sh,ult}, & 7\ days\ of\ moist-curing \\ \left[\frac{t}{55+t}\right]\varepsilon_{sh,ult}, & 1\ to\ 3\ days\ of\ steam-curing \end{cases}$ time development ***Equation 2-24***	$k_{td} = \frac{t}{61 - 4f'_{ci} + t}$ time development factor ***Equation 2-26***	$\beta_{as}(t) = 1 - \exp(-0.2\sqrt{t})$ time function for autogenous shrinkage ***Equation 2-28*** $\beta_{ds}(t - t_s) = \left[\frac{(t - t_s)}{0.035h^2 + (t - t_s)}\right]^{0.5}$ time-development function for drying shrinkage ***Equation 2-29***
Explanation of the Variables	• λ = % relative humidity • V/S = volume to surface ratio in [in.] • ψ = % ratio of fine aggregate to total aggregate by weight • c = cement content in [lbs/yd^3] • s = slump in [in.] • α = % air content • t = time after the end of the initial wet curing (days)	• V/S = volume-to-surface ratio in [in.] • H = relative humidity (%) • f'_{ci} = specified compressive strength of concrete at time of prestressing in [ksi]. If concrete age at time of initial loading is unknown at design time, f'_{ci} may be taken as $0.80f_c'$ in [ksi]. • t = maturity of concrete in [days]; relative to end of curing for creep calculations	• f_{cm} = mean compressive strength at 28 days in [MPa] = f'_c + 8 MPa • $\alpha_{as}, \alpha_{ds1}, \alpha_{ds2}$ = coefficient dependent on the type of cement strength class of cement: α_{as} / α_{ds1} / α_{ds2} 32.5 N: 800 / 3 / 0.013 32.5 R, 42.5 N: 700 / 4 / 0.012 42.5 R, 52.5 N, 52.5 R: 600 / 6 / 0.012 • RH = relative humidity of the ambient atmosphere in [%] • h = notational size of member in [mm] = $\frac{2A_c}{u}$ • t_s = concrete age at the beginning of drying in [days] • t = concrete age in [days]

Chapter 3 Computer Program Development

3.1 Introduction

The first version of the camber prediction program was developed by Schrantz (2008). Specific steps included the assemblage of the entire time-deflection algorithm with the numerical time-step approach using Visual Basic (VB) programming language. Further, her work included design of the user interfaces to enter the required values and to report the output data. The second version of the software was developed by Johnson (2012) after including a few crucial corrections. In this research study, a third version of the camber software is developed and later used for data analysis.

The input process with the previous camber software were time-consuming owing to the fact that it was not able to import from or export to a spreadsheet file. A user was required to enter all input variables separately and record the output data one at a time. In addition, some existing time-dependent concrete prediction models had become obsolete since the original version. Thus, new prediction models have been added. The new version of the application also comes with several modifications and new features to enhance the user experience.

The new camber software offers one MOE development model based on measured MOE, Two-Point MOE, and four different strength-based MOE development models, ACI 209 Normal, ACI 209 Backcalculate, *fib* MC 2010 Normal-Weight, and *fib* MC 2010 Backcalculate. Available concrete creep and shrinkage models are AASHTO LRFD 2014, ACI 209, and *fib* MC 2010.

This chapter continues with the presentation of the methodology including the logic of the time-dependent deformation computations and the modifications made to the previous versions. The discussions about the new features and prediction models are presented in Section 3.3. Later, Section 3.4 concludes the chapter by presenting the current input schema and the output structure.

3.2 Methodology

This section is composed of two main parts. Firstly, a discussion of the algorithm for time-dependent deflections is included, which was initially assembled by Schrantz (2012). Next, an explanation of the modifications made on the earlier versions is presented.

3.2.1 Algorithm for Time-Dependent Deflections

The derived equations in this section are based on the three fundamental assumptions: ‘a plane section remains plane’, the linear-elastic stress-strain behavior for stress-induced strains, and equilibrium. They are combined to construct the key relationship necessitated for the time-step method. Discussion of these assumptions is given in Section 2.2.3.

Figures 3-1 and 3-2 illustrate the algorithm to calculate the time-dependent deflections. The calculations are divided into five main groups: (1) initial calculations, (2) calculations for each time step and cross section, (3) updated strains and stresses, and (4) incremental and total camber. In addition to showing the algorithm, the reserved variable names used in the software are also provided to better compare the figures presented in Section 3.4.3. The notation used in Figures 3-1 and 3-2 is explained in Appendix A. Derivations of the equations are discussed by Schrantz (2012).

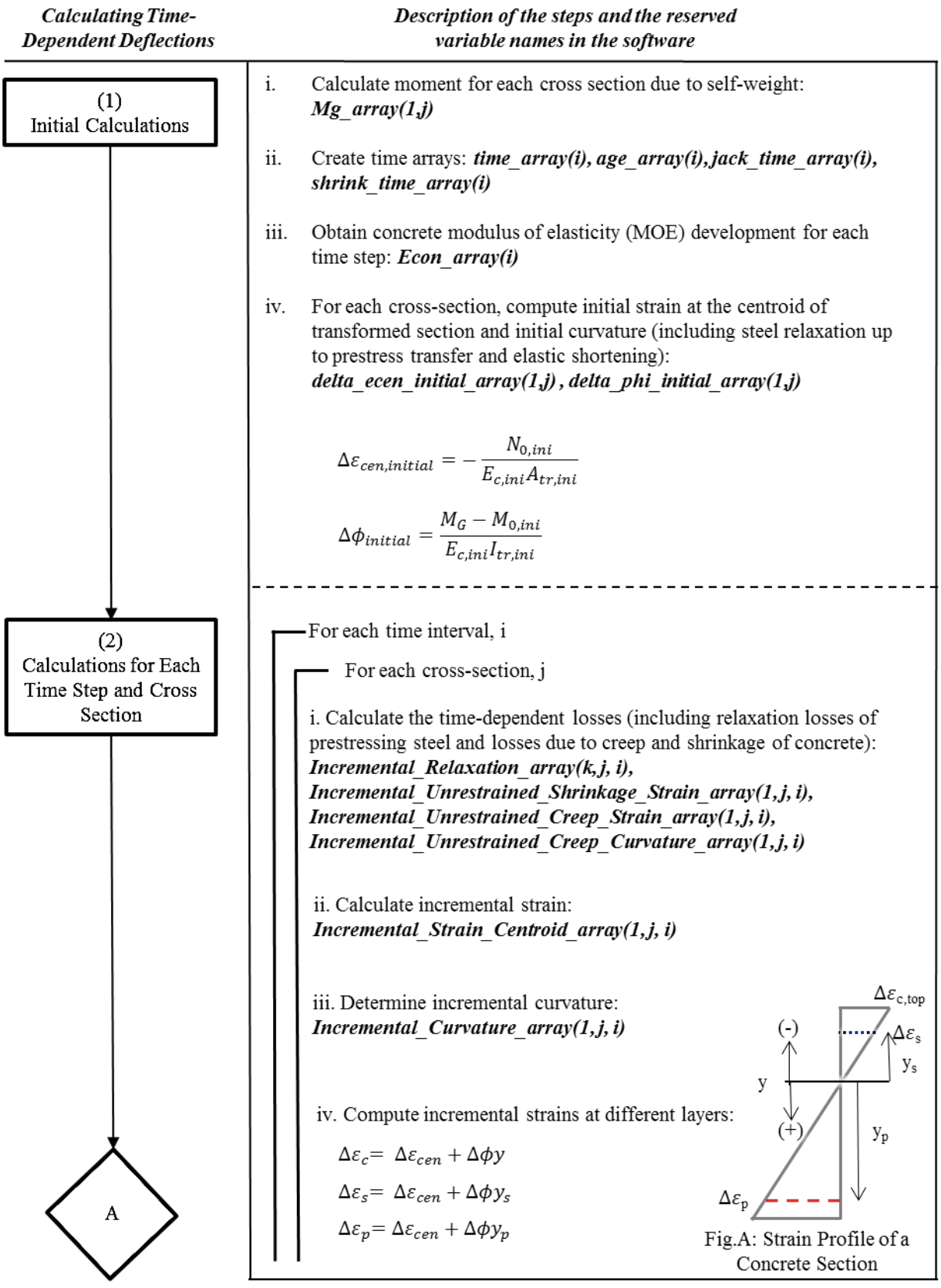

Figure 3-1: Methodology of Time-Deflection Calculations—Part 1

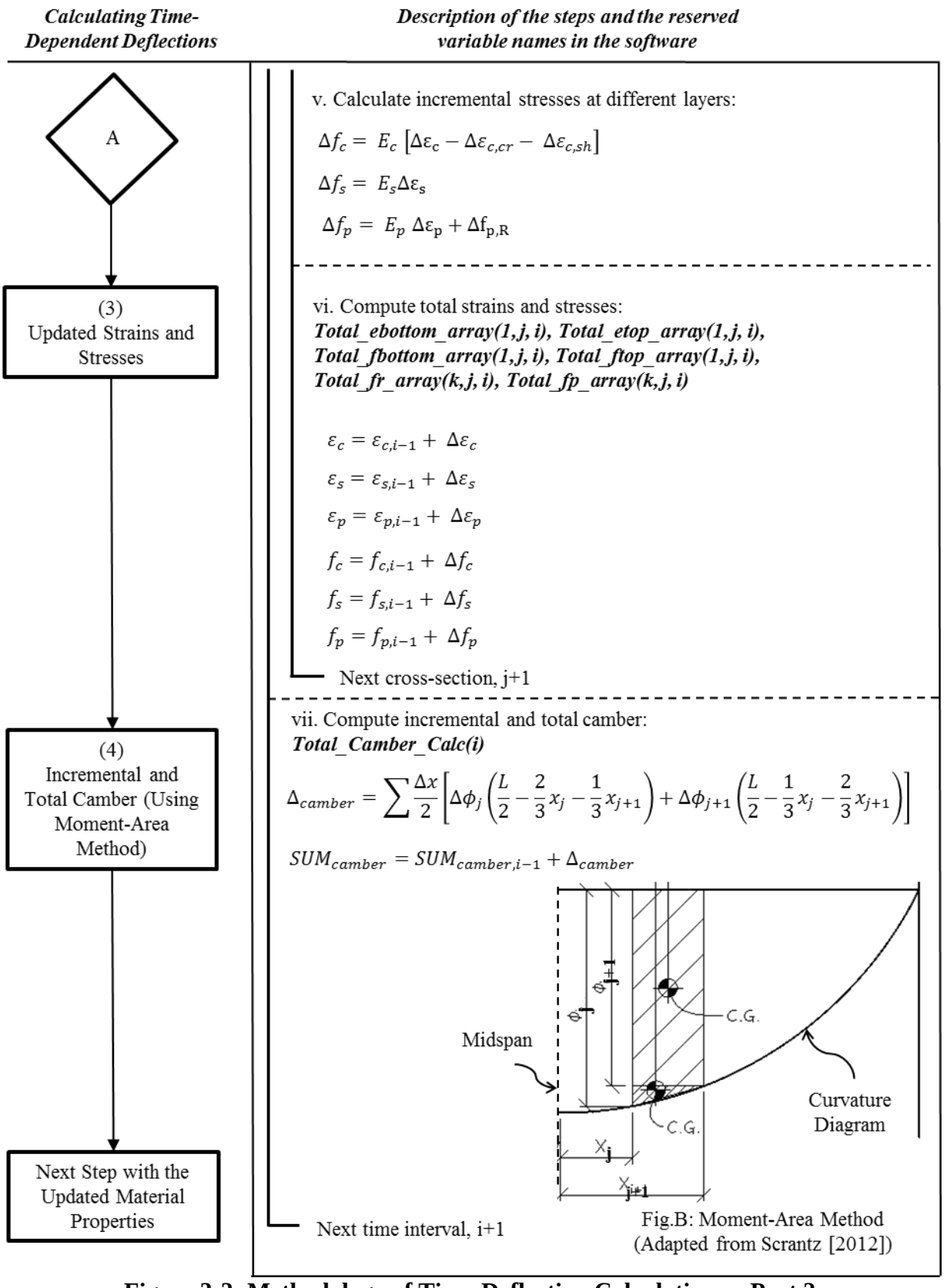

Figure 3-2: Methodology of Time-Deflection Calculations—Part 2

(1) Initial Calculations

Bending moment due to the self-weight is needed to compute the elastic shortening of the concrete. In the camber software, unit weight of the plain concrete is distributed uniformly over the girder length with an additional amount of 5 pcf to account for the reinforcement within a girder.

A time array is used to provide a mutual chronological time in all of the subroutines. Step sizes are based on a nonlinear function to better characterize the rapidly changing earlier behavior. The time arrays used in the computer software are also discussed in Section 3.4.1.

Modulus of elasticity (MOE) development is essential to obtain the trend of the material properties. MOE development can be formulated according to the two-point approach or the code-based approaches such as *fib* MC 2010 and ACI 209. MOE influences the relative stiffness of the steel and concrete materials; thus, the transformed-section properties change slightly at every time-step. Non-cracked section properties are also assumed.

The incremental step approach necessitates a starting point to construct the arrays in the next stage, and this is the reason behind the calculating the initial curvature and initial strain. The parameters in Step 1 should be considered separately from the remainder since the initial calculations are not based on the incremental approach rather they are total values.

(2) Calculations for Each Time Step and Cross Section

This step launches the loop for the time incremental calculations at each cross section. The steel relaxation, unrestrained creep and shrinkage deformations are time-dependent changes incorporated in the algorithm. The prestressed girders contain reinforcement steel (prestressed and non-prestressed) restraining free deformations due to creep and shrinkage. Therefore, the unrestrained term is used to emphasize the difference.

Creep deformations, which vary linearly over the cross section, need to be functioned in terms of curvature and strain unlike the unrestrained shrinkage deformation. The unrestrained shrinkage deformations are assumed to be constant over the girder depth. Unrestrained creep and shrinkage deformations can be modeled as described in AASHTO LRFD 2014, ACI 209, and *fib* MC 2010.

The incremental strain and curvature functions combining individual time-dependent deformations are given in Equations 3-1 and 3-2. They are derived directly from Equations 2-1, 2-2, 2-3, and 2-4 given in Section 2.2.3.2. Derivations of the equations were explained by Schrantz (2012). The notation can be found in Appendix A.

$$\Delta\varepsilon_{cen} = \frac{A_c}{A_{tr}}\left(\Delta\varepsilon_{cen,cr} + \Delta\varepsilon_{c,sh}\right) - \frac{\Delta\phi_{c,cr}\left(n_p \sum A_{p,k} y_{p,k} + n_s \sum A_{s,k} y_{s,k}\right)}{A_{tr}} + \frac{\frac{1}{E_c}\sum \Delta f_{p,R,k} A_{p,k}}{A_{tr}} \qquad \textbf{Equation 3-1}$$

$$\Delta\phi = \Delta\phi_{c,cr}\left(1 - \frac{n_p \sum A_{p,k} {y_{p,k}}^2 + n_s \sum A_{s,k} {y_{s,k}}^2}{I_{tr}}\right) - \frac{\left(\Delta\varepsilon_{cen,cr} + \Delta\varepsilon_{c,sh}\right)\left(n_p \sum A_{p,k} y_{p,k} + n_s \sum A_{s,k} y_{s,k}\right)}{I_{tr}} - \frac{\frac{1}{E_p} n_p \sum \Delta f_{p,R,k} A_{p,k} y_{p,k}}{I_{tr}} \qquad \textbf{Equation 3-2}$$

where, $\Delta\varepsilon_{cen}$ = incremental strain at the centroid of the transformed section

$\Delta\phi$ = incremental curvature

$\Delta\phi_{c,cr}$ = incremental curvature due to unrestrained creep

$\Delta\varepsilon_{cen,cr}$= incremental unrestrained creep strain in concrete at the centroid of the transformed section

$\Delta\varepsilon_{c,sh}$ = incremental unrestrained shrinkage strain in concrete at the centroid of the transformed section

$\Delta f_{p,R,k}$ = incremental change in stress in each prestress layer k due to relaxation

k = each layer of prestressed or non-prestressed reinforcement

After determining incremental strain and curvature, incremental strains at different layers are obtained with the assumption of the perfect bonding between the steel and concrete. At the same depth, the same amount of incremental strain is obtained for all constituents—concrete block and steel layers. The embedded Figure A in Figure 3-1 illustrates the position of strain values and the sign convention used in the camber software.

Theory of the linear-elastic stress-strain behavior provides the necessary relationship to calculate stresses over the girder depth. The incremental concrete stress excludes the unrestrained creep and shrinkage deformations since the strains due to creep and shrinkage do not induce stress (see Equation 2-2). The incremental relaxation loss is accounted for finding the incremental stress at the prestressing steel layers.

(3) Updated Strains and Stresses

After computing incremental strains and stresses, they are summed up with total values from the previous time step. Initial strains and curvatures from Step (1) are the beginning points.

(4) Incremental and Total Camber

Camber is calculated by using the moment-area method. In order to represent the storage conditions of the plant, girders are assumed to be symmetrical and simply-supported with a uniformly distributed self-weight. The camber trend is only influenced by the incremental curvatures. The embedded Figure B in Figure 3-2 displays the implementation of moment-area method.

3.2.2 Modifications Made to Previous Versions

This section presents the five major modifications within the camber prediction software:

- Relocation of input variables in a module,
- Improvement of source code to minimize errors,
- Improvement of combo-box controls,
- Inclusion of calculate button, and
- Separation of creep and shrinkage models in a new subroutine

Some of the modifications are aimed at fixing the errors. Other modifications were added to promote the user-friendly interface.

3.2.2.1 Relocation of Input Variables in a New Module

In the previous versions of the camber software, variables were specific to a Microsoft Windows form where they were introduced. In other words, variables were not shared with other modules and functions (subroutines). Therefore, all of the input variables are moved to a mutual module to globalize them. It also becomes useful to transfer them into a spreadsheet file.

3.2.2.2 Improvement of Source Code to Minimize Errors

User inputs were not previously examined to detect irrational values; indeed, the earlier versions of application allowed passing to the next forms without informing users about possible exceptions. Inputting letters or unreasonable numerical values was very likely to cause problems. In order to prevent it, if-statements are included to justify that user-input variables are reasonable. In addition, all of the inputs are arranged to pass through an algorithm called "Try…Catch" blocks. Errors are referred as exceptions in the .NET Framework. If an exception is caught during an execution, the blocks perform the final code instead of stopping it. In the new

version, the final code is written in a way to inform users about the type of exceptions and ask them to verify the input.

3.2.2.3 Improvement of Combo-Box Controls

A combo-box control allows users to select an item from a provided list. Later, a numerical value is assigned in the internal subroutines based on the label of the chosen item. If the label is modified somehow by a user, the assigned value can be zero. In order to avoid modifications to item names and to ensure inputting non-zero variables, the drop-down styles are changed. Nevertheless, some of the drop-down styles are kept same to allow custom values. For example, a user can define a custom coefficient rather than choosing one of the cement types given in *fib* MC 2010.

3.2.2.4 Inclusion of Calculate Button

In the previous versions, the corresponded subroutines were called at each time when an output form was loaded. For instance, an output form revealing total curvatures used to call the subroutines calculating incremental curvatures, but it did not call the subroutines computing the camber development. One of the conditions to permit exporting the output data was to have all of them computed. Consequently, all of the subroutines and functions are organized in sequence in a new form, and the process is launched by clicking the calculate button. After using this button, the restart button appears on the same form. It allows users to perform a new analysis while erasing all of the variables in the memory. The restart button is added to avoid adding up results in the following attempts, which was the case in the earlier versions.

3.2.2.5 Separation of Creep and Shrinkage Models

The creep and shrinkage models were computed in the lengthy subroutine called "time_interval_loop". It was hard to track the subroutine for the creep and shrinkage models in

the previous version. A subroutine including the calculations of them are created to add and to update recent creep and shrinkage models. The new subroutine labeled as "Creep_Shrinkage_TimeArrays" calculates the incremental creep coefficients and shrinkage strains according to the chosen model including *fib* MC 2010. Also, new creep and shrinkage models can be added in this subroutine in future versions.

3.3 New Features

In this section, new features added in the camber prediction software are explained. This section starts with the discussion of the implemented four new MOE development models: including 'Two-Point MOE Development Model', '*fib* MC 2010 Normal-Weight', '*fib* MC 2010 Backcalculate', and 'ACI 209 Backcalculate'. Next, the implementation of the *fib* MC 2010 creep and shrinkage model is explained. Also, the discussion of the established communication with a spreadsheet file is made. The last subsection explains the uncategorized new features.

3.3.1 New Modulus of Elasticity Development Models

3.3.1.1 Two-Point MOE Development Model Based on Measured MOE

The collected data from the previous research projects include the actual concrete modulus of elasticity (MOE) at transfer and at 28 days. It uses a modified version of the time development function as given in *fib* MC 2010. The coefficient (s), which depends on the strength class of cement, is backcalculated by utilizing the supplied transfer and 28-day MOE. Two-point MOE development model based on measured MOE (two-point MOE model) is illustrated in Figure 3-3. In the earlier version of the software, the two-point approach was derived from the Model Code (MC) 1990. The time development equation was identical to the current one, but age of concrete at prestress transfer, $t_{transfer}$, did not include the maturity. In the new version, a user can specify the concrete age with maturity (using curing temperature).

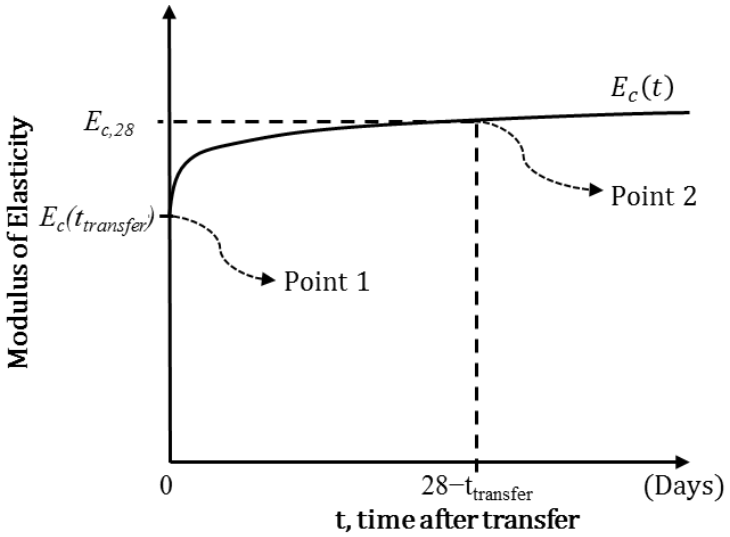

Figure 3-3: Illustration of Two-Point MOE Model

Derivation of the modified function can be seen below. Equations 3-3 and 3-4 are obtained from MC 2010.

$$E_c(t) = \left(\beta_{cc}(t)\right)^{1/2} \times E_{c,28} \qquad \textit{Equation 3-3}$$

$$\beta_{cc}(t) = exp\left\{s \times \left(1 - \sqrt{\frac{28}{t}}\right)\right\} \qquad \textit{Equation 3-4}$$

where, $E_c(t)$ = modulus of elasticity at an age of t in [days]

$\beta_{cc}(t)$ = function to describe the development with time

$E_{c,28}$ = modulus of elasticity at an age of 28 days

t = age of concrete in [days]

After inserting the given MOE at transfer, $E_c(t_{transfer})$, and 28 days, $E_{c,28}$, into Equation 3-3, it gives

$$E_c\left(t_{transfer}\right) = \sqrt{\beta_{cc}\left(t_{transfer}\right)} \times E_{c,28} \qquad \textit{Equation 3-5}$$

Replacing $\beta_{cc}\left(t_{transfer}\right)$ with the expression given in Equation 3-4 and rearranging Equation 3-5, the following function is obtained.

$$\left(\frac{E_c(t_{transfer})}{E_{c,28}}\right)^2 = exp\left\{s \times \left(1 - \sqrt{\frac{28}{t_{transfer}}}\right)\right\} \qquad \textbf{Equation 3-6}$$

Eliminating the exponential term after taking the natural logarithm of both sides gives

$$\ln\left(\frac{E_c(t_{transfer})}{E_{c,28}}\right)^2 = \ln\left[exp\left\{s \times \left(1 - \sqrt{\frac{28}{t_{transfer}}}\right)\right\}\right] \qquad \textbf{Equation 3-7}$$

$$2 \times \ln\left(\frac{E_c(t_{transfer})}{E_{c,28}}\right) = s \times \left(1 - \sqrt{\frac{28}{t_{transfer}}}\right) \qquad \textbf{Equation 3-8}$$

$$s = 2 \times \ln\left[\frac{E_c(t_{transfer})}{E_{c,28}}\right] \times \frac{1}{1 - \sqrt{\frac{28}{t_{transfer}}}} = 2 \times s^* \qquad \textbf{Equation 3-9}$$

The constant value, s^*, is obtained for the convenience of implementing the model in the software. The s term, coefficient which depends on the strength class of cement, is inserted into Equation 3-4 as:

$$\beta_{cc}(t) = exp\left\{2 \times \frac{\ln\left[\frac{E_c(t_{transfer})}{E_{c,28}}\right]}{1 - \sqrt{\frac{28}{t_{transfer}}}} \times \left[1 - \sqrt{\frac{28}{t}}\right]\right\} \qquad \textbf{Equation 3-10}$$

The square root of both sides is taken as shown in Equation 3-11 and it is simplified in Equation 3-12.

$$\left(\beta_{cc}(t)\right)^{1/2} = exp\left\{\frac{1}{2} \times 2 \times \frac{\ln\left[\frac{E_c(t_{transfer})}{E_{c,28}}\right]}{1 - \sqrt{\frac{28}{t_{transfer}}}} \times \left[1 - \sqrt{\frac{28}{t}}\right]\right\} \qquad \textbf{Equation 3-11}$$

$$\left(\beta_{cc}(t)\right)^{1/2} = exp\left\{\frac{\ln\left[\frac{E_c\left(t_{transfer}\right)}{E_{c,28}}\right]}{1-\sqrt{\frac{28}{t_{transfer}}}} \times \left[1-\sqrt{\frac{28}{t}}\right]\right\} \qquad \textit{Equation 3-12}$$

The constant part in Equation 3-12 is replaced with s^* in order to obtain the growth portion of the MOE development model given in Equation 3-3.

$$\left(\beta_{cc}(t)\right)^{\frac{1}{2}} = exp\left\{s^* \times \left(1-\sqrt{\frac{28}{t}}\right)\right\} \qquad \textit{Equation 3-13}$$

Figure 3-4 shows the routine created for the two-point MOE development model. The constant value, s^*, in Equation 3-13 is represented with "s_stiffness" in the Visual Basic (VB) routine. Also, square root of $\beta_{cc}(t)$ in Equation 3-3 is labeled as "beta_E(i)".

```
s_stiffness = CSng((Log(Eci_supp / Ec28_supp)) / (1 - (((28) / (AdjustedAge)) ^
0.5)))

'AdjustedAge is equal to t_transfer.
'Note: Log is the reserved name for natural base logarithmic function (ln) in VB.

For i = 1 To TimeIntervals

   beta_E (i) = CSng(Exp(s_stiffness * (1 - ((28 / age_array(i)) ^ 0.5))))

'age_array() is the concrete age (days) relative to the casting. It includes the
maturity.

   Econcrete_array(i) = Ec28_supp * beta_E(i)

Next

Ec_initial = Eci_supp
Ec28 = Ec28_supp

'Eci_supp is the supplied initial concrete modulus of elasticity.
'Ec28_supp is the supplied initial concrete modulus of elasticity at 28-day.
'CSng is used to convert expression to a single type.
```

Figure 3-4: Routine for Two-Point MOE Development

3.3.1.2 *fib* Model Code 2010 MOE Model

Cement type, aggregate type, and 28-day concrete strength are needed to compute MOE development according to *fib* MC 2010 (for normal-weight concrete). The provided strength type—design or actual—is also required. The programming code implementing the new MOE model is shown in Figure 3-5.

The codes, not shown in the figure, assign a numerical value for the coefficients based on the cement and aggregate types. Cement types are listed as "42.5R, 52.5N, 52.5R", "32.5R, 42.5N" and "32.5N". The variable name "s_fib" is used in the VB routine to save the associated coefficient. Similarly, aggregate types are grouped into four categories: "basalt, dense limestone", "quartzite", "limestone", and "sandstone". A VB variable labeled as "alpha_e_fib" is the coefficient based on the selected aggregate type. Alternatively, both of the coefficients can be submitted numerically by a user.

```
If StrengthType = "Actual" Then

   Ec28 = CSng((21.5 * 10 ^ 3 * alpha_e_fib * n_E_fib * (fc28_MOE / 145.0377 / 10)
^ (1 / 3)) * 145.0377 / 1000) 'in ksi

ElseIf StrengthType = "Specified" Then

   Ec28 = CSng((21.5 * 10 ^ 3 * alpha_e_fib * n_E_fib * ((fc28_MOE / 145.0377 + 8)
/ 10) ^ (1 / 3)) * 145.0377 / 1000) 'in ksi
End If

'n_E_fib is a coefficient depend on oven-dry density of lightweight concrete. It
is taken as 1.0 for normal-weight concrete.  '1 MPa = 145.0377 psi

For i = 1 To TimeIntervals

'TimeIntervals is the number of times segments
   beta_cc(i) = CSng(Exp(s_fib * (1 - Sqrt(28 / age_array(i)))))

'age_array() is the concrete age (days) relative to the casting. It includes the
maturity.
```

➔Cont'd

```
➔Cont'd
   Econcrete_array(i) = CSng(Sqrt(beta_cc(i)) * (Ec28)) 'in ksi

Next

   Ec_initial = CSng(Sqrt(beta_cc(1)) * (Ec28)) 'in ksi

'beta_cc(1) is associated with the value at transfer
'CSng is used to convert an expression to a single type.
```

Figure 3-5: Routine for *fib* Model Code 2010 (Normal-Weight) MOE Development

3.3.1.3 Backcalculated *fib* Model Code 2010 Model

The difference between the backcalculated and regular *fib* MC 2010 is the way to obtain the coefficient depends on the strength class, s. This coefficient is acquired by making use of two compressive strength points in the "backcalculated" version; while, it is picked from the tabulated list in the normal-weight version.

A user is directed to provide aggregate type, concrete strengths at transfer and 28 days after transfer for the backcalculated *fib* MC 2010 MOE model. Additionally, a user is asked to choose one of the strength types—specified-design or expected-actual—since *fib* MC 2010 amplifies the specified-design value by offsetting it.

Derivation of the coefficient and the time-development function is explained in the following equations. Development of strength with time is described in *fib* MC 2010 as:

$$f_{cm}(t) = \beta_{cc}(t) \times f_{cm} \qquad \textbf{\textit{Equation 3-14}}$$

$$\beta_{cc}(t) = exp\left\{s \times \left(1 - \sqrt{\frac{28}{t}}\right)\right\} \qquad \textbf{\textit{Equation 3-15}}$$

where, $f_{cn}(t)$ = mean compressive strength at an age of t in [days]

$\beta_{cc}(t)$ = function to describe the development with time

f_{cm} = mean compressive strength at an age of 28 days

t = age of concrete in [days] (taking into account temperature during curing)

s = coefficient which depends on the strength class of cement

Inserting the supplied strength values at prestress transfer $t_{transfer}$ = in (taking into account temperature during curing) into Equation 3-15 gives

$$E_{ci}(t_{transfer}) = \beta_{cc}(t_{transfer}) \times E_{ci} \qquad \textbf{Equation 3-16}$$

Inserting the expression provided in Equation 3-15 and rearranging Equation 3-16 give

$$\ln\left(\frac{E_{ci}(t_{transfer})}{E_{ci}}\right) = \ln\left[exp\left\{s \times \left(1 - \sqrt{\frac{28}{t_{transfer}}}\right)\right\}\right] \qquad \textbf{Equation 3-17}$$

$$\ln\left(\frac{E_{ci}(t_{transfer})}{E_{ci}}\right) = s \times \left(1 - \sqrt{\frac{28}{t_{transfer}}}\right) \qquad \textbf{Equation 3-18}$$

Solving Equation 3-18 for the s term

$$s = \ln\left[\frac{E_{ci}(t_{transfer})}{E_{ci}}\right] \frac{1}{1 - \sqrt{\frac{28}{t_{transfer}}}} \qquad \textbf{Equation 3-19}$$

Rewriting Equation 3-14 with the expression derived in Equation 3-19 give

$$\beta_{cc}(t) = exp\left\{\frac{\ln\left[\frac{E_{ci}(t_{transfer})}{E_{ci}}\right]}{1 - \sqrt{\frac{28}{t_{transfer}}}} \times \left[1 - \sqrt{\frac{28}{t}}\right]\right\} \qquad \textbf{Equation 3-20}$$

The constant part in Equation 3-20 is replaced with s to obtain time-development function.

$$\beta_{cc}(t) = exp\left\{s \times \left(1 - \sqrt{\frac{28}{t}}\right)\right\} \qquad \textbf{Equation 3-21}$$

The s term is represented with “s_fib” in the Visual Basic (VB) application. A selected portion of the code for the backcalculated *fib* MC 2010 MOE model is shown in Figure 3-6.

```
If StrengthType = "Actual" Then

   Ec28 = CSng((21.5 * 10 ^ 3 * alpha_e_fib * n_E_fib * (fc28_MOE / 145.0377 / 10) ^
(1 / 3)) * 145.0377 / 1000) 'in ksi

ElseIf StrengthType = "Specified" Then

   Ec28 = CSng((21.5 * 10 ^ 3 * alpha_e_fib * n_E_fib * ((fc28_MOE / 145.0377 + 8) /
10) ^ (1 / 3)) * 145.0377 / 1000) 'in ksi

'n_E_fib is a coefficient depending on oven-dry density of lightweight concrete.
It is taken as 1.0 for normal-weight concrete.
'alpha_e_fib is a coefficient of aggregate type.
'1 MPa = 145.0377 psi
End If

If StrengthType = "Actual" Then

   s_fib = CSng((Log(fci_MOE / fc28_MOE)) / (1 - (28 / AdjustedAge) ^ 0.5))

ElseIf StrengthType = "Specified" Then

   s_fib = CSng((Log((fci_MOE / 145.0377 + 8) / (fc28_MOE / 145.0377 + 8))) / (1 - (28
/ AdjustedAge) ^ 0.5))

'AdjustedAge is equal to t_transfer.
End If

For i = 1 To TimeIntervals

   beta_cc(i) = CSng(Exp(s_fib * (1 - Sqrt(28 / age_array(i)))))
 'age_array() is the concrete age (days) relative to the casting. It includes the
maturity.

   Econcrete_array(i) = CSng(Sqrt(beta_cc(i)) * (Ec28)) 'in ksi
Next
   Ec_initial = CSng(Sqrt(beta_cc(1)) * (Ec28)) 'in ksi ,

'beta_cc(1) is associated with the value at transfer
'fci_MOE is the supplied initial concrete strength.
'fc28_MOE is the supplied  concrete strength at 28-day.
'CSng is used to convert expression to a single type.
```

Figure 3-6: Routine for Backcalculated *fib* MC 2010 MOE Development Model

3.3.1.4 Backcalculated ACI 209 MOE Model

The backcalculated ACI MOE Model utilizes strength values at transfer and 28 days to fit the MOE time-development curve as given in ACI 209R-92. The parameters α and β are backcalculated by using the strength values. ACI 209R-92 describes the time-development of compressive strength as:

$$(f'_c)_t = \frac{t}{\alpha + \beta \times t}(f'_c)_{28} \qquad \textit{Equation 3-23}$$

where, $(f'_c)_t$ = compressive strength at an age of t in [days]

t = age of concrete since the casting in [days]

α, β = parameters depend on the type of cement and curing

Using the equilibrium at t = 28 days and solving for α give the following expression.

$$\alpha = 28 \times (1 - \beta) \qquad \textit{Equation 3-24}$$

The expression of α is inserted into Equation 3-23 as:

$$(f'_c)_t = \frac{t}{28 - \beta \times 28 + \beta \times t}(f'_c)_{28} \qquad \textit{Equation 3-25}$$

Using the supplied strength value at t = $t_{initial}$ (age of concrete at prestress transfer) give

$$(f'_c)_{initial} = \frac{t_{initial}}{28 - \beta \times 28 + \beta \times t_{initial}}(f'_c)_{28} \qquad \textit{Equation 3-26}$$

The following expressions show rearranged Equation 3-26 to solve for β.

$$\beta = \frac{28 - t_{initial}\left[\frac{(f'_c)_{28}}{(f'_c)_{initial}}\right]}{28 - t_{initial}} \qquad \textit{Equation 3-27}$$

Moreover, the same growth method is also utilized for AASHTO LRFD 2014 MOE Model since it does not suggest or specify any time growth equations. ACI 209 MOE development is simply multiplied by the K_1 factor at all ages. Figure 3-7 supplies the routine for the backcalculated ACI 209 MOE development.

```
beta_MOE_AA = CSng((AdjustedAge * (fc28_MOE / fci_MOE) - 28) / (AdjustedAge - 28))

'AdjustedAge is equal to t_initial.
alpha_MOE_AA = CSng(28 * (1 - beta_MOE_AA))

For i = 1 To TimeIntervals

   fconcrete_array(i) = Max((age_array(i) / (alpha_MOE_AA + (beta_MOE_AA *
age_array(i)))) * fc28_MOE, fci_MOE) 'in psi

'age_array() is the concrete age (days) relative to the casting.
‘fconcrete_array(i) is capped with fci_MOE for the compatibility reasons.

   Econcrete_array(i) = CSng(33 * K1_MOE_AA * ((wc_MOE) ^ 1.5) * ((fconcrete_array(i))
^ 0.5) / 1000) 'in ksi

' K1_MOE_AA is the correction for the source of aggregate and specific to AASHTO
LRFD 2014 model. For ACI 209, it is equal to 1.00
Next i

   Ec_initial = CSng(33 * K1_MOE_AA * ((wc_MOE) ^ 1.5) * ((fci_MOE) ^ 0.5) / 1000)
'in ksi
   Ec28 = CSng(33 * K1_MOE_AA * ((wc_MOE) ^ 1.5) * ((fc28_MOE) ^ 0.5) / 1000) 'in ksi

'fci_MOE is the supplied initial concrete strength.
'fc28_MOE is the supplied concrete strength at 28-day
'CSng is used to convert expression to a single type.
```

Figure 3-7: Routine for Backcalculated ACI 209 MOE Development Model

3.3.1.5 Sample Output for MOE Development Models

A sample case is used to show the software's capability of computing MOE development. The output of the casting group H (SCC) from the Hillabee Creek Bridge Project is plotted in Figure 3-8. This subsection is not intended to compare the various MOE development models.

The MOE and strength development can be seen the figure. ACI 209 and *fib* MC 2010 employ the strength-based approach. The regular MOE models use the actual strength at 28 days and the coefficient(s) that are suggested for the use with the relevant model. On the other hand, backcalculated models use the actual strengths at transfer and at 28 days. The coefficients are backcalculated accordingly.

The MOE value at transfer, shown as t=0 in the figure, is used to predict the deformations such as strain, curvature, and camber at transfer. Therefore, the accuracy of the material prediction models at transfer depends on the initial MOE.

Backcalculated and regular models intersect at 28 days relative to the concrete casting. This point is expressed with the label of "28days-TransferTime" for ACI 209 and with the label of "28days-EqvAge" for *fib* MC 2010. "TransferTime" is the chronological age without any temperature effects. In contrast, "EqvAge" represents the maturity of concrete (age of concrete including the temperature effects up to transfer). The models intersecting at these specific points support the initial assumptions.

The regular and backcalculated MC 2010 model compute significantly larger MOE than the other strength-based models since the constant that depends on the type of aggregate (α_E) is taken as 1.2. The discrepancy between the regular and backcalculated models reveal the difference between the backcalculated coefficients (or parameters) and the suggested coefficients (or parameters).

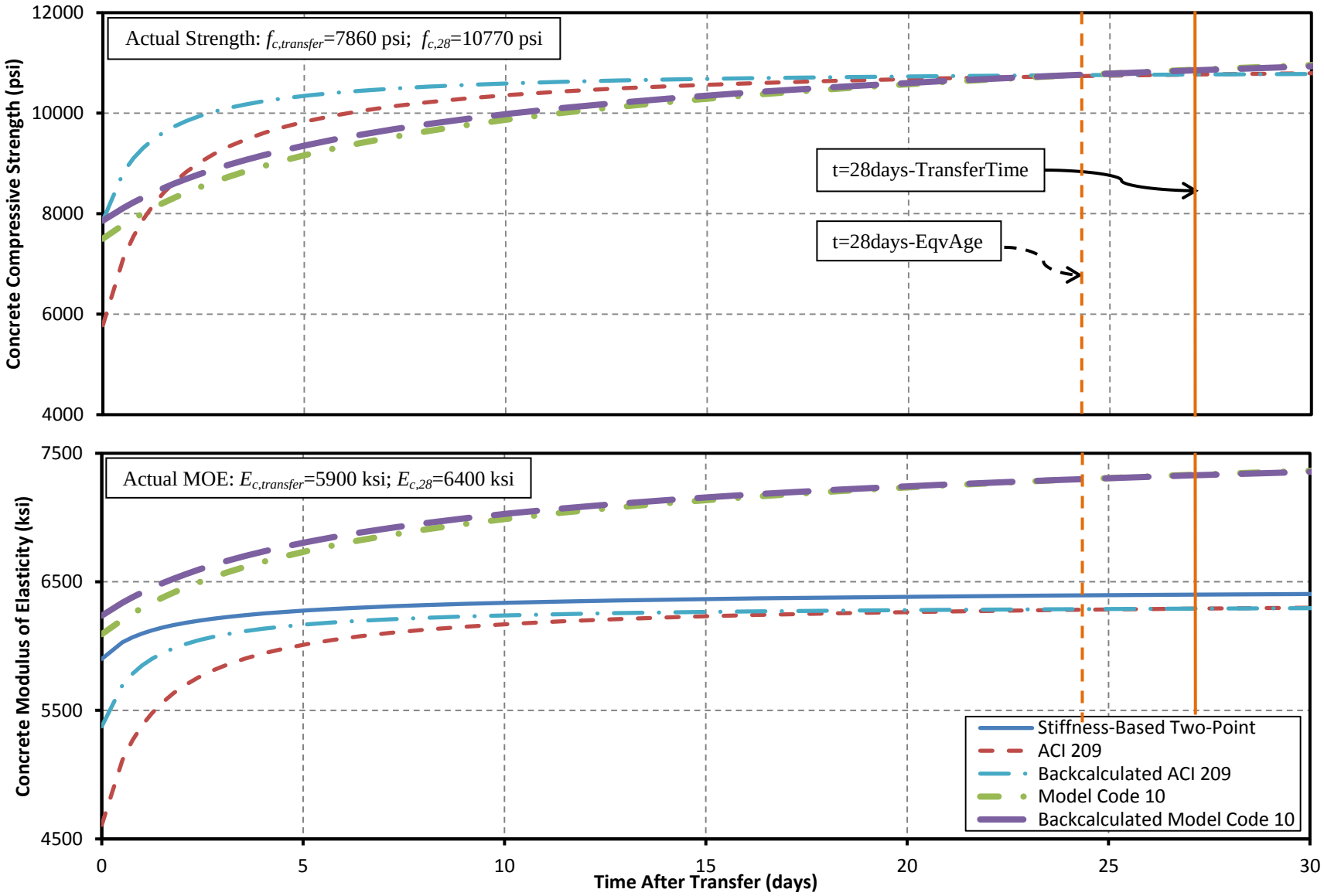

Figure 3-8: Sample Output for Strength and MOE Development Models

3.3.2 New Creep and Shrinkage Model

The implementation of the *fib* MC 2010 creep and shrinkage models for normal-weight concrete is considered in this section. Table 3-1 provides the required parameters to predict creep and shrinkage behavior.

Table 3-1: Required Variables for MC 2010 Creep and Shrinkage Model

Used Variable		**Definition**	**Is it required for**	
In *fib* MC 2010	**In VB application**		**Creep?**	**Shrinkage?**
f_{cm}	fcm_fib_CrSh	mean compressive strength at the age of 28 days in [psi]	Y	Y
T	age_array( )	age of concrete in [days]	Y	Y
RH	RH	relative humidity of the ambient environment in [%]	Y	Y
H	h_fib_CrSh	notional size of member in [in] (= $2A_c/u$)	Y	Y
t_o	creep_AdjustedAge	age of concrete at loading in [days], including temperature adjustment and the effect of type of cement	Y	N
$(t-t_s)$	shrink_time_array( )	duration of drying in [days]	N	Y
	CementType_fib_CrSh	strength class of cement	N	Y

3.3.2.1 *fib* Model Code 2010 Creep Model

The MC 2010 creep model and the notation used in this section are provided in Table 2-7 in Section 2-3.6. Implementation of the MC 2010 creep model in the VB source code is achieved in three steps. In the first step, the notional creep coefficient, φ_0, is calculated. It is a function of the mean compressive strength, the relative humidity, notional size of member, and the age of concrete at loading. The formulation is shown in Equation 3-28, and Figure 3-9 further explains the implementation.

$$\varphi_0 = \varphi_{RH}\beta(f_{cm})\beta(t_0) \qquad \textit{Equation 3-28}$$

```
 'Step 1: Calculating the notional creep coef part

   phi_RH_fib = CSng((1 + (1 - RH / 100) / (0.1 * (h_fib_CrSh * 25.4) ^ (1 / 3)) *
((35 / (fcm_fib_CrSh / 145.0377)) ^ 0.7)) * ((35 / (fcm_fib_CrSh / 145.0377)) ^
0.2))

   beta_fcm_fib = CSng(16.8 / ((fcm_fib_CrSh / 145.0377) ^ 0.5))

   beta_to_fib = CSng(1 / (0.1 + creep_AdjustedAge ^ 0.2))

   notional_creep_co = phi_RH_fib * beta_fcm_fib * beta_to_fib

'The units are converted to SI system. 1 in = 25.4mm, 1 psi = 1/145.0377 MPa
```

Figure 3-9: Routine for *fib* MC 2010 Creep Model—Step 1

In the second step, the time-development of creep coefficient, $\beta_c(t,t_0)$, is calculated. The function is given in Equation 3-29. The term, β_H, is a function of notional size of member, relative humidity, and mean compressive strength.

$$\beta_c(t,t_0) = \frac{(t - t_0)}{\beta_H + (t - t_0)} \qquad \textit{Equation 3-29}$$

The third and last step, which is shown in Equation 3-30, includes obtaining the creep coefficient from the notional creep coefficient and the time-development. The VB code for the second and third step can be found in Figure 3-10. The incremental creep coefficient, "delta_beta_c(i)", is calculated for each time step.

$$\varphi(t, t_0) = \varphi_0 \beta_c(t, t_0) \qquad \textit{Equation 3-30}$$

```
For i = 1 To TimeIntervals

'Step 2: Development of creep with time

   beta_h_fib = CSng(Min(1.5 * h_fib_CrSh * 25.4 * (1 + (1.2 * RH / 100) ^ 18) +
250 * ((35 / (fcm_fib_CrSh / 145.0377)) ^ 0.5), 1500 * (35 / (fcm_fib_CrSh /
145.0377)) ^ 0.5))

'The units are converted to SI system. 1 in = 25.4mm, 1 psi = 1/145.0377 MPa

   beta_c_begin(i) = CSng(Max((age_array(i - 1) - AdjustedAge) / (beta_h_fib +
(age_array(i - 1) - creep_AdjustedAge)), 0) ^ 0.3)

   beta_c_end(i) = CSng(Max((age_array(i) - AdjustedAge) / (beta_h_fib +
(age_array(i) - creep_AdjustedAge)), 0) ^ 0.3)

   delta_beta_c(i) = beta_c_end(i) - beta_c_begin(i)

'Step 3: Total creep coefficient

   Ultimate_Creep_Coefficient = notional_creep_co

   Incremental_Creep_Coefficient_array(i) = notional_creep_co * delta_beta_c(i)

   Total_Creep_Coefficient = Total_Creep_Coefficient +
Incremental_Creep_Coefficient_array(i)

Next i
```

Figure 3-10: Routine for *fib* MC 2010 Creep Model—Steps 2&3

3.3.2.2 *fib* Model Code 2010 Shrinkage Model

The explanation of the MC 2010 shrinkage model and the notation used in this subsection are provided in Table 2-8 in Section 2.3.7. It calculates the autogenous and drying shrinkage separately unlike the AASHTO LRFD and ACI 209 shrinkage models. The MC 2010 shrinkage model is made compatible for the time-step approach in three steps. The first step covers the calculation of autogenous shrinkage strain, $\varepsilon_{cas}(t)$, provided in Equation 3-31. The term, $\varepsilon_{cas0}(f_{cm})$, depends on the strength class of cement and the mean compressive strength. The term, $\beta_{as}(t)$, is the time-development function. Figure 3-11 shows the routine for the first step of the *fib* MC 2010 shrinkage model.

$$\varepsilon_{cas}(t) = \varepsilon_{cas0}(f_{cm})\beta_{as}(t) \qquad \textit{Equation 3-31}$$

```
For i = 1 To TimeIntervals
'Step 1 : Notional autogenous shrinkage coefficient and incremental time function

   epsilon_cas0_fib = CSng(((-alpha_as_fib * (((fcm_fib_CrSh / 145.0377) / 10) / (6
+ (fcm_fib_CrSh / 145.0377) / 10)) ^ 2.5) * 10 ^ -6))
'alpha _as_fib is the coefficient depend on the strength class of cement
'The units are converted to SI system. 1 in = 25.4mm, 1 psi = 1/145.0377 MPa
   beta_as_fib_begin(i) = CSng(1 - Exp(-0.2 * Sqrt(age_array(i - 1))))
   beta_as_fib_end(i) = CSng(1 - Exp(-0.2 * Sqrt(age_array(i))))

   beta_as_fib_delta(i) = beta_as_fib_end(i) - beta_as_fib_begin(i)
Next i
```

Figure 3-11: Routine for *fib* MC 2010 Shrinkage Model—Step 1

In the second step, drying shrinkage function, $\varepsilon_{cds}(t,t_0)$, is executed, and the function is given in Equation 3-32. The term, $\varepsilon_{cds0}(f_{cm})$, depends on the strength class of cement and the mean compressive strength; the term, $\beta_{RH}(RH)$, is a function of the relative humidity, the strength class of cement, and the mean compressive strength. The term, $\beta_{ds}(t - t_s)$, is the time-development function for the drying shrinkage.

$$\varepsilon_{cds}(t, t_s) = \varepsilon_{cds0}(f_{cm})\beta_{RH}(RH)\beta_{ds}(t - t_s) \qquad \textit{Equation 3-32}$$

The total shrinkage strain, $\varepsilon_{cs}(t,t_0)$, is obtained at the third step. It is the summation of the autogenous shrinkage and the drying shrinkage as provided in Equation 3-33. Figure 3-12 shows the routine for the second and third steps.

$$\varepsilon_{cds}(t, t_s) = \varepsilon_{cas}(t) + \varepsilon_{cds}(t, t_s) \qquad \textit{Equation 3-33}$$

```
For i = 1 To TimeIntervals
'Step 2 :
'Notional drying shrinkage coefficient, RH coefficient and incremental time function

   epsilon_cds0_fib = CSng(((220 + 110 * alpha_ds1_fib) * Exp(-alpha_ds2_fib *
(fcm_fib_CrSh / 145.0377))) * 10 ^ -6)

'alpha _ds1_fib and alpha _ds2_fib  are the coefficients depending on the strength
class of cement
   beta_s1_fib = CSng(Math.Min((35 / (fcm_fib_CrSh / 145.0377)) ^ 0.1, 1))

   If RH >= 40 And RH < 99 * beta_s1_fib Then
   beta_RH_fib = CSng(-1.55 * (1 - (RH / 100) ^ 3))
   ElseIf RH >= 99 * beta_s1_fib Then
   beta_RH_fib = 0.25
   End If

   beta_ds_fib_begin(i) = CSng(Max((shrink_time_array(i - 1) / (0.035 * (h_fib_CrSh *
25.4) ^ 2 + shrink_time_array(i - 1))), 0) ^ 0.5)

   beta_ds_fib_end(i) = CSng(Max((shrink_time_array(i) / (0.035 * (h_fib_CrSh * 25.4) ^
2 + shrink_time_array(i))), 0) ^ 0.5)
'The units are converted to SI system. 1 in = 25.4mm, 1 psi = 1/145.0377 MPa

   beta_ds_fib_delta(i) = beta_ds_fib_end(i) - beta_ds_fib_begin(i)

'Step 3 : Total and incremental shrinkage strain
   For j = 1 To NumberCS

'NumberCS is a user-specified value defining number of cross sections for the analysis.

   Incremental_Unrestrained_Shrinkage_Strain_array(1, j, i) = epsilon_cas0_fib *
beta_as_fib_delta(i) + epsilon_cds0_fib * beta_RH_fib * beta_ds_fib_delta(i)

'First term represents the autogenous shrinkage and the second part represents the
drying shrinkage.

   Next j
Next i
```

Figure 3-12: Routine for *fib* MC 2010 Shrinkage Model—Steps 2&3

3.3.2.3 Sample Output for Creep and Shrinkage Prediction Models

The casting group L (VC) from the Hillabee Creek Bridge Project is analyzed to show the extent of the software's capability. The AASHTO LRFD, ACI 209, and MC 2010 creep and shrinkage models are graphed in Figure 3-12. Additionally, the autogenous and drying parts of *fib* MC 2010 are included in the figure.

The creep coefficients at transfer are zero owing to the fact that creep develops once the prestress transfer occurs. Growing trend of creep is consistent with the creep definition—the continuous time-dependent deformation under the sustained load.

The AASHTO LRFD and ACI 209 shrinkage models start to develop deformations when the concrete begins to dry. Similarly, the drying component of *fib* MC 2010 develops with the start of drying. Nonetheless, the autogenous part of *fib* MC 2010 grows once the concrete has reached setting. Casting group L (VC) started drying about 8 hours before the prestress transfer. This delay explains the reason why the shrinkage strain is not zero at prestress transfer. Moreover, *fib* MC 2010 has relatively higher total shrinkage strain at transfer due to the autogenous component.

MC 2010 estimates the largest creep and shrinkage amounts at the early ages. The predicted strain and camber with *fib* MC 2010 are found to be the largest for this time period as well because creep and shrinkage deformations govern the time-dependent behavior.

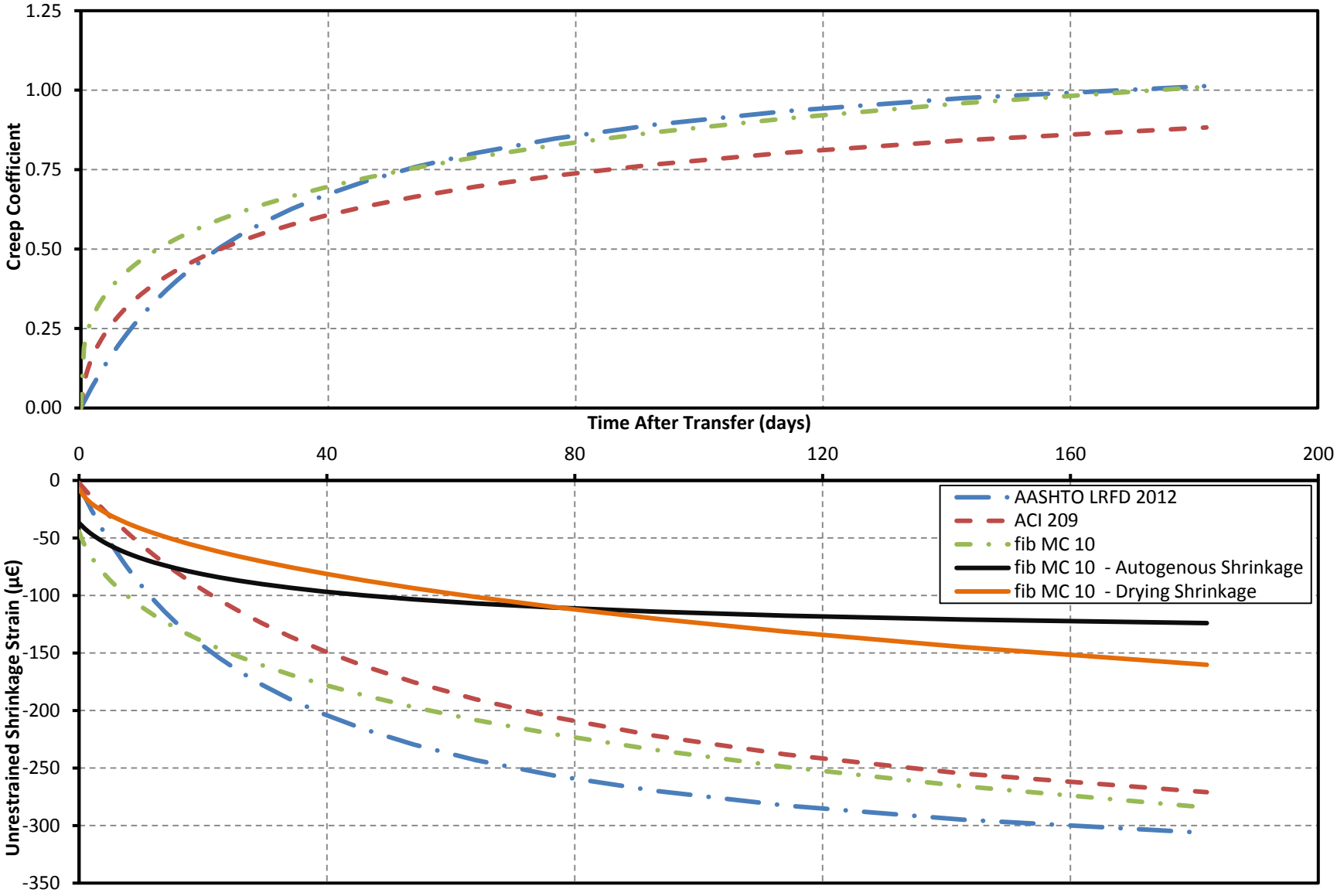

Figure 3-13: Sample Output for Creep and Shrinkage Models

3.3.3 Importing from and Exporting to a Spreadsheet File

The computer software is now able to import input values from a spreadsheet file and to export data to a spreadsheet. In the earlier versions, users were forced to enter input values one by one and to record output data by hand for each analysis. In addition, the software was not able to keep a record of the analysis.

Enabling the communication with a spreadsheet file has improved the performance of the software while minimizing the total analysis duration. The source code of the software is entirely rearranged to enable data transmission between the software and a Microsoft Excel (2010) spreadsheet file. The Excel file extensions, '*.xls' and '*.xlsx', are made use of, owing to the fact that they are widely used.

Exporting the input data gives the opportunity for verifying inputs and keeping a record of an analyzed project. Similarly, importing the input data allows users to analyze a girder repeatedly with different prediction models. Furthermore, exporting the output data enables users to have all of the calculated data saved as an Excel spreadsheet, which can later be used for plotting and comparison purposes. The feature of importing from and exporting to a spreadsheet file is explained in detail in Appendix J.

3.3.4 Miscellaneous Features

This subsection introduces several more features:

- Benchmark point for making the predicted strains compatible with the measured strains,
- Equivalent effective prestress,
- User-defined layers to obtain strain development,
- Definition of actual and design strengths
- Modification of predicted creep coefficient and shrinkage strain
- Project name, and
- Other uncategorized features.

The new features are provided to advance the capability of the software along with enhancing the user experience.

3.3.4.1 Benchmark Point

This feature is solely for researchers. Researchers use a reference data point for establishment of measured deformations. The related time is referred as benchmark point. Further, it is used to eliminate the developed shrinkage strain prior to a user-specified time point and to make the predicted strains compatible with the measured values. In the new version, a user is asked to pinpoint the benchmark point and later the shrinkage strain prior to the benchmark point is reported in the spreadsheet file.

Shrinkage development of a prestressed girder is partially illustrated in Figure 3-14. The AASHTO LRFD and ACI 209 models start to develop shrinkage strain following the ending of curing. The elements of the *fib* MC 2010 shrinkage model use distinct inception points.

Autogenous shrinkage starts to develop once the fresh concrete is cast; however, the drying portion of shrinkage starts to grow after the curing.

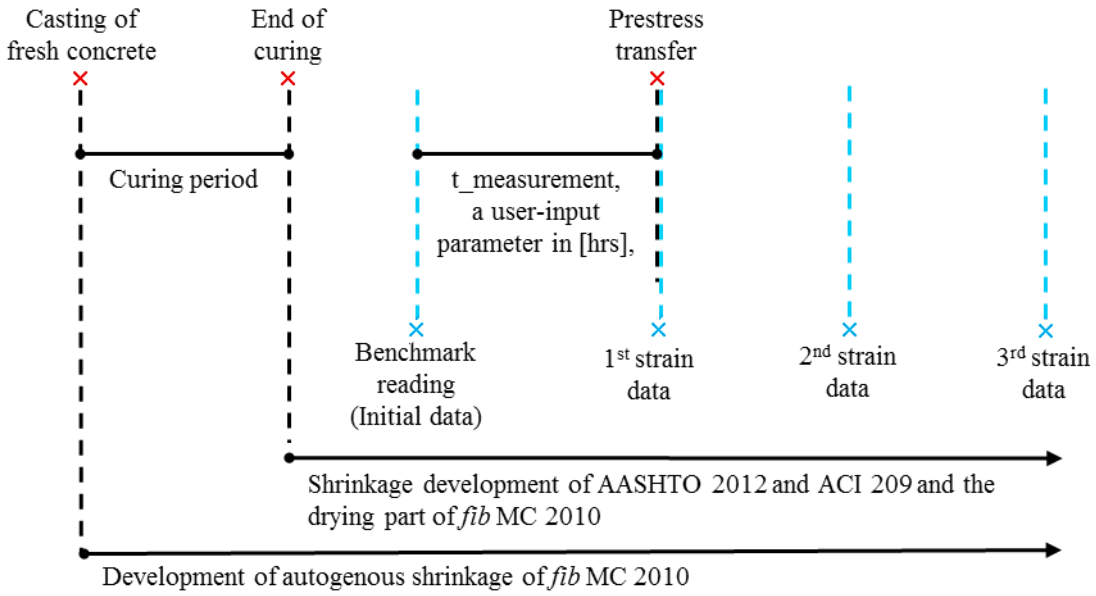

Figure 3-14: Illustration of the Benchmark Reading

The benchmark reading represents the initially recorded strain data. The first, second and third strain data are obtained by subtracting the benchmark value. For that reason, the computer software is programmed to account for the shrinkage strain prior to the benchmark point. Shrinkage is the major time-dependent loss at this time period.

Analyses of the girders in the Hillabee Creek Bridge Project and the AASHTO Type I Project indicate that the developed shrinkage at the benchmark point can be significant. This value is between -35 με and -60 με for *fib* MC 2010 model, and it reaches as much as -10 με for AASHTO LRFD and ACI 209 models.

3.3.4.2 Equivalent Effective Prestress Values

The equivalent effective prestress values are obtained for simplified reporting purposes. The goal is to report a value of effective prestress, $f_{pe,}$ that is responsible of all of the main

prestressing steel. The computer software uses the layer approach for defining the prestressing strand layout. A layer is a set of strand located at the same cross-sectional depth and a layer group is a subset of a layer having same characteristics such as debonded length or draping location (Schrantz 2012).

A user is allowed to define up to 30 prestressing steel layer groups, and stress values of each layer group are outputted individually. A routine is added to represent the individual layer groups as one equivalent steel layer. Figure 3-15 illustrates the terminology. Equations 3-34, 3-35, and 3-36 provide the functions used for this purpose.

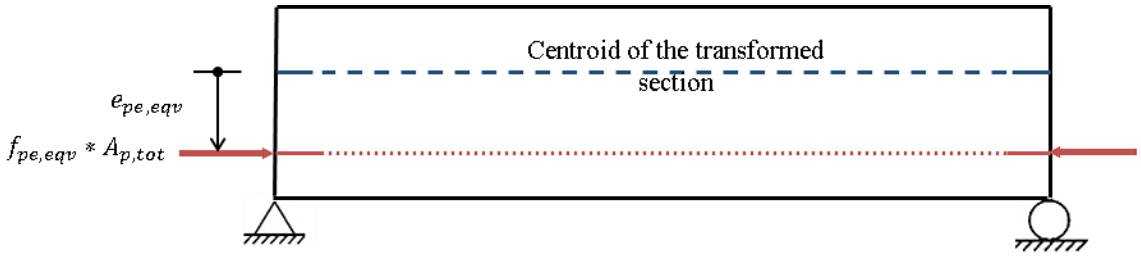

Figure 3-15: Equivalent Effective Prestress and Eccentricity

$$y_{pe,eqv} = \frac{\sum M_{pe,k}}{\sum F_{pe,k}} = \frac{\sum A_{p,k} f_{pe,k} y_{p,k}}{\sum A_{p,k} f_{pe,k}} \qquad \textit{Equation 3-34}$$

$$f_{pe,eqv} = \frac{\sum F_{pe,k}}{A_{p,tot}} = \frac{\sum A_{p,k} f_{pe,k}}{\sum A_{p,k}} \qquad \textit{Equation 3-35}$$

$$e_{pe,eqv} = y_{tr} - y_{pe,eqv} \qquad \textit{Equation 3-36}$$

where, $y_{pe,eqv}$ = distance to equivalent effective prestress layer from extreme bottom fiber at a cross section

$M_{pe,k}$ = moment due to effective prestress of a prestress layer

$F_{pe,k}$ = effective prestress force at a prestress layer

$A_{p,k}$ = total area of strands in a prestressing steel layer

$y_{p,k}$ = distance from each prestressing layer to the extreme bottom fiber

$f_{pe,k}$ = effective prestress amount in a layer

$f_{pe,eqv}$ = equivalent effective prestress amount at a cross section

$A_{p,tot}$ = total prestressing area in a cross section

y_{tr} = distance from centroid of the section to the extreme bottom fiber

$e_{pe,eqv}$ = eccentricity of the equivalent effective prestress layers

The equivalent effective prestress and eccentricity can be used to verify the internal time-step calculations and to compare them with other camber methods. Some of the existing methods are explained in Section 2.2.2. In the camber software, "fpe_avgmidpsan(i)" and "fpe_avgsupport(i)" are the reserved array names for the equivalent effective prestress at midspan and supports. "ep_avgmidpsan(i)"and "ep_avgsupport(i)" are the reserved array names for the eccentricity at midspan and supports.

Also, the prestressing steel layers with an effective prestress larger than 100 ksi are considered for the calculations in order to eliminate lightly stressed strands on the top flange.

3.3.4.3 User-Defined Layers to Obtain Strain Development

The earlier versions of the software were not able to provide output data allowing a direct comparison with the collected strain data. Strain values were available only at the predetermined girder locations such as individual steel layers and the top, bottom, and centroid of a girder. The new version brings the option to enter additional strain gage locations. In an exported output file, the midspan strain developments can be obtained. The array, "Total_estraingages_array(1, j, i, m)", keeps the values at all cross sections and it can be used for future research studies.

3.3.4.4 Definition of Design and Actual Strength Values

A user is asked to specify both actual and design concrete strengths in the new version. One of the reasons is to satisfy the compatibility among the existing models. To illustrate, *fib* MC 2010 uses an equation to offset the specified-design type of strength differently from the other models. Another reason is to prevent users from the confusion when they advance to the selection of a prediction model. For this purpose, both of the actual and design strengths are provided as an available option at later steps of inputting.

If the actual strength values are not available, specified design strength values can be inputted as the expected actual strength. If the expected overstrength factors are known for the specific project, the expected actual strength values can be obtained by inputting the overstrength factors as guided by the camber prediction software.

3.3.4.5 Modification of Predicted Creep Coefficient and Shrinkage Strain

In the new version, predicted creep coefficient and shrinkage strain can be adjusted separately with user-defined factors. The user-defined factors for creep and shrinkage are directly multiplied by the predicted creep coefficient and shrinkage strain. For *fib* Model Code 2010, the autogenous and drying shrinkage predictions can be multiplied by separate factors.

This feature allows a user to change the code-based factors (for example, the AASHTO LRFD shrinkage model suggests to increase predicted shrinkage strain with 20% if concrete is exposed to moist curing less than 5 days.). Also, a user can enter various factors and investigate the sensitivity of creep and shrinkage predictions on time-dependent responses such as strains, curvatures, and cambers. In this manner, creep and shrinkage can be modified based on known properties of local concrete mixtures. Figure K-22 shows a screenshot of this feature.

3.3.4.6 Project Name

Assigning a project name has been quite useful to keep track of the studied analysis. A project name is entered at the beginning of the analysis. If a user skips this, the computer's local time and date becomes the project name. Later on, the computer software uses the project name to label the exported spreadsheet files.

3.3.4.7 Other Improvements

In addition to these six features, other changes are also made. In the previous version, the output was limited to 40 cross sections and 40 time intervals. These limits are eliminated in the spreadsheet version. The minimum interval amount for them is kept the same as 1.

Another feature added is to allow users defining design and actual (if known) unit weight of plain concrete. The design value is used to calculate the moment due to the self-weight, and the actual self-weight may be used for the MOE prediction models. Therefore, a user is given an option to enter distinct unit weight only for the use of internal self-weight calculations.

3.4 Current Algorithm

In this section, the current algorithm is discussed. The time-related variables are clarified. Later, the input variables and schema are explained. The last section explains and maps the subroutines and the key output arrays. This section also aims at guiding researchers to add new features or to modify the existing camber software.

3.4.1 Time-Related Variables

Schrantz (2012), first developer of the software, derived a nonlinear time function to implement the time-step approach. She utilized the strength development function of the CEB 90 model. The same time-development model is used in *fib* MC 2010. Thus, the function from Schrantz's work is implemented with some modifications. It can be seen in Equation 3-37. The variables used in the time array are user-specified.

$$time\_array(i) = \begin{cases} 0.00, & i = 1 \\ MaxTime \times \left[1 - \frac{1}{0.2} \ln \left| \frac{i}{TimeIntervals} \right| \right]^{-2}, & i \geq 2 \end{cases} \qquad \textbf{Eqn. 3-37}$$

where, $MaxTime$ = total analysis length after prestress transfer in [days]

$TimeIntervals$ = number of time intervals to be used in the analysis

Initial value of 'time_array' is forced to be equal to zero in the new version for the data comparison reasons. Neither the created time functions nor the output data were initially aligned to the exact prestress transfer time in the previous versions. Table 3-2 describes the deviation of the initial time points from the prestress transfer time.

Table 3-2: Comparison of Initial Time Values

TimeIntervals	MaxTime (days)	time_array(1) (days) (old)	time_array(1) (days) (new)
40	120	0.32	0.00
	180	0.48	0.00
	240	0.63	0.00
	300	0.79	0.00
	360	0.95	0.00

Table 3-3 demonstrates how the time-related arrays are defined and when they are used. In Figure 3-16, time-related variable and array names are shown. The straight lines represent the chronological age. The curved lines show the concrete age including the maturity at transfer. The variables are user-input parameters; whereas, the arrays are used in the routines.

Table 3-3: Time Array Functions Used in the Software

time_array( )	Equation 3-37
Used when calculating	the time-development trends not covered below
age_array( )	=time_array( ) + AdjustedAge
Used when calculating	the strength development of AASHTO LRFD 2014, ACI 209, and *fib* MC 2010
	the MOE development of AASHTO LRFD 2014, ACI 209, *fib* MC 2010, and two-point models
	autogenous shrinkage part of *fib* MC 2010
jack_time_array( )	=time_array( ) + TransferTime + JackingTime
Used when calculating	the prestress relaxation loss
shrink_time_array( )	=time_array( ) + TransferTime - (SteamPeriod or MoistPeriod)
Used when calculating	the shrinkage strain development of AASHTO LRFD, ACI 209
	the drying shrinkage part of *fib* MC 2010

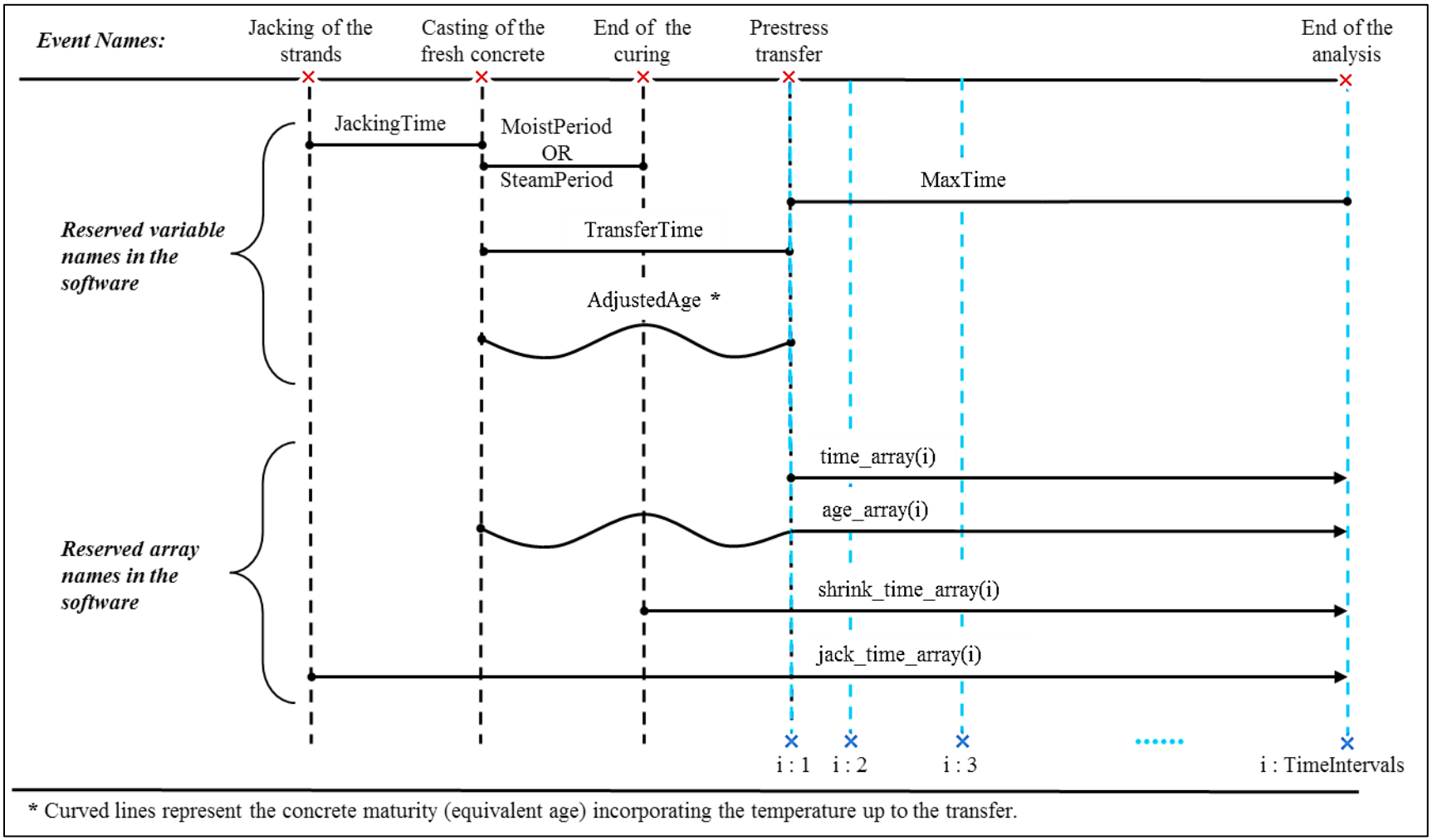

Figure 3-16: Reserved Time-Related Variable and Array Names

3.4.2 Input Variables and Schema

The new version of the software introduces two options for entering the variables. When the ‘wizard’ option is selected, a user is required to continue with thirteen different user-guided forms. A user can find the explanations for each input value. Second option is the ‘importing a spreadsheet’. For this purpose, a user needs to prepare an Excel spreadsheet, and the variables have to occupy the certain cells. An input template can be produced after using the “wizard” option. Similarly, a formatted template is included in Figure J-5 in Appendix J. Both of the choices are demonstrated in Figures 3-17 and 3-18.

All of the required variables and their explanations can also be seen in the figures. Some of the properties can be defined more than one way. For example, expected actual concrete strength values can be entered by hand or computed using the expected overstrength factors. Also, the required variables for the MOE development depend on the selected model. Likewise, each creep and shrinkage model requires separate input. These variations are represented with capital letters following the numbers.

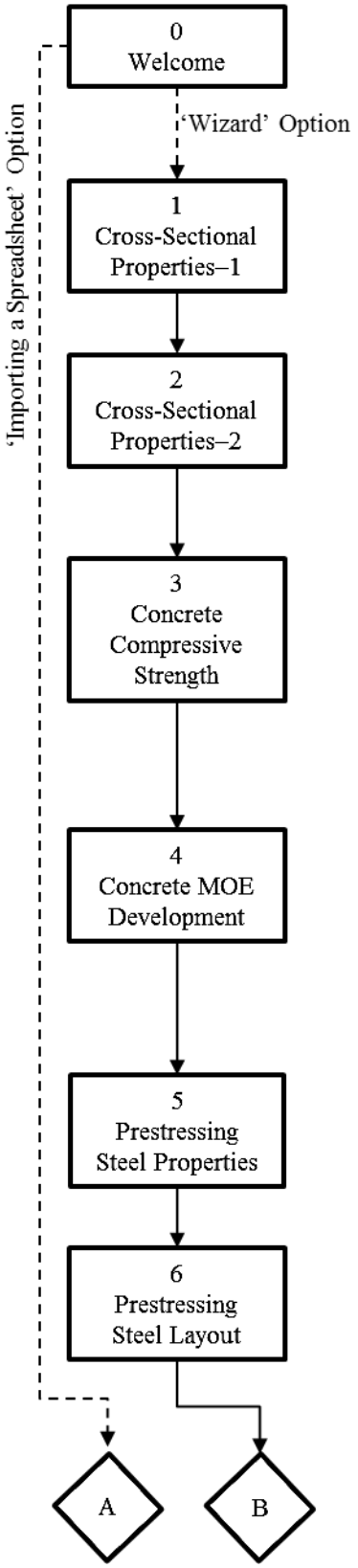

User-Input Variables	*Explanation*
N/A	Select the way to make input: 'Wizard' or 'Importing a Spreadsheet'
(1) ProjectName **(2)** Cross-Section Type	**(1)** Name of the project that will be presented in the output. **(2)** Choose user-defined or one of the standard cross section
(1) Ag **(2)** Ig **(3)** yb **(4)** h **(5)** L	**(1)** Gross cross-sectional area in [in.^{2}] **(2)** Gross moment of inertia in [in.^{4}] **(3)** Centroid of the concrete only section (from bottom) in [in.] **(4)** Depth of the girder in [in.] **(5)** Length of the girder in [in.]
(1) fci **(2)** fc28 **(3)** wc **(4A)** OSi, OS28 **(4B)** fci_actual, fci28_actual, wc_actual	**(1)** & **(2)** Specified comp. strength at initial prestress and at 28 days in [psi] **(3)** Unit weight of plain concrete in [pcf] (used for dead load calculations) **(4A)** Expected overstrength factors **(4B)** Expected actual values.
(1A) Eci_supp, Ec28_supp **(1B)** StrengthType, CementTypeACI, CuringType, K1_MOE_AA **(1C)** StrengthType, K1_MOE_AA **(1D)** StrengthType, AggregateTypefib, CementTypefib **(1E)** StrengthType, AggregateType	**(1A)** Stiffness-based model: MOE of concrete girder at initial p.s. transfer and 28 days in [ksi] StrengthType: Define whether to use specified or actual strength. **(1B)** ACI 209 : K1_MOE_AA is 1.00 for ACI 209 model. **(1C)** ACI 209 backcalculate **(1D)** *fib* MC 2010 **(1E)** *fib* MC 2010 backcalculate
(1) Ep **(2)** fpu **(3)** fpy	**(1)** MOE of prestressing steel in [ksi] **(2)** Ultimate strength of prestressing steel in [ksi] **(3)** Yield strength of p.s.in [ksi]
(1) np1, np2 , … np30 **(2)** Ap1, Ap2, … Ap30 **(3)** yp1_mid, … yp30_mid **(4)** fpj_1, fpj_2, … fpj_30 **(5)** DL1, DL2, … DL30 **(6)** GT1, GT2, … GT30 **(7)** ST1, ST2, … ST30	**(1)** Number of strands in a layer group **(2)** Cr.-sec. area of a strand in [in.^{2}] **(3)** Distance to centroid of a ps. layer (from bottom) at the midspan in [in.] **(4)** Jacking stress in [ksi] **(5)** Layer group detail length in [in.] **(6)** Type of p.s. layout **(7)** Type of strands

Note: The capital letters adjacent to the numbers represent the available choices and one of the letters must be selected to advance.

Figure 3-17: Input Schema—Steps 1–6

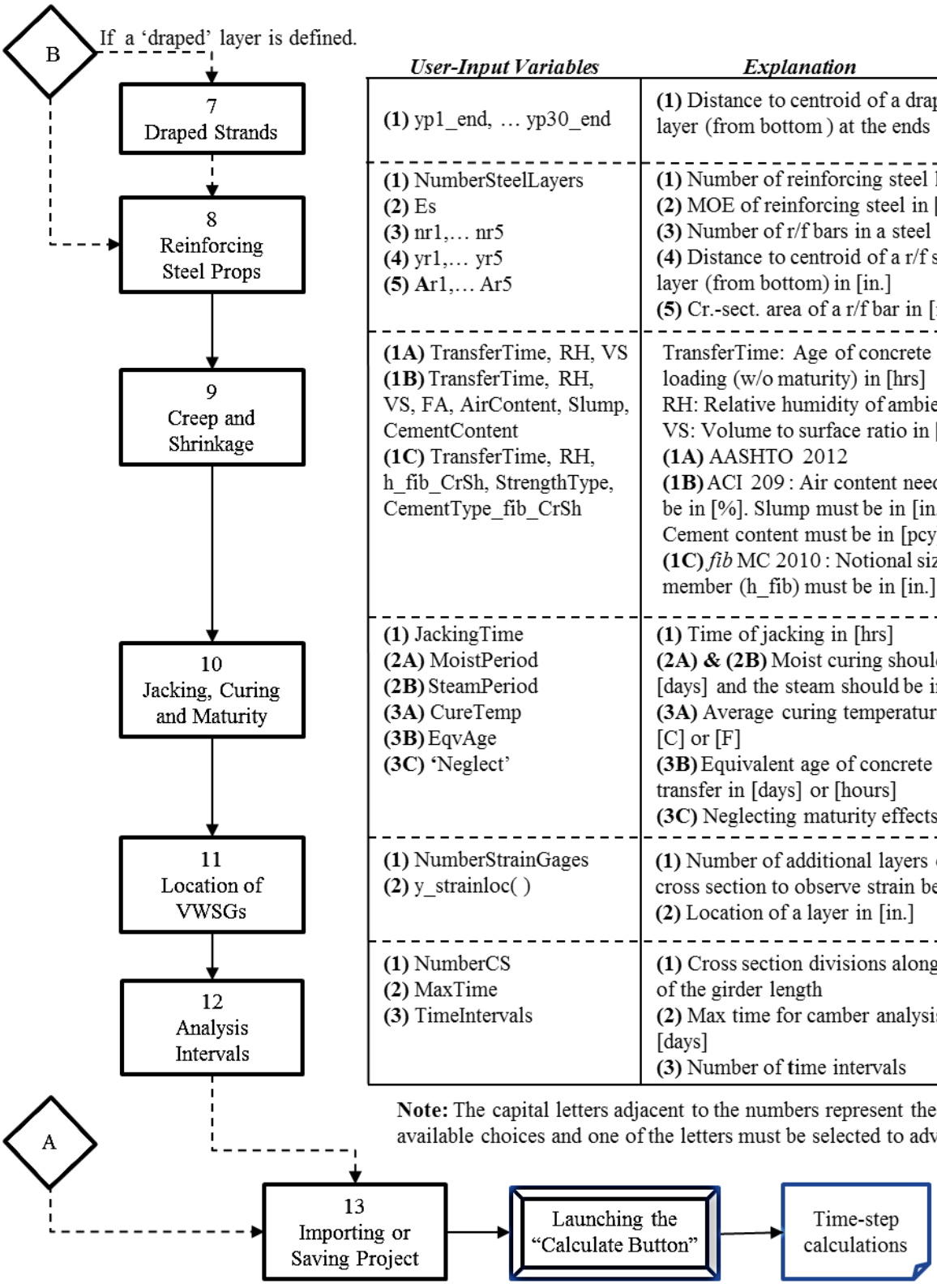

User-Input Variables	*Explanation*
(1) yp1_end, … yp30_end	**(1)** Distance to centroid of a draped. layer (from bottom) at the ends in [in.]
(1) NumberSteelLayers **(2)** Es **(3)** nr1,… nr5 **(4)** yr1,… yr5 **(5)** **A**r1,… Ar5	**(1)** Number of reinforcing steel layers **(2)** MOE of reinforcing steel in [ksi] **(3)** Number of r/f bars in a steel layer **(4)** Distance to centroid of a r/f steel layer (from bottom) in [in.] **(5)** Cr.-sect. area of a r/f bar in [in.^{2}]
(1A) TransferTime, RH, VS **(1B)** TransferTime, RH, VS, FA, AirContent, Slump, CementContent **(1C)** TransferTime, RH, h_fib_CrSh, StrengthType, CementType_fib_CrSh	TransferTime: Age of concrete at loading (w/o maturity) in [hrs] RH: Relative humidity of ambient [%] VS: Volume to surface ratio in [in.] **(1A)** AASHTO 2012 **(1B)** ACI 209 : Air content needs to be in [%]. Slump must be in [in.]. Cement content must be in [pcy]. **(1C)** *fib* MC 2010 : Notional size of member (h_fib) must be in [in.].
(1) JackingTime **(2A)** MoistPeriod **(2B)** SteamPeriod **(3A)** CureTemp **(3B)** EqvAge **(3C)** 'Neglect'	**(1)** Time of jacking in [hrs] **(2A) & (2B)** Moist curing should be in [days] and the steam should be in [hrs] **(3A)** Average curing temperature in [C] or [F] **(3B)** Equivalent age of concrete at transfer in [days] or [hours] **(3C)** Neglecting maturity effects
(1) NumberStrainGages **(2)** y_strainloc( )	**(1)** Number of additional layers on a cross section to observe strain behavior **(2)** Location of a layer in [in.]
(1) NumberCS **(2)** MaxTime **(3)** TimeIntervals	**(1)** Cross section divisions along half of the girder length **(2)** Max time for camber analysis in [days] **(3)** Number of time intervals

Note: The capital letters adjacent to the numbers represent the available choices and one of the letters must be selected to advance.

Figure 3-18: Input Schema—Steps 7–13

The new version offers eight MOE development models and five creep and shrinkage models (if the variations such as light-weight concrete and backcalculated versions are considered separately). This research study investigates the MOE development model based on measured MOE: Two-Point MOE Model. Four strength-based MOE development models are included of future studies: ACI 209 Normal, ACI 209 Backcalculate, *fib* MC 2010 Normal-Weight and *fib* MC 2010 Backcalculate. The creep and shrinkage models used in this research are AASHTO LRFD 2014, ACI 209, and *fib* MC 2010 Normal-Weight. Figure 3-18 shows the user-guided form for the MOE development models. All of the user-guided forms can be found in Appendix K.

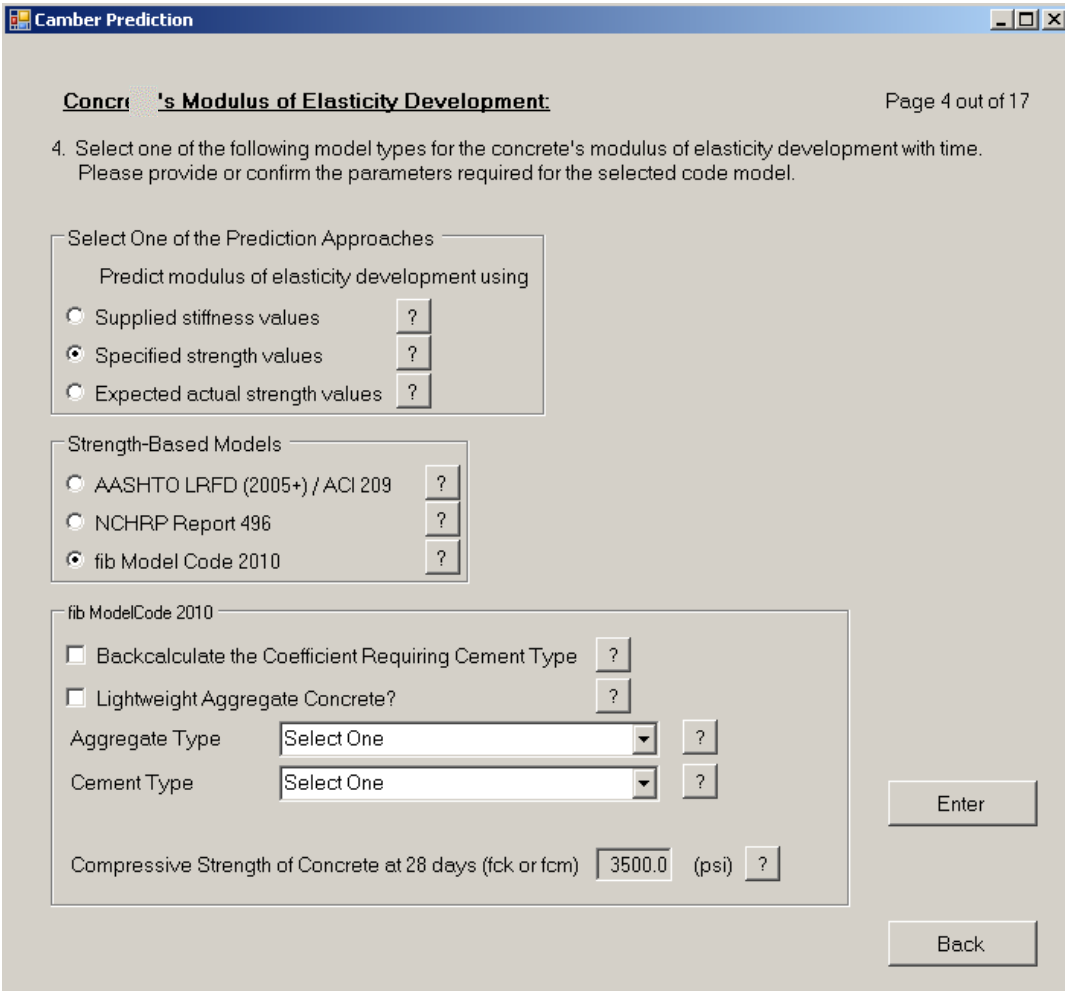

Figure 3-19: User-Guided Input Form for MOE Development Models

3.4.3 Subroutines and Output Data

In this chapter, created subroutines are introduced. Calling a subroutine runs the code held within it and reveals various looped arrays at the end. Subroutines are used to divide the lengthy routines into manageable parts. The sequence of the subroutines is important due to the tied relationships.

The arrays are generated by the loops represented with the indices i, j, k, or m. The letter i represents the loop for the time interval; the letter j is for the cross section. The letter k is for each prestressing or reinforcing steel layer; the letter m indicates a loop for user-input strain gage locations. A user can input up to thirty prestressed steel layers, five reinforcing steel layers, and six midspan strain gage layers. The illustration in Figure 3-20 explains the idea of the indices j, k and m. The index i is explained in Section 3.4.1.

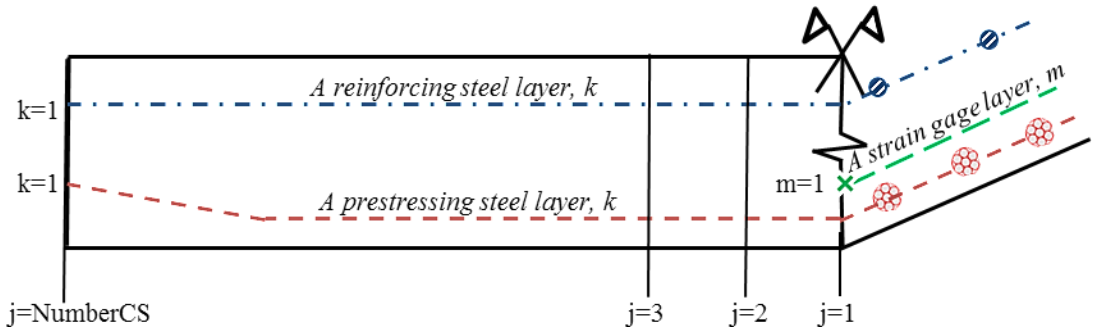

Figure 3-20: Illustration of the Indices j, k, and m

The indices determine the size and dimension of the arrays. For instance, "Total_fbottom_array(1,j,i)" is a 3D array with a size of [1+1]×[j+1]×[i+1]. Ones are added since the first element of the VB arrays is indexed by subscript of zero. For this array, initial dimension with a size of [1+1] is not actively used, but it is kept the same way with the earlier versions for the compatibility. This array loops through every cross section j and every time interval i.

The subroutines and the important output variables are demonstrated in Figures 3-21 and 3-22. Output variables are demonstrated in order to explain the available output data and to help debugging the software. They can be used to modify the exported data for the future studies. Methods to modify them are explained in Section J.3.3 in Appendix J. The logic of the time-dependent deformations is explained in Section 3.2.1.

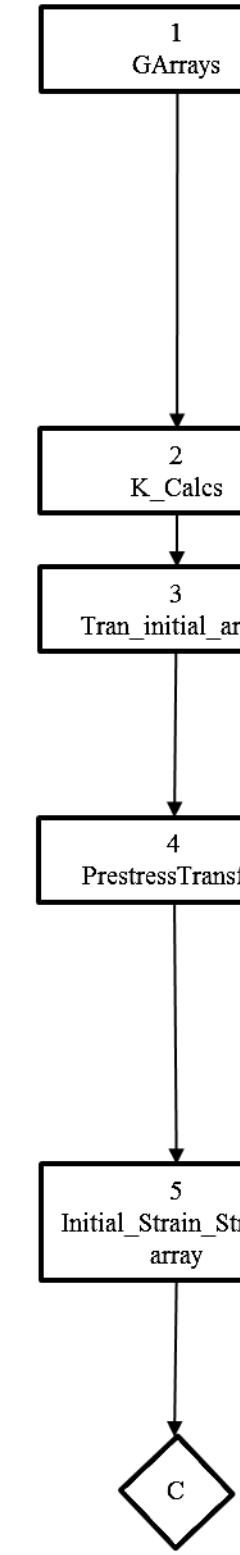

Created Subroutines	*Key Output Variables*	*Explanation*
1 GArrays	**(1)** yp_array(k, j) **(2)** Mg_array(1, j) **(3)** time_array(i) **(4)** age_array(i) **(5)** jack_time_array(i) **(6)** shrink_time_array(i) **(7)** Ec_initial, Ec28 **(8)** fconcrete_array(i) **(9)** Econ_array(i) **(10)** Acon_array(1,j,i)	**(1)** Distance from each prestressing steel layer to the extreme bottom fiber at each cross-section in [in.] **(2)** Moment due to self-weight in [kft] **(3) & (4) & (5) & (6)** Nonlinear time arrays in [days] **(7)** MOE at initial p.s. transfer and at 28 days in [ksi]. Initial value is used to calculate the initial strain and camber. The 28-day value is only reported. **(8)** Comp. strength development in [psi] **(9)** MOE development in [ksi] **(10)** Net concrete area without steel layers in [in.^{2}]
2 K_Calcs	The coefficients required for creep and shrinkage calculations are made as stated in ACI 209 and AASHTO 2012.	
3 Tran_initial_array	**(1)** Atr_initial_array(1, j) **(2)** ytr_initial_array(1, j) **(3)** Itr_initial_array(1, j)	**(1) & (2) & (3)** User-supplied values are used to calculate the initial transformed properties at each cross section j. **(1)** Cross-sectional area in [in.^{2}] **(2)** Distance from centroid of the section to the extreme bottom fiber [in.] **(3)** Moment of inertia in [in.^{4}]
4 PrestressTransfer	**(1)** fpbt_array(k, j) **(2)** delta_ecen_initial_array(1, j) **(3)** delta_phi_initial_array(1, j) **(4)** fpt_array(k, j)	**(1) & (2) & (3) & (4)** The arrays are created for each cross section j and they do not include any shrinkage losses. **(1)** Stress in each prestressing steel layer (k) immediately before the transfer in [ksi] **(2)** Initial strain at the centroid immediately before the prestress transfer **(3)** Initial curvature immediately before the transfer in [1/in.] **(4)** Stress in each prestressing steel layer k immediately after the transfer in [ksi]
5 Initial_Strain_Stress_ array	**(1)** initial_fc_array(1, j) **(2)** initial_fc_array(2, j) **(3)** initial_fcen_array(1, j)	**(1) & (2) & (3)** The arrays are used to calculate initial concrete stresses just after the transfer for each cross section j. They are the starting points of the time-step approach. They include p.s. steel relaxation up to the transfer and elastic shortening. **(1)** At the extreme bottom fiber in [ksi] **(2)** At the extreme top fiber in [ksi] **(3)** At the centroid of the trans. sect. in [ksi]

Note: The value(s) in the parenthesis represents the loop(s) that the array goes through. Max 'i' is 'TimeIntervals', max 'j' is 'NumberCS', and max 'k' is 'NumberLayerGroups' or 'NumberSteelLayers'. The array dimensions and sizes depend on the employed variables.

Figure 3-21: Sequence of Subroutines and Key Output Variables—Part 1

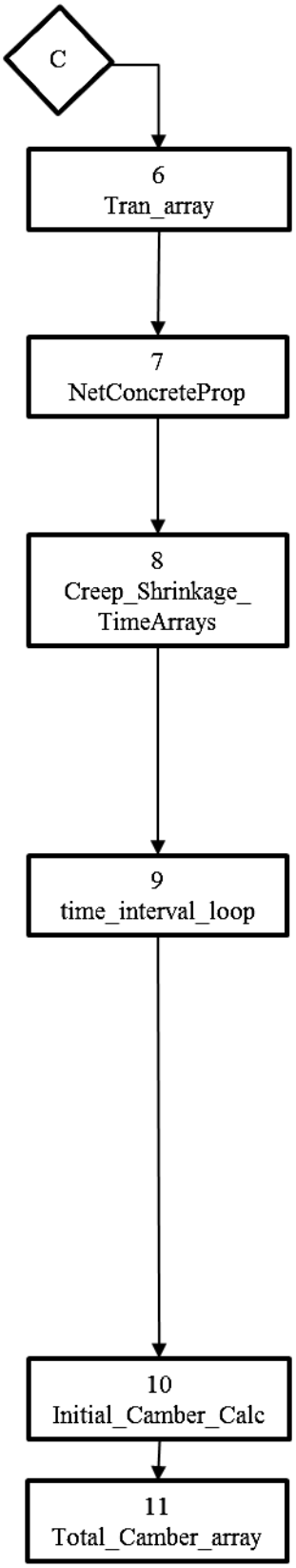

Key Output Variables	*Explanation*
(1) Atr_array(1, j,i) **(2)** ytr_array(1, j,i) **(3)** Itr_array(1, j,i)	**(1) & (2) & (3)** Time development of the cross-sectional properties is obtained at each cross section j and at each time interval i. It is a function of the concrete MOE development. **(1)** Cross-sectional area in [in.^{2}] **(2)** Distance from centroid of the section to the extreme bottom fiber in [in.] **(3)** Moment of inertia in [in.^{4}]
(1) yc_net_initial_array(1,j) **(2)** yc_net_array(1,j,i)	**(1) & (2)** Distance from centroid of the net concrete section to the extreme bottom fiber at each cross-section in [in.] **(1)** At prestress transfer **(2)** At each time interval (i)
Similar array names are used for the different creep and shrinkage models. **(1)** Ultimate_Creep_Coefficient **(2)** Incremental_Creep_Coefficient_array(i) **(3)** Incremental_Unrestrained_Shrinkage_Strain_array(1, j, i) **(2) & (3)** Creep coefficients are determined at each time interval; in contrast, shrinkage strains are calculated for each cross section at each time interval. **(4)** Ultimate_Shrinkage_Strain **(5)** Strain_t_measurement Developed shrinkage strain up to a user-defined benchmark point.	
The arrays below are in a time-loop represented by 'i'. The arrays with the letters 'j', 'k', or 'm' are further executed for each cross section, each steel layer, or each user-defined strain location, respectively. Curvatures are in [1/in.], stress values are in [ksi], and distances are in [in.]. **(1)** Incremental_Relaxation_array(k, j, i): Prestress relaxation losses **(2)** Incremental_Unrestrained_Creep_Strain_array(1, j, i) **(3)** Incremental_Unrestrained_Creep_Curvature_array(1, j, i) **(4)** Incremental_Curvature_array(1, j, i) , Total_Curvature_array(1, j, i) **(5)** Incremental_Strain_Centroid_array(1, j, i) , Total_ecen_array(1, j, i) **(6)** Total_ebottom_array(1, j, i), Total_etop_array(1, j, i): Strains at bot. and top **(7)** Total_estraingages_array(1, j, i, m): Strains at additional layers **(8)** Total_fcen_array(1, j, i): Concrete stress at centroid of the trans. section **(9)** Total_fbottom_array(1, j, i), Total_ftop_array(1, j, i): Concrete stresses **(10)** Total_fr_array(k, j, i), Total_fp_array(k, j, i): R/f and p.s. steel stresses **(11)** ep_avgmidpsan(i), ep_avgsupport(i): Equivalent eccentricity of ps. layers **(12)** fpe_avgmidpsan(i), fpe_avgsupport(i): Equivalent effective prestress	
(1) Initial_Camber_Calculation	**(1)** Initial camber value at midspan just after p.s. transfer in [in.]. It does not include any shrinkage or creep losses.
(1) Total_Camber_Calc(i)	**(1)** Camber development—utilizing p.s. steel relaxation, elastic shortening of conc., creep and shrinkage losses—at midspan in [in.]

Figure 3-22: Sequence of Subroutines and Key Output Variables—Part 2

Chapter 4 Experimental Methods

4.1 Introduction

Four research projects including a total of fifty-one girders are investigated for the time-dependent deformations. The data are obtained from the four prestressed girder research studies: the Hillabee Creek Bridge Project, the AASHTO Type I Project, the Alabama HPC Project, and the T-Beam Project—they are referenced as Projects 1, 2, 3, and 4, respectively. Temperature corrections for internal strain and camber are discussed. Then, selected input variables for the use of the predictions are also presented. This part of the study is used to gather data to run the camber prediction software to predict time-dependent responses such as bottom-flange strain, midspan curvature, and midspan camber.

4.2 Data Gathering

4.2.1 Project 1: The Hillabee Creek Bridge Project

4.2.1.1 Overview

The purpose of the Hillabee Creek Bridge Project was to compare the performance of precast prestressed bridge girders cast with vibrated concrete (VC) and self-consolidated concrete (SCC) mixtures. The girders studied in this research were designed and fabricated for an actual bridge constructed on State Route 22 over Hillabee Creek in Tallapoosa County, Alabama. The fabrication of these girders was completed in the fall of 2010 at Hanson Pipe and Precast in Pelham, Alabama. Johnson (2012) detailed the experimental method to obtain strain and camber readings up to the erection of the bridge girders.

Half of the specimens were cast with self-consolidated concrete (SCC), and other half were cast with vibrated concrete (VC). All twenty-eight bulb-tee girders in this project were produced with a 15-degree skew enabling the proper alignment of the bridge.

The identification of the specimens was made as shown in Figure 4-1. Concrete type CVC is mentioned as the vibrated concrete (VC) in this research. Specimen design, material properties, strain measurement and camber measurement are explained by summarizing Johnson's thesis (2012).

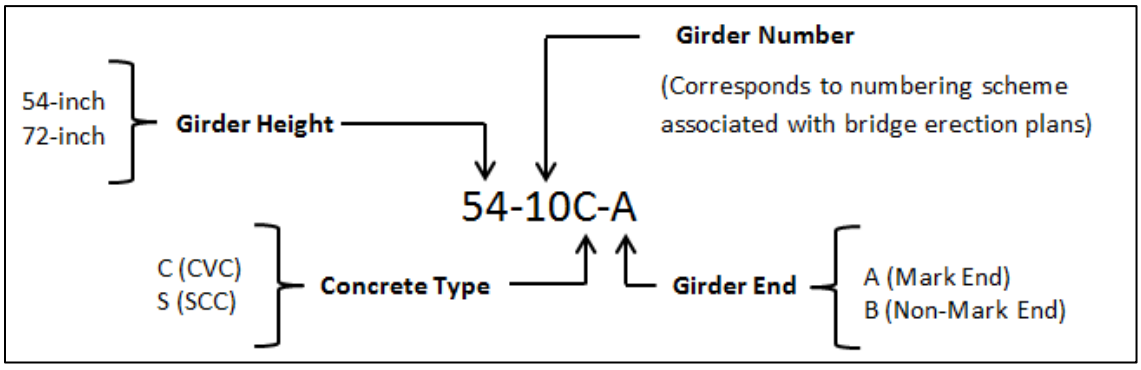

Figure 4-1: Hillabee Creek Bridge - Girder Identification Scheme (Dunham 2011)

4.2.1.2 Specimen Design

The BT-54 girders are 97 ft. 10 in. long and the BT-72 girders are 134 ft. 2 in. long. Figure B-1 in Appendix B shows the cross-sectional dimensions of the BT-54 and BT-72 sections.

The BT-54 girders are designed with seven-wire, Grade 270, low-relaxation, ½-inch diameter strands with a jacking stress (f_{pj}) of 202.5 ksi. The same strand arrangement is used for all of the BT-54 girders. The BT-72 girders were designed with seven-wire, Grade 270, low-relaxation, ½-inch "special(oversize)" diameter strands with a jacking stress of 202.5 ksi. All of the BT-72 girders have the same strand arrangement. Further, BT-54 and BT-72 girders have a two-point draping configuration. In order to debond some strands, they were encased in plastic casing and sealed with tape. In addition to the fully prestressed strands, BT-54 and BT-72 girders have seven-wire, Grade 270, low relaxation, ½-inch diameter strands with a jacking stress of 32.7 ksi in the top flange. Figure B-2 in Appendix B shows the strand profile for the BT-54 and BT-72 girders. Figure B-3 shows the steel arrangement for the BT-54 girders at midspan and girder ends. Figure B-4 illustrates the steel arrangement for the BT-72 girders.

Stirrups, bottom steel confinement bars (D-bars), straight bars (S-bars), and V-bars were the four bar shapes used for the BT-54 and BT-72 girders. Figure B-5 depicts the mild steel configuration for the BT-54 and BT-72 girders.

4.2.1.3 Material Properties

Mixture designs used for VC and SCC concrete can be seen in Table 4-1. Type III portland cement and slag cement were used for the both concrete mixtures. As a coarse aggregate, #67 limestone was used for the VC mixture; whereas, #78 limestone was used for the SCC mixture. Moreover, the SCC mixture had higher sand-to-total aggregate ratio than VC

mixture. The type and amount of admixtures were also different. An air-entraining admixture (Darex AEA EH), a high-range water-reducing admixture (ADVA Cast 575), a viscosity-modifying admixture (V-Mar 3), and a hydration-stabilizing mixture (Recover) were used as chemical admixtures.

Table 4-1: Project 1—Summary of Concrete Mixture (Johnson 2012)

Item	BT-54		BT-72	
	SCC	CVC	SCC	CVC
Water Content (pcy)	266	238	265	234
Cement Content (pcy)	758	696	760	708
GGBF Slag Content (pcy)	134	124	135	125
w/cm	0.30	0.29	0.30	0.28
SSD Coarse Agg. #78 (pcy)	1528	0	1550	0
SSD Coarse Agg. #67 (pcy)	0	1923	0	1950
SSD Fine Agg. (pcy)	1384	1163	1370	1179
s/agg (by weight)	0.48	0.38	0.47	0.38
Air-Entraining Admixture (oz/cy)	0.3	0.3	0.2	0.2
HRWR Admixture (oz/cy)	11	8	11	7
Viscosity-Modifying Admixture (oz/cy)	2	0	4	0
Hydration-Stabilizing Admixture (oz/cy)	2	1	2	1
Total Air Content (%)*	4.1	4.2	4	3.2

*Average of air content was determined from fresh concrete test results.

Table B-1 in Appendix B reveals the fresh concrete properties tested by the Auburn University researchers. 6-inch by 12-inch concrete cylinders were molded and accelerated cured under the curing tarp with the girders. They were tested in conformity with ASTM C 39 (2005) and ASTM C 469 (2002) in order to determine the concrete strength and the modulus of elasticity, respectively. The hardened concrete properties are given in Table 4-2.

For BT-54s, the half-inch diameter strands—with an area of 0.153 in.^{2}—were provided by Strand-Tech Martin, Inc. from Summerville, South Carolina. The half-inch "special" strands—with an area of 0.167 in.^{2}—used for the BT-72 girders, were provided by American Spring Wire from Houston, Texas. Modulus of elasticity (MOE) of the prestressing tendons was

28,600 ksi. Grade 60 rebar was in conformity with ASTM A615 and used as a non-prestressed reinforcing steel. MOE of the reinforcing steel was 29,000 ksi.

Table 4-2: Project 1—Hardened Concrete Properties (Johnson 2012)

	Release			28 Days	
Casting Group	**Age (hrs)**	**f'_{ci} (psi)**	**E_{ci} (ksi)**	**$f'_{c,28}$ (psi)**	**$E_{c,28}$ (ksi)**
A (SCC)	24	9010	6200	10240	6400
B (CVC)	23	8790	7100	10590	7400
C (SCC)	24	8680	6300	10800	6600
D (CVC)	24	7860	6700	9670	6900
E (SCC)	24	7940	6100	10180	6200
E (CVC)	25	8760	6400	10360	6800
Specified BT-54	-	5200	-	6000	-
F (SCC)	24	8120	5800	10490	6300
G (CVC)	23	8290	6700	10770	7000
H (SCC)	19	7860	5900	10770	6400
I (CVC)	22	8770	7100	10850	7300
J (SCC)	22	8220	5800	10550	6400
K (CVC)	20	8320	6800	11050	7700
L (SCC)	19	6930	5700	10070	6000
L (CVC)	20	7710	6600	10510	6900
Specified BT-72	-	5800	-	8000	-

4.2.1.4 Strain Measurement

Before concrete was cast, the vibrating-wire strain gauges (VWSGs) were installed within the girder sections for the purpose of obtaining internal strain and temperature trends. The Geokon, Inc. VCE-4200 VWSGs were used, and the gauge drawing is included in Figure B-6 in Appendix B. In addition to the recorded strains, the embedded thermistor measures the temperature data, which are used for temperature corrections later. Figure B-7 demonstrates the plan of instrumented VWSGs. An illustration of the installed gauge in the bottom flange can be seen in Figure 4-2.

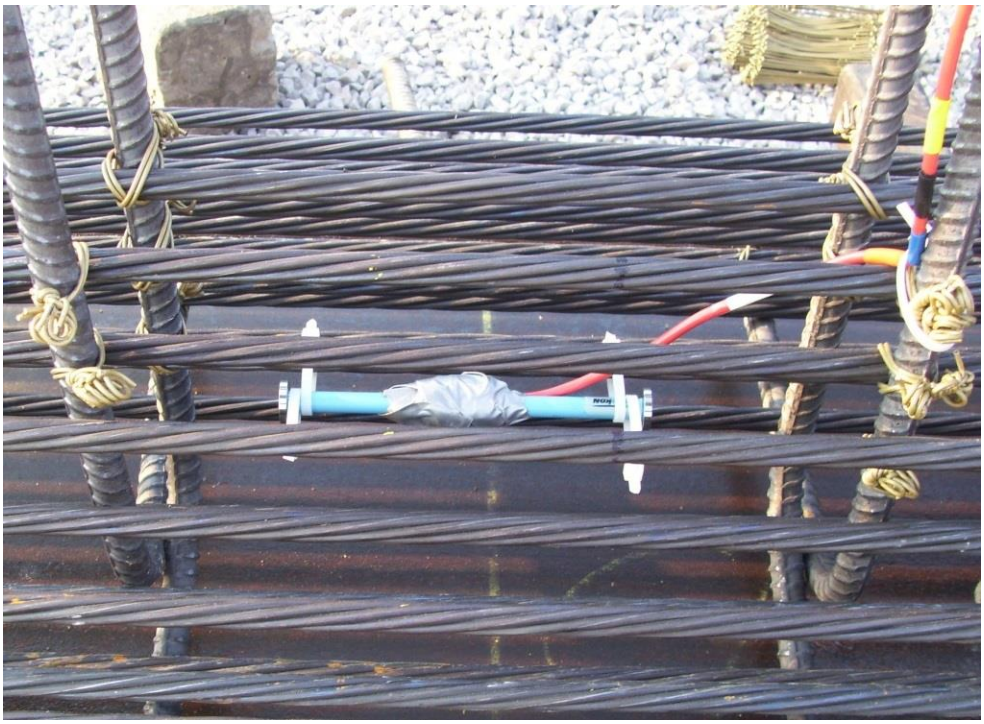

Figure 4-2: Gage Located in the Bottom Flange (Johnson 2012)

Figure 4-3 gives the configuration of the Data Acquisition System (DAS) used in this research. DAS was designed to be a stand-alone system and composed of two multiplexers, a battery system, and a CR1000 datalogger. The collected strain data for all of the girders are summarized in Table 4-3 and 4-4.

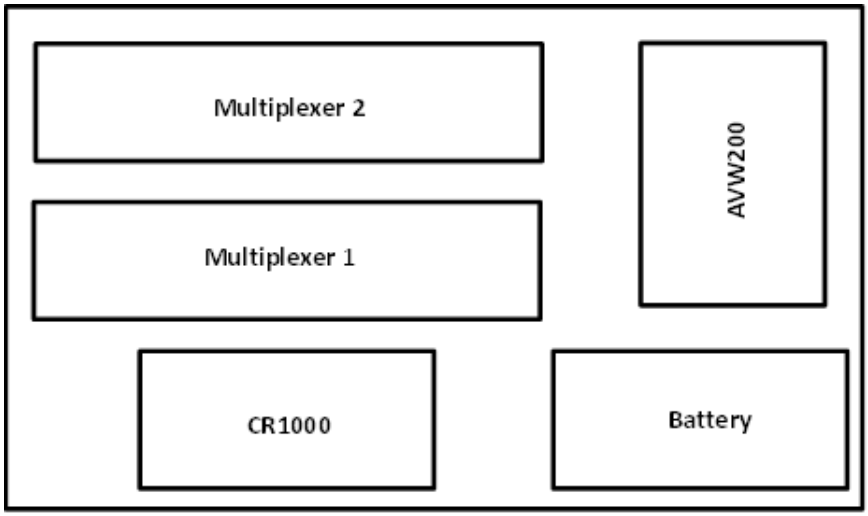

Figure 4-3: Configuration of the VWSG Data Acquisition System (Johnson 2012)

4.2.1.5 Camber Measurement

Surveying and a tensioned-wire system were the two methods used in this research project to record camber. The tensioned-wired system was used for one girder in each casting group with an exception. Both of the girders in the casting group E, 54-7S and 54-8C, were measured with the tension-wired system. The rest of the recordings were completed with the surveying method. For the surveying method, readings were taken at 9 inches from each end, midspan, and $1/6^{th}$ and $5/6^{th}$ of span locations. For the tensioned-wire system, the value on the ruler was recorded to the nearest 0.01 in. while the cylindrical 30-pound weight was tensioning the steel wire as depicted in Figure 4-4. Camber readings were made immediately after sunrise in order to prevent the deflections due to daily temperature gradient. The length of the data availability was included in Table 4-3 and 4-4.

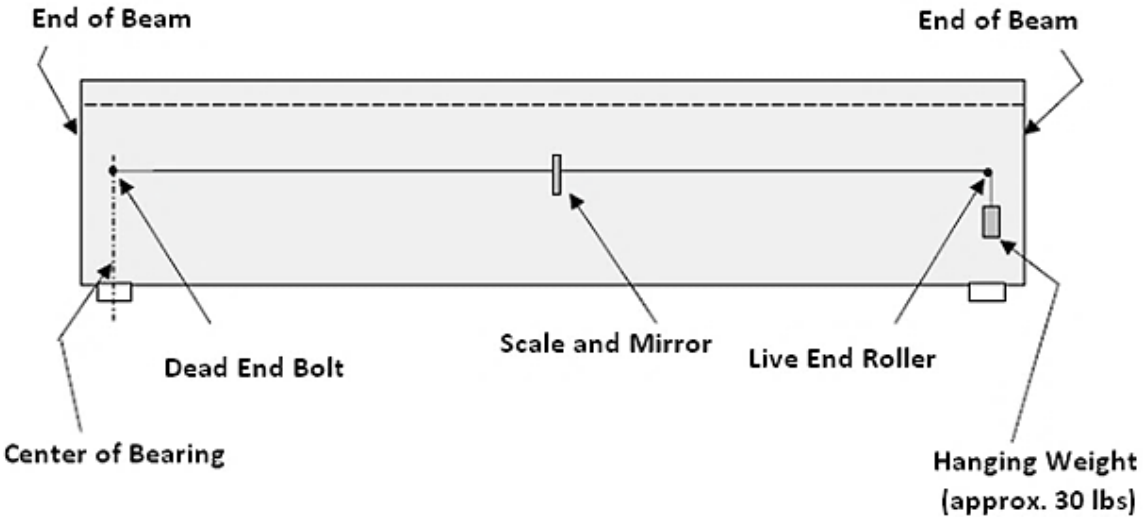

Figure 4-4: Schema of the Tensioned-Wire System (Johnson 2012)

Table 4-3: Project 1 (BT-54)—Summary of Collected Data

Project Name	Girder Type	Casting Group	MOE [1] (ksi) at		Maturity Calc.? [2]	Temp Corr.? [3]	Girder Name	Length of Meas. (day)		VWSG Locations (in) [4]			
			Transfer	28-day				Camber	Strain	#1	#2	#3	#4
Hillabee Creek Bridge (Girders were stored outdoors)	**BT-54**	A (SCC) [5]	6200	6400	Y (Using 54-5S)	Y	54-2S	219	219	6.0	N/A	N/A	N/A
							54-5S	219	219	6.0	19.5	37.5	52.0
							54-6S	219	219	6.0	19.5	37.5	52.0
		B (VC) [5]	7100	7400	Y (Using 54-9C)	Y	54-9C	217	217	6.0	19.5	37.5	52.0
							54-10C	217	217	6.0	19.5	37.5	52.0
							54-13C	217	217	6.0	N/A	N/A	N/A
		C (SCC)	6300	6600	Y (Using 54-4S)	Y	54-1S	212	212	6.0	N/A	N/A	N/A
							54-3S	212	212	6.0	N/A	N/A	N/A
							54-4S	212	212	6.0	19.5	37.5	52.0
		D (VC)	6700	6900	Y (Using 54-11C)	Y	54-11C	211	211	6.0	19.5	37.5	52.0
							54-12C	211	211	6.0	N/A	N/A	N/A
							54-14C	211	N/A	N/A	N/A	N/A	N/A
		E (SCC)	6100	6200	Y	Y	54-7S	205	205	6.0	19.5	37.5	52.0
		E (VC)	6400	6800	Y	Y	54-8C	205	205	6.0	19.5	37.5	52.0

[1] MOE stands for modulus of elasticity of concrete. Presented values are obtained from the lab-tested cylinder samples.

[2] Maturity is calculated with the temperature data obtained from the strain gages.

[3] Temperature values from four strain gages are used to apply temperature correction for strains and cambers. Girders having one gage are corrected with the girder having four gages from the same casting group.

[4] VWSG stands for vibrating-wire strain gage. Distance is from the bottom of the girder.

[5] SCC stands for self-consolidated concrete mix. VC stands for vibrated concrete mix.

Table 4-4: Project 1 (BT-72)—Summary of Collected Data

Project Name	Girder Type	Casting Group	MOE [1] (ksi) at		Maturity Calc.? [2]	Temp Corr.? [3]	Girder Name	Length of Meas. (day)		VWSG Locations (in) [4]			
			Transfer	28-day				Camber	Strain	#1	#2	#3	#4
Hillabee Creek Bridge (Girders were stored outdoors)	**BT-72**	F (SCC)	5800	6300	Y (Using 72-7S)	Y	72-1S	196	196	8.8	N/A	N/A	N/A
							72-7S	196	196	8.8	24.0	51.0	70.0
		G (VC)	6700	7000	Y (Using 72-8C)	Y	72-8C	192	192	8.8	24.0	51.0	70.0
							72-14C	192	192	8.8	N/A	N/A	N/A
		H (SCC)	5900	6400	Y (Using 72-4S)	Y	72-3S	191	191	8.8	N/A	N/A	N/A
							72-4S	191	191	8.8	24.0	51.0	70.0
		I (VC)	7100	7300	Y (Using 72-10C)	Y	72-10C	189	189	8.8	24.0	51.0	70.0
							72-13C	189	189	8.8	N/A	N/A	N/A
		J (SCC)	5800	6400	Y (Using 72-5S)	Y	72-2S	185	185	8.8	N/A	N/A	N/A
							72-5S	185	185	8.8	24.0	51.0	70.0
		K (VC)	6800	7700	Y (Using 72-12C)	Y	72-11C	184	184	8.8	N/A	N/A	N/A
							72-12C	184	184	8.8	24.0	51.0	70.0 [6]
		L (SCC)	5700	6000	Y	Y	72-6S	182	182	8.8	24.0	51.0	70.0
		L (VC)	6600	6900	Y	Y	72-9C	182	182	8.8	24.0	51.0	70.0

[1] MOE stands for modulus of elasticity of concrete. Presented values are obtained from the lab-tested cylinder samples.

[2] Maturity is calculated with the temperature data obtained from the strain gages.

[3] Temperature values from four strain gages are used to apply temperature correction for strains and cambers. Girders having one gage are corrected with the girder having four gages from the same casting group.

[4] VWSG stands for vibrating-wire strain gage. Distance is from the bottom of the girder.

[5] SCC stands for self-consolidated concrete mix. VC stands for vibrated concrete mix.

[6] Strain data of the gauge 4 are only available up to 7 days.

4.2.2 Project 2: AASHTO Type I

4.2.2.1 Overview

Auburn University Highway Research Center (AUHRC) investigated the effects of self-consolidating concrete (SCC) in precast-prestressed concrete bridge girders. This research project was carried out by Boehm (2008) and funded by Alabama Department of Transportation (ALDOT). Within the scope of this project, six full-scale AASHTO Type I girders were monitored for strain and camber development by Schrantz (2012) and subjected to transfer length and flexural testing at the end by Boehm (2008). Schrantz (2012) developed a camber application—utilizing the time-step approach—and analyzed the time-dependent deformations of the girders up to the casting of concrete decks.

Two VC girders and four SCC girders were cast in May 2007 at Hanson Pipe and Precast in Pelham, Alabama. After testing the girders for the initial transfer length, all of the girders were transported to the Auburn University Structural Research Laboratory. Later, a cast-in-place concrete deck was placed on each girder.

Figure 4-5 describes the identification of the specimens. STD is referred as vibrated concrete (VC) in this study. The 28-day strength level of moderate strength concrete was determined to range from 6600 psi to 9800 psi. The high strength concrete girders attained a strength value between 13,100 and 13,600 psi at 28 days. The difference between Girders 1 and 2 in a same group was the shear reinforcement patterns. In the following subsections, specimen design, material properties, strain measurement, and camber measurement are discussed. The research conducted by Boehm (2008) and Schrantz (2012) are summarized in the next subsections. Table 4-9 gives the summary of collected data acquired from this research study.

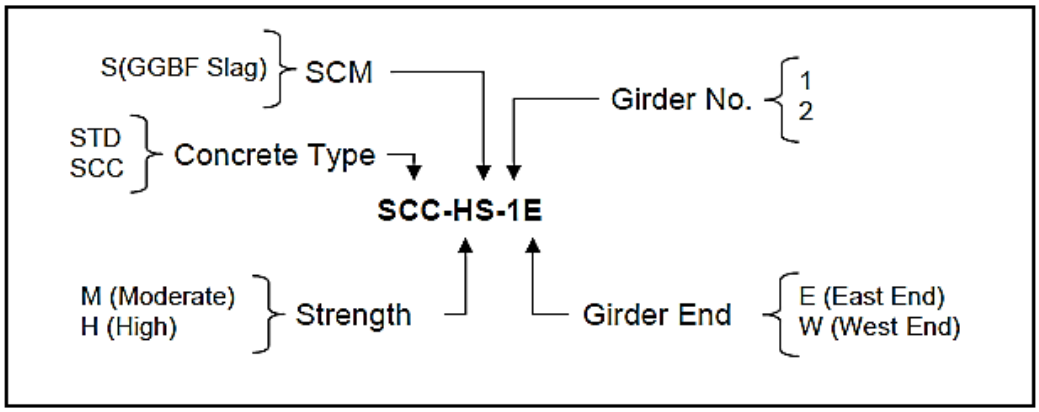

Figure 4-5: Project 2—Girder Identification Scheme (Boehm 2008)

4.2.2.2 Specimen Design

Each of the AASHTO Type I girders were 40-ft long and designed with eight prestressing strands. Cross-sectional dimensions are provided in Figure C-1 in Appendix C. Seven wire, Grade 270, low-relaxation, ½-in. "special" diameter strands were utilized and they were straight and fully bonded. Six of the strands located in the bottom flange were jacked with an amount of 202.5 ksi. Two of the strands in the top flange were jacked with an amount of 30.5 ksi. Shear reinforcement was included along the girder length, and confining steel reinforcement was placed at the girder ends. Figure C-2 illustrates the steel arrangement. Figure C-3 demonstrates the mild steel spacing.

4.2.2.3 Material Properties

Three mixture designs were used for AASHTO Type I girders, which were batched at Hanson Pipe & Precast. Table 4-5 provides the mixture constituents, water-cement ratios, sand-aggregate ratios, and air content. Table C-1 in Appendix C contains the fresh concrete properties.

Compressive strengths of concrete were tested with 6-inch by 12-inch concrete cylinders. Table C-2 presents the concrete strength at various ages and under different curing conditions.

Table 4-6 provides the initial concrete properties from the match-cured samples, and the 28-day properties from the cylinders in conformity with the ASTM Standards.

Table 4-5: Project 2—Concrete Mixtures (Adapted from Boehm [2008])

Mixture Constituents	Units (per yd^3)	Mixtures		
		STD-M	SCC-MS	SCC-HS
Water	gal	32.4	34.2	31.2
Cement (Type III)	lb	640	553	650
GGBF Slag (Grade 100)	lb	0	237	279
Water/Cement	n/a	0.42	0.36	0.28
# 78 Crushed Limestone	lb	2034	1608	1601
Red Bluff Sand	lb	1110	1317	1267
Sand/Aggregate	n/a	0.37	0.47	0.46
Air-Entraining Admixture	fl oz	0.6	0.6	0.6
HRWR Admixture	fl oz	19.2	51.0	93.0
Viscosity-Modifying Admixture	fl oz	0	16.0	0
Retarding Admixture (Delvo)	fl oz	19.2	24.0	28.0
Air (%)*	n/a	3.2	2.8	1.5

*Average of air content was determined from fresh concrete test results.

Table 4-6: Project 2—Hardened Concrete Properties (Adapted from Boehm [2008])

	Release			28 Days	
Girder ID	**Age (hrs)**	**f'_{ci} (psi)**	**E_{ci} (ksi)**	**$f'_{c,28}$ (psi)**	**$E_{c,28}$ (ksi)**
STD-M-1	18	4780	5700	6600	6750
STD-M-2	18	4780	5700	7200	7300
SCC-MS-1	18	5540	5250	9780	7400
SCC-MS-2	18	5540	5250	9790	7500
SCC-HS-1	18	10430	7000	13160	8600
SCC-HS-2	18	10430	7000	13580	8300

The low-relaxation, Grade 270, seven-wire, ½-inch "special" strands—with an area of 0.164 $in.^2$—were supplied by American Spring Wire Corporation in Houston, Texas. In order to remove surface debris, the strands were wiped with a cotton cloth before prestressing. MOE of the prestressing steel was 28,900 ksi. ASTM A615 Grade 60 reinforcing bars were used as the mild steel reinforcement. MOE of the non-prestressing steel was 29,000 ksi.

4.2.2.4 Strain Measurement

The vibrating-wire strain gauges (VWSGs) were Geokon, Inc. VCE-4200. They were installed in order to obtain the strain development and the associated temperature values. Later, the readings were acquired with the Campbell Scientific's CR10X automatic data acquisition system. The table at the end of the following section summarizes the availability of collected strain data from this research study.

4.2.2.5 Camber Measurement

The camber readings of the prestressing girders were made with the surveyor's method and the tension-wire system (0.01-inch-precision steel rule). The survey was done at 2 inches from each end and every quarter length (including the midspan). The table at the end of the next section presents the availability of collected camber data.

4.2.3 Project 3: HPC BT-54

4.2.3.1 Overview

The aim of the HPC BT-54 project was to quantify the accuracy of available prediction methods for camber and prestress losses in high performance concrete (HPC) girders. Five AASHTO BT-54 girders investigated in this research were designed and cast for Bent 5 and Bent 6 of the Uphapee Creek HPC Showcase Bridge in Macon County, Alabama. Girders 1 and 2 were cast in December 18th, 1998; Girder 3 and 4 were cast in January 28th, 1999. Girder 5 was cast in February 3rd, 1999. All of the fabrication was completed in Sherman Prestressed Concrete in Pelham, Alabama. They were monitored for strain and camber development.

Specimen design, material properties, strain measurement and camber measurement are summarized in the following subsections according to the studies completed by Glover and Stallings (2000), Stallings and Eskildsen (2001), and Stallings et al. (2003).

4.2.3.2 Specimen Design

The span length of five BT-54 girders is 112 feet 4 inches between the centers of simple neoprene bearing pads. Figure D-1 in Appendix D provides the cross-sectional view of the girders.

Fully prestressed strands are seven-wire, Grade 270, low-relaxation, 0.6 in. diameter with a specified jacking stress (f_{pj}) of 202.5 ksi. 18 of them are straight and fully bonded. 10 of them are debonded at 48 in. from the ends. 14 strands are draped at 120 in. from the midspan. Lightly prestressed strands are seven-wire, Grade 270, low-relaxation, 0.5 in. diameter with a specified jacking stress of 50 ksi. They are straight, fully bonded and located in the top flange. Figure D-2 illustrates the profile of prestressed beams and Figure D-3 demonstrates the steel and strand arrangement at midspan and girder ends.

4.2.3.3 Material Properties

Table 4-7 lists the concrete mixture design corresponding to the saturated-surface-dry (SSD) condition. The girders were fabricated with eighteen pours. #67 crushed limestone was used as a coarse aggregate for the first twelve castings, and #7 crushed limestone was used for the last six pours.

Table 4-7: Project 3—Concrete Mixtures (Adapted from Stallings et al. [2003])

Mixture Constituents	Mixtures HPC BT-54 - 1, 2, 3, 4, and 5
Water	237 lb/yd^3
Cement (Type III)	752 lb/yd^3
Type C Fly Ash	132 lb/yd^3
Water/Cement	0.30
#67 or #7 Crushed Limestone	1843 lb/yd^3
#89 Natural Sand	383 lb/yd^3
#100 Natural Sand	733 lb/yd^3
Sand/Aggregate	N/A
Superplasticizers (MB Rheobuild® 1000)	14 oz per 100 lb of cementitious material
Retarder (MB Delvo®)	1.4 oz per 100 lb of cementitious material
Air Entrainment (MB Micro Air®)	0.44 oz per 100 lb of cementitious material
Air (%)*	4.2
*Average of air content was determined from fresh concrete test results.	

Hardened concrete properties were tested with 4-inch by 8-inch concrete cylinders. They were match-cured until the prestress transfer and they were stored outside the production yard nearby the BT-54 girders. Compressive strength was determined according to AASHTO T 22 (1997) “Standard Specification for Compressive Strength of Cylindrical Concrete Specimens”. Modulus of elasticity values were obtained according to ASTM C 469 (1996). Table 4-8 gives the hardened concrete properties. The measurements from the concrete cylinders do not include any corrections taking account of the cylinder size. Tables D-1 and D-2 reveal the hardened concrete properties.

Table 4-8: Project 3—Hardened Concrete Properties (Adapted from Stallings et al. [2003])

Property	Number of Specimens	Range	Mean	Coefficient of variation (%)
f'_{ci} (at t≈20 hrs) (psi)	36	8040 to 9810	8540	6.4
$f'_{c,28}$ (psi)	36	8440 to 11060	9920	7.6
$E_{ci} \approx E_{c,28}$ (ksi)	32	4300 to 7100	5740	11.7

Fully prestressed strands with 0.6 in. diameter have a cross-sectional area of 0.217 in^2. Lightly prestressed strands with 0.5 in. diameter have a cross-sectional area of 0.153 in^2. MOE of the strands were reported as 27,500 ksi.

4.2.3.4 Strain Measurement

Geokon's Mode1 4911 Vibrating Wire Rebar Strain Meter was used to measure the internal strains. The strain data were collected with the Campbell Scientific's CRI0X. The availability of collected strain data obtained from this research study can be found in Table 4-7.

4.2.3.5 Camber Measurement

The surveyor's level with the carpenter's tape was utilized to measure the camber growth on the girders. The measurements were made to the nearest $^1/_{16}$ inch. The camber measurements had been made at various times of the day in the first 100 days. Later, researchers tried to minimize the temperature effects by measuring the readings in the early morning.

Table 4-9: Projects 2 and 3—Summary of Collected Data

Project Name	Type of Mix	Girder Name [1]	MOE [2] (ksi) at Transfer	MOE [2] (ksi) at 28-day	Maturity Calc. ? [3]	Temp Corr.? [4]	Length of Meas. (day) Camber	Length of Meas. (day) Strain	VWSG Locations (in) [5] #1	VWSG Locations (in) [5] #2	VWSG Locations (in) [5] #3
AASHTO Type I (Girders were stored outdoors)	VC [6]	STD-M-1	5700	6750	Y	Y	110	110	3.3	11.9	24.4
		STD-M-2	5700	7300	Y [7]	Y	110	110	3.3	12.4	23.5
	SCC [6]	SCC-MS-1	5250	7400	Y	Y	160	160	3.3	12.8	24.3
		SCC-MS-2	5250	7500	Y	Y	167	167	3.3	12.9	24.1
		SCC-HS-1	7000	8600	Y	Y	214	214	3.0	12.9	24.3
		SCC-HS-2	7000	8300	Y	Y	214	214	3.4	13.0	24.1
HPC BT-54 (Girders were stored outdoors)	VC	Girder 1	5740 [8]		Y[9]	N[10]	353	311	6.5	51.3	N/A
		Girder 2					353	311	6.5	51.3	N/A
		Girder 3					300	270	6.5	51.3	N/A
		Girder 4					300	270	6.5	51.3	N/A
		Girder 5					292	264	6.5	51.3	N/A

[1] M and H stand for moderate and high strength, respectively. S stands for GGBF Slag used in the mix.

[2] MOE stands for modulus of elasticity of concrete. Presented values are obtained from the lab-tested cylinder samples.

[3] Maturity is calculated by using the temperature data of relevant strain gages.

[4] Temperature values from three strain gages are used to apply temperature correction for strains and cambers.

[5] VWSG stands for vibrating-wire strain gage. Distance is from the bottom of the girder.

[6] SCC stands for self-consolidated concrete mix. VC stands for vibrated concrete mix.

[7] Early age temperature data of STD-M-1 are also used to calculate the maturity of STD-M-2.

[8] 32 MOE values at various ages from release to 56-day were averaged.

[9] Maturity calculations are carried out by using the representative temperature values of Pour #10 from the same project.

[10] Temperature corrections cannot be applied since temperature values at the reading time are not available.

4.2.4 Project 4: T-Beams

4.2.4.1 Overview

Alabama Department of Transportation (ALDOT) sponsored research to investigate the bond behavior of prestressed strands in SCC girders. Sixteen T-beams were fabricated in the Auburn University Structural Engineering Laboratory. They were monitored for camber development in addition to the actual transfer length testing. The girders were four different sizes and labeled with "A", "B", "C", and "D". Also, each girder with different length was cast with four different mixtures, and girders with 16 different combinations were obtained. One VC mixture and three SCC mixtures were used. Figure 4-6 depicts the girder identification. Three girders represented with "A", "B", and "C" will be considered within the scope of this study.

Levy (2007) explained the design and fabrication of experimental specimens, and her research was summarized in the following subsections; namely, specimen design, material properties, strain measurement and camber measurement.

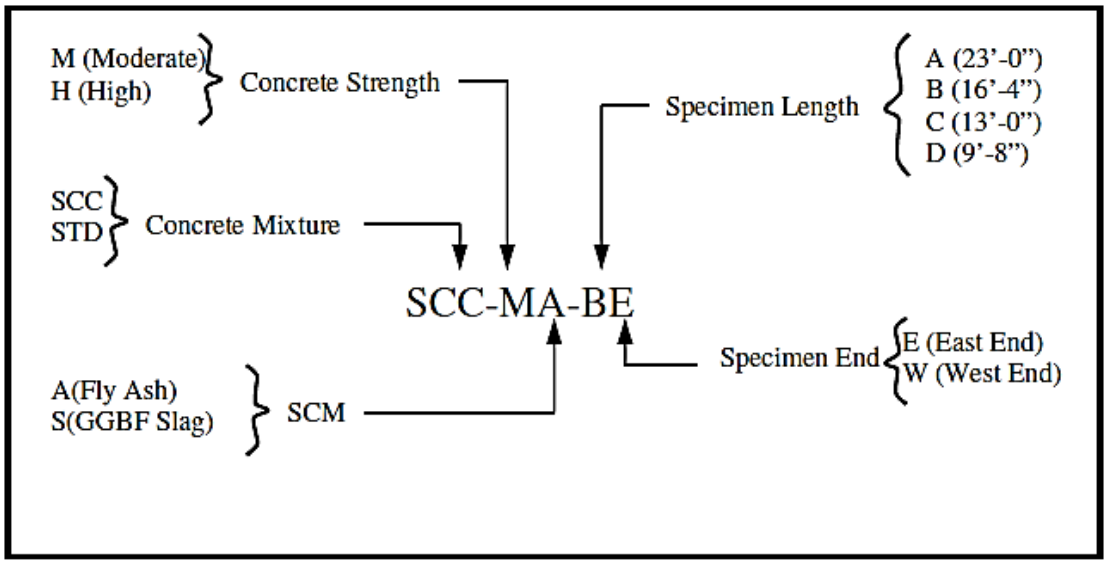

Figure 4-6: Project 4—Girder Identification Scheme (Levy 2007)

4.2.4.2 Specimen Design

The sizes of the girders can also be found in Figure 4-6. Figure E-1 in Appendix E shows the dimensions of the cross-section and the arrangement of steel. T-Beams were designed with seven-wire, Grade 270, low-relaxation, ½-in. "special" strands with a jacking stress of 214.5 ksi. The strands were straight and fully developed and cleaned with a cotton rag to eliminate the surface debris. Longitudinal and transverse non-prestressed reinforcement consisted of #3 steel reinforcing bars. Longitudinal bars were designed as compression reinforcement. U-stirrups were used to provide shear reinforcement. The stirrup spacing of the beams can be seen in Figure E-2.

4.2.4.3 Material Properties

Table 4-10 shows the four different concrete mixtures used in the research project. The coarse aggregate type was #78 dolomitic limestone, and the fine aggregate type was natural river sand. Table E-1 tabulates the fresh concrete properties.

Table 4-11 illustrates the hardened concrete properties. The properties were obtained from the 4-inch by 8-inch cylinders. They were air-cured and stored in the same conditions as the actual beams. Each property is the average of the tested three cylinders. Additionally, Table E-2 presents further hardened properties. The strength tests were performed in accordance with AASHTO T 22(1997) and ASTM C39 (1998). The MOE of concrete was obtained according to ASTM C469 (1998).

Half-inch "special" strands had a cross-sectional area of 0.164 in^2 and a MOE value of 28,900 ksi. The strands were transported from American Spring Wire Corporation in Houston, Texas. The #3 bars were ASTM A615 Grade 60 reinforcement, and they had a MOE value of 29,000 ksi.

Table 4-10: Project 4—Concrete Mixture Proportions (Adapted from Levy [2007])

Mixture Constituents	Mixture			
	STD-M	SCC-MA	SCC-MS	SCC-HS
Water (pcy)	270	270	270	260
Cement (pcy)	640	525	375	650
Fly Ash (pcy)	0	225	0	0
GGBF Slag (pcy)	0	0	375	279
w/cm	0.40	0.36	0.36	0.28
Coarse Agg. (pcy)	1964	1607	1613	1544
Fine Agg. (pcy)	1114	1316	1323	1265
s/agg	0.37	0.46	0.46	0.46
Air-Entraining Admixture (oz/cwt)	0.33	0.00	0.00	0.00
Mid-Range Water Reducing Admixture (oz/cwt)	4.0	4.0	6.0	6.0
High-Range Water Reducing Admixture (oz/cwt)	3.5	4.0	4.5	5.0
Viscosity-Modifying Admixture (oz/cwt)	0.0	2.0	2.0	2.0
Air (%)	11.0	2.0	5.0	3.0

Table 4-11: Project 4—Hardened Concrete Properties (Adapted from Levy [2007])

	Release			28 Days	
Girder ID	Age (hrs)	f'_{ci} (psi)	E_{ci} (ksi)	$f'_{c,28}$ (psi)	$E_{c,28}$ (ksi)
STD-M - A, B, C	72	5000	4900	6320	5150
SCC-MA - A, B, C	30	5500	4900	8540	5400
SCC-MS- A, B, C	72	5300	4950	9170	6950
SCC-HS- A, B, C	30	9990	6050	13380	7050

4.2.4.4 Camber Measurement

The surveyor's level and a rod with 0.01 in. gradations were utilized to measure the camber development of T-Beams. The girders had been stored in the lab; therefore, the temperature corrections were not needed. Table 4-12 summarizes the availability of data.

Table 4-12: Project 4—Summary of Collected Data

Project Name	Type of Mix	Girder Name [1]	MOE [2] (ksi) at Transfer	MOE [2] (ksi) at 28-day	Maturity Calc. ? [3]	Temp Corr.? [4]	Length of Meas. (day) Camber	Length of Meas. (day) Strain
T-Beams (Girders were stored indoor)	VC [5]	STD-M-A	5000	6320	Y	N	90	N/A
		STD-M-B			Y	N	90	
		STD-M-C			Y	N	90	
	SCC [5]	SCC-MA-A	4900	5400	Y	N	201	
		SCC-MA-B			Y	N	201	
		SCC-MA-C			Y	N	201	
		SCC-MS-A	4950	6150	Y	N	56	
		SCC-MS-B			Y	N	56	
		SCC-MS-C			Y	N	56	
		SCC-HS-A	6050	7050	Y	N	15	
		SCC-HS-B			Y	N	15	
		SCC-HS-C			Y	N	15	

[1] M and H stand for moderate and high strength, respectively. The following letters A and S stand for Fly Ash, and GGBF Slag, respectively. Last letters, A, B and C represent the length of girders. (A = 276 in, B = 196 in., C = 156 in.)

[2] MOE stands for modulus of elasticity of concrete. Presented values are obtained from the lab-tested cylinder samples.

[3] Maturity is calculated by using the thermocouples embedded at the strand depth.

[4] Temperature profiles were not available at the time of camber measurement. Also, temperature corrections may have an insignificant influence on the results since the T-Beam girders were stored indoor.

[5] SCC stands for self-consolidated concrete mix. VC stands for vibrated concrete mix.

4.3 Temperature Corrections for Internal Strain and Camber

4.3.1 Overview

The prestressed girders stored outside were directly exposed to sunlight, wind, and other environmental effects. It was likely that the outside prestressed girders encountered a non-uniform temperature distribution over a girder depth when researchers took strain and camber readings.

The software predicting the time-dependent deflections is developed with an assumption that temperature remains uniform. For the purpose of comparing predictions and the actual data, raw strain and camber readings are adjusted relative to a uniform internal temperature of 20 $^{\circ}$C (68 $^{\circ}$F).

The temperature values at the time of recording were obtained in $^{\circ}$C from the thermistors embedded into the strain gages. The temperature histories were available for the Hillabee Creek Bridge Project and the AASHTO Type I girders. Strain and camber corrections are made by using simplified cross sections. Figures 4-7 and 4-8 show the simplified cross sections and the assumed thermal gradients for the Hillabee Creek Bridge Project. Similarly, Figure 4-9 illustrates the simplified cross section for the AASHTO Type I girders. The simplified dimensions were chosen to be as close as the cross-sectional area, centroid, and moment of inertia of original section. Also, the temperature gradients were assumed to be constant on the flanges and linear on the web.

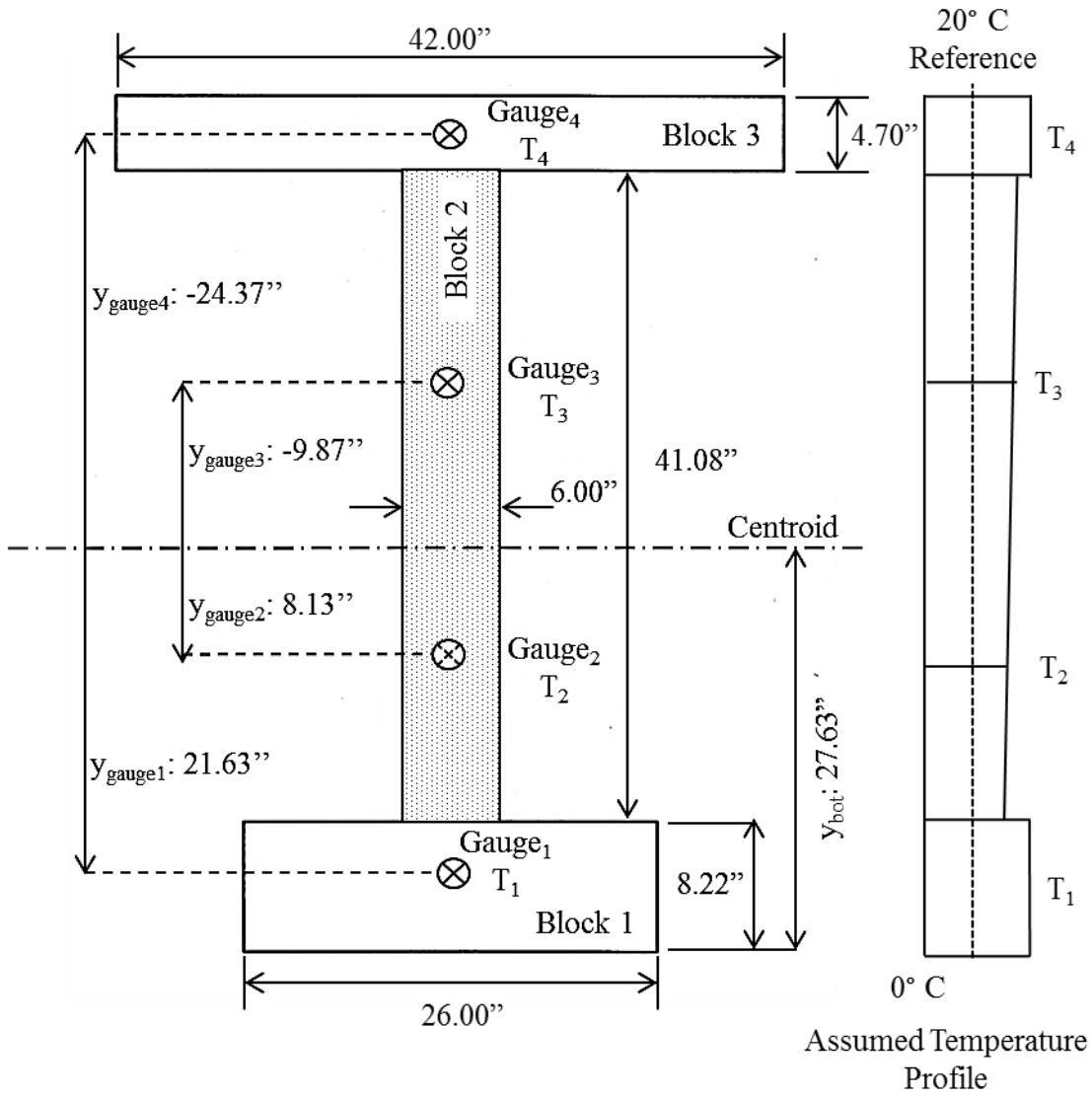

Block 1	Block 2	Block 3
Area : 213.8 in^2	Area : 246.5 in^2	Area : 197.6 in^2
$I_{wrt.centroid}$: 119404 in^4	$I_{wrt.centroid}$: 34977 in^4	$I_{wrt.centroid}$: 142904 in^4

Figure 4-7: Project 1—Simplified BT-54 for Temperature Correction

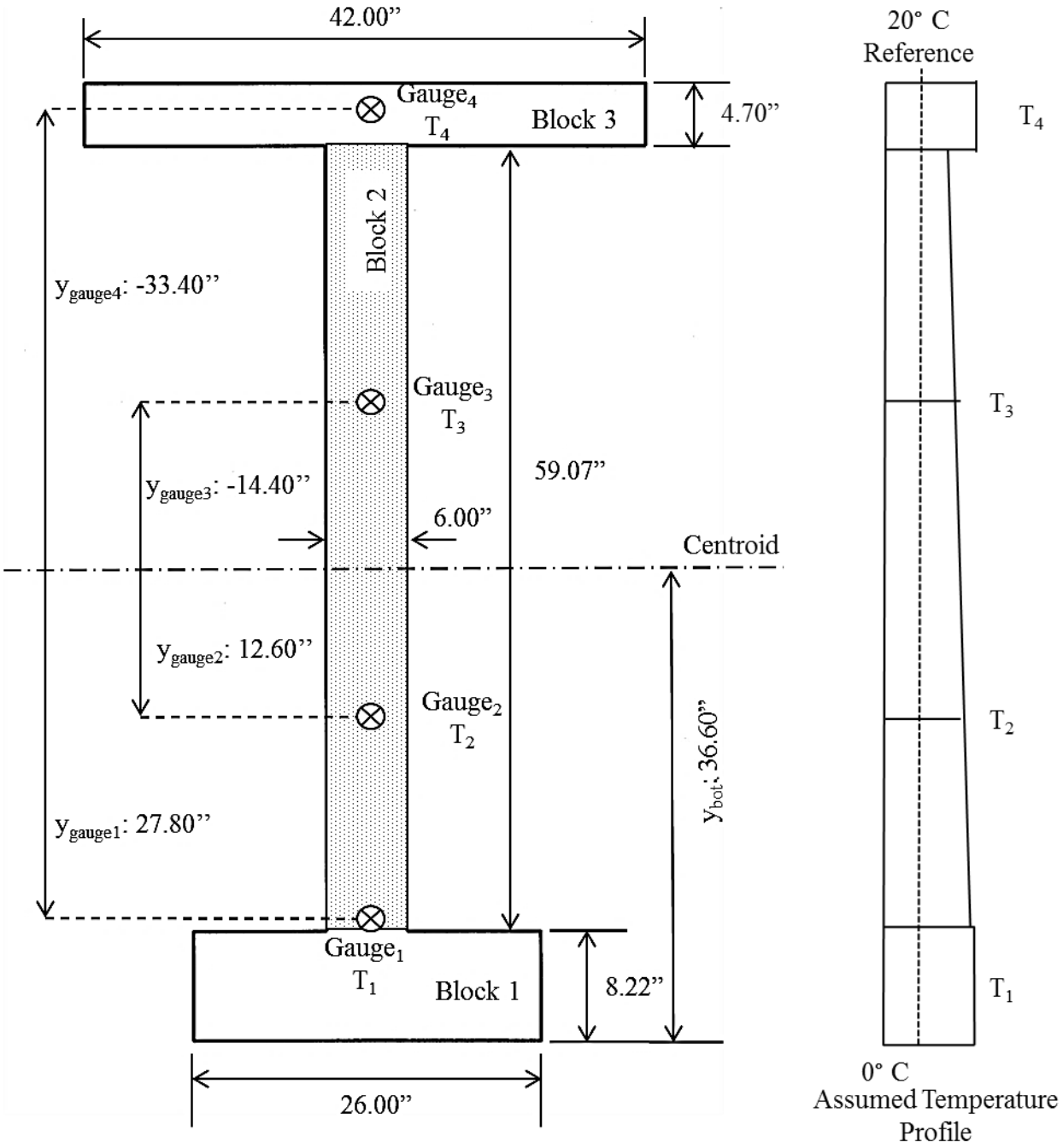

Block 1	Block 2	Block 3
Area : 213.8 in^2	Area : 354.4 in^2	Area : 197.6 in^2
$I_{wrt.centroid}$: 226870 in^4	$I_{wrt.centroid}$: 103532 in^4	$I_{wrt.centroid}$: 216213 in^4

Figure 4-8: Project 1—Simplified BT-72 for Temperature Correction

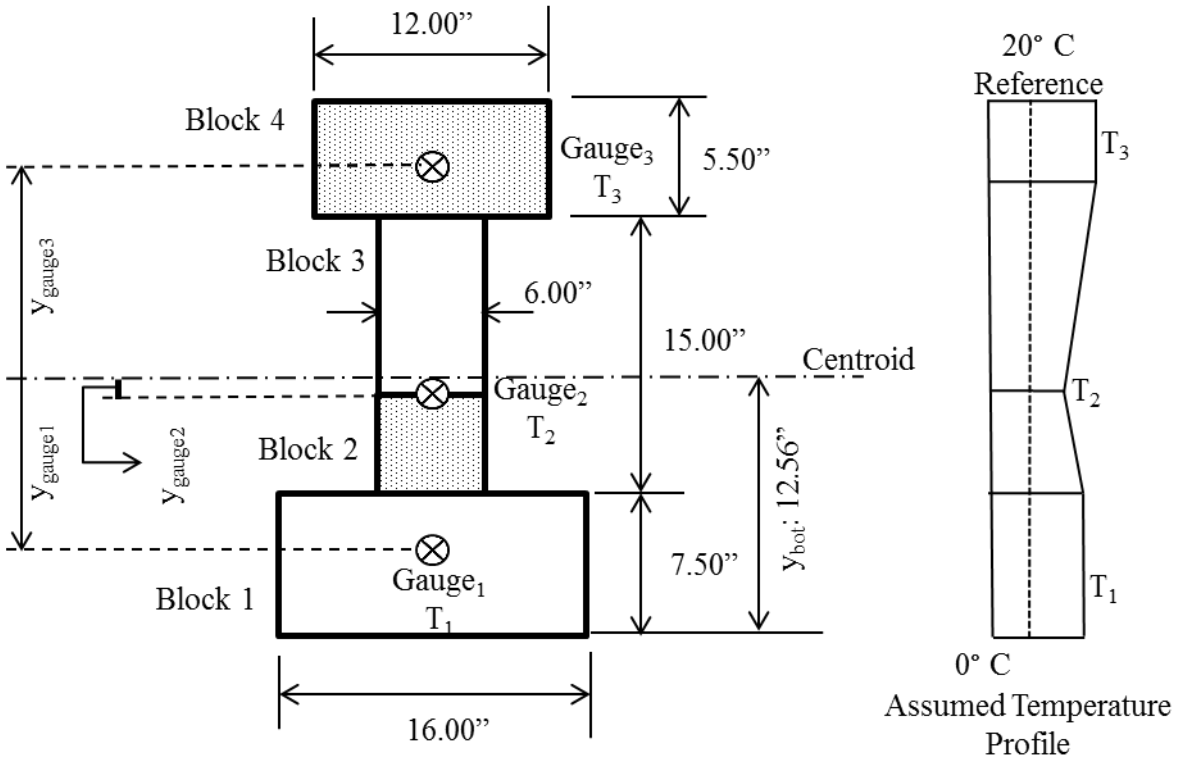

Figure 4-9: Project 2—Simplified Section for Temperature Correction

Equations 4-1 and 4-2 show the relationship to obtain the strain and curvature changes due to varying temperature on a girder depth. Linear-elastic material behavior, ‘plane section remains plane’, and equilibrium were the assumptions utilized to obtain them. The derivations of the equations can be found in Johnson’s research (2012). Keske (2014) made some modifications to Johnson’s method. Keske (2014) also measured the CTE values of the SCC and VC girders and the findings are listed in Table 4-13 along with the employed CTE values. CTE for the saturated condition was in in accordance with AASHTO T 336.

$$\Delta\varepsilon_{cen,t} = \frac{CTE \int \Delta T dA'}{A'} \qquad \textit{Equation 4-1}$$

$$\Delta\phi_t = \frac{CTE \int \Delta T y dA'}{I} \qquad \textit{Equation 4-2}$$

where, $\Delta\varepsilon_{cen,t}$ = the strain change at the centroid of the cross section due to temperature change in [με]

$\Delta\phi_t$ = change in curvature of a concrete cross section due to temperature changes on the cross section in [με/in.]

CTE = coefficient of thermal expansion of concrete in [με/°C]

ΔT = temperature gradient of the cross section from 20°C in [°C]

A' = simplified cross-sectional area in [in^2]

I = simplified cross-sectional moment of inertia with respect to the centroid in [in.^{4}]

Table 4-13: Coefficients of Thermal Expansion (CTE)

Concrete	Measured (Keske 2014)				Used in this research	
	Dry		Saturated			
	με/°C	με/°F	με/°C	με/°F	με/°C	με/°F
SCC Girder	13.3	7.4	9.4	5.2	12.5	7.0
VC Girder	12.2	6.8	9.2	5.1	11.5	6.4

4.3.2 Adjustment of Recorded Internal Strains

The internal strain readings are corrected in two steps. First, temperature change within the VWSG member is considered since the steel wire encounters temperature-dependent expansion or contraction. It is expressed in Equation 4-3. The given coefficient of thermal expansion (CTE) value for VWSGs was supplied by the producer. Second, raw strain values are corrected to eliminate the effect of nonlinear temperature distribution over the concrete cross section. Equation 4-4 takes account of the thermal effects of the strain gauges and concrete cross-section. Figure 4-10 shows an example of corrected set of internal strains.

$$\varepsilon_{rec,gt} = \varepsilon_{rec} + T_g \times CTE_g \qquad \textbf{\textit{Equation 4-3}}$$

where, $\varepsilon_{rec,gt}$ = recorded strain corrected for gauge temperature in [με]

ε_{rec} = recorded raw strain in [με]

T_g = gauge temperature relative to 20°C in [με/°C]

CTE_g = coefficient of thermal expansion for the VWSG in [με/°C]

= 12.2 με/°C (6.8 με/°F)

$$\varepsilon_T = \varepsilon_{rec,gt} + \Delta\varepsilon_{cen,t} + \Delta\phi_t \times y \qquad \textbf{\textit{Equation 4-4}}$$

where, ε_T = corrected strain taking account of the thermal effects of strain gauges and concrete cross-section

$\Delta\varepsilon_{cen,t}$ = the strain change at the centroid of the cross section due to temperature change in [με] (given in Equation 4-1)

$\Delta\phi_t$ = change in curvature of a concrete cross-section due to temperature change on the cross section in [με /in.] (given in Equation 4-2)

y = distance from the centroid to the girder depth where strain reading is made in [in.] (+, downward)

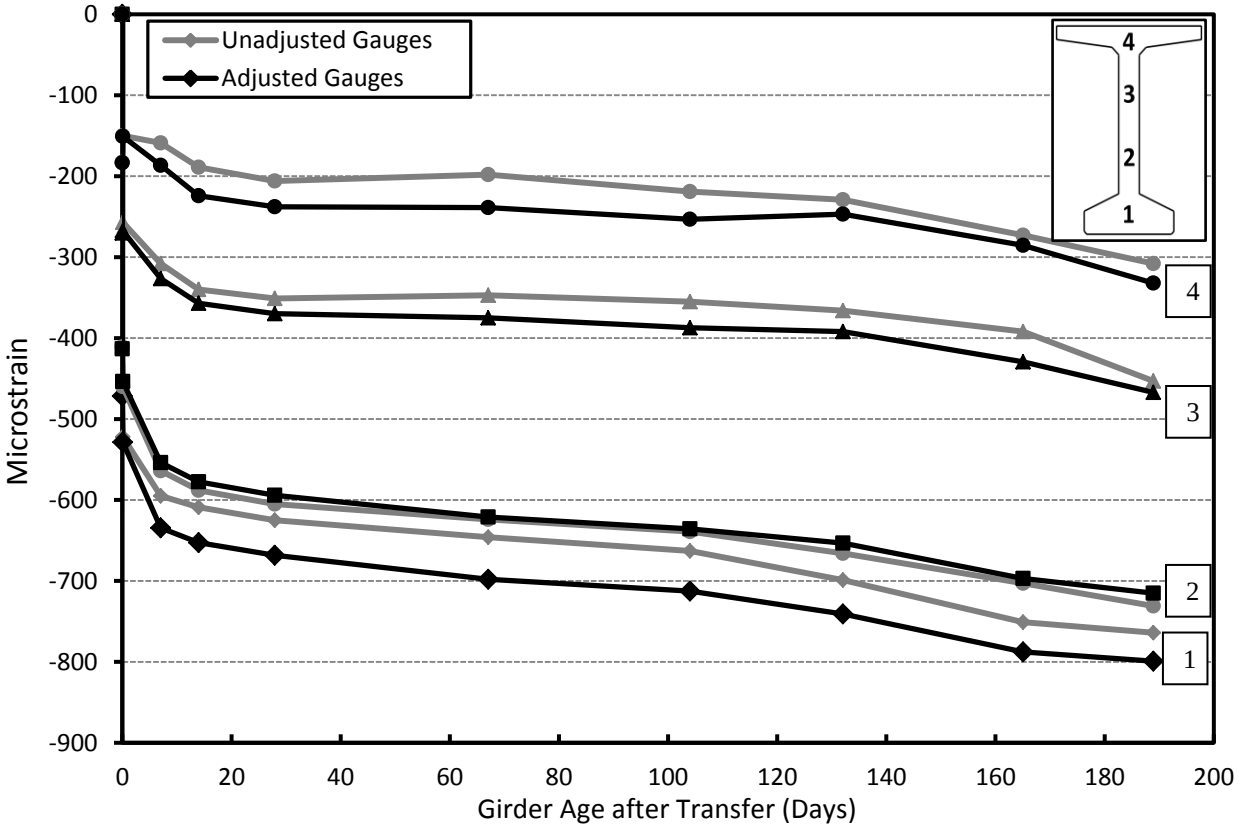

Figure 4-10: Adjusted Strains for 72-10C

4.3.3 Adjustment of Measured Camber Values

For the purpose of adjusting the camber readings, the non-linear temperature profile was assumed constant along the girder length and that the beam is simply supported. Camber measurements are adjusted with two corrections as shown in Equation 4-5 using a procedure like that described by Johnson (2012). The baseline correction is included because temperature gradient was significant at the time of initial camber reading. Another correction was to include the temperature gradient effect for each camber reading. Figure 4-11 shows a sample camber data adjusted according to the equation below.

$$\Delta_{adj} = (\Delta_{meas} + \Delta_{baseline.corr}) - \Delta_{temp,corr} \qquad \textit{Equation 4-5}$$

where, Δ_{adj} = adjusted camber in [in.]

Δ_{meas} = recorded camber without any thermal adjustments in [in.]

$\Delta_{baseline.corr}$ = $\frac{\Delta\phi_{i,t}(L^2)}{8}$ = correction for the baseline reading

$\Delta\phi_{i,t}$ = change in baseline curvature due to initial temperature gradient in [με/in.] (given in Equation 4-2)

$\Delta_{temp,corr}$ = $\frac{\Delta\phi_t(L^2)}{8}$ = correction for each camber reading in [in.]

$\Delta\phi_t$ = change in curvature due to temperature gradient in [με/in.] (given in Equation 4-2)

L = length of the girder in [in.]

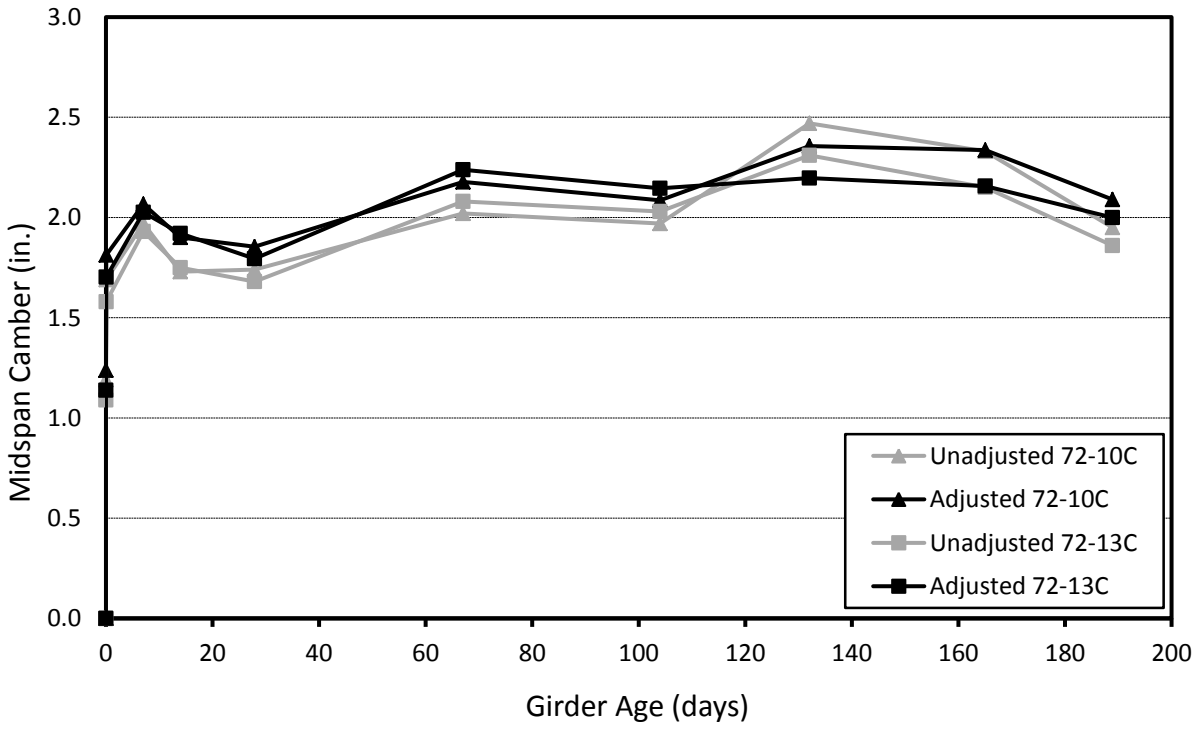

Figure 4-11: Adjusted Cambers for Casting Group I

4.4 Selected Input Variables

The scope of this research involves the comparison of the prediction models. AASHTO LRFD 2014, ACI 209 and *fib* MC 2010 are compared with the collected data from four different projects as well as each other. The input variables used for the girders in Projects 2 and 4 are listed in Table F-1 in Appendix F. The full list of input parameters for the girders in Projects 1 and 3 are given in Table F-2. The adjusted slump values are explained by Schrantz (2012) and Johnson (2012). The benchmark reading represents the elapsed time from the prestress transfer to the benchmark reading for strain predictions.

Curing type is selected as accelerated curing for Projects 1, 2, and 3. Project 4 is investigated for both accelerated and non-accelerated curing properties. Accelerated curing indicates that curing temperature is elevated above normal curing temperature due to the exposure of sun, the tarp/enclosure, or the external application of steam or heat. Concrete with non-accelerated curing does not have any external heating effects and does not experience as much temperature increase as with accelerated curing. "Steam" curing is taken to mean accelerated curing, and "moist" curing indicates non-accelerated curing.

The prediction models were formulated with different variables, and they were based on the common construction practice of the specific country or region. *fib* MC 2010 was established explicitly for the European construction practice; in contrast, AASHTO LRFD and ACI 209 were modeled according to the U.S. practice. The European and ASTM standards differ from each other in terms of the cement classifications, the requirements, and the material testing methods. Therefore, these standards do not offer direct equivalents. The cement types are discussed in detail in Appendix I.

The investigated research projects were carried out according to the governing U.S. standards. All of the cement types in these projects were Type III, and they had high early

strength for the purpose of prestressing application. Therefore, "42.5 R, 52.5 N, 52.5 R" is selected as the strength class of cement for the use of the *fib* MC 2010 model. The aggregate types used for this research were #67, #7, and #78 limestone, and they are assumed to match with the type of "basalt, dense limestone aggregates".

The equivalent age calculations are carried out according to Equation 4-6 as given in *fib* MC 2010. Equivalent ages are used only for the *fib* MC 2010 prediction model. The early-age temperature profile of the girders in Project 1 is provided in Figures B-8–B-20 in Appendix B. The temperature profile for girders in Project 2 is plotted in Figure C-4. The early age temperature profile for the girders in Project 3 is obtained from Pour #10 given in Figure D-4. Strength-maturity curves for the girders in Project 4 are provided in Figures E-3, E-4, E-5, and E-6.

$$t_{0,T} = \sum \Delta t_i exp\left\{13.65 - \frac{4000}{273 + T(\Delta t_i)}\right\} \qquad \textbf{\textit{Equation 4-6}}$$

where, $T(\Delta t_i)$ = temperature in [°C] during the time period Δt_i in [days]

Chapter 5 Results and Discussion

5.1 Introduction

Camber deflections and effective prestress forces are the basic design-critical aspects related to time-dependent deformations. Camber measurements are obtained directly, but loss of prestress force is represented by bottom-flange strains. Curvature measurements at midspan are also obtained since camber predictions are made according to the moment-area method.

In this chapter, bottom-flange strains, curvatures, and cambers are predicted with the new version of the camber prediction software. The used concrete MOE development model was a two-point MOE development model based on measured MOE (two-point MOE model). The material prediction models for creep and shrinkage of concrete were composed of AASHTO LRFD 2014, ACI 209, and fib Model Code 2010. They are compared to actual responses of the Hillabee Creek Bridge (Project 1), AASHTO Type I (Project 2), HPC (Project 3), and T-Beam (Project 4) girders. Then, the results are discussed to highlight the key points.

Further discussions about data collections are made in Section 4.2. Data used for plotting the graphs in this chapter can be found in Appendices H and G. Also, the graphs used in this chapter are scaled differently for each case.

5.2 Statistical Evaluation of the Error between Predicted and Measured Values

Unbiased estimate of the standard deviation of the fractional errors (UE-StDev) is used to evaluate the error between the predicted and measured values. In the unbiased case, sample standard deviation is divided by ‘n-1’ instead of ‘n’ to calculate the sample variance (Dekking et

al. 2005). For this research, UE-StDev is used as a way to evaluate the predicted strains, curvatures, and cambers. Additionally, the average of the fractional errors is utilized to support the unbiased estimates and evaluate the distribution of predictions. Equation 5-1 shows the function for UE-StDev. Equation 5-2 shows how to calculate the fractional *growth* error, which represents the error of prediction *growth* relative to measured *growth*.

$$S = \sqrt{\frac{1}{n-1}\sum_{i}^{n}\Delta_i^2} \qquad \textbf{\textit{Equation 5-1}}$$

where, S = unbiased estimate of the standard deviation of the fractional error

n = number of data points

Δ_i = fractional error of the i[th] data point

$$\Delta = \frac{(x - x_{initial})_{predicted} - (x - x_{initial})_{measured}}{(x - x_{initial})_{measured}} \qquad \textbf{\textit{Equation 5-2}}$$

where, x = strain, curvature, or camber at the time considered

$x_{initial}$ = strain, curvature, or camber at the initial time considered

Selecting the best prediction according to UE-StDev eliminates the negative sign. Understanding whether the case is regularly over- or underpredicted becomes impossible. Table 5-1 demonstrates three different cases. Case 1 overpredicts all of the responses such as strain, curvature, or camber. Case 2 overpredicts them on average; while, Case 3 underpredicts entirely. All of the cases produce the same amount of unbiased estimates despite the non-uniformity. To avoid the confusion, the average of the fractional errors is also considered.

Table 5-1: Comparison of Cases with Different Fractional Error Distribution

	Fractional Error					**UE-StDev**	**Average**
	Data#1	Data#2	Data#3	Data#4	Data#5		
Case 1	0.02	0.05	0.05	0.25	0.25	0.18	0.12
Case 2	-0.15	-0.10	0.00	0.20	0.25	0.18	0.04
Case 3	-0.25	-0.25	-0.05	-0.05	-0.02	0.18	-0.12

5.3 Project 1: The Hillabee Creek Bridge Girders

5.3.1 Total Creep Coefficient and Total Shrinkage Strain

The creep and shrinkage values are the key elements determining the predicted time-dependent deformations. Curvature and camber *growth* significantly depends on creep; in contrast, strain *growth* depends on both shrinkage and creep.

Figure 5.1 demonstrates the total creep coefficient and total shrinkage strain (not ultimate creep coefficient and shrinkage strain) predicted up to the erection. The erection times for the Hillabee Creek Bridge Project are between 182 days and 219 days.

The estimated creep coefficients fall between 0.86 and 1.10. ACI 209 predicts the least ultimate creep coefficient for most of the cases; in contrast, *fib* MC 2010 estimates the largest creep on average. Further, the predicted creep coefficients for the SCC and VC girders are very close.

The shrinkage strains are predicted to be within -240 με and -330 με. The *fib* MC 2010 model calculates the autogenous and drying shrinkage separately unlike the ACI 209 and AASHTO LRFD 2014 models. The total shrinkage strains reported on the figure exclude the shrinkage prior to the benchmark reading and show the values used for the time-dependent calculations. The shrinkage strain predictions with MC 2010 range from -36 με to -54 με prior to the benchmark reading. For the other two models, they are determined to be less than -6 με.

fib MC 2010 predicts the least shrinkage in magnitude, and it does not reflect a sharp difference for the SCC and VC girders. The ACI 209 and AASHTO LRFD shrinkage predictions for the SCC girders turn out to be larger in magnitude than the ones for the VC girders. Additionally, ACI 209 predicts a larger shrinkage strain than AASHTO LRFD when it comes to the SCC girders.

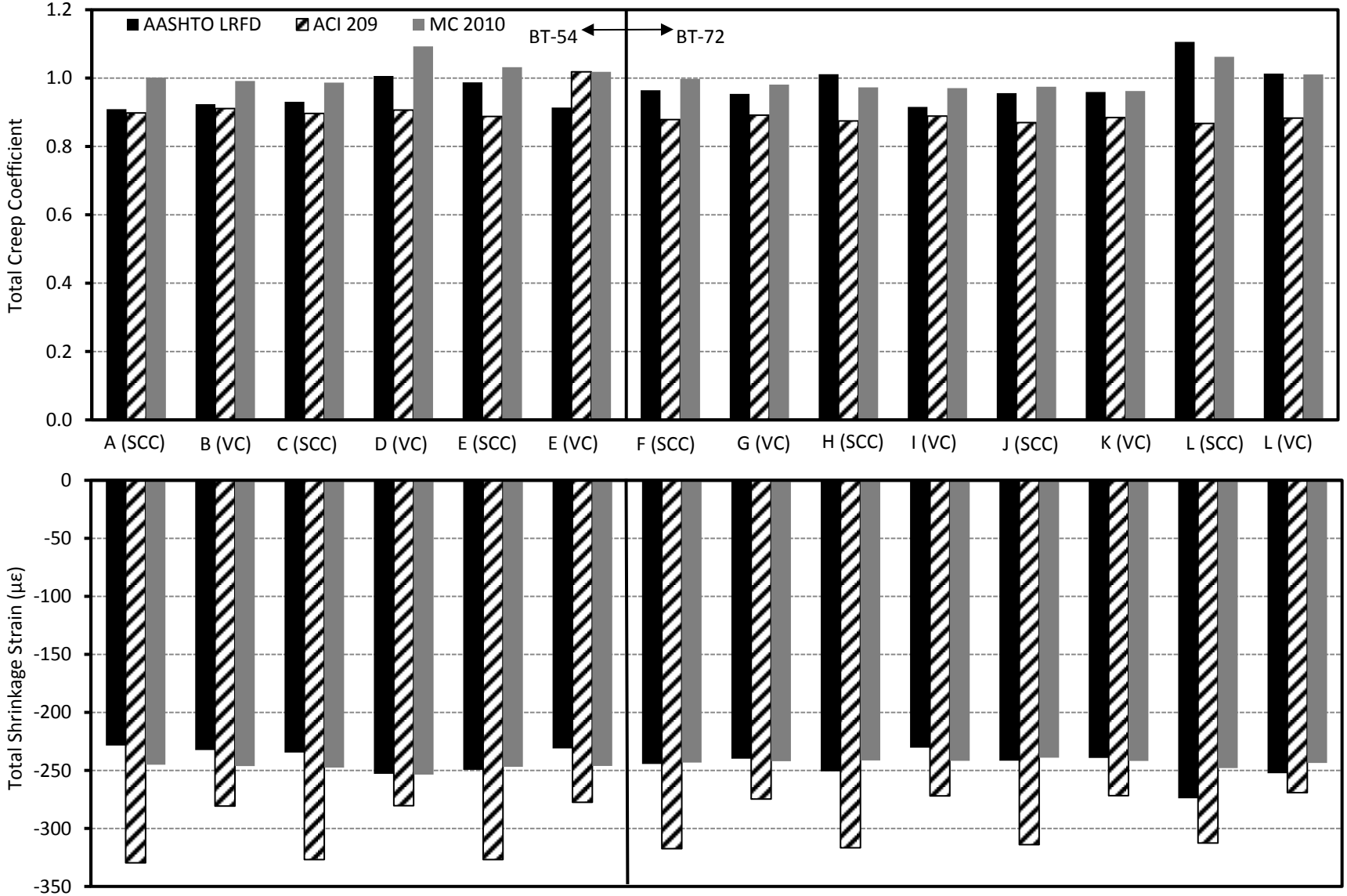

Figure 5-1: Total Creep and Shrinkage Predictions for Each Casting Group—Project 1

5.3.2 Bottom-Flange Strain Analyses

(1 of 3) BT-54 Girders—Project 1

Seven BT-54 girders were cast with self-consolidating concrete (SCC), and seven BT-54 girders were cast with vibrated concrete (VC). The bottom-flange gage, Gage 1, was located in the flange at 6.0 in. from bottom of the girder.

Bottom-flange strains are obtained to represent the prestress loss. The strain *growth* depends on shrinkage and creep. Figures 5.2 and 5.3 demonstrate the trends of measured and predicted internal strains at immediately after transfer, at 56 days, and at erection. Data used for these graphs can be found in Table G-2 in Appendix G.

The points nearest to the origin illustrate the values just after transfer. All of the BT-54 values representing the strains immediately after transfer fall very close to the equality line. At transfer, the SCC girders are predicted better than the VC girders.

On the other hand, internal strains are overpredicted at later ages. Most of the predictions are beyond the +20% error line. Predictions for the VC girders are slightly better than the SCC girders. *fib* MC 2010 predicts bottom-flange strains a little better than other models at 56 days; in contrast, AASHTO LRFD predicts them slightly better at erection.

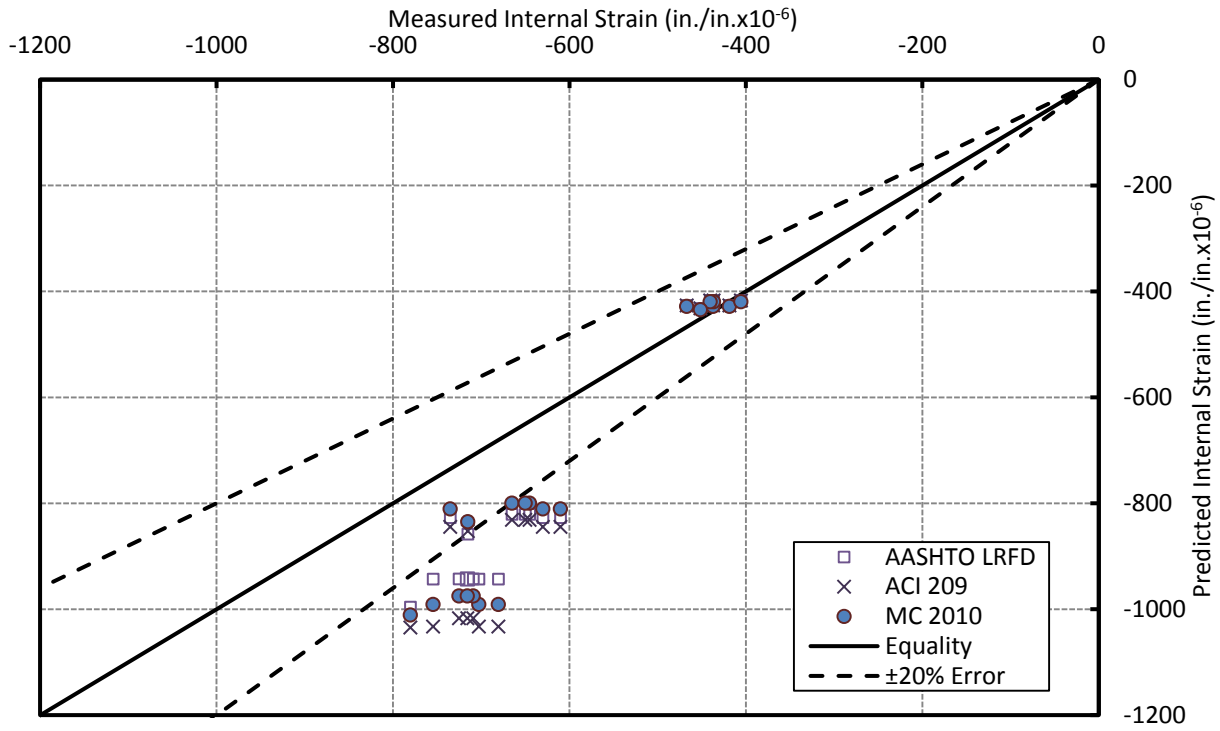

Figure 5-2: Predicted vs. Measured Bottom-Flange Strains—SCC BT-54

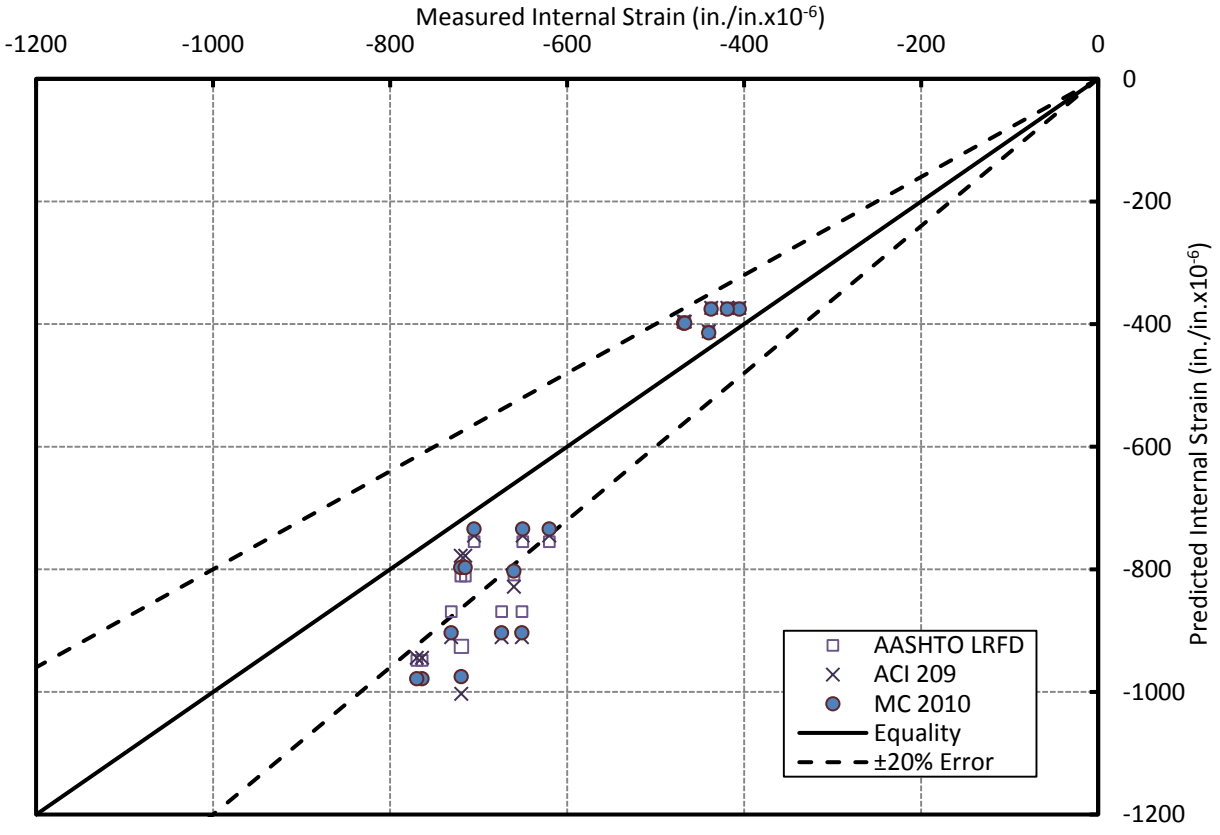

Figure 5-3: Predicted vs. Measured Bottom-Flange Strains—VC BT-54

(2 of 3) BT-72 Girders—Project 1

Seven SCC and seven VC BT-72 girders were analyzed for the bottom-flange strain located at 8.8 in.. Trends of strain predictions can be seen in Figures 5.4 and 5.5. The whole data set is provided in Table G-2.

The internal strains immediately after transfer are predicted better than the ones at the later ages. The initial strains of the SCC girders are predicted a little better than the VC girders.

At 56-day and erection, the estimated internal strains are overpredicted. They fall near the +20% error line. Predictions for the VC girders are better than the ones for SCC similar to the initial strains. Also, the three prediction models reveal similar estimations for the bottom-flange strain.

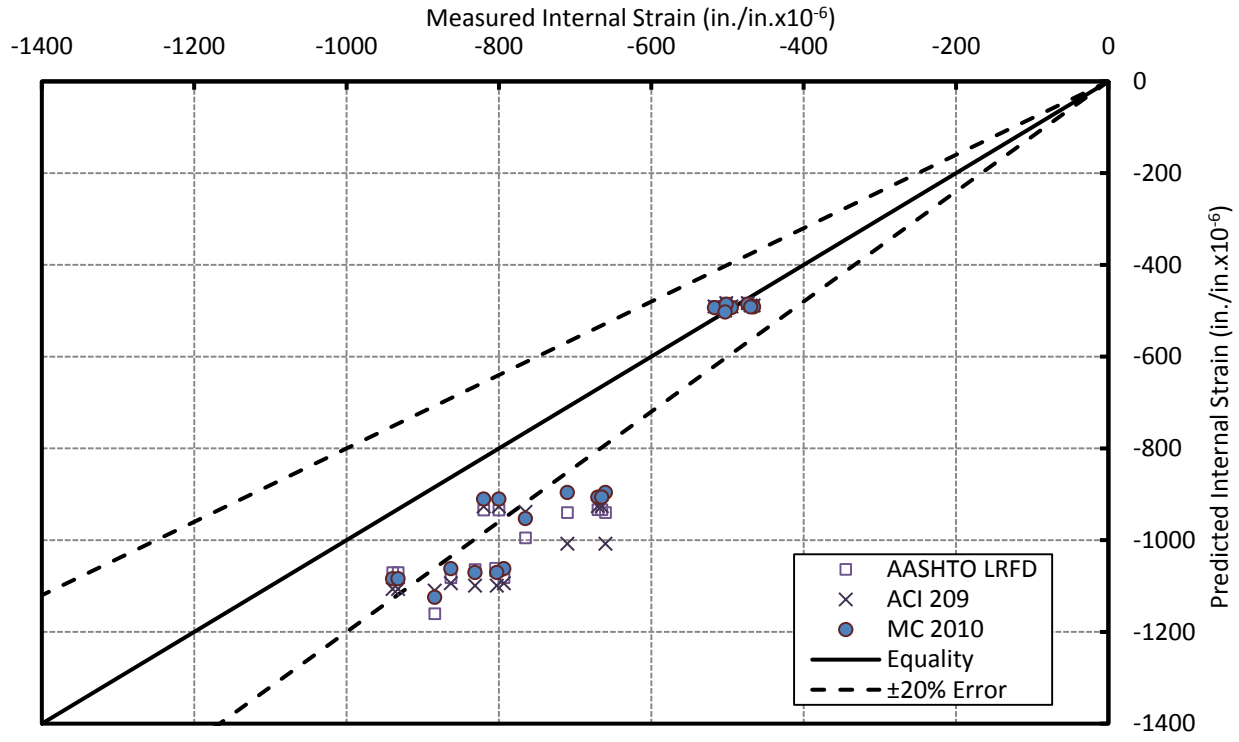

Figure 5-4: Predicted vs. Measured Bottom-Flange Strains— SCC BT-72

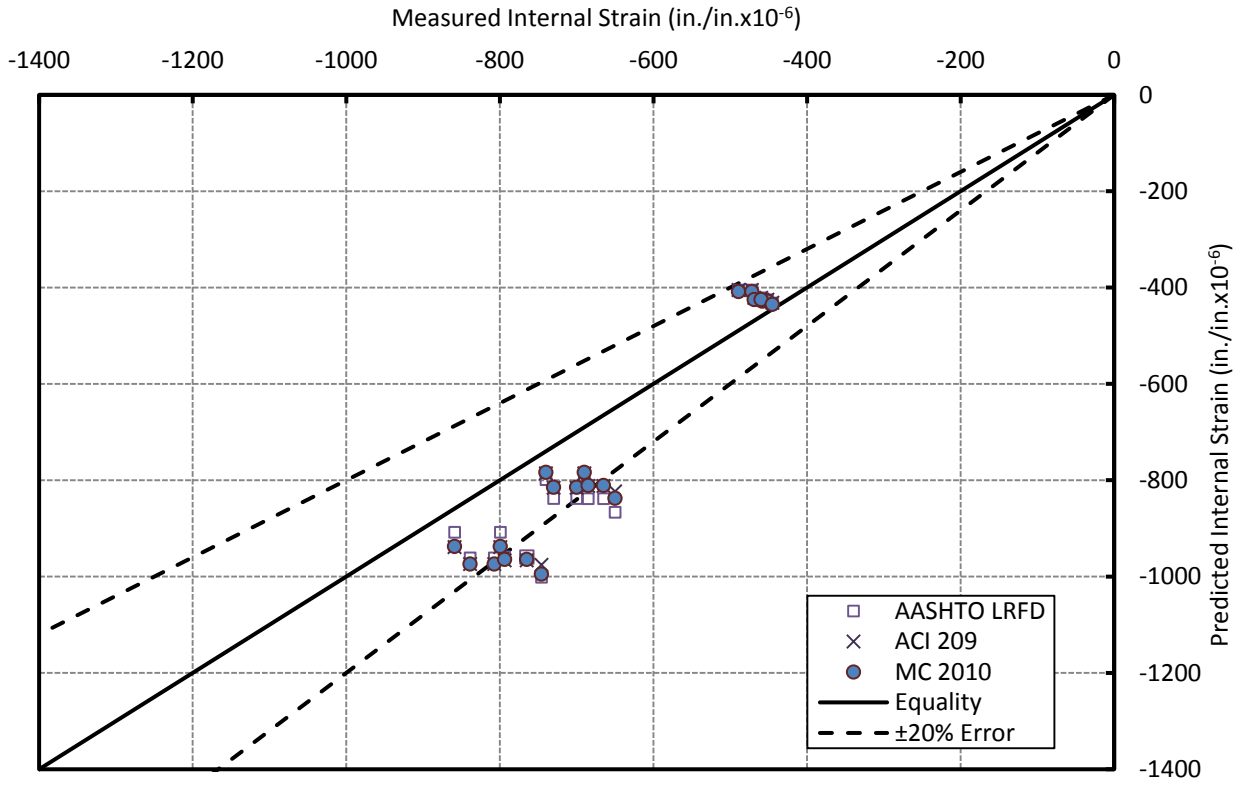

Figure 5-5: Predicted vs. Measured Bottom-Flange Strains— VC BT-72

(3 of 3) Statistical Evaluation of Error for Predicted Bottom-Flange Strains—Project 1

The AASHTO LRFD shrinkage model states to increase the shrinkage strain 20% when concrete is exposed to drying before five days of non-accelerated curing. The 17-hour (5/7 day) curing—the girders in Project 1 are cured less than 17 hours unlike Projects 2, 3, and 4—is the estimated approximate amount if it is exposed to accelerated curing as explained in Section 2.3.7. The analyses performed using the 20% increase in shrinkage strain predictions are labeled as AASHTO LRFD +20 in this thesis.

The calculations for the unbiased estimate of the standard deviation of the prediction errors (UE-StDev) can be found in Section 5.2. Figure 5.6 summarizes the analyses of AASHTO LRFD, AASHTO LRFD +20, ACI 209, and MC 2010. Data used for these graphs can be found in Table H-1 in Appendix H. Values closer to zero mean more accurate predictions.

Strain *growth* is obtained by subtracting the strains at transfer from the strains at later ages. Seven data points are used for this calculation except for the BT-54 VC. The BT-54 VC girders have six data points. Erection times for these girders range from 184 days to 219 days. 100% error at transfer represents a strain value of about 465 με; while, 100% error at later ages represents a value of about 265 με.

At transfer, the strains are mostly underpredicted. In contrast, the strain *growth* predictions are all overestimated at later ages. The bottom-flange strains give an idea about the prestress losses since the prestress strands are concentrated at the bottom flange.

The strains are evaluated in four groups: (i) different prediction models are compared, (ii) comparison of AASHTO LRFD and AASHTO LRFD +20 is made, (iii) the BT-54 and BT-72 girders are compared to each other, and (iv) the comparison of the SCC and VC girders is made.

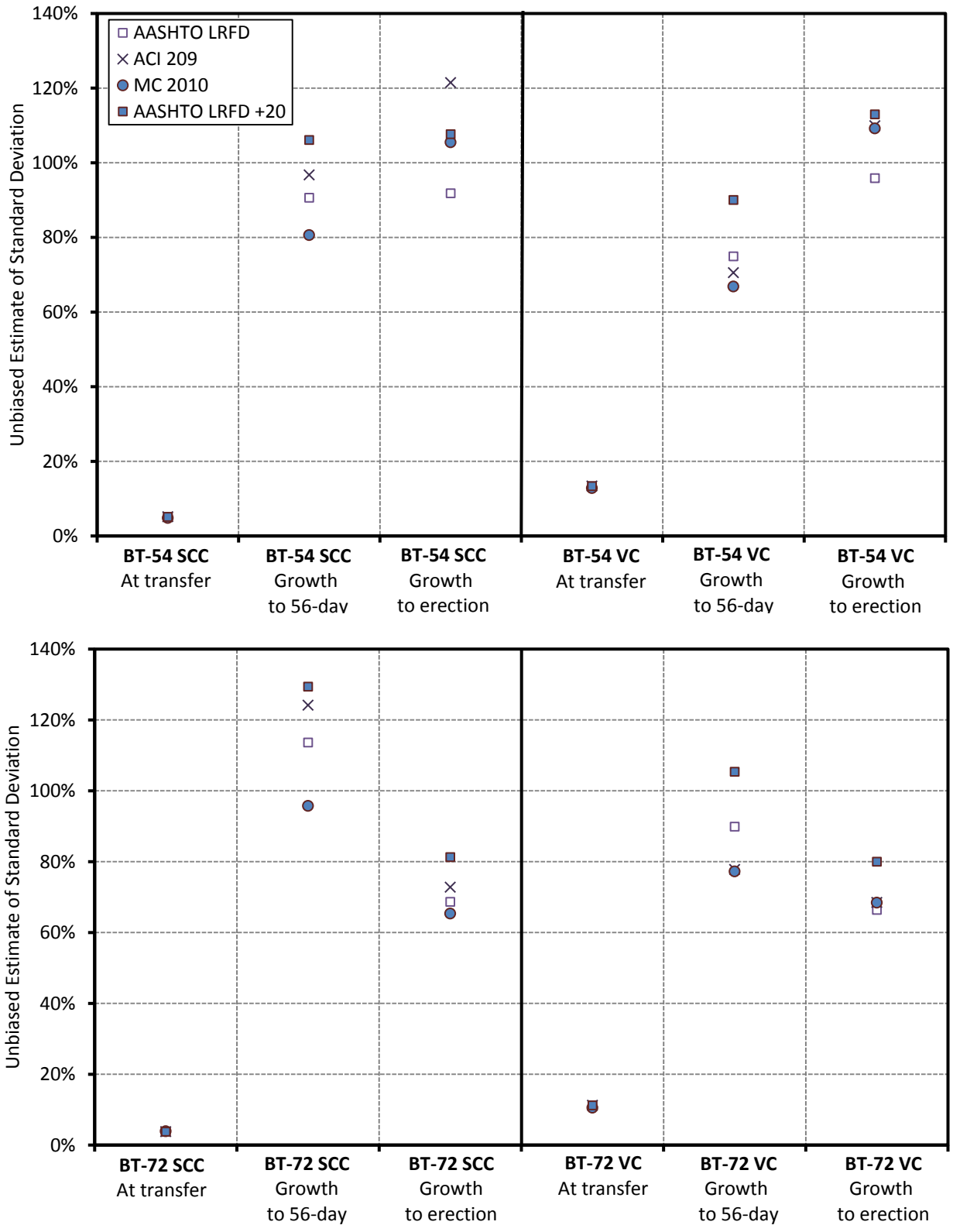

Figure 5-6: Fractional Errors—Bottom-Flange Strains—Project 1

i. Comparison of AASHTO LRFD, ACI 209 and *fib* MC 2010

Only *growth* errors are considered since the initial predictions are same no matter what the prediction model is. *fib* MC 2010 estimates the strain *growth* to 56-day with the least error possibly due to the eliminated autogenous shrinkage up to the benchmark reading. AASHTO LRFD generally best estimates the strain *growth* to erection than AASHTO LRFD.

ii. Comparison of AASHTO LRFD and AASHTO LRFD +20

AASHTO LRFD +20 includes the 20% increase in the shrinkage strain predictions. AASHTO LRFD estimates the bottom-flange strains more accurately. Project 1 is the only project checked for this increase. The curing durations of these girders were recorded below 17 hours, and they may have not been accurate. All in all, the 20% increase in shrinkage strain predictions is not reasonable for the bottom-flange strain predictions.

iii. Comparison of BT-54 and BT-72 girders

The creep and shrinkage predictions were somewhat same for the BT-54 and BT-72 girders; thus, the effect of the geometry on the time-dependent behavior can be seen explicitly. Both of the BT-54 and BT-72 girders are estimated accurately, at transfer. For the BT-54 girders, the error in strain *growth* increases with age unlike the BT-72 girders. The predicted strains for the BT-54 girders are slightly better at 56 days; while, the predictions for the BT-72 girders are fairly better at erection.

iv. Comparison of the SCC and VC girders

Initial strains for the SCC girders are slightly better than the strain for the VC girders. At 56 days, strain *growth* of the VC girders is predicted a little bit better. At erection, both of the SCC and VC girders have the same fractional error since the predicted creep and shrinkage were same. In terms of the bottom-flange strains—and the prestress losses, the SCC and VC girders behave more or less similarly.

5.3.3 Curvature Analyses

(1 of 3) BT-54 Girders—Project 1

Curvature readings were possible for the four SCC and the four VC girders. The gauges were located at 6.0 in. and at 52 in. from the bottom.

Comparison of midspan curvature is made since camber predictions utilize the moment-area method. Curvature *growth* depends largely on creep. Figures 5-7 and 5-8 demonstrate the predicted and measured midspan curvatures at immediately after transfer, at 56-day after transfer, and at erection. The data used for the graphs are given in Table G-3 in Appendix G.

The initial curvature predictions are mostly overpredicted, and fall within the +20% error line. The VC girders seem to predict the initial curvature slightly better than the SCC girders.

The long-term predictions remain mostly within the ±20% error lines, and they are generally overestimated. The VC girders are predicted more accurately than the SCC girders at later ages. *fib* MC 2010 seems to predict curvatures less accurately than AASHTO LRFD and ACI 209. The total values can be misleading to compare the prediction models since the initial errors are reflected in the errors at later ages.

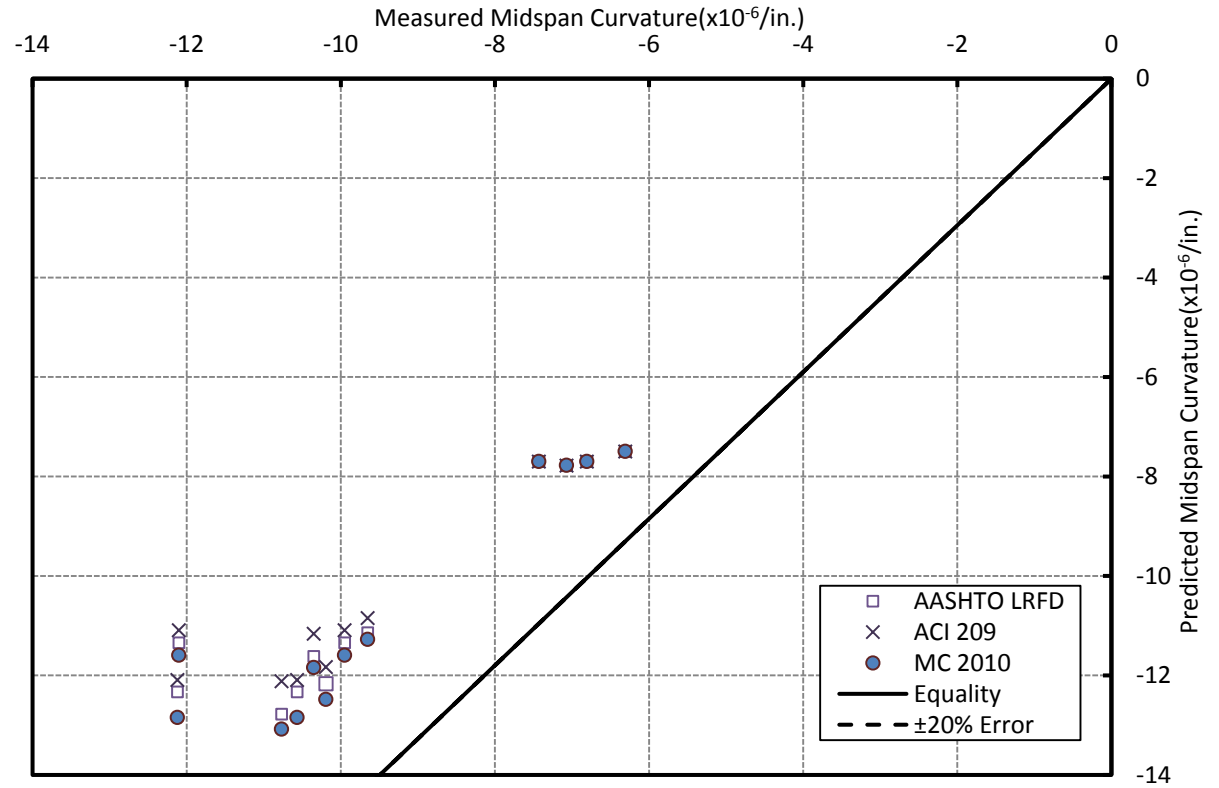

Figure 5-7: Predicted vs. Measured Midspan Curvature—SCC BT-54

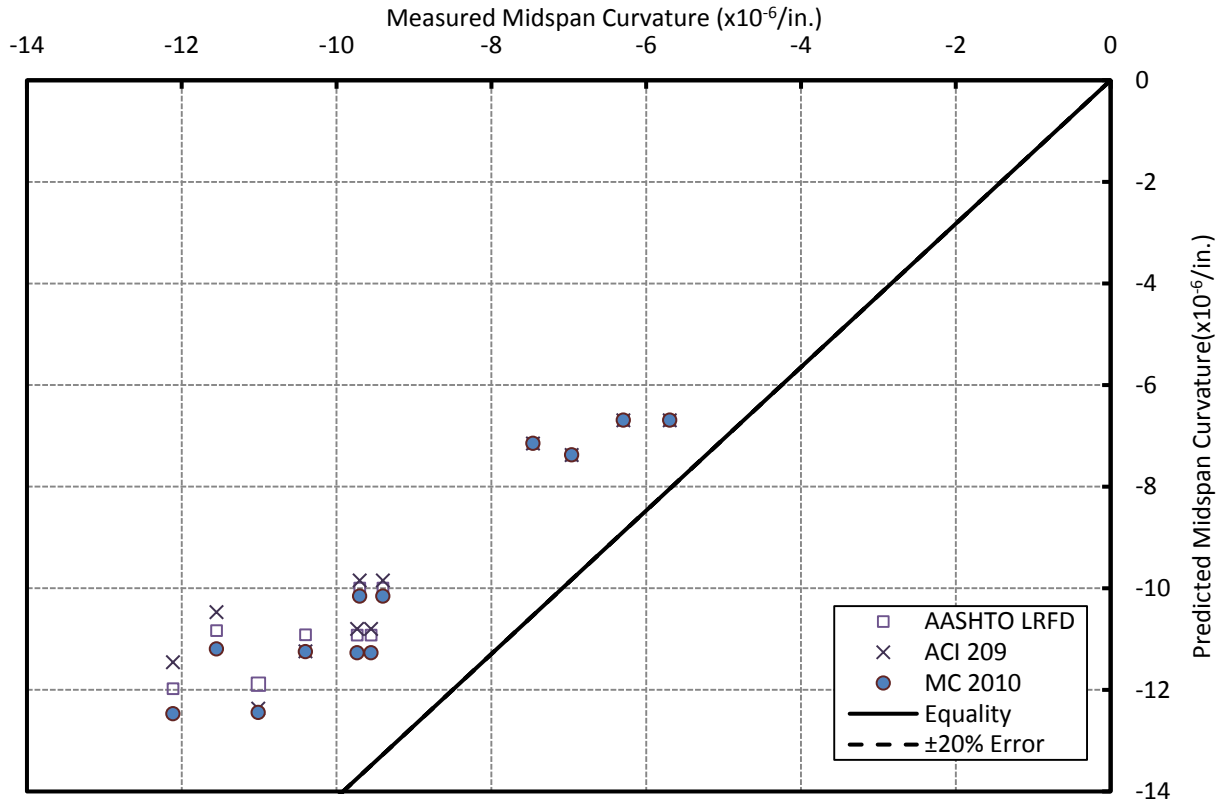

Figure 5-8: Predicted vs. Measured Midspan Curvatures—VC BT-54

(2 of 3) BT-72 Girders—Project 1

The curvature calculations were possible for the four SCC and the four VC BT-72 girders. The curvature values are calculated by using the gages at 8.8 in. and at 70 in. from the bottom. However, the girder—72-12C, a VC girder in the casting group K—has the strain readings available at 8.8 in. and at 51.0 in..

The curvature predictions are plotted in Figures 5-9 and 5-10. The initial curvatures are overpredicted. The predictions for the VC girders seem to be more reliable and they fall mostly within the ±20% error lines.

At the later ages, the VC girders remain within the ±20% error lines; the SCC girders have curvature predictions falling beyond the +20% error line. The initial errors are obviously reflected in the long-term predictions. The ACI 209 prediction model gives a little more accurate results for the SCC girders; however, it is hard to draw a conclusion for the VC girders.

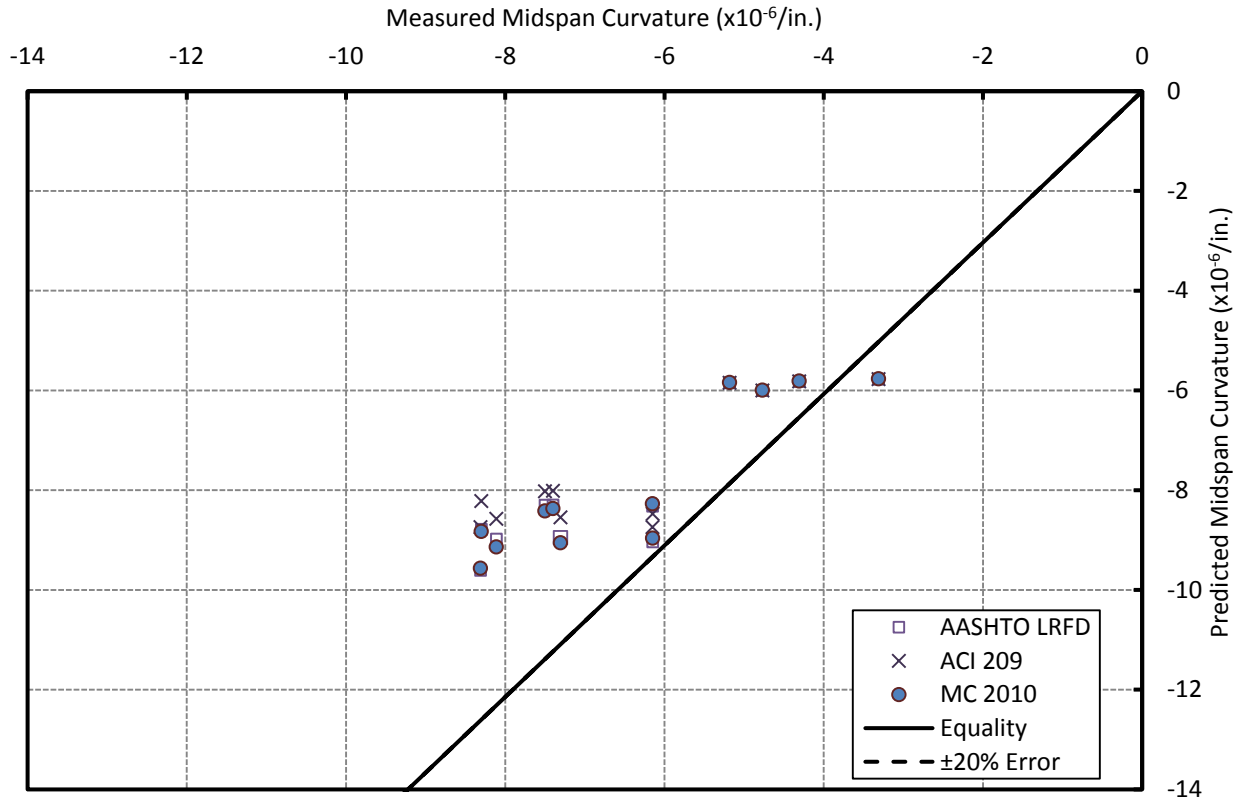

Figure 5-9: Predicted vs. Measured Midspan Curvatures— SCC BT-72

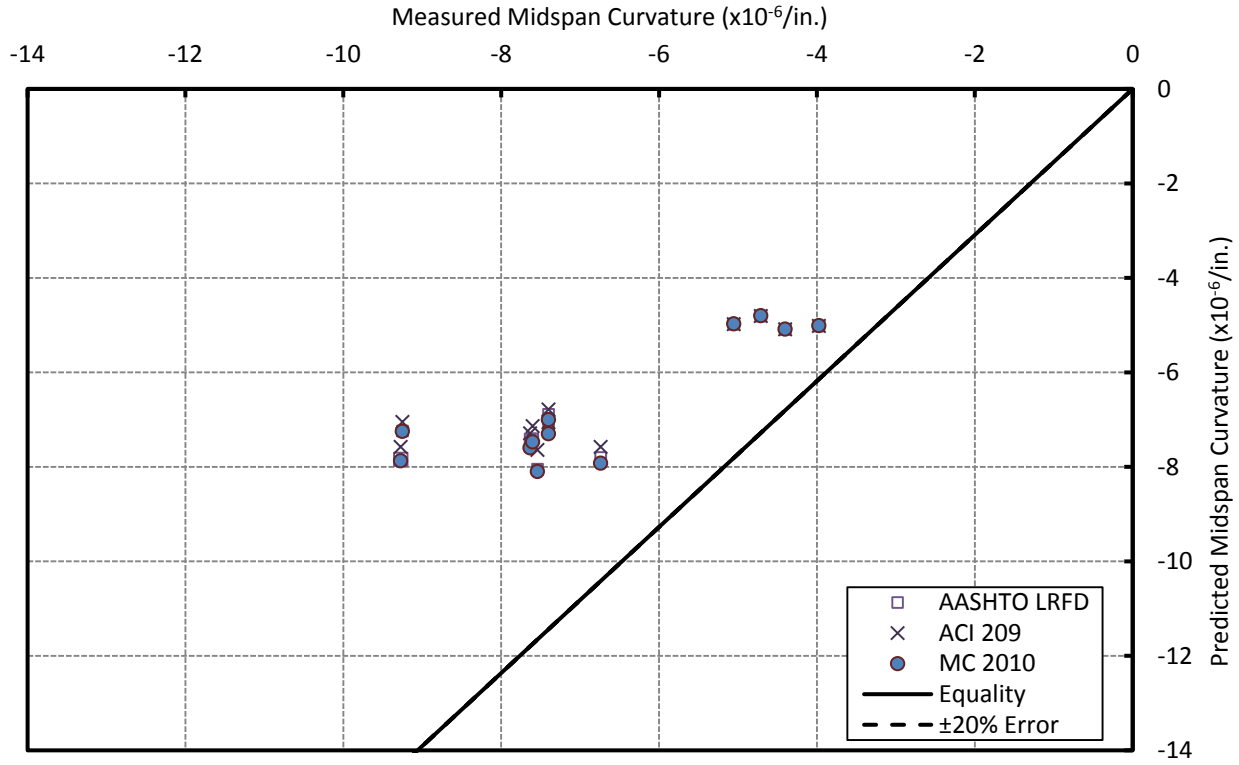

Figure 5-10: Predicted vs. Measured Midspan Curvatures—VC BT-72

(3 of 3) Statistical Evaluation of the Error for the Predicted Curvatures—Project 1

Figure 5.10 illustrates the evaluated analyses for the bottom-flange strains. The scale is different than the scale used for the strain analyses. The data used for plotting can be found in Table H-2 in Appendix H. Four data points are used for each calculation.

The initial predictions are all overpredicted. The *growth* values are composed of the under- and overestimations. On average, the BT-54 girders are overpredicted, and the BT-72 girders are underpredicted.

100% error for the BT-54 girders represents a curvature amount of 6.3×10^{-6} 1/in. at transfer; whereas, the 100% error represents a curvature value of 3.7×10^{-6} 1/in. for the *growth*. For the SCC BT-72 girders, it is about 3.3×10^{-6} 1/in. for the initial curvature and the *growth*, and it climbs up to 4.0×10^{-6} 1/in. for the VC BT-72 girders.

The comparisons are investigated in three main categories: (i) different prediction models are compared to each other, (ii) AASHTO LRFD and AASHTO LRFD +20 are compared, (iii) comparison of BT-54 and BT-72 girders is made, and (iv) the SCC and VC girders are compared.

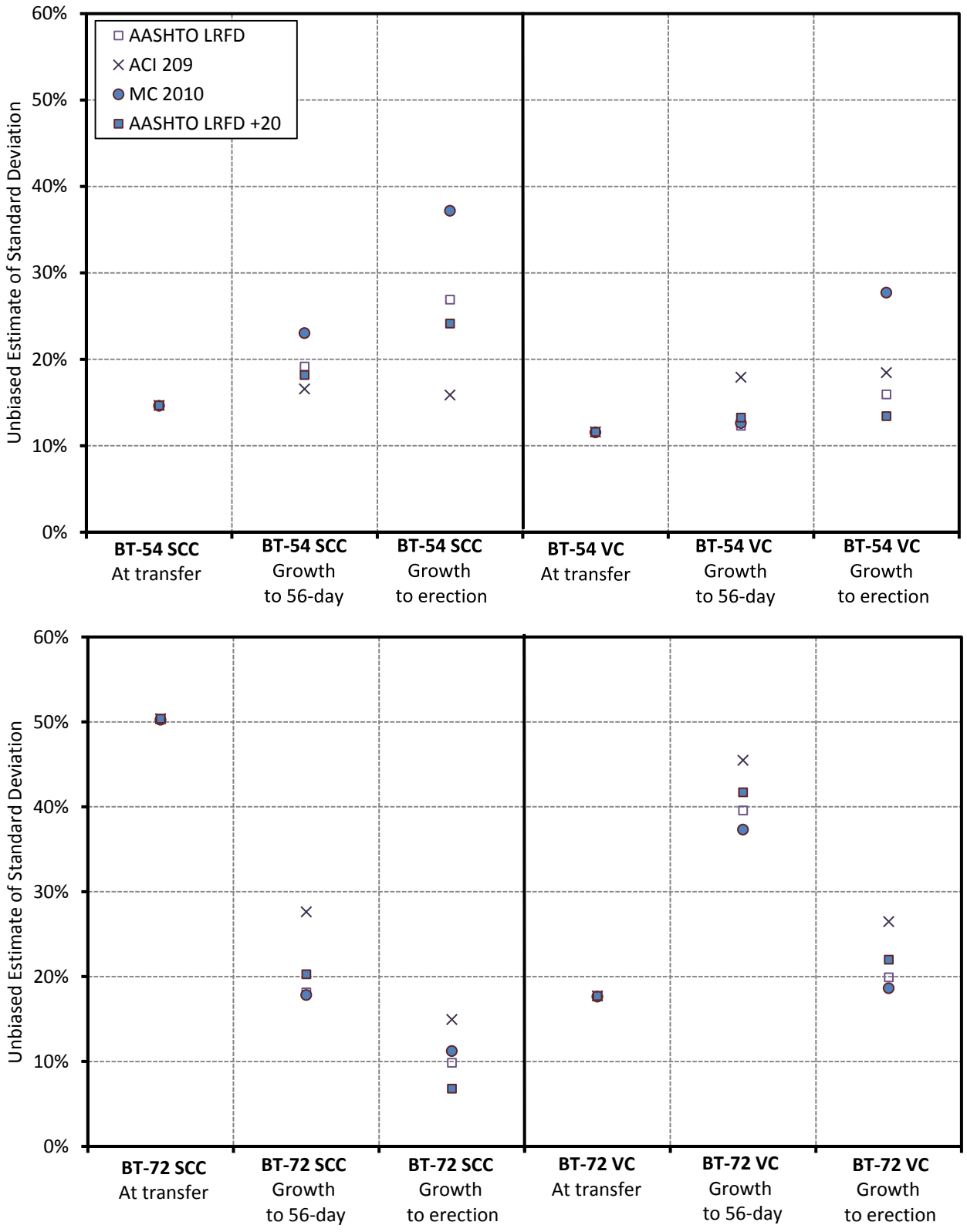

Figure 5-10: Fractional Errors—Midspan Curvatures—Project 1

i. Comparison of AASHTO LRFD, ACI 209 and *fib* MC 2010

The initial values are predicted with the same amount of error for the different prediction models. The unbiased estimates show that the prediction models estimate the curvature *growth* somewhat similar. On the other hand, the arithmetical average of the errors reveal that ACI 209 is the best model for the overpredicted BT-54 girders, and *fib* MC 2010 gives the most precise predictions for the underpredicted BT-72 girders. This conclusion is consistent with the rank of predicted total creep coefficients: ACI 209 estimates the least creep for the underpredicted BT-54 girders and MC 2010 estimates the greatest creep for the overpredicted BT-72 girders.

ii. Comparison of AASHTO LRFD and AASHTO LRFD +20

AASHTO LRFD +20 includes the 20% increase in the shrinkage strain predictions. It estimates the curvature *growth* of the overpredicted BT-54 girders more accurately. AASHTO LRFD estimates the curvature growth of the underpredicted BT-72 girders more accurately.

iii. Comparison of BT-54 and BT-72

At transfer, the BT-54 girders are better predicted than the BT-72 girders. At later ages, the BT-72 girders are predicted a little better than the BT-54 girders. The errors in the predictions of the BT-54 girders increase at erection; however, the errors for the BT-72 girders decrease on average. Having the non-uniform distribution of estimations complicates the comparison of the BT-54 and BT-72 girders.

iii. Comparison of girders with SCC and VC mixes

For the overpredicted BT-54 girders, the VC girders are predicted slightly better than the SCC girders. However, the SCC girders have more accurate estimations for the underpredicted BT-72 girders. Drawing a conclusion for the SCC and VC girders can be misleading due to the non-uniform distribution.

5.3.4 Camber Analyses

(1 of 3) BT-54 Girders—Project 1

Midspan cambers are analyzed for the seven SCC and the seven VC BT-54 girders as shown in Figures 5.11 and 5.12. They include the camber predictions just after transfer, at 56 days, and at erection. The BT-54 girders were 1174 inches in length.

The initial predictions are mostly overestimated. They depend on the modulus of elasticity; estimations are calculated similarly regardless of the prediction model. The VC girders are predicted more accurately than the SCC girders. The modulus of elasticity for the VC girders was 8% greater than the SCC girders.

At later ages, the predictions are all overestimated. Camber *growth* depends largely on creep. Most of the SCC girders and half of the VC girders have predictions falling beyond the +20% error line. Among the prediction models, ACI 209 predicts the least camber, and *fib* MC 2010 estimates the greatest camber. However, deciding the accuracy of the prediction models can be misleading by looking at the total cambers. Thus, the camber *growth* will be considered for the statistical evaluation in the last subsection.

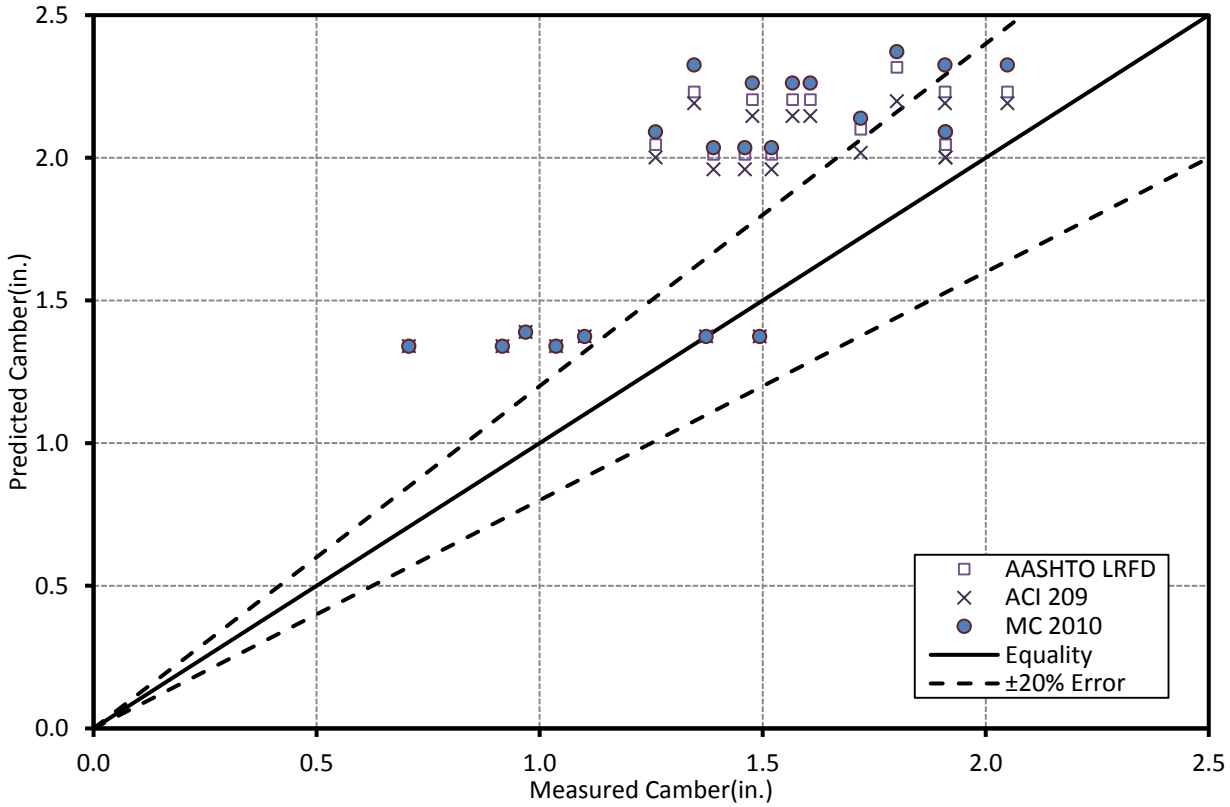

Figure 5-11: Predicted vs. Measured Midspan Cambers—SCC BT-54

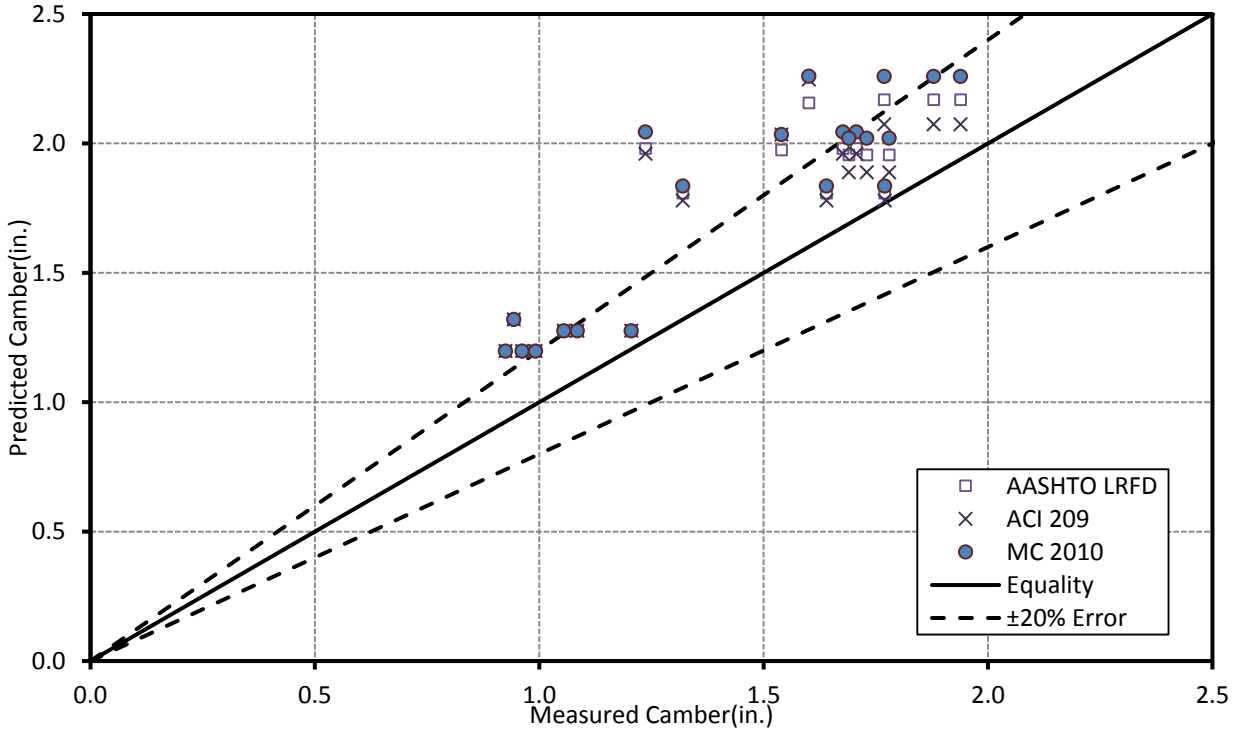

Figure 5-12: Predicted vs. Measured Midspan Cambers—VC BT-54

(2 of 3) BT-72 Girders—Project 1

Seven SCC and seven VC BT-72 girders are analyzed for camber. The predicted and measured cambers are plotted in Figures 5.13 and 5.14. They consist of the midspan cambers immediately after transfer, at 56 days, and at erection. The length of the BT-72 girders was 1620 inches.

The initial camber predictions are overestimated and not based on the selected prediction model since they depend on the elastic properties. The VC girders have more accurate estimations than the SCC girders. The modulus of elasticity of the VC girder was 15% less than the MOE of the VC girders.

The predictions at later ages are also overestimated. The VC girders are predicted more accurately than the SCC girders. The ACI 209 camber predictions are the least in amount; while, the *fib* MC 2010 camber predictions are the greatest. The accuracy of the prediction models will be discussed in the following subsection by evaluating the camber *growth*.

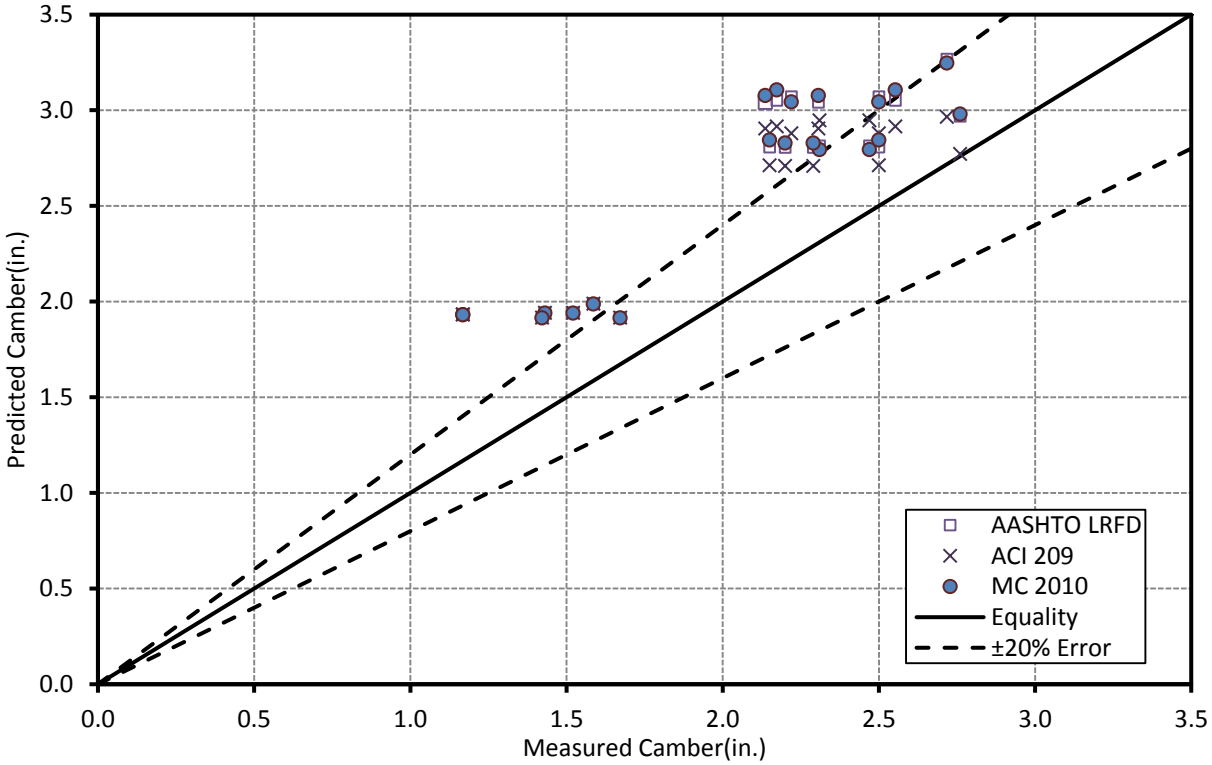

Figure 5-13: Predicted vs. Measured Midspan Cambers— SCC BT-72

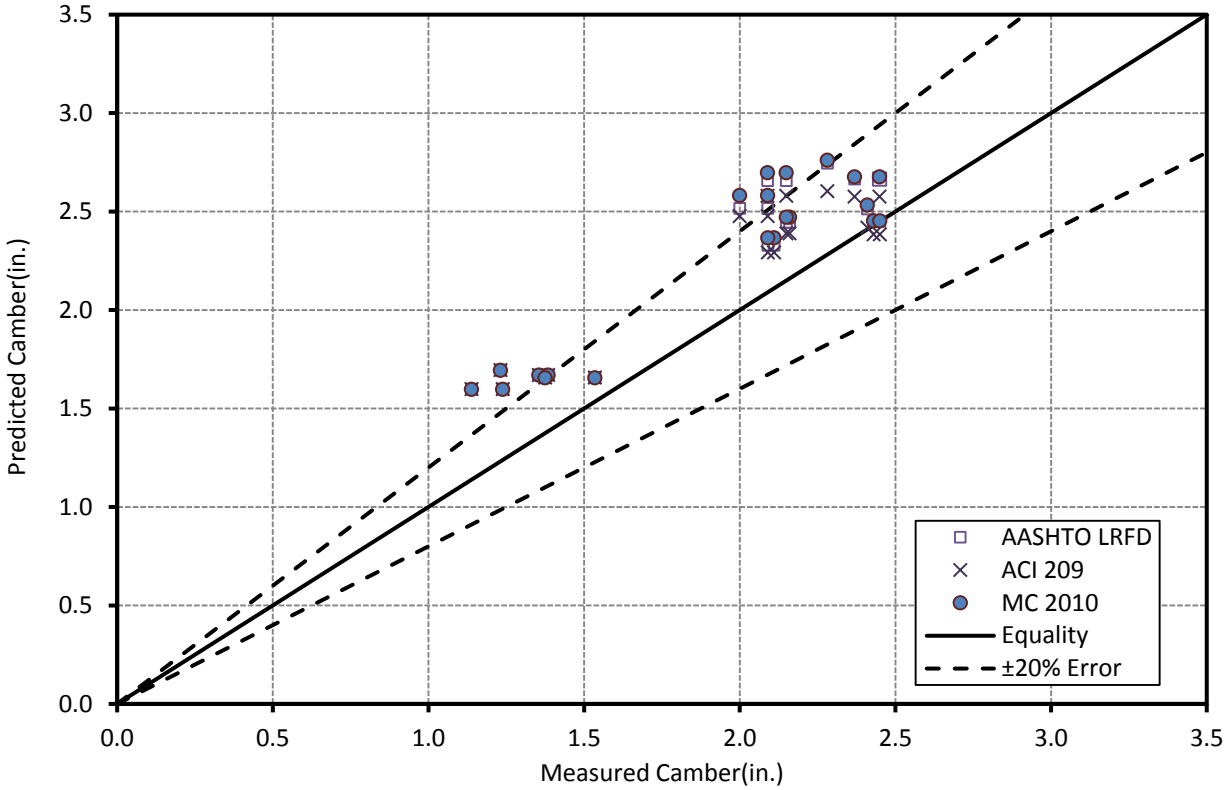

Figure 5-14: Predicted vs. Measured Midspan Camber—VC BT-72

(3 of 3) Statistical Evaluation of the Error for Predicted Cambers—Project 1

The unbiased estimates plotted in Figure 5.15 are evaluated to quantify the errors in the camber predictions. The graph is scaled differently from the earlier evaluations. Camber *growth* was determined by subtracting the initial camber from the cambers at later ages. Six points are used for the calculations, and erection date for these girders extends from 184 days to 219 days. Data used for these graphs can be found in Table H-3 in Appendix H.

At transfer and erection, the camber predictions are entirely overestimated. At 56 days, the *growth* predictions are overestimated on average. 100% error for the BT-54 girders represents a camber error of 0.90 in. at transfer; whereas, the 100% error represents a camber of 0.35 in. for the *growth* predictions. For the BT-72 girders, it is about 1.26 in. at transfer, and it is 0.89 in. for the *growth* estimations.

On the other hand, Johnson (2012) identified that cracking due to temperature gradient and existing hold-down points are the potential reasons behind the errors. He stated that the cracking occurred after the formwork removal may not have been accounted accurately even though the temperature corrections were applied. Also, he observed that the hold-down points may have limited the girders to move upward at transfer. The hold down-points can be seen in Figure B-2 in Appendix B.

The results are discussed in four aspects: (i) different prediction models are compared to each other, (ii) AASHTO LRFD and AASHTO LRFD +20 are compared to each other, (iii) the differences between the BT-54 and BT-72 girders are contrasted, and (iv) the comparison of the SCC and VC girders are completed.

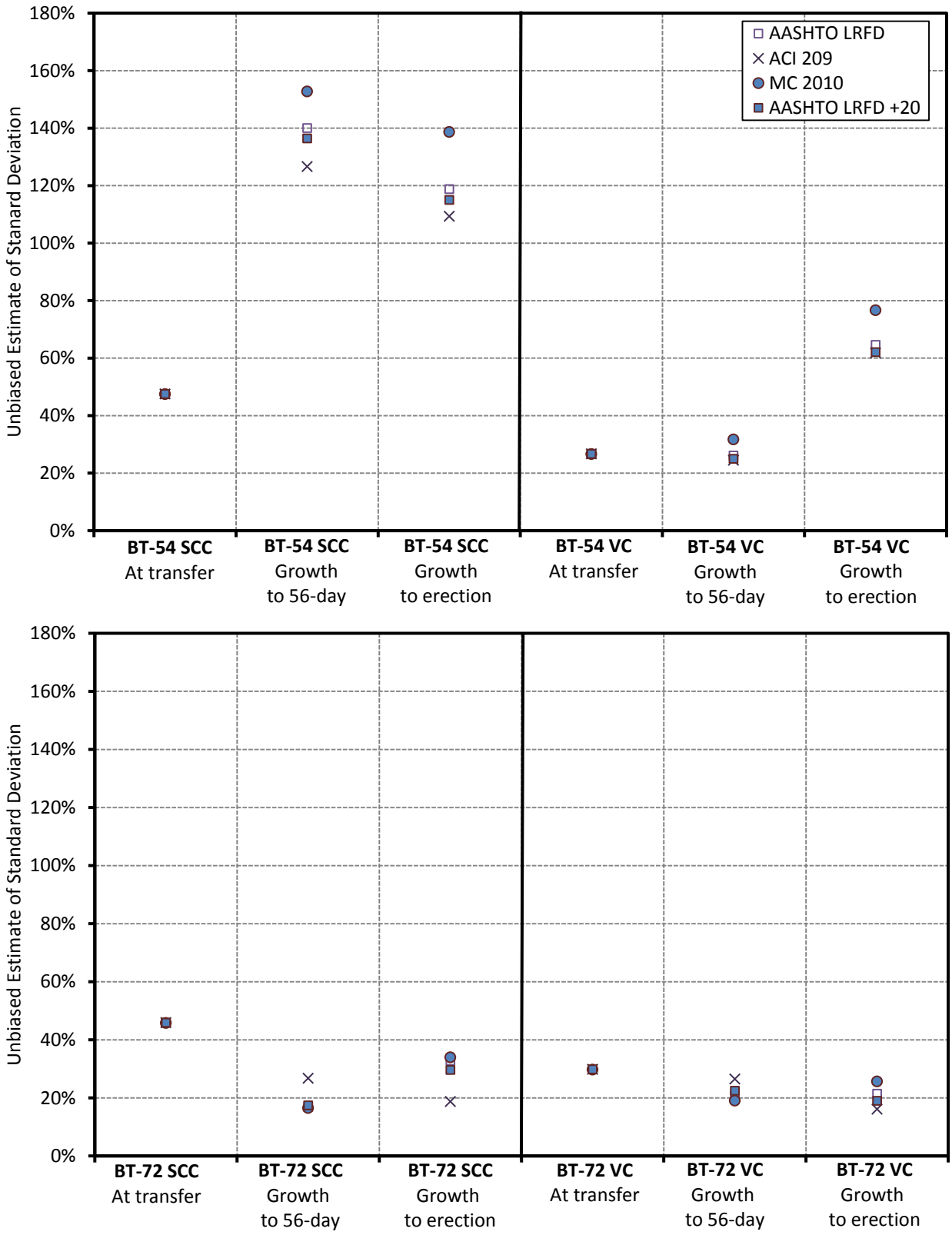

Figure 5-15: Fractional Errors—Midspan Cambers—Project 1

i. Comparison of AASHTO LRFD, ACI 209 and *fib* MC 2010

The initial cambers are not controlled by the chosen prediction models but based on the elastic properties. The same initial predictions are obtained for all methods. At 56 days, AASHTO LRFD and ACI 209 better predict the camber *growth* for the BT-54 girders than *fib* MC 2010. AASHTO LRFD and MC 2010 better estimate the 56-day *growth* for the BT-72 girders than ACI 209. At erection, ACI 209 reveals the best camber estimations. AASHTO LRFD predictions are better than MC 2010. The prediction models with the least and greatest creep predictions estimate the least and greatest camber *growt*h in the same order.

ii. Comparison of AASHTO LRFD and AASHTO LRFD +20

AASHTO LRFD +20 includes the 20% increase in the shrinkage strain predictions and estimates the camber *growth* with a little more accuracy than AASHTO LRFD.

iii. Comparison of BT-54 and BT-72 girders

At transfer, both BT-54 and BT-72 girders are predicted with the same accuracy. The errors in the BT-54 girders increase gradually at later ages unlike the BT-72 girders. At later ages, BT-72 is estimated remarkably better than BT-54.

iv. Comparison of girders with SCC and VC mixes

At transfer, VC is predicted more precisely than SCC, which is largely related with the initial MOE. At later ages, the VC predictions are better than the SCC girders. Additionally, the *growth* errors in the SCC BT-54 girders are considerably large probably due to the camber reading errors.

5.4 Project 2: AASHTO Type I

5.4.1 Total Creep Coefficient and Total Shrinkage Strain

Creep and shrinkage deformations are the main reasons for the rising or falling trends of the time-dependent responses. Strain predictions at later ages are under control of the estimated shrinkage and creep. The long-term curvature and camber estimations significantly rely on the creep deformation.

For the AASHTO Type I girders, the total creep coefficient and total shrinkage strain are predicted up to the erection and plotted in Figure 5-16. The erection days for STD-M, SCC-MS, and SCC-HS are 110, 167 and 214, respectively.

The estimated total creep coefficient varies between 0.76 and 1.22. The least ultimate creep coefficients for STD-M and SCC-MS are obtained with the ACI 209 model; whereas, AASHTO LRFD reveals the highest creep for them. Yet, AASHTO LRFD predicts the highest creep predictions for the high-strength girders. The AASHTO LRFD and *fib* MC 2010 predictions drop for the SCC-HS girders even though the analysis duration is greater.

The shrinkage strains are predicted within the range of -190 με and -300 με. The MC 2010 shrinkage model excludes shrinkage prior to the benchmark point calculated to be between -26 με and -57 με. For other predictions models, it is not greater than -5 με as provided in Table G-1 in Appendix G.

The *fib* MC 2010 and ACI 209 strain predictions tend to elevate in magnitude as the concrete strength increases; while, the AASHTO LRFD predictions drop considerably for the SCC-HS girders. AASHTO LRFD estimates the highest shrinkage amount for STD-M and SCC-MS, and *fib* MC 2010 predicts the least shrinkage in magnitude. ACI 209 predicts the largest shrinkage for the SCC-HS girders.

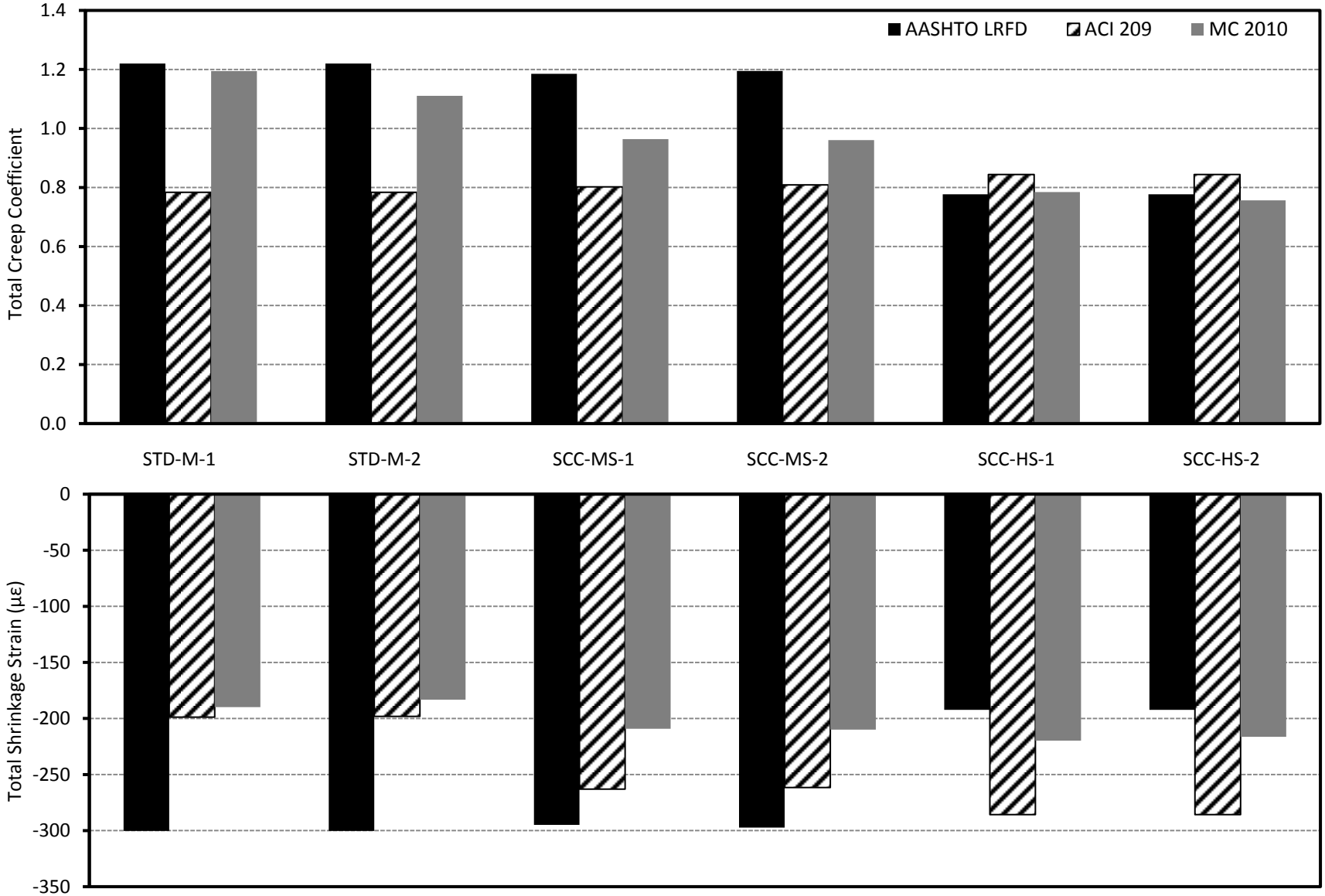

Figure 5-16: Total Creep and Shrinkage Predictions—Project 2

5.4.2 Bottom-Flange Strain Analyses

(1 of 4) STD-M Girders

Two moderate-strength Type I girders were produced with the VC mixtures. Bottom VWSG, Gage 1, was located in the flange at 3.3 in. from bottom of the girder. Also, the recorded strain values were corrected to account for the temperature gradient.

Figure 5-17 represents the trend of measured and predicted bottom-flange strais at immediately after transfer, at 56 days, and at 110 days. The points closest to the origin illustrate the values just after transfer. Initial values are estimated less than the measured ones and they fall very close to the -20% error line.

At later ages, AASHTO LRFD predicts the shrinkage very close to the equality line. *fib* MC 2010 seems to predict better than ACI 209. Predictions at later ages fall mostly within the ±20% error line.

(2 of 4) SCC-MS Girders

Two moderate-strength Type I girders were cast with the SCC mixtures. GGBF slag was also used different than the STD-M girders. Bottom VWSG, Gage 1, was located in the flange at 3.3 in. from bottom of the girder.

Figure 5-18 shows the measured versus predicted internal strains. Initial values are predicted very close to the equality line. At later ages, *fib* MC 2010 and ACI 209 predict the bottom-flange strains more accurately. The AASHTO LRFD predictions fall above the +20% error line.

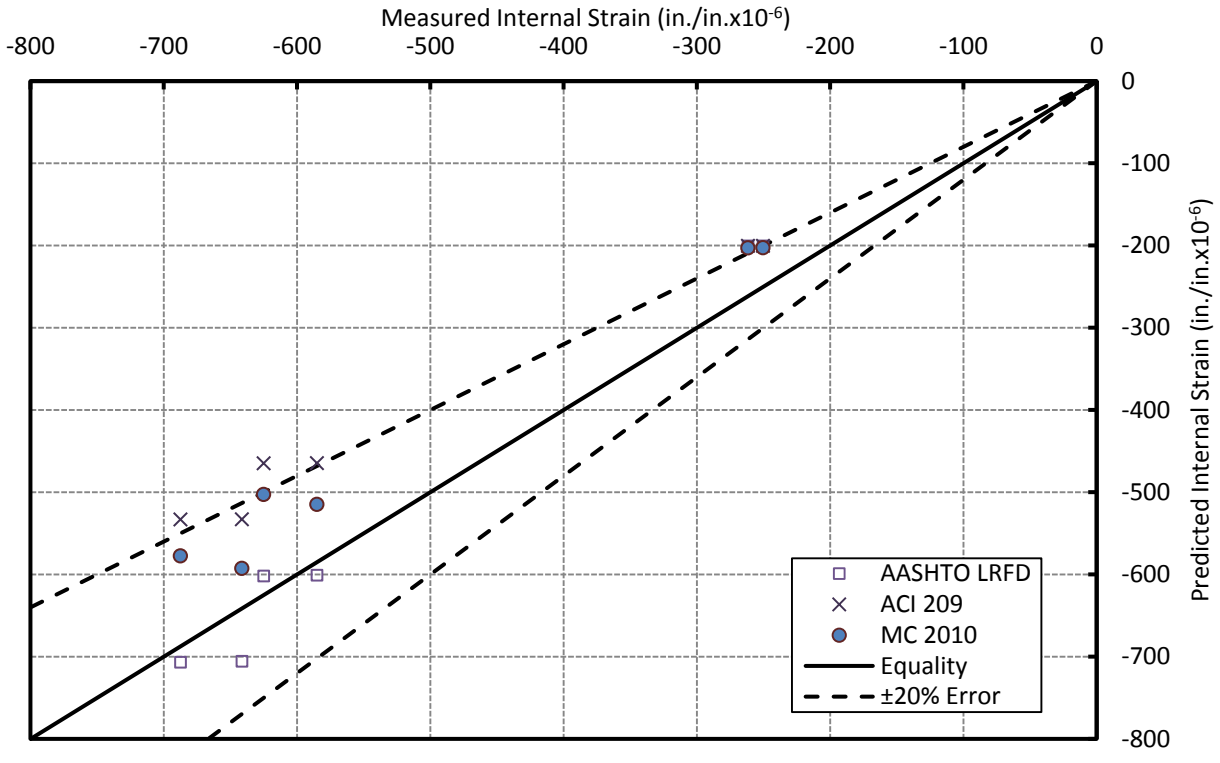

Figure 5-17: Predicted vs. Measured Bottom-Flange Strains—Type I—STD-M

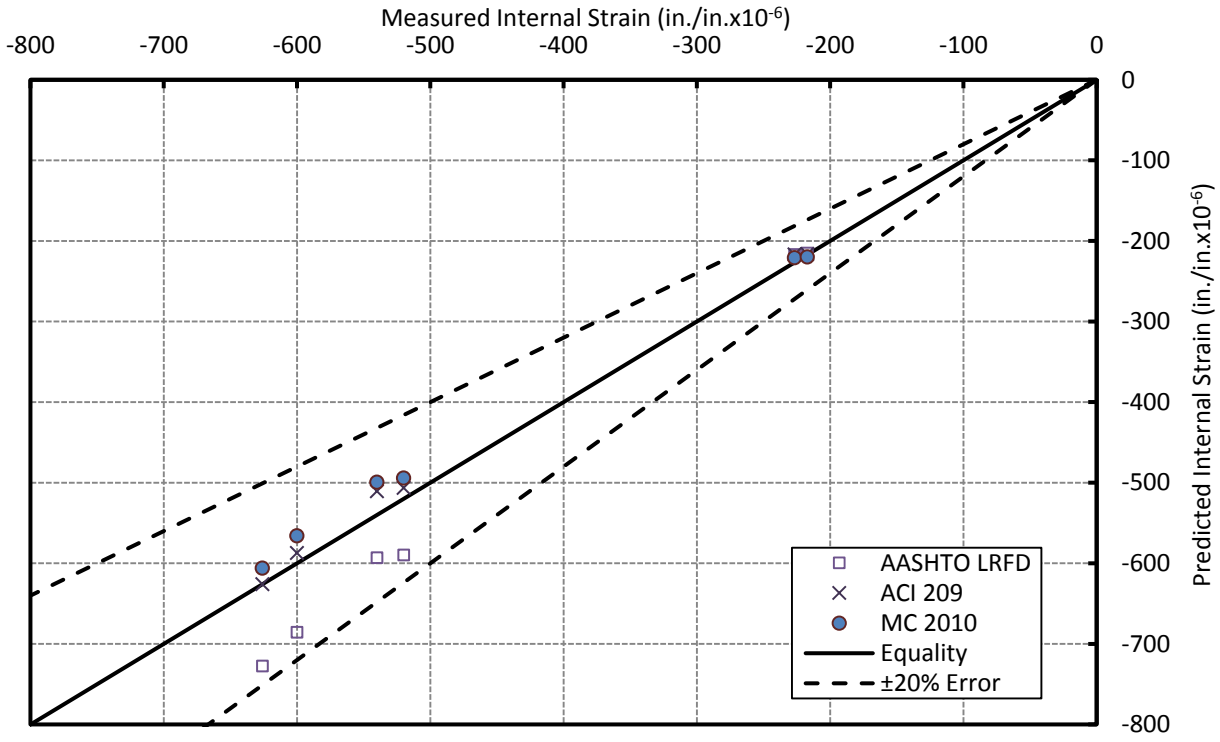

Figure 5-18: Predicted vs. Measured Bottom-Flange Strains—Type I—SCC-MS

(3 of 4) SCC-HS Girders

Two high-strength Type I girders were cast with the SCC mixtures. Bottom VWSG, Gage 1, was located in the flange at 3.0 in. for the first girder and at 3.4 in. for the second.

Figure 5-19 represents the strain predictions and readings at immediately after transfer, at 56 days, at 110 days, and at 214 days after transfer.

The initial predictions are estimated accurately. Nonetheless, the bottom-flange strains are overpredicted at later ages, and fall beyond the 20% error line. *fib* MC 2010 seems to be the best model for the long-term strains.

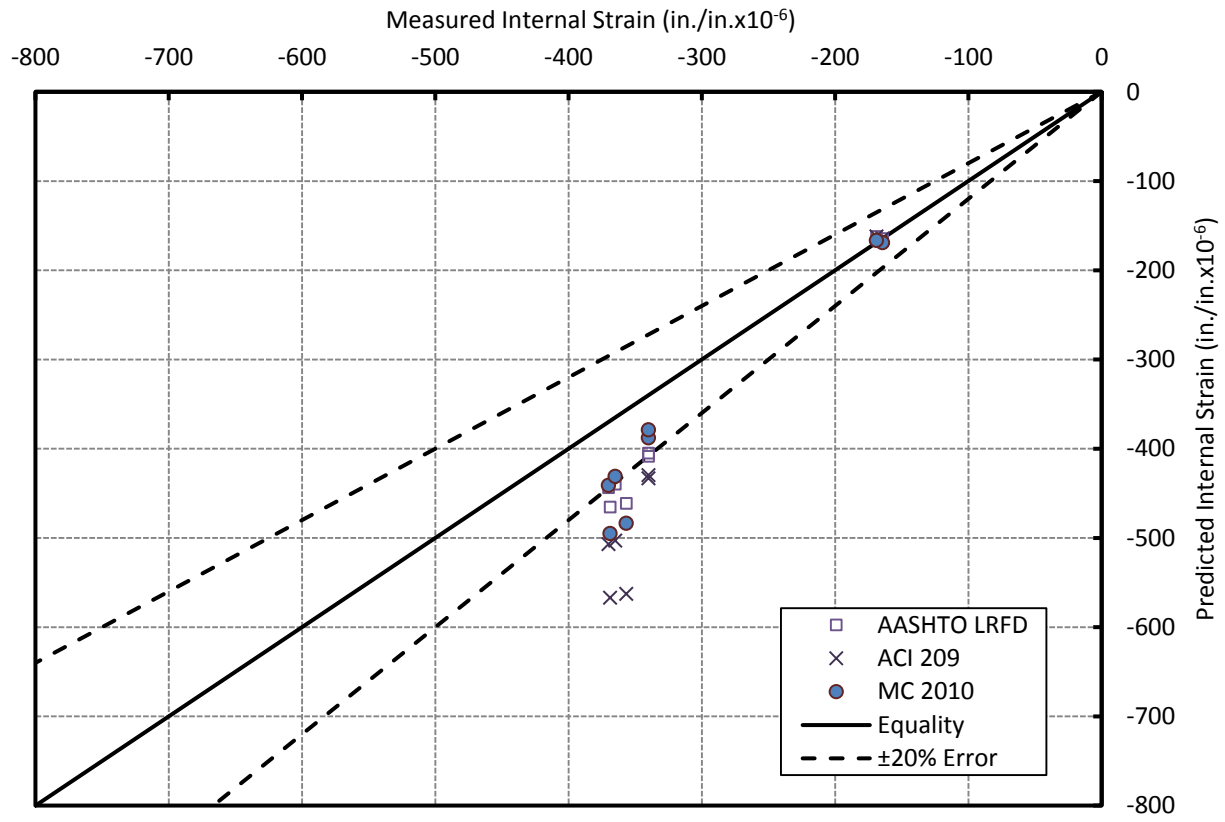

Figure 5-19: Predicted vs. Measured Bottom-Flange Strains—Type I—SCC-HS

(4 of 4) Statistical Evaluation of Error for Predicted Bottom-Flange Strains—Project 2

Figure 5.20 demonstrates the unbiased estimates of the standard deviation of the fractional errors. Data used for the graph can be found in Table H-1. *Growth* values are obtained by subtracting the strains at transfer from the strains at later ages.

Two data points were available for the calculations but using more data points may have been more reasonable. Yet, two data points have small variance. At the same time, the unbiased estimations are greater than the averaged errors.

The recorded strain values were only available up to 56 days for the SCC-MS girders. 100% error for STD-M and SCC-MS represents a strain value of about 265 με; while, 100% error for SCC-HS represents a value of about 185 με.

At transfer, the strains are mostly underpredicted. The strain *growth* for STD-M and SCC-MS cannot be classified as over- or underpredicted. For that reason, the average of the fractional errors will be discussed. The strain *growth* of the SCC-HS girders, on the other hand, is overpredicted.

The errors are contrasted with each other in two categories: (i) comparison of AASHTO LRFD, ACI 209 and *fib* MC 2010 is made, and (ii) the STD-M, SCC-MS and SCC-HS girders are compared to each other.

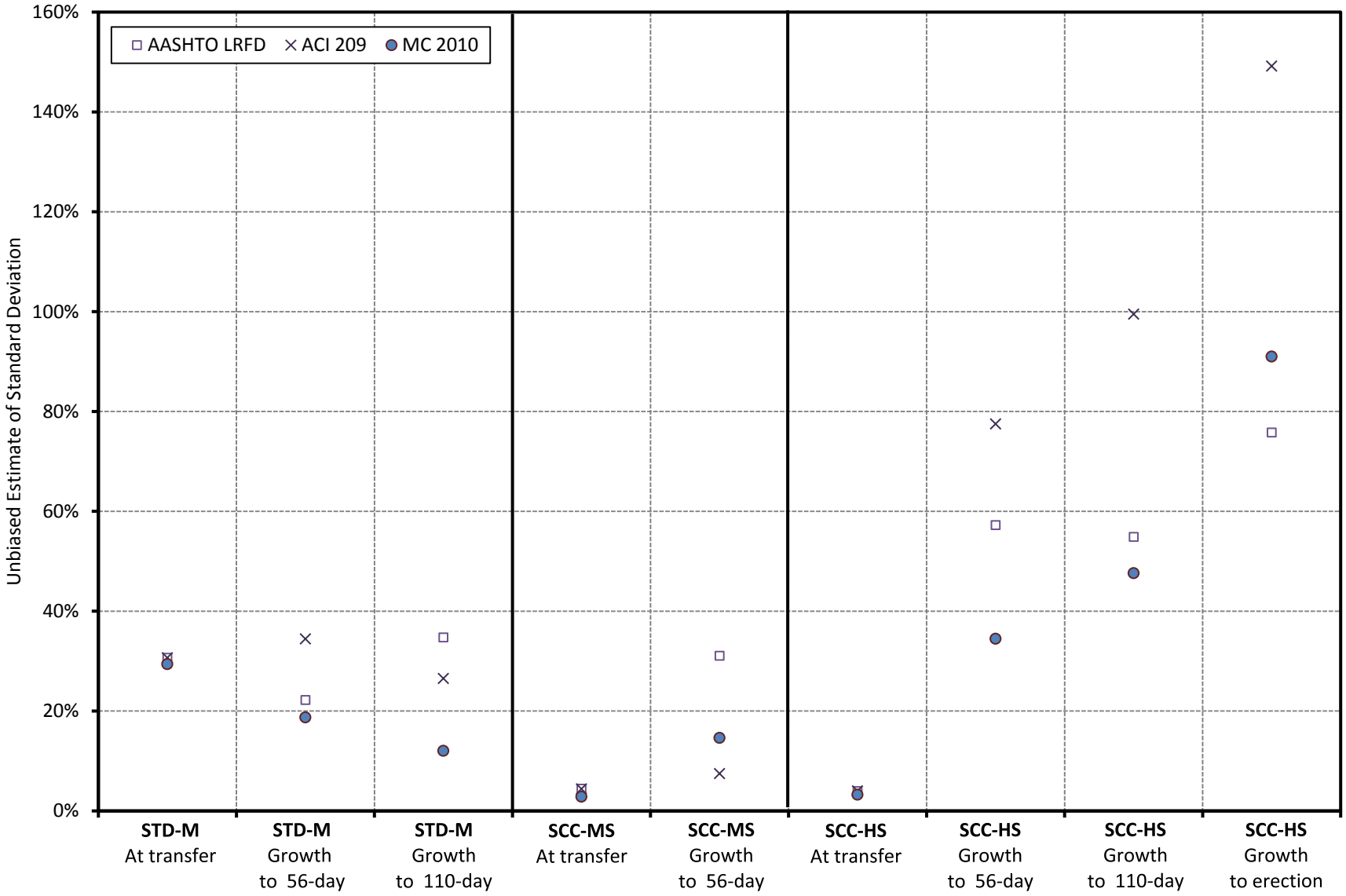

Figure 5-20: Fractional Errors - Bottom-Flange Strains at Midspan—Project 2

i. Comparison of AASHTO LRFD, ACI 209 and *fib* MC 2010

fib MC 2010 estimates the initial strains slightly better due to the excluded autogenous shrinkage prior to the benchmark reading. At later ages, the irregular data sets such as over- and underpredictions require comparing the arithmetical average of the fractional errors. The arithmetical averages reveal that the strain *growth* is overpredicted, and *fib* MC 2010—predicting the least shrinkage—reveals significantly better estimations.

ii. Comparison of STD-M, SCC-MS and SCC-HS girders

At transfer, strain values of the STD-M girders have the worst estimations possibly due to the errors involved in the modulus of elasticity testing. STD-M generally underpredicts the initial strain unlike the other two girder sets.

At later ages, the SCC-HS girders have the least accurate predictions which are all overpredicted. The accuracy of the STD-M and SCC-MS girders is somewhat similar, and it is hard to draw a conclusion whether they are over- or underpredicted even by comparing the average errors.

5.4.3 Curvature Analyses

(1 of 4) STD-M Girders

The recorded curvature values were obtained by using the top and bottom gages of the two STD-M girders. Figure 5-21 demonstrates the predicted and measured internal strains at immediately after transfer, at 56 days, and at 110 days after transfer.

The curvatures are estimated less than the measured ones and none of the predictions do not fall under the -20% error line. At later ages, *fib* MC 2010 and AASHTO LRFD seem to predict the curvatures better than ACI 209. Also, the initial errors are reflected in the predictions at later ages.

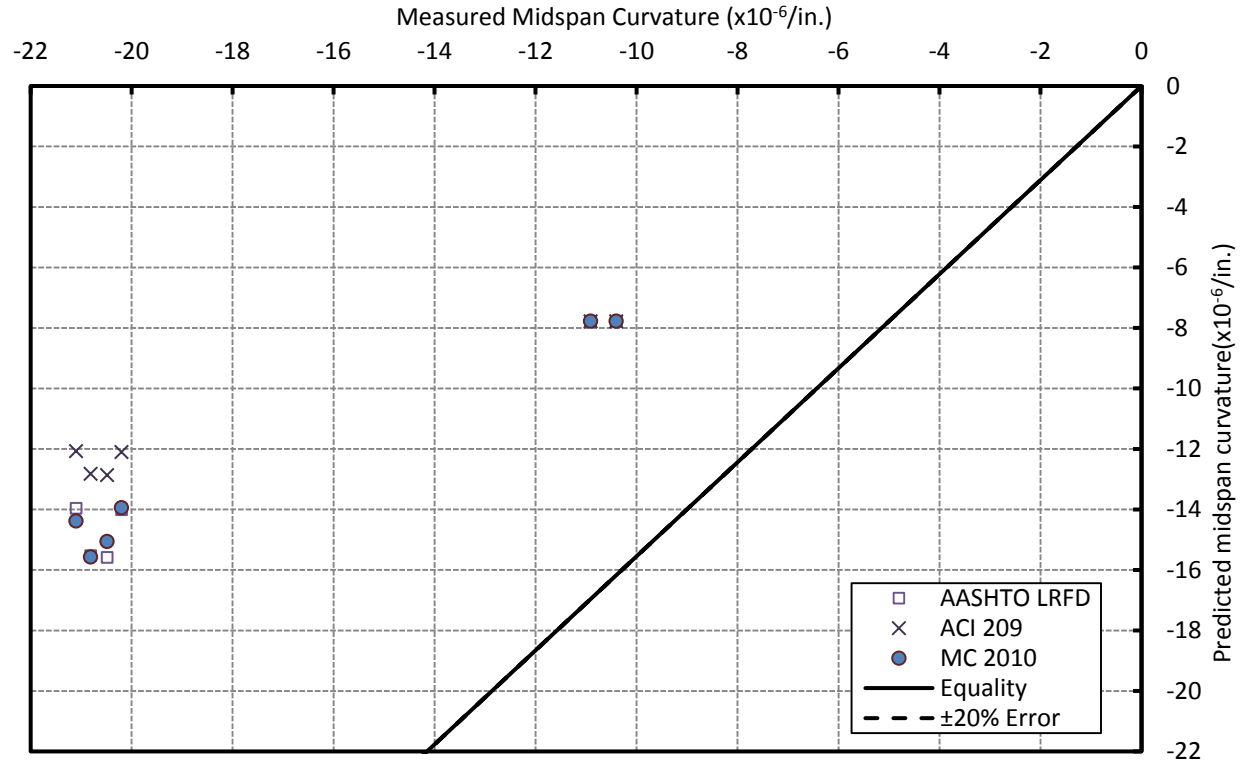

Figure 5-21: Predicted vs. Measured Midspan Curvatures—Type I—STD-M

(2 of 4) SCC-MS Girders

The top and bottom strains are used to calculate the recorded curvatures. Figure 5-22 illustrates the trend of the measured versus predicted curvatures.

Initial values are predicted within the ±20% error line. At later ages, the predictions are underpredicted mostly, and they are not as good as the ones at transfer. AASHTO LRFD—predicting the greatest creep—reveals the most accurate estimations for the SCC-MS girders.

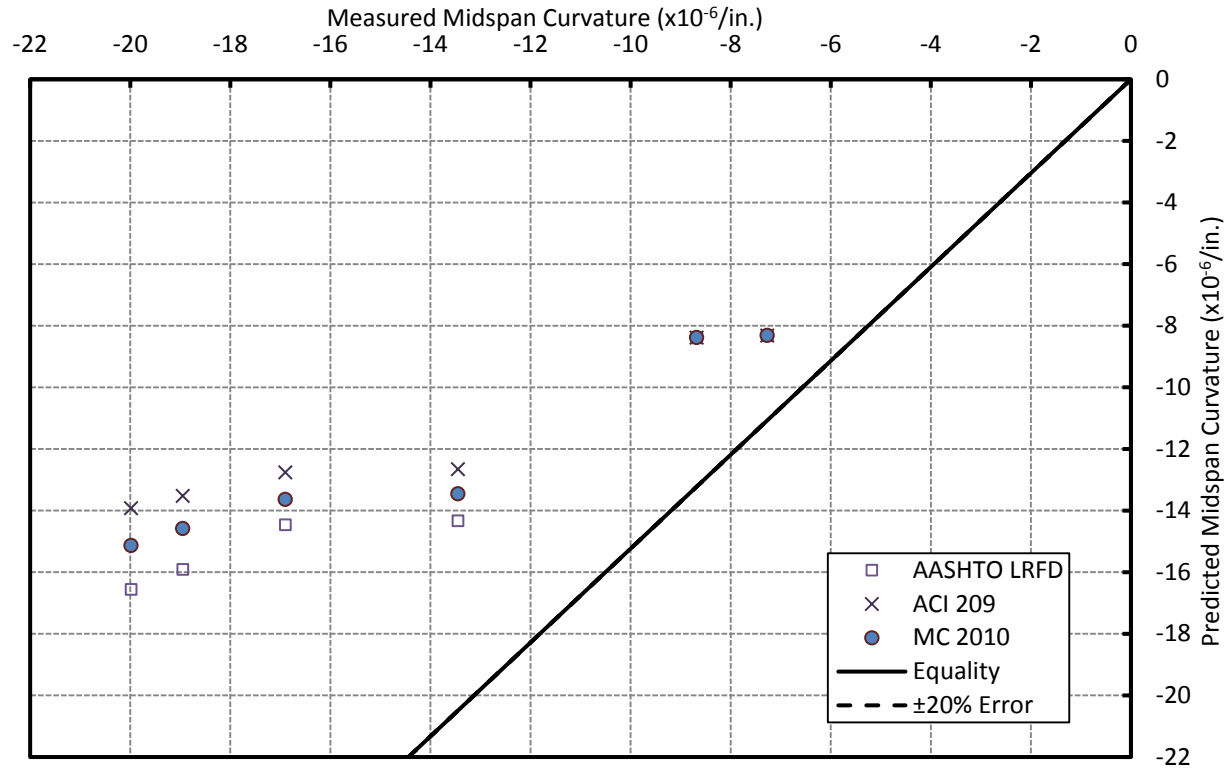

Figure 5-22: Predicted vs. Measured Midspan Curvatures—Type I—SCC-MS

(3 of 4) SCC-HS Girders

Figure 5-23 shows the predicted versus measured curvatures just after transfer, at 56 days, 110 days, and 214 days after transfer.

The points closest to the origin illustrate the values predicted immediately after transfer. The initial predictions are overpredicted and placed close to the +20% error line. The long-term estimations are overpredicted for most of the rime, but they remain close to the equality line.

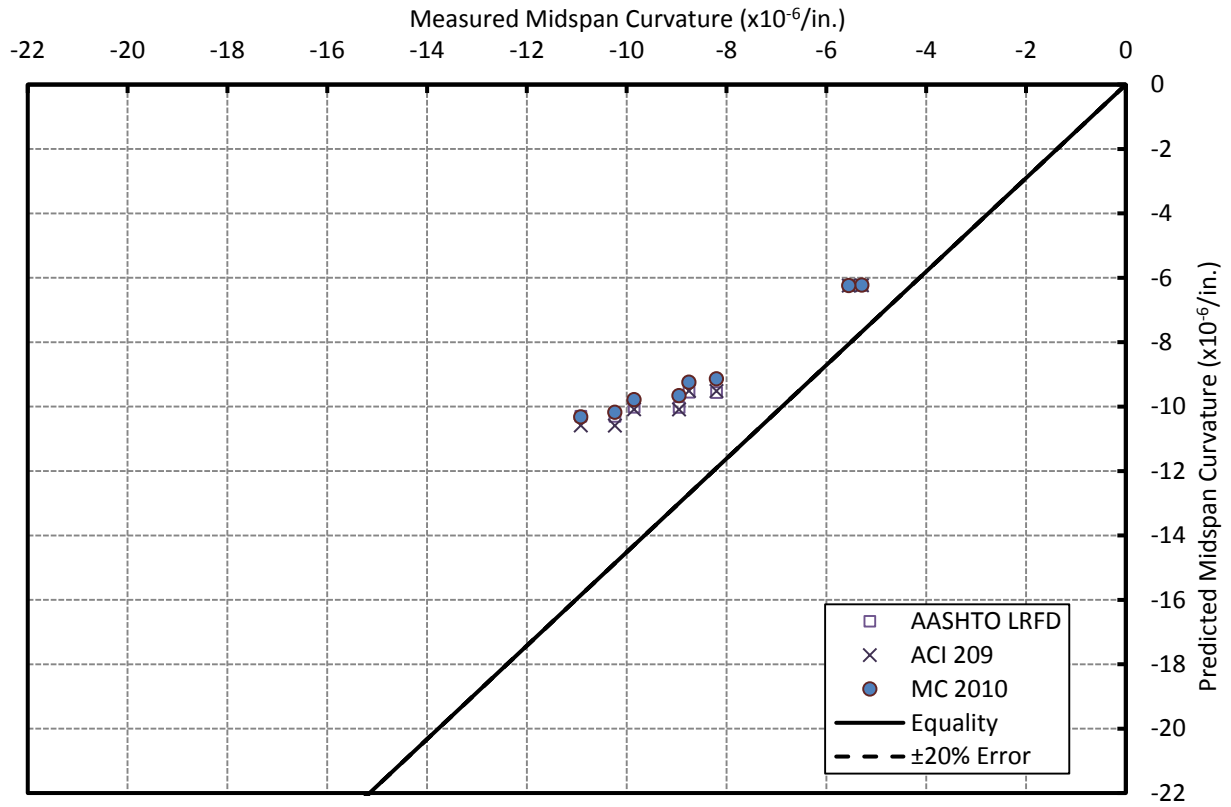

Figure 5-23: Predicted vs. Measured Midspan Curvatures—Type I—SCC-HS

(4 of 4) Statistical Evaluation of the Error for Predicted Curvatures—Project 2

The unbiased estimates are plotted in Figure 5.24. The scale of the graph is different than the one for the unbiased estimate of strain in Section 5.4.2. Data used for the graph can be found in Table H-2 in Appendix H. The *growth* is calculated by subtracting the values at transfer from the ones at later ages. 100% error for STD-M, SCC-MS, and SCC-HS represents an average curvature amount of 10.4×10^{-6} 1/in., 7.8×10^{-6} 1/in., and 4.5×10^{-6} 1/in., respectively.

For the STD-M girders, the initial curvature and the curvature *growth* are underpredicted. The initial values of the SCC-MS girders are overpredicted on average, and the *growth* curvatures are underpredicted. The initial values of the SCC-HS girders are overpredicted, and it is hard to classify the *growth* values of the SCC-HS girders.

The comparison of the curvature predictions is discussed in two aspects: (i) comparison of AASHTO LRFD, ACI 209, and *fib* MC 2010 is made, and (ii) the STD-M, SCC-MS, and SCC-HS girders are compared.

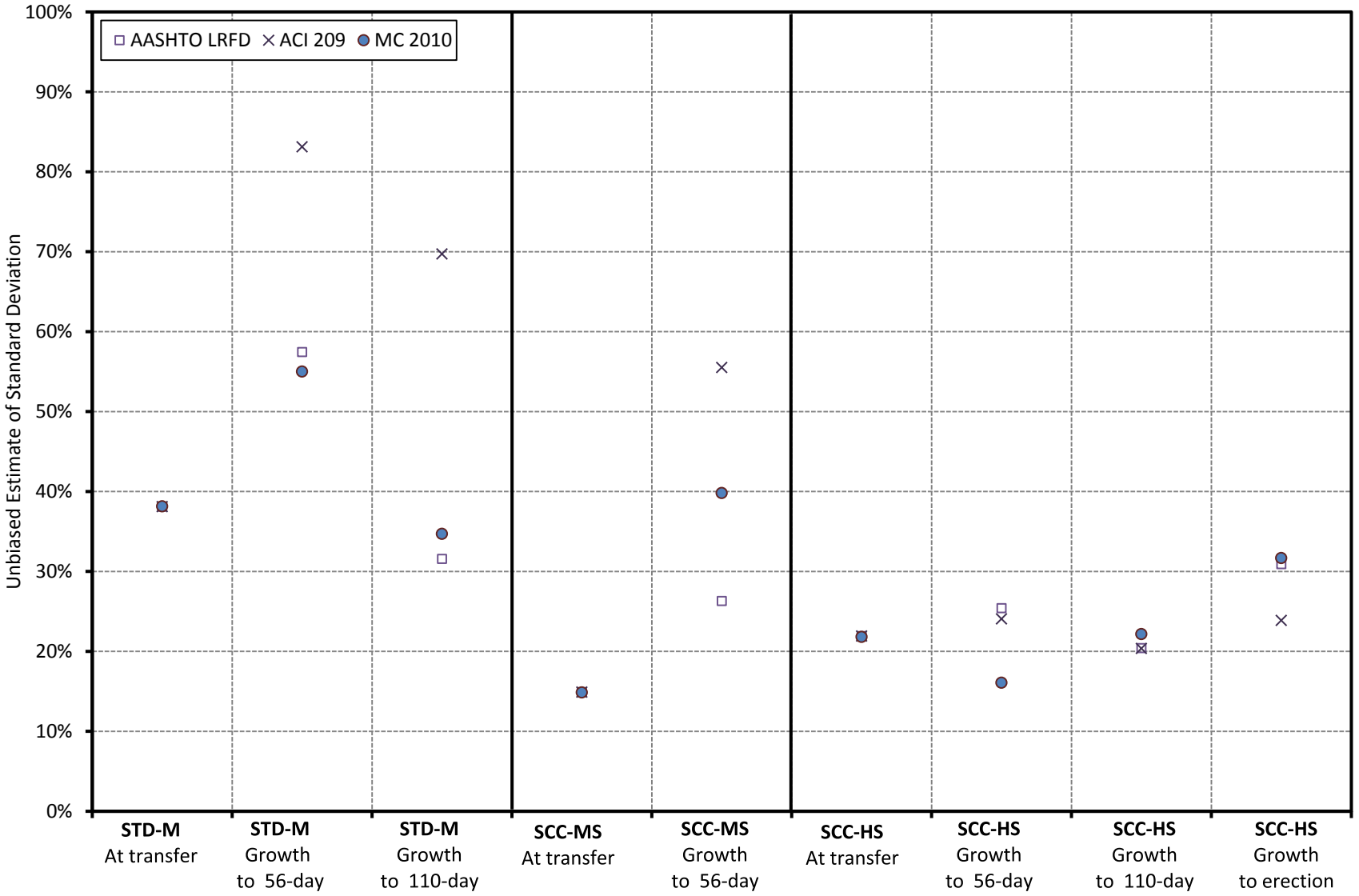

Figure 5-24: Fractional Errors—Midspan Curvatures—Project 2

i. Comparison of AASHTO LRFD, ACI 209, and *fib* MC 2010

The transfer values are predicted with the same accuracy regardless of the prediction model since the initial predictions are tied up with the elastic properties. For the STD-M and SCC-MS girders, the *growth* values are constantly underpredicted. The best predictions for them are obtained with the AASHTO LRFD model having the highest creep predictions. It proves that the curvature predictions are governed by creep.

On the other hand, the unbiased estimates of the SCC-HS girders can be misleading since they include underpredictions and overpredictions. As a result, the average of fractional errors is evaluated, and the ACI 209 prediction model is the most accurate model for the SCC-HS girders.

ii. Comparison of STD-M, SCC-MS and SCC-HS girders

SCC-MS girders are best predicted at transfer. At later ages, the best predicted girder group is the SCC-HS girders, and the second one is SCC-MS. The SCC-HS girders—having underpredictions and overpredictions unlike STD-M and SCC-MS—are better predicted than other two girder types.

5.4.4 Camber Analyses

(1 of 4) STD-M Girders

Time-dependent camber analyses are carried out for the cambers immediately after transfer, at 56 days, and at 110 days after transfer. The plot of the predictions and measurements for two STD-M girders can be seen in Figure 5-25. The STD-M girders were 480-inch long.

The initial cambers are predicted with an error less than 20%. They are estimated with the same amount regardless of the prediction model. At later ages, most of the camber predictions remain within the ±20% error line. AASHTO LRFD and MC 2010 are estimated close to the equality line more times than ACI 209. All in all, the camber predictions have a mixed distribution.

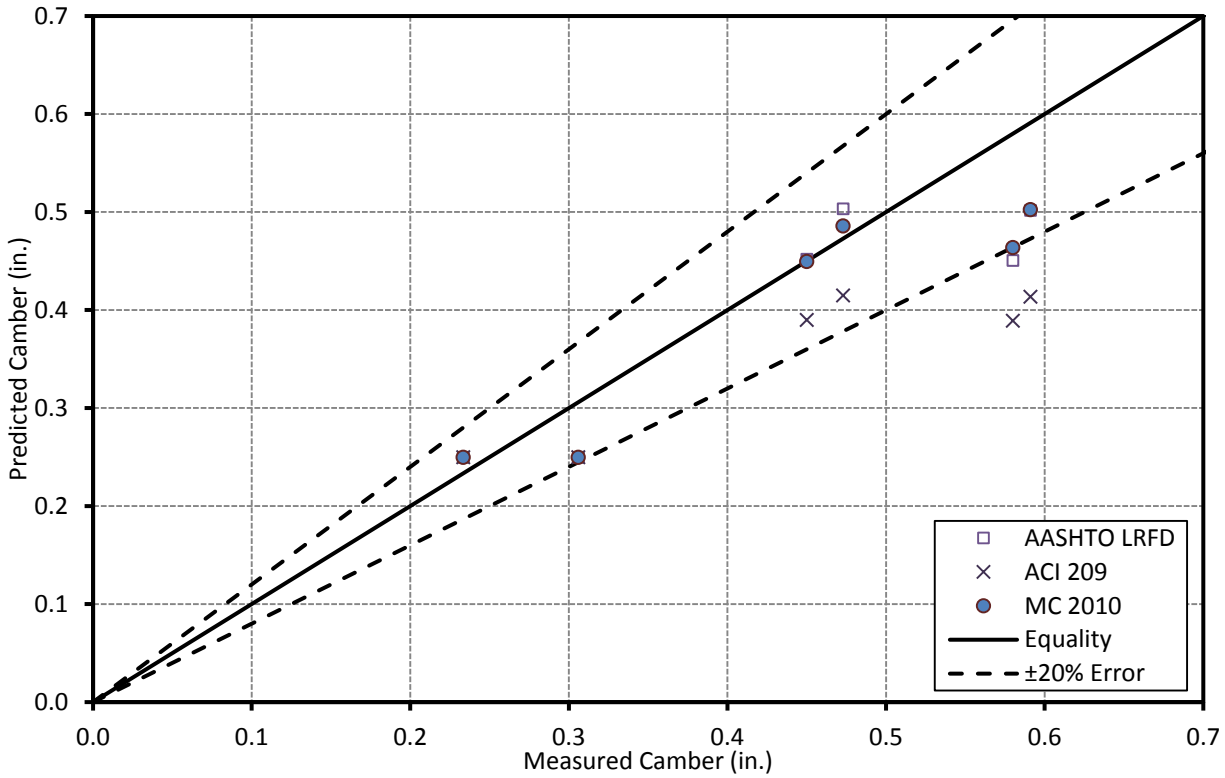

Figure 5-25: Predicted vs. Measured Midspan Cambers—Type I—STD-M

(2 of 4) SCC-MS Girders

For the two 480-inch long STD-M girders, the predicted and measured cambers are shown in Figure 5-26. The plot includes the cambers immediately after transfer, at 56 days, 110 days, and 167 days.

Overestimations are observed for all of the initial camber predictions and most of the long-term predictions. At transfer, one of the girder sets falls close to the +20% error line and another one falls close to the equality line; additionally, the trend remains the same for the long-term predictions. This means that the *growth* is predicted more accurately than the errors indicated in the plot. The ACI 209 and *fib* MC 2010 predictions are closer to the equality than the AASHTO LRFD predictions.

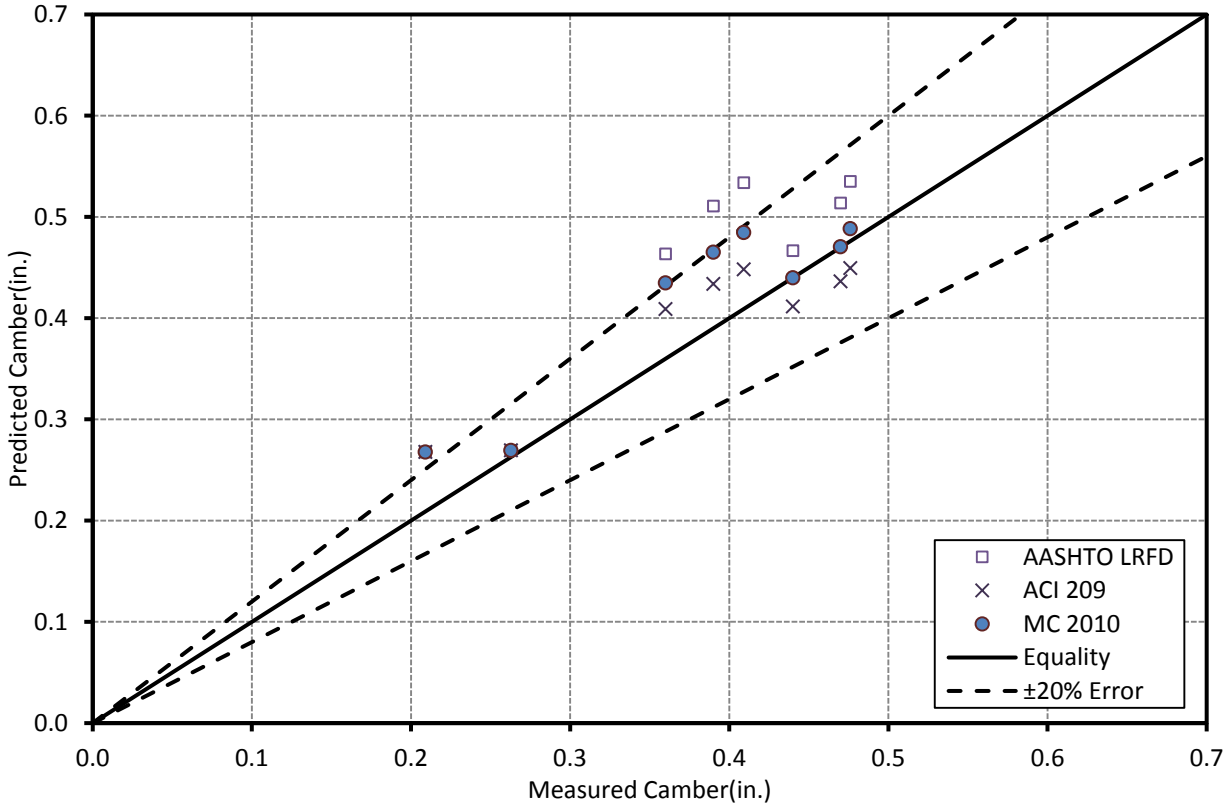

Figure 5-26: Predicted vs. Measured Midspan Cambers—Type I— SCC-MS

(3 of 4) SCC-HS Girders

The camber predictions of the two SCC-HS girders are compared to the measurements in Figure 5-27. The plot includes the cambers immediately after transfer, at 56 days, 110 days, and 214 days. The SCC-HS girders were 480-inch long.

The initial and long-term cambers are completely overpredicted. Most of the predictions are beyond the +20% error line. At later ages, MC 2010 predicts the least camber; whereas, ACI 209 estimates the largest camber.

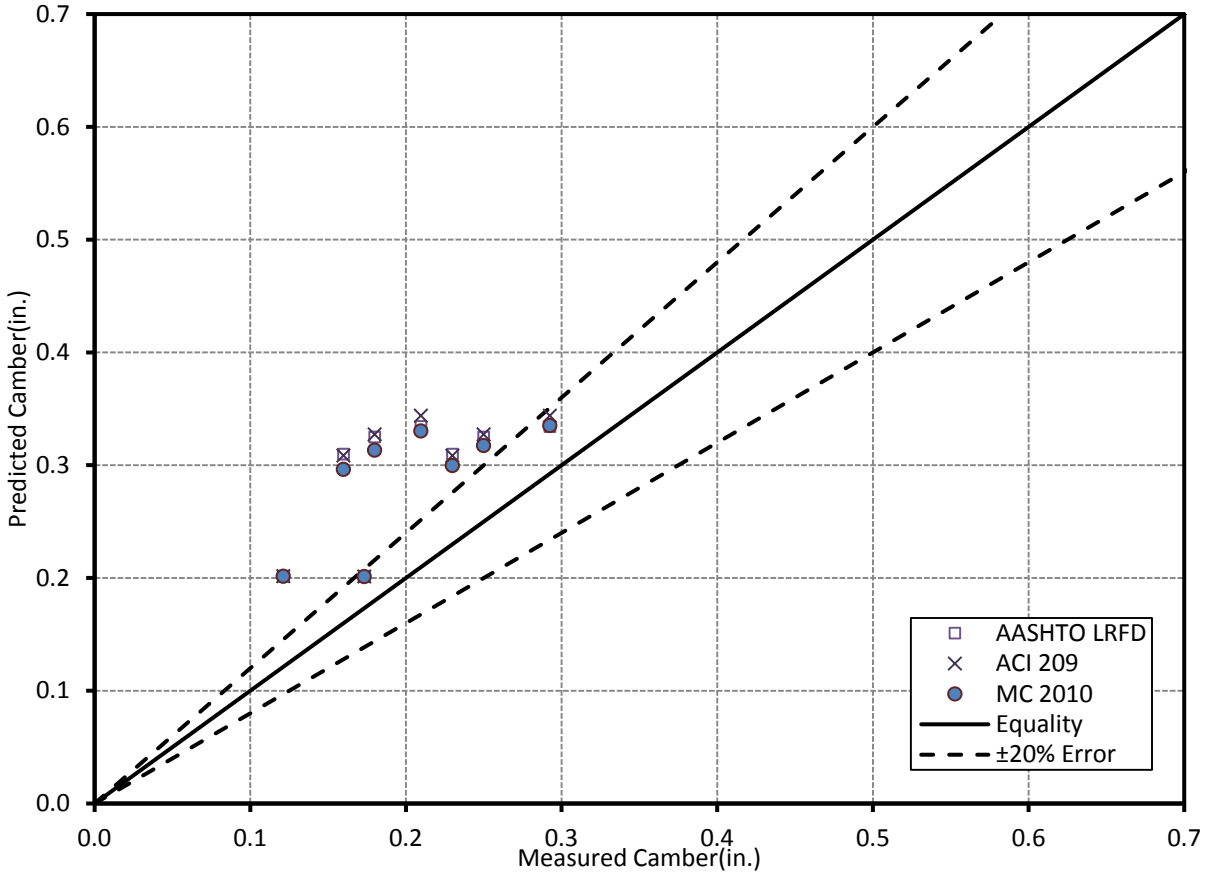

Figure 5-27: Predicted vs. Measured Midspan Cambers—Type I— SCC-HS

(4 of 4) Statistical Evaluation of the Error for Predicted Cambers—Project 2

Unbiased estimates plotted in Figure 5-28 show the fractional error in camber predictions. The data is provided in Table H-3 in Appendix H. The figure shown below is scaled differently than the related figures in the previous sections.

The *growth* prediction is the difference between the long-term and the initial camber. Two camber data was available for the unbiased calculations; consequently, the errors plotted below are much greater than the average of errors. 100% error for STD-M, SCC-MS, and SCC-HS represents an average camber of 0.28 in., 0.19 in., and 0.08 in., respectively. Also, the measurement errors for the short-span girders can significantly affect the results since the precision of camber measurements was 0.01 in.

The STD-M girders are underpredicted at transfer, and they have a mixed distribution of predictions at later ages. The SCC-MS girders are overpredicted entirely at transfer, and the *growth* is mostly underpredicted. The SCC-HS girders are all overpredicted at transfer and at later ages.

The camber predictions are evaluated in two categories: (i) comparison of AASHTO LRFD, ACI 209 and *fib* MC 2010 is made, and (ii) the STD-M, SCC-MS and SCC-HS girders are compared.

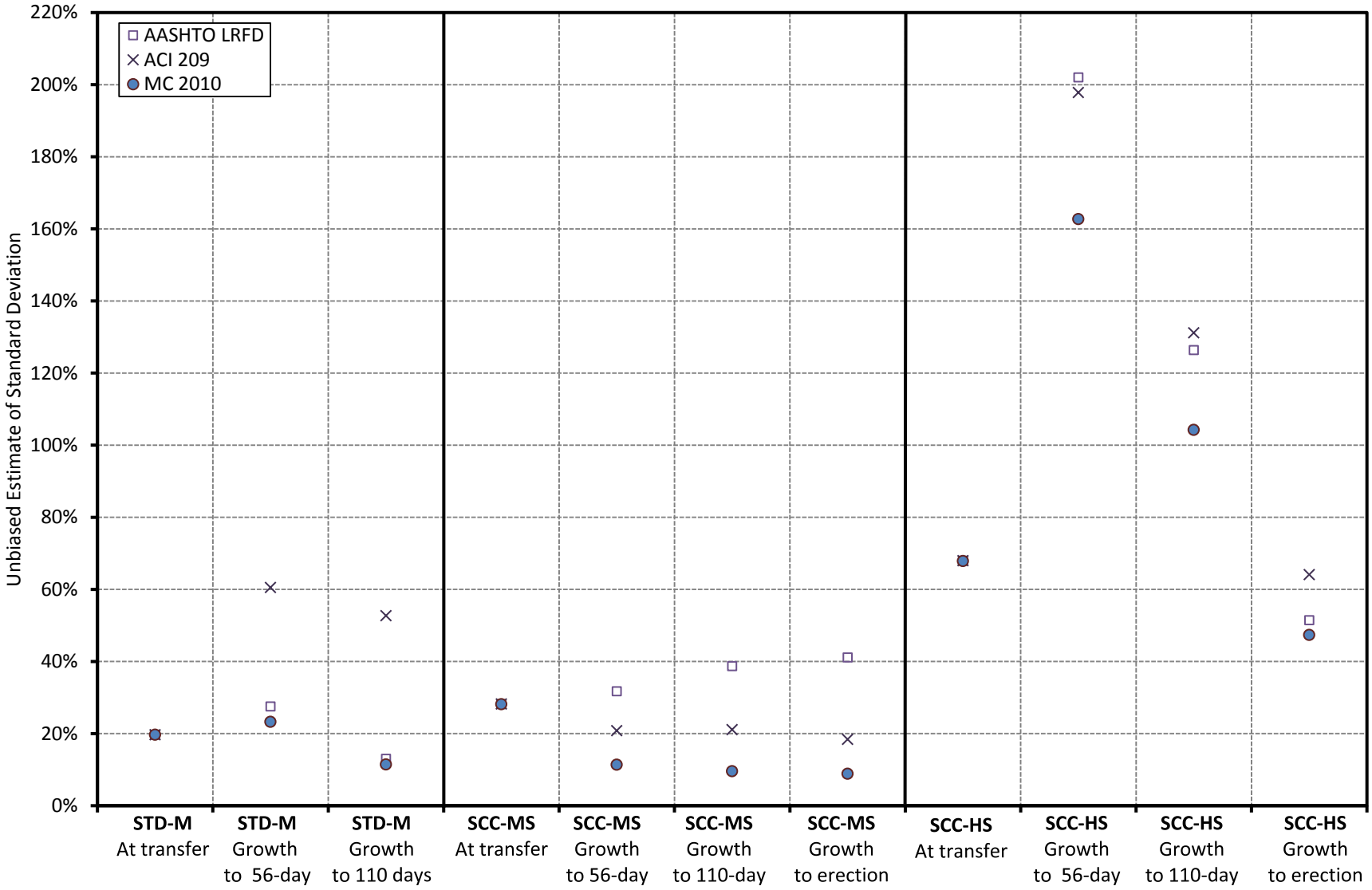

Figure 5-28: Fractional Errors—Midspan Cambers—Project 2

i. Comparison of AASHTO LRFD, ACI 209 and *fib* MC 2010

The same predictions are obtained at transfer regardless of the prediction models. The *growth* of the STD-M, SCC-MS, and SCC-HS girders is predicted most accurately by MC 2010.

ACI 209—estimating the least creep—underpredicts camber *growth* for the STD-M girders and becomes the least accurate model. For SCC-HS, ACI 209—estimating the greatest creep—overpredicts midspan camber and becomes the least accurate model as well. As a result, the accuracy of the models is determined by the creep predictions and distribution of camber predictions.

ii. Comparison of STD-M, SCC-MS and SCC-HS girders

According to the fractional errors, the STD-M and SCC-MS girders are better predicted than SCC-HS at erection and later ages. However, the related errors for the SCC-HS predictions are better than SCC-MS.

5.5 Project 3: HPC BT-54

5.5.1 Total Creep Coefficient and Total Shrinkage Strain

The long-term predictions such as strain, curvature, and camber depend on the predicted creep and shrinkage deformations. For the HPC BT-54 girders, the total creep coefficient and the total shrinkage strain up to 180 days are plotted in Figure 5-29.

The estimated total creep coefficient ranges from 0.88 to 1.04. ACI 209 estimates the least creep; in contrast, *fib* MC 2010 predicts the most. Furthermore, this trend is consistent with the findings of the Hillabee Creek Bridge Project—composed of BT-54 and BT-72 girders.

The shrinkage strains are predicted within the range of -235 με and -285 με. The shrinkage strain prior to the benchmark readings are calculated as 0 με. *fib* MC 2010 estimates the greatest shrinkage strain in magnitude, and AASHTO LRFD reveals the least.

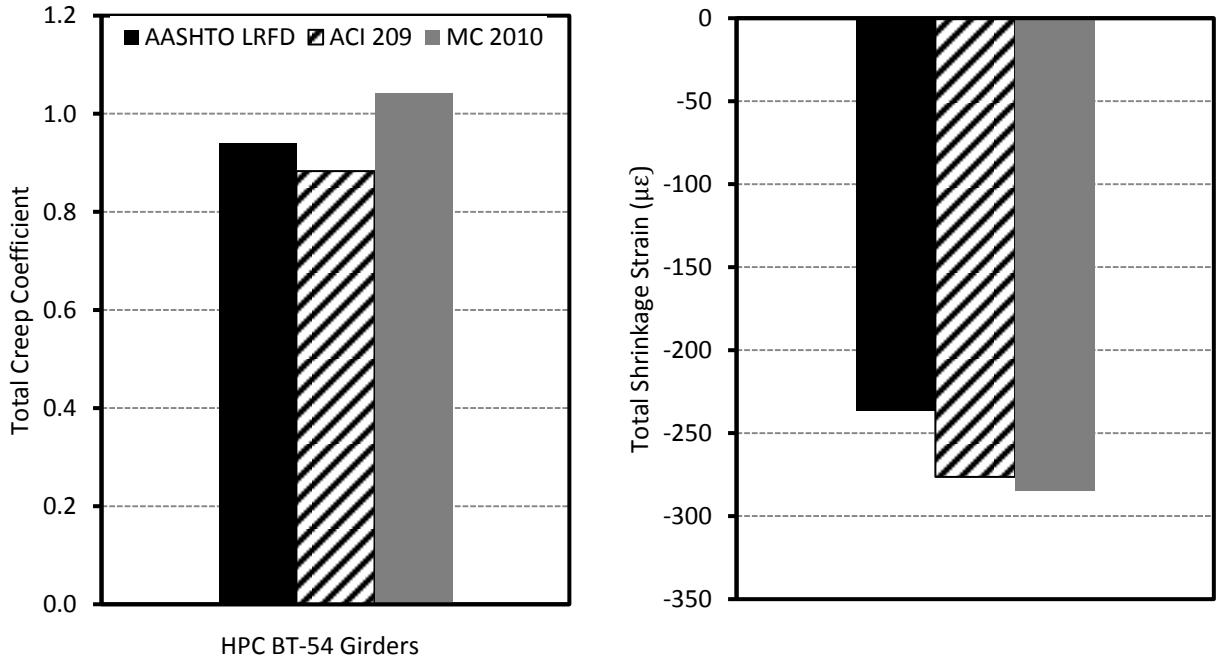

Figure 5-29: Total Creep and Shrinkage Predictions—Project 3

5.5.2 Bottom-Flange Strain Analyses

Five VC BT-54 girders were monitored for the strain development. Bottom-flange gages were located in the flange at 6.5 in. from bottom of the girder. Temperature corrections accounting for the thermal gradients were not applied due to the lack of temperature data.

Figure 5.30 shows the trend of the predicted and measured internal strains at 1 day, 56 days, and 180 days after transfer. Although the girders were monitored almost for a year, the 180-day strain was chosen to be compatible with other projects.

The strains at 1 day fall within the ±20% error lines. AASHTO LRFD and ACI 209 underpredict the 1-day strains; whereas, *fib* MC 2010 mostly overpredicts them with the best accuracy. At later ages, most of the predictions are overpredicted and remain within the 20% error line. AASHTO LRFD and ACI 209 predict the strain *growth* close to the equality line.

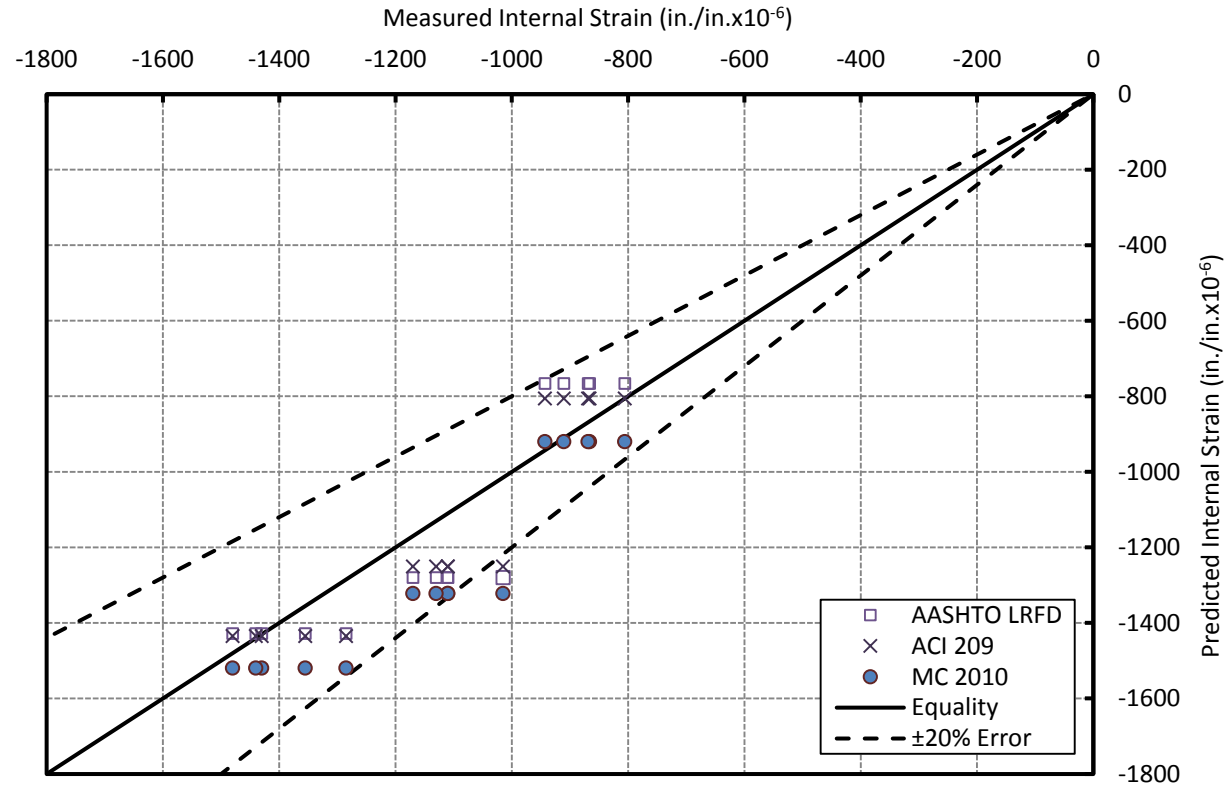

Figure 5-30: Predicted vs. Measured Bottom-Flange Strains—Project 3

Statistical Evaluation of Error for Predicted Bottom-Flange Strains—Project 3

The unbiased estimates of the standard deviation of the fractional errors are illustrated in Figure 5.31. Data points can be found in Table H-1. *Growth* is obtained by subtracting the strains at later ages from the ones at 1 day.

Five data points are used to evaluate the strain trend. 100% error for the 1-day strain represents a value of 905 με; whereas, 100% error for the *growth* at 56 days and 180 days represent strains of 220 με, and 480 με, respectively. The strains at 1 day have under- and overpredictions; while, the strain *growths* are all overpredicted.

The errors are analyzed in two categories: (i) the comparison of AASHTO LRFD, ACI 209 and *fib* MC 2010 is made, and (ii) the HPC girders are compared to the VC BT-54 girders analyzed in the Hillabee Creek Bridge Project (Project 1).

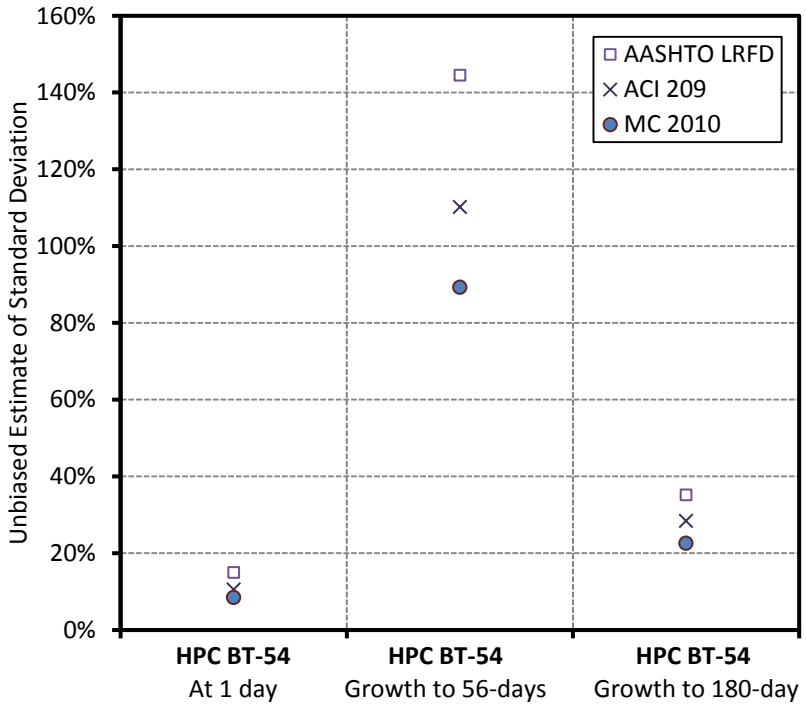

Figure 5-31: Fractional Errors—Bottom-Flange Strains—Project 3

i. Comparison of AASHTO LRFD, ACI 209 and *fib* MC 2010

The overpredicting *fib* MC 2010 model estimates the 1-day strain better than the underpredicting AASHTO LRFD and ACI 209 models. *fib* MC 2010 reveals the best predictions at later ages. The second best model is ACI 209. Also, the *growth* is obtained relative to the 1-day (after the transfer) readings. AASHTO LRFD develops about 150 με less bottom-flange strain at 1 day than MC 2010; as a result, the accuracy of the models at later ages may be misrepresented.

ii. Comparison of the VC BT-54 girders in Project 1 and Project 3

The VC BT-54 girders in Project 3 had been produced 11 years before the VC BT-54 girders in Project 1. In order to carry out the time-dependent analysis, the similar inputs for concrete properties and time of events were entered, but the total prestressing force and its layout were the major difference. The girders in Project 3 had 70% (1845 kips / 1115 kips) more prestressing force than the girders in Project 1. Also, the *growth* of Project 3 is obtained relative to the 1-day readings (relative to transfer).

The *growth* to 56-day of the Project 1 is better predicted in terms of fractional and average errors. However, the *growth* to erection of Project 1 is predicted less accurately than *growth* to erection of Project 3. In addition, the models revealing the most and least accurate predictions for Project 1 are not consistent with the models in Project 3. The discrepancies of strain *growth* can be explained by the initial measurement used to calculate the *growth*.

5.5.3 Curvature Analyses

The curvature analyses were carried out for the four BT-54 girders. Bottom and top gauges were located at 6.5 in. and 51.3 in., respectively. Figure 5.32 shows the trend of the measured and predicted internal strains at 1 day, 56 days, and 180 days after transfer. The 180-day curvature was chosen mainly to be consistent with other projects.

The curvatures at 1 day fall within the ±20% error lines. AASHTO LRFD and ACI 209 underpredict the 1-day curvatures. At later ages, the predictions are mostly overpredicted and they remain close to the equality line.

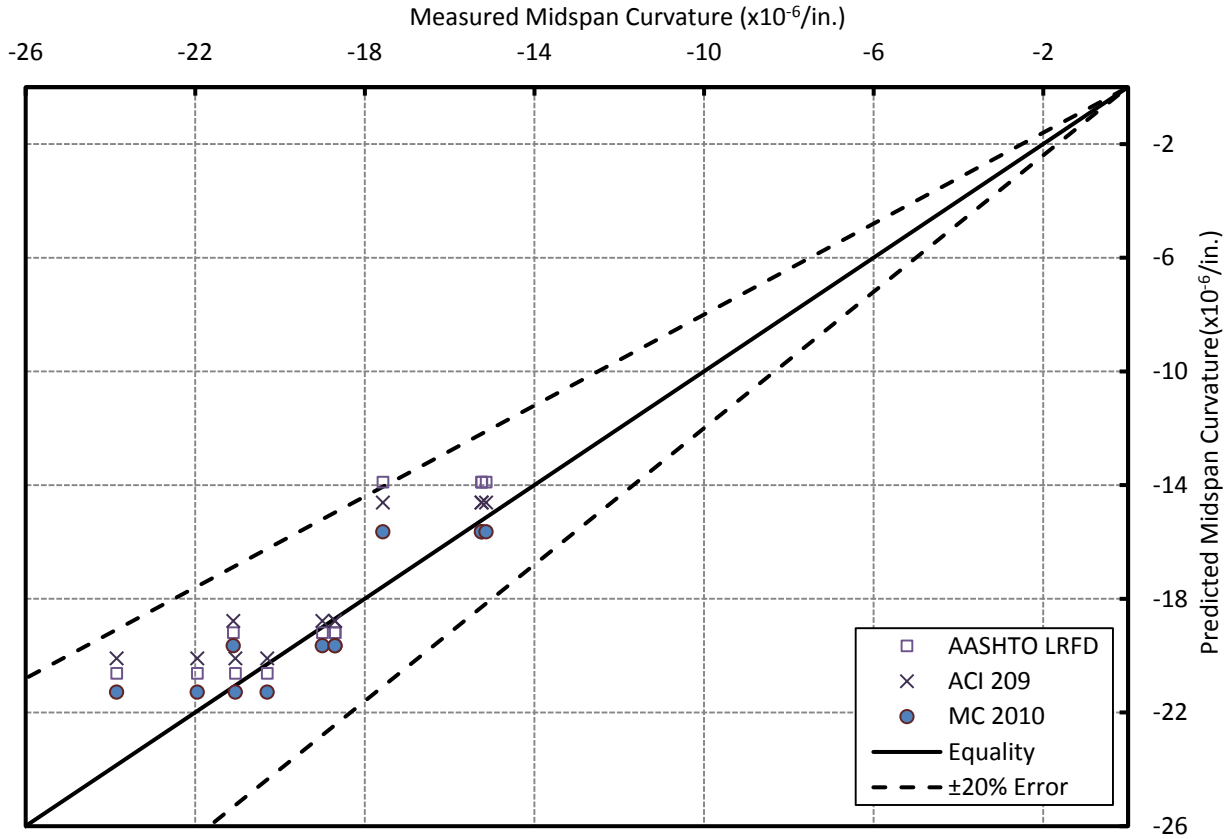

Figure 5-32: Predicted vs. Measured Midspan Curvatures—Project 3

Statistical Evaluation of the Error for Predicted Curvatures—Project 3

Figure 5.33 shows the unbiased estimates of the standard deviation of the fractional errors. The graph is scaled differently than the relevant strain graph. The *growth* values are determined by subtracting the 1-day curvatures from the long-term curvatures.

100% error for the 1-day curvature represents a value of 16.8×10^{-6} 1/in.; while, 100% error for the *growth* represents a curvature amount of 4.5×10^{-6} 1/in.. The 1-day curvatures are mostly underpredicted, and the long-term curvatures are mostly overpredicted.

The errors are discussed in two categories: (i) the comparison of AASHTO LRFD, ACI 209, and *fib* MC 2010 is discussed first, and (ii) the Project 3 girders are contrasted to the VC BT-54 girders in Project 1.

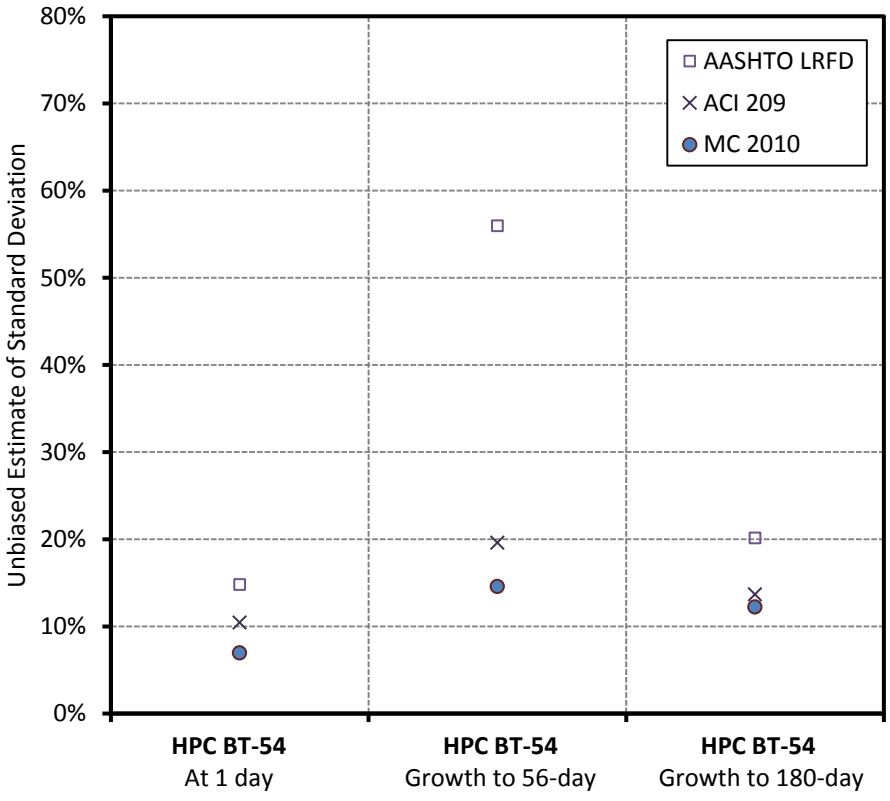

Figure 5-33: Fractional Errors—Midspan Curvatures—Project 3

i. Comparison of AASHTO LRFD, ACI 209 and *fib* MC 2010

The HPC girders have under- and overpredictions; as a result, the average of the fractional errors are additionally considered. At 1-day, *fib* MC 2010 supplies the best unbiased and average estimations. At later ages, ACI 209 and *fib* MC 2010 better predict the curvatures in terms of the unbiased estimates. In addition, the comparison of the average fractional errors shows that ACI 209 is the best model. The growth is obtained by using the 1-day readings (relative to transfer) and the prediction models do not develop same amount of curvature at 1 day. Consequently, the accuracy of the models at later ages may be misrepresented.

ii. Comparison of the VC BT-54 girders in Project 1 and Project 3

The prestressing layout is the major difference between the BT-54 girders analyzed in different projects. Both of the girders are overpredicted on average at transfer and later ages. At transfer, the fractional and actual errors are very close to each other.

At later ages, the girders in Project 3 reveal more accurate predictions in accordance to the unbiased fractional errors. Nevertheless, the actual errors challenge this conclusion and show that the predictions for Project 1 are more accurate.

Also, the curvature *growth*—depends largely on creep predictions—is predicted more accurately than the strain *growth*—depends on shrinkage and creep predictions—in Projects 1 and 3.

In addition, the models revealing the most and least accurate predictions for Project 1 are not consistent with the models in Project 3. This can be explained by the initial measurement used for the *growth*.

5.5.4 Camber Analyses

The girders in Project 3 were studied for the camber predictions at transfer, 56 days, and 180 days from transfer. Figure 5-34 shows the predicted and measured cambers. The measured cambers do not include the corrections accounting of the thermal gradient.

The cambers at 1 day are predicted very precisely except for one girder set. At later ages, most of the girders are overpredicted. The greatest camber predictions were obtained by MC 2010, and the least predictions were obtained by ACI 209. The same trend is obtained in curvature predictions as well since curvature and camber predictions depend on creep predictions. Also, the cambers for the Project 3 girders develop up to about 5.0 inches; whereas, the cambers for the related Project 1 girders were not greater than 3.0 inches.

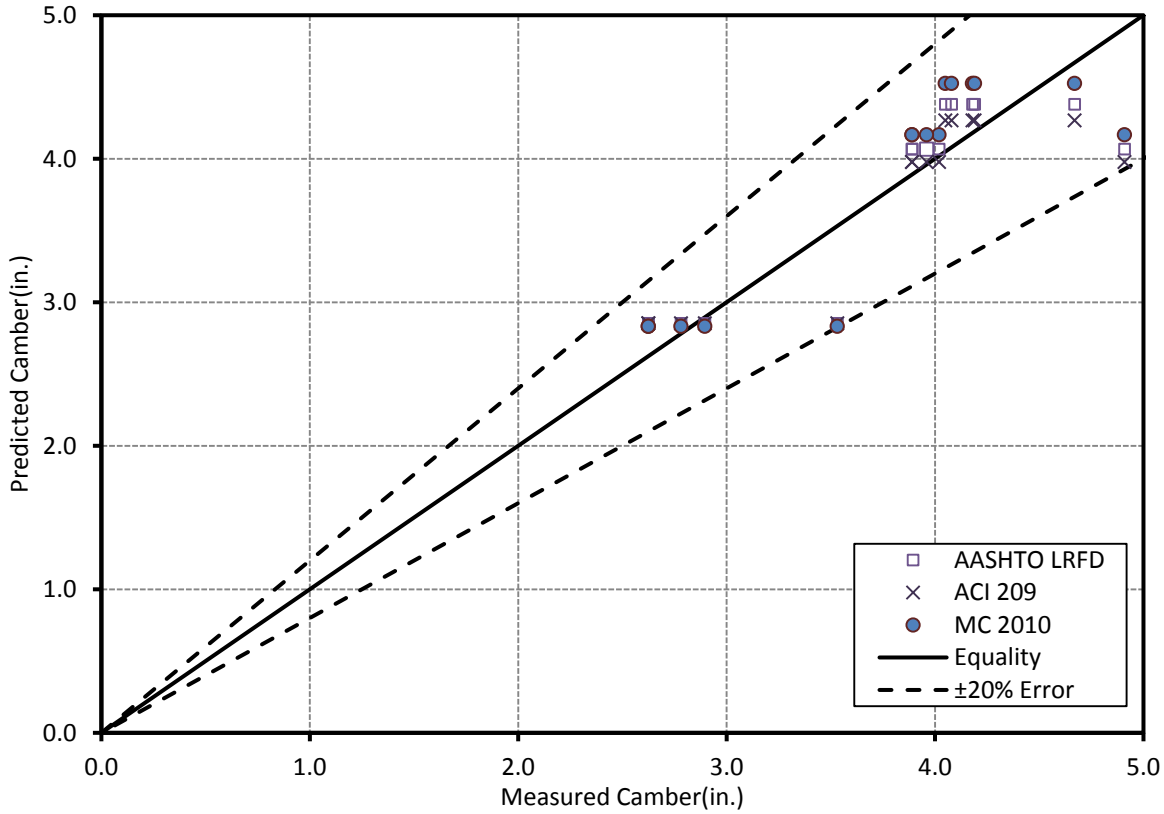

Figure 5-34: Predicted vs. Measured Midspan Cambers—Project 3

Statistical Evaluation of the Error for Predicted Cambers—Project 3

The unbiased estimates of the fractional errors are plotted in Figure 5.35. The figure is scaled differently than the previous graphs. The camber *growth* is the difference between long-term cambers and cambers at transfer.

100% error for the camber at transfer is equal to a camber error of 3.3 inches; in contrast, 100% error for the camber *growth* is equal to a camber error of 1.1 inches. The cambers at transfer and 56 days are mostly overpredicted. The 180-day cambers are entirely overpredicted.

The comparisons are investigated in two aspects: (i) different prediction models are compared to each other, and (ii) the Project 3 girders are contrasted to the VC BT-54 girders in the Project 1.

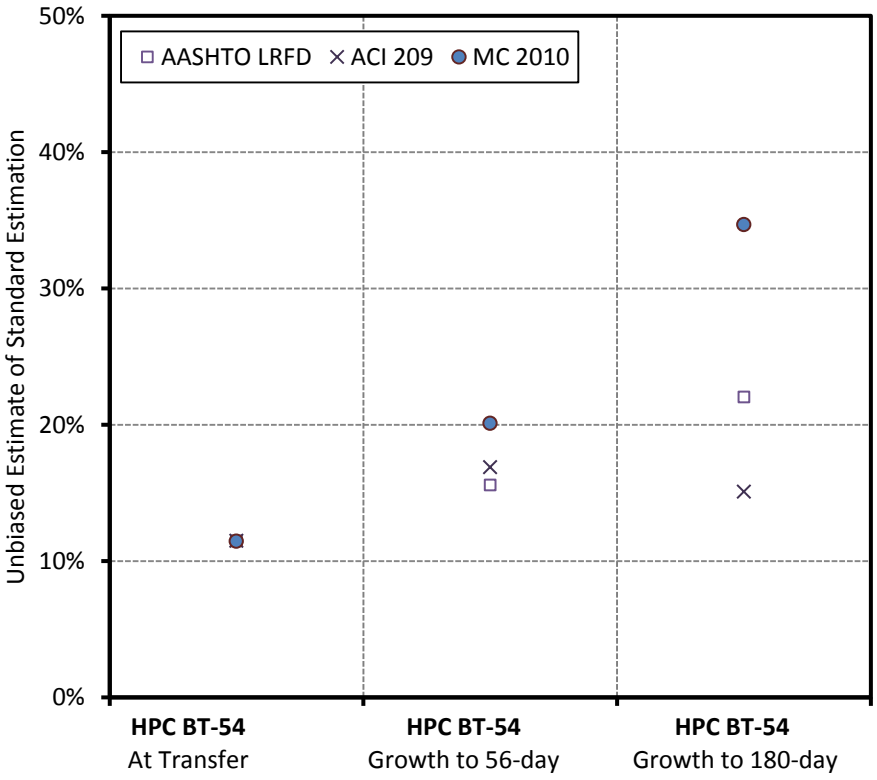

Figure 5-35: Fractional Errors—Midspan Cambers—Project 3

i. Comparison of AASHTO LRFD, ACI 209 and *fib* MC 2010

The initial predictions are predicted with the same accuracy no matter what the prediction model is due to the dependency on elastic properties. At later ages, ACI 209 reveals the best camber estimations; whereas, MC 2010 reveals the least accurate. It is in line with the creep predictions. Also, the error escalates as the duration of camber analysis increases.

ii. Comparison of the VC BT-54 girders in Project 1 and Project 3

The Project 3 girders were designed with 70% more prestressing force, and material properties were quite similar with the Hillabee Creek Bridge girders. The measured camber at erection was about 5.0 inches for the Project 3 girders, and about 2.5 inches for the Project 2 girders.

Both of the girders are mostly overpredicted at transfer and later ages. At transfer, the Project 3 girders are better predicted possibly due to the accuracy of the recorded MOE. Similarly, the *growth* predictions for the Project 3 girders are more accurate.

Also, the models revealing the most and least accurate camber predictions for Project 1 are consistent with the models in Project 3.

5.6 Project 4: T-Beams

5.6.1 Total Creep Coefficient and Total Shrinkage Strain

Twelve T-Beams are studied for the camber development. The strain and the curvature estimations are not investigated because strains were not measured. The camber analyses are performed for the girders with a span length of 276, 196, and 156 inches, and they are repeated for each of the four casting groups.

Long-term responses such as strain, curvature, and camber are substantially influenced by the predicted creep and shrinkage deformations. Total creep coefficient and total shrinkage strains are graphed in Figure 5-36. The STD-M, SCC-MA, SCC-MS, and SCC-HS girders are analyzed up to 90, 200, 56 and 14 days, respectively.

The analyses with the accelerated and non-accelerated curing properties are completed for the comparison reasons. Maturity values of T-Beams are obtained from the strength-maturity curves given in Figures E-3, E-4, E-5 and E-6 in Appendix E. The girders are all assumed to be accelerated-cured, accordingly. The analyses with non-accelerated curing properties are provided for the comparison reasons.

The estimated total creep coefficients vary from 0.42 to 2.03. The large variability is due to the duration of the analyses performed. The AASHTO LRFD creep predictions with accelerated curing properties are remarkably less than the ones with the non-accelerated. On the other hand, the ACI 209 predictions with the accelerated curing properties are slightly greater than its predictions with the non-accelerated.

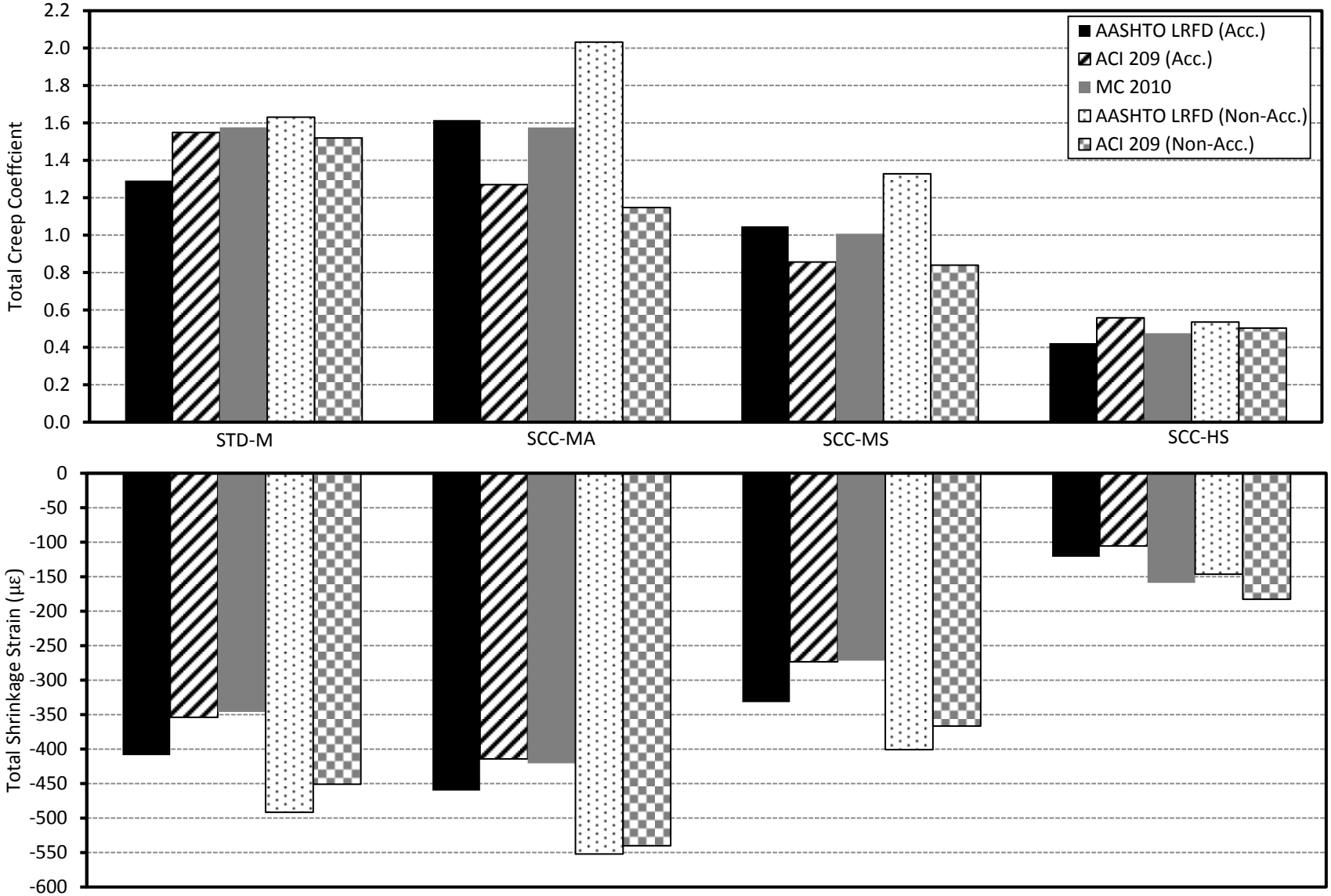

Figure 5-36: Total Creep and Shrinkage Predictions—Project 4

For the STD-M girders, *fib* MC 2010 predicts the largest creep coefficient; in contrast, AASHTO LRFD has the least creep estimation. For the SCC-MA and SCC-MS girders, AASHTO LRFD reveals the largest creep coefficient while ACI 209 creep estimations are the least. Further, ACI 209 gives the largest creep prediction for the SCC-HS girders; while, AASHTO LRFD predicts the least creep coefficient for them.

The shrinkage strain predictions vary from -105 με to -552 με. The strain analyses with accelerated curing are found to be considerably less than the ones with non-accelerated curing. The shrinkage strains up to the benchmark readings are not included for T-Beams. AASHTO LRFD estimates the largest shrinkage strain in magnitude for STD-M, SCC-MA, and SCC-MS; whereas, *fib* MC 2010 predicts the least. Furthermore, *fib* MC 2010 estimates the greatest shrinkage strain in magnitude for SCC-HS; while, ACI 209 gives the least.

5.6.2 Camber Analyses

(1 of 5) STD-M Girders

Camber analyses for three different girder sizes are plotted in Figure 5-37. The graph compares the predictions to the measurements immediately after transfer, at 14 days, 56 days and 90 days after transfer. The span length of the A, B, and C girders were 276, 196, and 156 inches, respectively.

The initial cambers are underpredicted. At later ages, total cambers are underpredicted on average by AASHTO LRFD unlike ACI 209 and *fib* MC 2010. The prediction models are examined better in the subsection about the statistical evaluation.

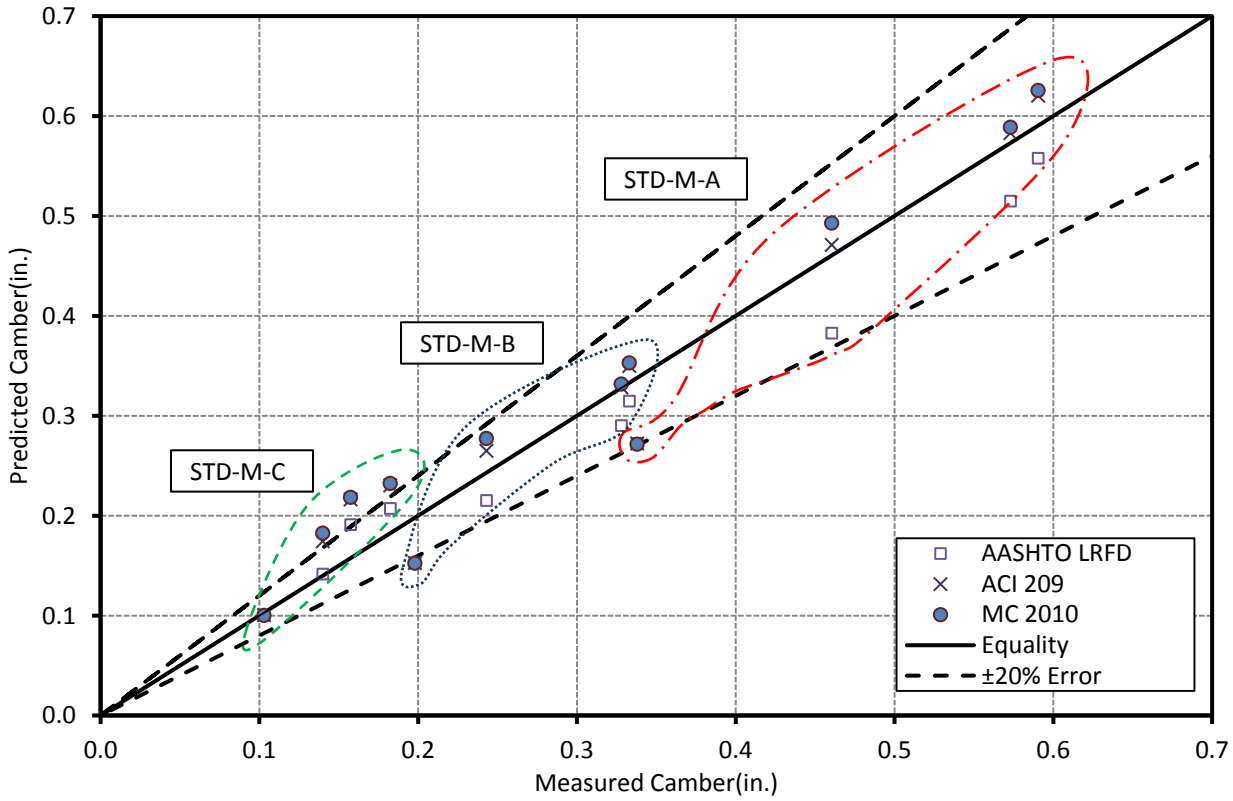

Figure 5-37: Predicted vs. Measured Midspan Cambers—T-Beams—STD-M

(2 of 4) SCC-MA Girders

The camber analyses for SCC-MA girders are illustrated in Figure 5-38. It includes the cambers immediately after transfer, at 56 days, 90 days, and 200 days after transfer.

The initial cambers for SCC-MA-B are best predicted. At later ages, most of the predictions are overpredicted. The ACI 209 estimations are very close to the equality line.

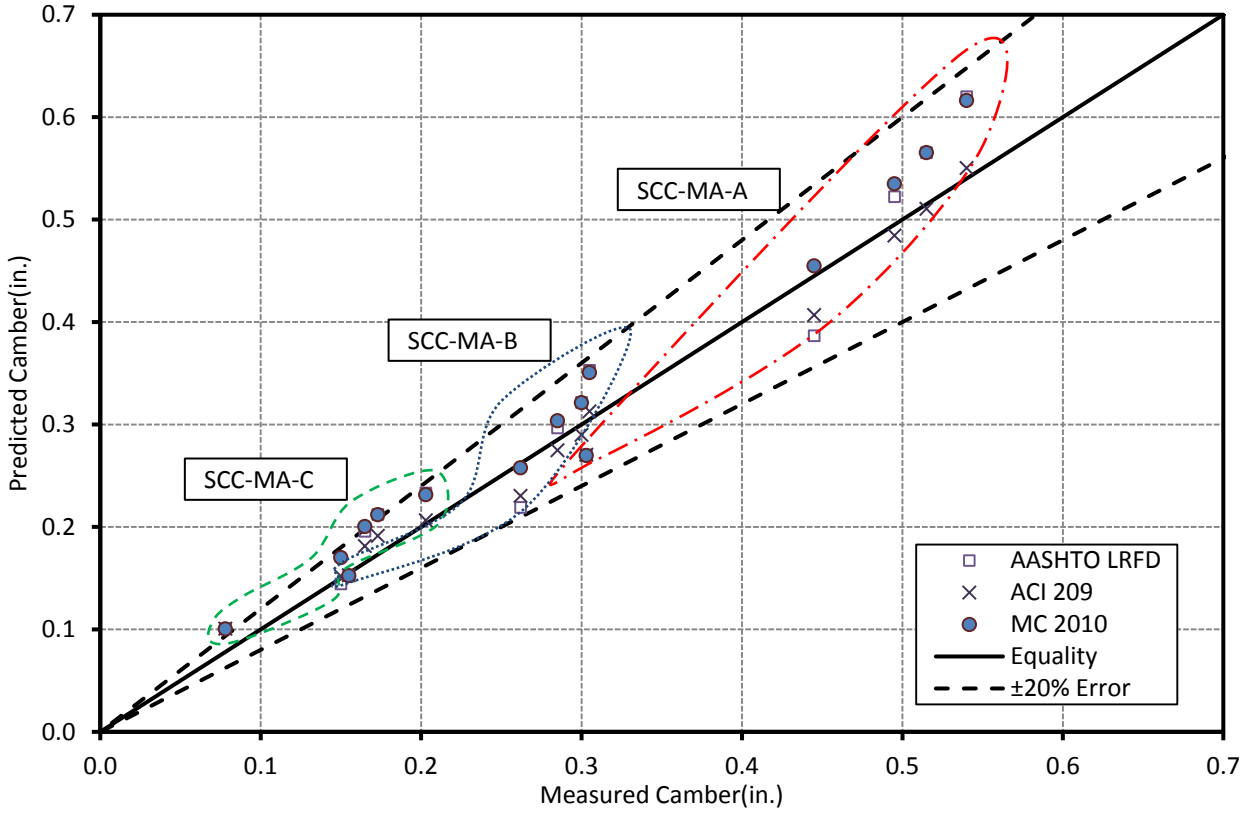

Figure 5-38: Predicted vs. Measured Midspan Cambers—T-Beams—SCC-MA

(3 of 4) SCC-MS Girders

Figure 5-39 shows the camber analyses for the SCC-MS girders just after transfer, at 14 days, and 56 days after transfer.

At transfer, the predictions fall within the ±20% error lines. The error elevates at later ages. The camber development from 14 days to 56 days is not as much as the predicted amounts. At later ages, most of the camber predictions remain within the ±20% error lines. MC 2010 reveals the largest camber predictions; in contrast, AASHTO LRFD reveals the least camber predictions. It is consistent with the creep coefficient predictions.

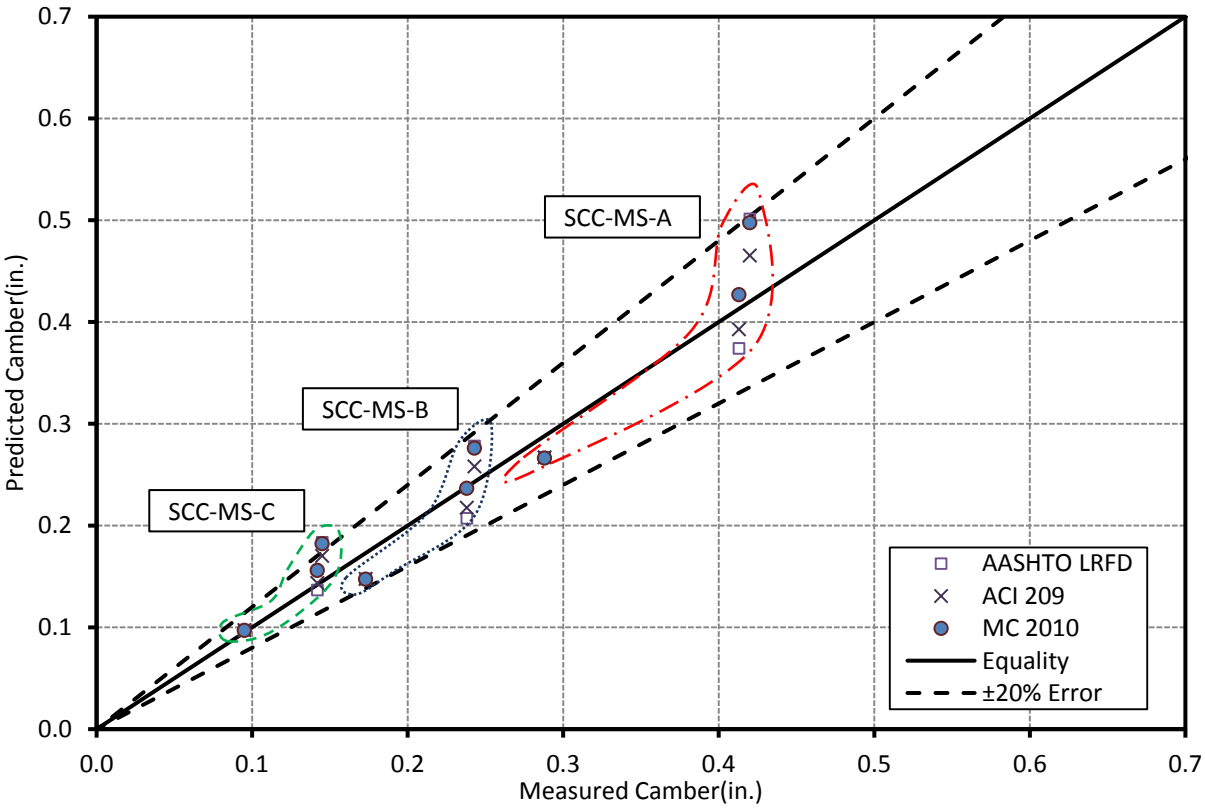

Figure 5-39: Measured vs. Predicted Internal Strains—T-Beams—SCC-MS

(3 of 4) SCC-HS Girders

The camber estimations and measurements for the SCC-HS girders are plotted in Figure 5-40. The comparison of cambers can be seen immediately after transfer and at 14 days after transfer. The initial cambers are not predicted very accurately. At 14 days, the prediction for the shortest span falls beyond the +20% error lines. The measurement error can be an issue for these girders due to the precision of the method to read cambers.

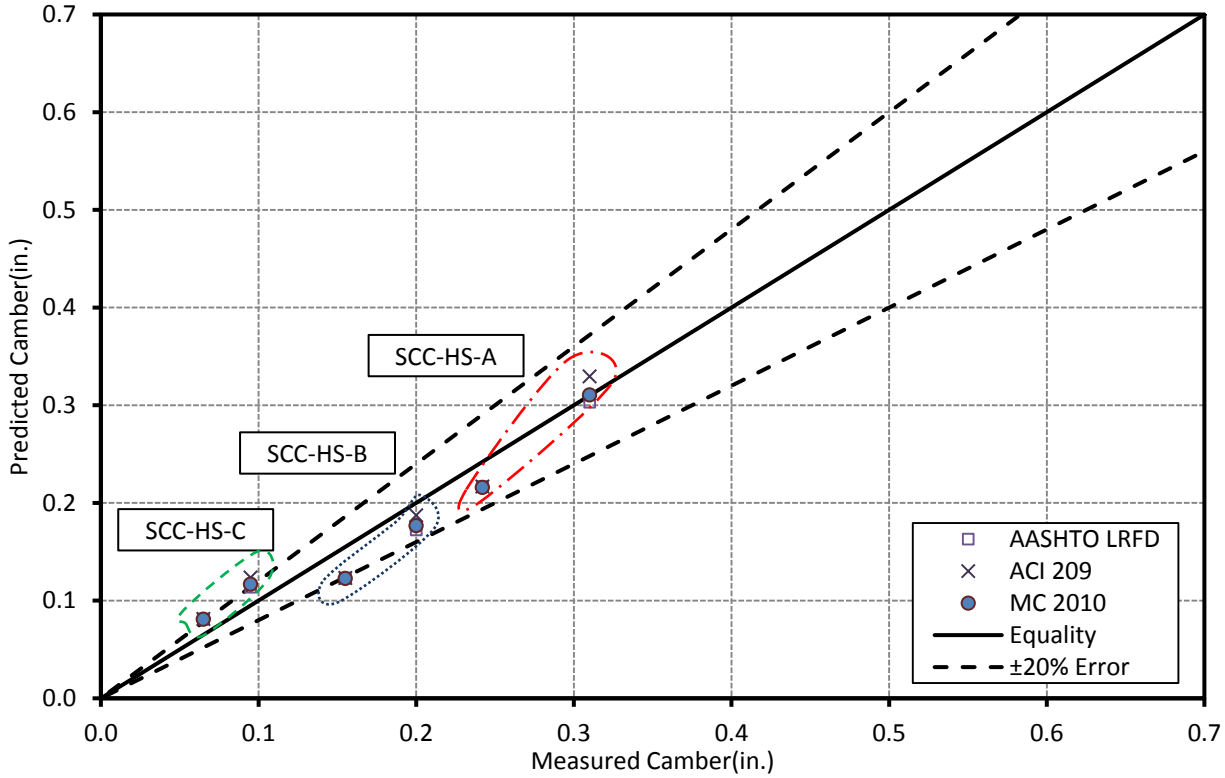

Figure 5-40: Predicted vs. Measured Midspan Cambers—T-Beams—SCC-HS

(4 of 4) Statistical Evaluation of the Error for Predicted Cambers—Project 4

The unbiased estimates plotted in Figure 5-41 show the fractional errors in camber predictions. In spite of the different span lengths, three girders for each casting group are evaluated together since the similar creep and shrinkage predictions are made for them. The span lengths for the A, B, and C girders were 276, 196, and 156 inches, respectively.

The figure is scaled differently than the previous graphs. The camber *growth* is determined by taking the difference between the long-term cambers and the initial cambers. The analyses with the non-accelerated properties are also included for comparison purposes.

100% error for the camber at transfer represents a camber error of 0.18 inches; in contrast, 100% error for the camber at later ages is equal to a camber error of 0.12 inches. The slight camber amounts shed the lights on the possible measurement errors since the precision of test methods was not any better than 0.01 inches.

STD-M, SCC-MS, and SCC-HS underpredict the initial camber on average; while, SCC-MA overpredict them. At later ages, the *growth* is overpredicted except for the 14-day predictions of the moderate-strength girders.

The results are studied in three groups: (i) different prediction models are compared to each other, (ii) the casting groups are contrasted to each other, and (iii) the comparison of the analyses with accelerated and non-accelerated properties is made.

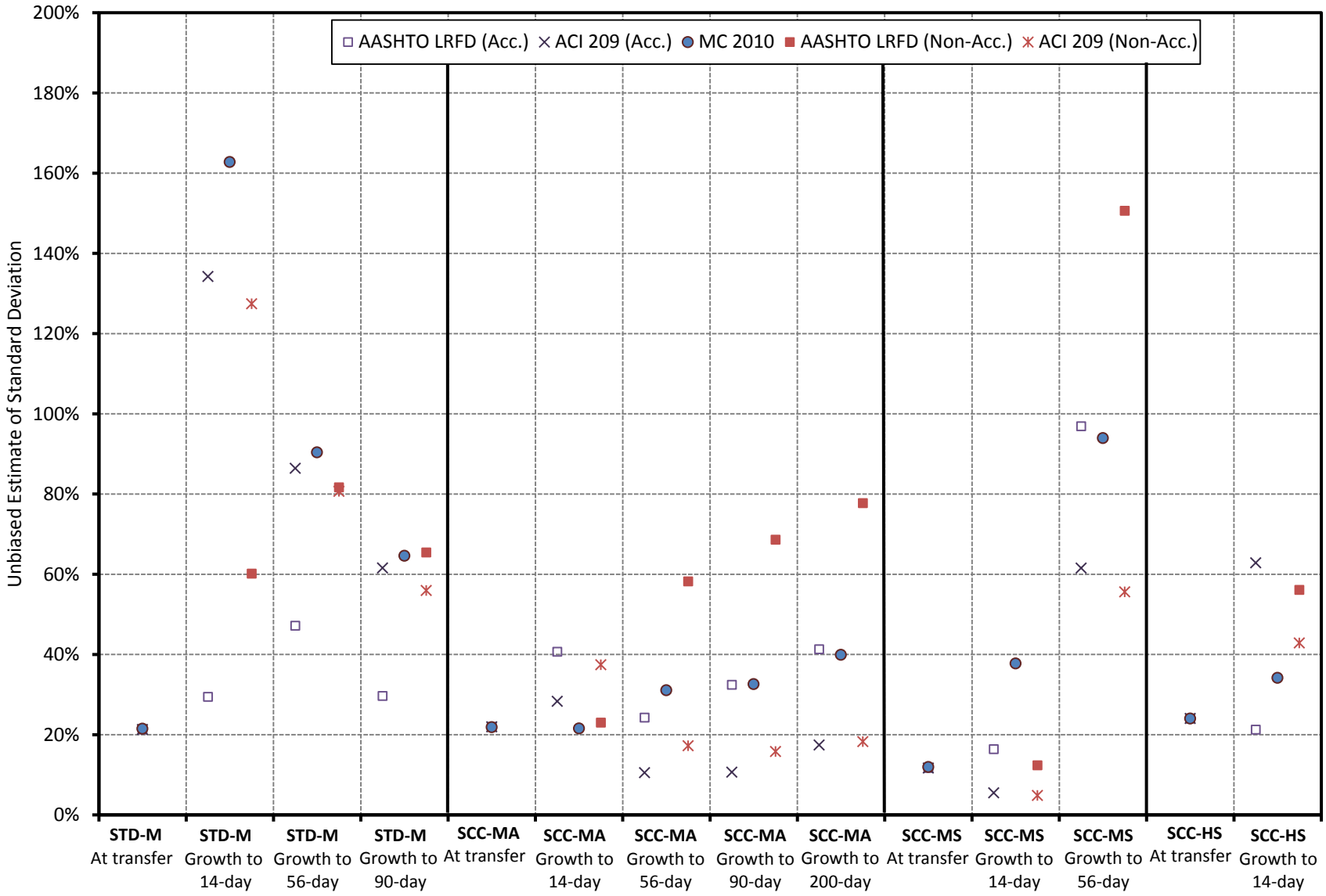

Figure 5-41: Fractional Errors—Midspan Cambers—Project 4

i. Comparison of AASHTO LRFD, ACI 209 and *fib* MC 2010

Initial predictions depend on the elastic properties and therefore free from the chosen creep and shrinkage prediction model. AASHTO LRFD estimates the camber *growth* most accurately for STD-M; in contrast, ACI 209 reveals the most accurate *growth* for SCC-MA and SCC-MS. MC 2010, on the other hand, predicts the camber *growth* least accurately for STD-M, SCC-MA, and SCC-MS. The data for the SCC-HS cambers were available up to 14 days, and AASHTO LRFD reveals the best predictions at that age.

ii. Comparison of STD-M, SCC-MA, SCC-MS, and SCC-HS

At transfer, the predictions for SCC-MS are best estimated among the four casting groups, which can be related to the initial MOE. At later ages, the SCC-MA girders have the most accurate predictions; conversely, the STD-M girders have the least accurate predictions on average. Also, the accuracy of the camber measurements may have influenced the overall trend.

iii. Comparison of the prediction models with accelerated and non-accelerated properties

AASHTO LRFD with the accelerated curing properties predicts the cambers more accurately than AASHTO LRFD with the non-accelerated properties. ACI 209 with the accelerated curing shows slightly less accuracy than ACI 209 with the non-accelerated curing. AASHTO LRFD is more sensitive to the curing properties than ACI 209 as also observed in the creep predictions in Figure 5-36.

Although special effort had not been applied to accelerate the curing, the strength-maturity curves indicate that T-Beams were accelerated cured. The hydration process must have elevated the internal temperature to the sufficient level.

5.7 Discussion of Results

5.7.1 Bottom-Flange Strain Analyses

5.7.1.1 Overview

The strain analyses were completed for the bottom flange in order to have a better idea about the prestress losses and the time-dependent deflections. The bottom-flange strains are the best indicators of the prestress losses since the centroid of the fully prestressed strands is located within the bottom flange. The strain *growth* is caused by the time-dependent deflections such as shrinkage and creep. Accuracy of the shrinkage and creep predictions can be investigated better after analyzing the curvature and camber.

5.7.1.2 Bottom-Flange Strain Readings at Midspan

Table 5-2 shows arithmetical average of the recorded bottom-flange strains. In Projects 1 and 2, the strain readings were corrected to take account of thermal gradients. The concrete age at *growth* is the least age among the different girders for a group. Approximate prestress losses can be found by multiplying the strain amount with the MOE of prestressing steel. To illustrate, a strain of -100 με is equal to a prestress loss of 2.9 ksi for strands with a MOE of 29,000 ksi.

Table 5-2: Average of Initial and Growth Strain Readings

Project # and Identification			Age at Growth (days)	Bottom-Flange Strain ($x10^{-6}$ in./in.)		
				Initial	Growth	Ratio
1	BT-54	SCC	205	-437	-287	**66%**
		VC	205	-439	-279	**64%**
	BT-72	SCC	182	-489	-374	**76%**
		VC	182	-463	-338	**73%**
2	STD-M	VC	110	-256	-408	**159%**
	SCC-MS	SCC	160	-222	-399	**180%**
	SCC-HS	SCC	214	-167	-196	**117%**
3	BT-54	VC	180	-879	-519	**59%**

In Section 2.3, the factors affecting the time-dependent deflections are explained. Accordingly, initial readings depend on the elastic properties such as MOE of concrete and prestress layout. In Project 2, SCC-HS has the least initial strain readings despite the similar prestress force and its layout, and this is corresponded to the MOE of concrete at transfer. Also, total prestress force explains the difference in the initial strains between the VC BT-54 girders in Projects 1 and 3.

Moreover, the strain *growth* is driven majorly by creep and shrinkage as explained in Section 2.3. Creep and shrinkage depend on several factors such as concrete mixture, ambient conditions, and curing type. BT-72 develops greater strain *growth* than BT-54 in Project 1 possibly due to the effect of creep curvature. Similarly, the moderate-strength girders in Project 2 develop greater strain *growth* than the related high-strength girders because of the different concrete mixture. All in all, the strain readings shown in Table 5-2 are consistent with the expectations, and it can also give a preliminary idea about the range of strains and prestress losses.

5.7.1.3 Bottom-Flange Strain Predictions at Midspan

Bottom-flange strain predictions for Projects 1, 2, and 3 are briefly discussed in this section. The strain analyses are investigated thoroughly in Sections 5.3.2, 5.4.2, and 5.5.2. The initial strain predictions are more accurate than the *growth* predictions. MC 2010 reveals the same bottom-flange strains at transfer with other two prediction models when the shrinkage up to the benchmark point is excluded.

Table 5-3 tabulates the best models according to the unbiased estimates at erection. It also provides the prediction trend and the unbiased estimates of strain errors. The moderate-strength girders are predicted more accurately than the high-strength girders. The moderate-

strength girders have the combination of over- and underpredictions; however, the high-strength girders are generally overpredicted. The current shrinkage and creep models are accurate for the moderate-strength girders, but they may not be as good at estimating the high-strength girders.

Table 5-3: Summary of Strain Growth at Erection

Project # and Identification			Prediction Trend*	Best Model wrt UE-StDev	UE-StDev (%)	UE-StDev (με)
1	BT-54	SCC	O	AASHTO LRFD	92	260
		VC	O	AASHTO LRFD	96	262
	BT-72	SCC	O	MC 2010	65	234
		VC	O	AASHTO LRFD	66	215
2	STD-M	VC	M	MC 2010	12	51
	SCC-MS	SCC	M	ACI 209	6	23
	SCC-HS	SCC	O	AASHTO LRFD	76	147
3	BT-54	VC	O	MC 2010	23	105

* 'O', 'M', and 'U' stand for overpredicted, mixed, and underpredicted, respectively. The trends are for the entire prediction set at erection.

In Projects 1 and 2, AASHTO LRFD usually gives the most accurate predictions for the high-strength girders; however, the high-strength girders in Project 3 are predicted most accurately by MC 2010.

For the overpredicted cases, the best predictions are obtained by the model predicting the least shrinkage except for Project 3. The *growth* is calculated with respect to the 1-day strain in Project 3.

The Project 3 girders having greater prestress force are predicted more accurately than the Project 1 girders. The VC girders are predicted a little better than the SCC girders in Project 1, yet fractional errors for VC and SCC are considerably large. The BT-72 girders are predicted more accurately than the BT-54 girders. BT-54 and BT-72 have overpredicted bottom-flange strains and almost the same creep coefficient and shrinkage estimates strain despite the geometry difference.

The strain analyses may have errors rooted in the input variables and the strain readings. The input parameters such as slump, air content, concrete strength, or MOE can be inaccurate. Samples used for material testing might not represent the total girder behavior well enough due to the probable imperfections. MC 2010 may have been implemented incorrectly since it was functioned according to the European Standards. In addition to the input variables, readings obtained from the strain gages may be erroneous. The strain gages may have been dislocated or even damaged while the concrete was being poured.

5.7.2 Curvature Analyses

5.7.2.1 Overview

Curvature is analyzed to understand the effects of creep predictions primarily at midspan. Initial and *growth* curvatures can be studied separately. The initial values primarily depend on MOE of a girder and arrangement of prestressing strands; while, the *growth* estimations depend significantly on creep curvature. Creep curvature is determined by multiplying creep coefficient and initial curvature. Contrary to strain *growth,* curvature *growth* depends on initial curvature. Besides, understanding the curvature growth can untangle the interaction of creep and shrinkage for strain growth.

5.7.2.2 Midspan Curvature Readings

As the distance between the strain gages increase, the curvature readings become less sensitive to the likelihood of dislocation of gages. Therefore, the curvature readings are obtained by taking the top- and bottom-flange strains and dividing them with the vertical distance. Arithmetic average of the curvature readings are provided in Section 5.7.3.2.

5.7.2.3 Midspan Curvature Predictions

Midspan curvature predictions for Projects 1, 2, and 3 are discussed in depth in Sections 5.3.3, 5.4.3, and 5.5.3, respectively. The curvature predictions at transfer are same regardless of the chosen prediction model. They are more accurate than the *growth* predictions except for the SCC BT-72 girders. The non-uniformity is caused by the casting group J having the least initial reading.

The best prediction models are listed in accordance to the fractional errors in Table 5-4. The curvature predictions for the moderate-strength girders are mostly underpredicted. AASHTO

LRFD predicts the curvature *growth* best; on the other hand, ACI 209 estimates it least accurately. For the underpredicted estimates, the best model also predicts the greatest creep.

Table 5-4: Summary of the Curvature Growth at Erection

Project # and Identification			Prediction Trend*	Best Model wrt UE-StDev	UE-StDev (%)	UE-StDev (x10^{-6}/in.)
1	BT-54	SCC	M	ACI 209	16	0.6
		VC	O	AASHTO LRFD	16	0.6
	BT-72	SCC	M	AASHTO LRFD & MC 2010	10	0.3
		VC	M	AASHTO LRFD & MC 2010	19	0.8
2	STD-M	VC	U	AASHTO LRFD	32	3.2
	SCC-MS	SCC	U	AASHTO LRFD	26	2.2
	SCC-HS	SCC	M	ACI 209	24	1.3
3	BT-54	VC	M	MC 2010	12	0.8

* 'O', 'M', and 'U' stand for overpredicted, mixed, and underpredicted, respectively. The trends are for the entire prediction set at erection.

For the high-strength girders, the predictions have a mixed distribution. This is the reason why the curvature predictions are more accurate than the relevant strain predictions.

The curvatures at later ages are influenced by the interaction of creep curvature and moment of inertia. The BT-54 girders are overpredicted on average, but the BT-72 girders are underpredicted on average.

For the high-strength girders, the curvature *growth* is estimated more accurately than the strain *growth*. Still, there can be errors originated in the input variables and the strain readings as explained in Section 5.7.1.3.

5.7.3 Camber Analyses

5.7.3.1 Overview

The camber predictions are based on the moment-area method as explained in Section 3.2.1. Initial camber predictions are determined by the elastic properties. Camber *growth*, on the other hand, depends on creep predictions similar to the curvature *growth*. However, curvature is analyzed separately because camber analysis is the summation of the varying curvatures (not only midspan curvature) along the length of a girder.

5.7.3.2 Midspan Camber Readings

Arithmetical averages of the midspan curvature and camber readings are provided in Table 5-5. The initial curvatures and cambers were measured just after transfer for the all projects. Also, it includes the least concrete age among the girders within the same group.

Table 5-5: Average of Initial and Growth Measurements

Project # and Identification			Age at Growth (days)	Curvature ($x10^{-6}$ 1/in.)			Midspan Camber (in.)		
				Initial	Growth	Ratio	Initial	Growth	Ratio
1	BT-54	SCC	205	-6.9	-4.0	**58%**	1.09	0.59	**54%**
		VC	205	-6.6	-4.0	**61%**	1.02	0.66	**65%**
	BT-72	SCC	182	-4.4	-3.1	**70%**	1.42	0.95	**67%**
		VC	182	-4.5	-3.3	**72%**	1.32	0.88	**67%**
2	STD-M	VC	110	-10.7	-10.0	**94%**	0.27	0.26	**96%**
	SCC-MS	SCC	160	-8.0	-11.3	**142%**	0.24	0.21	**88%**
	SCC-HS	SCC	214	-5.4	-5.2	**95%**	0.15	0.10	**67%**
3	BT-54	VC	180	-15.8	-6.0	**38%**	2.89	1.34	**46%**

Initial curvature and camber deflections depend largely on the elastic properties such as MOE of concrete, girder length, and eccentrically applied prestress force. In Project 1, BT-72 exhibits less initial curvature than BT-54; conversely, the initial camber of BT-72 is greater than the initial readings of BT-54. High-strength girders demonstrate greater MOE than the moderate-strength girders; thus, the high-strength girders have less curvature and camber in Project 2.

Different initial values between the VC BT-54 girders in Projects 1 and 3 can be explained by the total prestress force.

Curvature and camber *growth* depends largely on the creep-induced curvature. The larger the initial curvature is, the larger the creep-induced curvature becomes—assuming the same creep deflections. Consequently, the curvature and camber *growth* readings are grounded on the initial readings, and it clarifies why the *growth* follows a similar trend with the initial readings.

Besides, curvature readings are determined from the strain readings; camber readings were mostly obtained with the surveyor's method. Comparing them can also give an idea about the performance of different testing methods.

5.7.3.3 Midspan Camber Predictions

Midspan camber predictions for Projects 1, 2, 3, and 4 are reported in detail in Sections 5.3.4, 5.4.4, 5.5.4, and 5.6.2, respectively. The initial camber predictions are generally more accurate than the *growth* predictions, and they do not differ with the selected prediction model.

Initial errors may have been minimized if the following possibilities had been precluded. Recorded MOE may not represent actual girders because of imperfections existing in them and curing techniques applied to samples. Also, temperature gradient emanated from the cement hydration questions accuracy of the readings. The hold-down locations (existing only for Projects 1 and 3) may have restrained the upward movement and affected initial readings.

Fractional errors for all of the girders can be found in Table H-3 in Appendix H. The cambers were measured with a precision of 1/16 in. for Project 3 and with a precision of 0.01 in. for Projects 1 and 2. The camber measurements of Project 4 were achieved with the surveyor's method.

Table 5-6 presents the best models according to the fractional errors at erection. It also provides the prediction trend and related camber errors. The SCC-HS girders in Project 4 are not tabulated since the camber readings were available up to 15 days.

Table 5-6: Summary of the Camber Growth at Erection

Project # and Identification			Prediction Trend*	Best Model wrt UE-StDev	UE-StDev (%)	UE-StDev (in.)
1	BT-54	SCC	O	ACI 209	109	0.34
		VC	O	ACI 209	62	0.22
	BT-72	SCC	O	ACI 209	19	0.16
		VC	O	ACI 209	16	0.13
2	STD-M	VC	M	MC 2010	11	0.03
	SCC-MS	SCC	M	MC 2010	9	0.02
	SCC-HS	SCC	O	MC 2010	47	0.04
3	BT-54	VC	O	ACI 209	15	0.19
4	STD-M	VC	O	AASHTO LRFD	30	0.04
	SCC-MA	SCC	O	ACI 209	17	0.03
	SCC-MS	SCC	O	ACI 209	62	0.05
	SCC-HS	SCC	N/A	N/A	N/A	N/A

* 'O', 'M', and 'U' stand for overpredicted, mixed, and underpredicted, respectively. The trends are for the entire prediction set at erection.

The moderate-strength girders are predicted significantly better than the high-strength girders. The VC girders are better predicted than the SCC girders. In other words, the creep models predict the moderate-strength girders and the VC girders better than the high-strength girders and the SCC girders. For the moderate-strength girders, it is hard to draw a conclusion about the most accurate model. The high-strength girders in Projects 1 and 3 are best predicted by ACI 209. The BT-72 girders are predicted more accurately than the BT-54 girders as observed in strain and curvature predictions.

For the prediction models, the larger the creep coefficient is estimated, the greater the camber is predicted at midspan. Therefore, the model predicting the least creep coefficient reveals the most accurate estimations for the overpredicted cases.

The camber analyses can include measurement errors and errors in the input parameters. For instance, the camber errors are less than 0.05 in. for Project 2, but the precision of the surveyor's method to measure camber was 0.01 in.. The input parameters used for the time-dependent analysis may not be accurate. Material testing method might not represent girder properties well due to the imperfections. Also, the MC 2010 prediction model may not have been implemented accurately because it was based on the European construction practice.

5.7.4 Creep and Shrinkage Predictions

Strain, curvature, and camber *growth* are grounded on creep and shrinkage predictions. Strain *growth* is influenced considerably by two elements: shrinkage and creep. The leading element for strain *growth* varies with the depth of a girder. The curvature and camber *growth*s, on the other hand, depend largely on creep. This section summarizes creep and shrinkage predictions and ties them up with bottom-flange strain, curvature, and camber predictions. The high-strength girders in Project 4 are not considered since they were analyzed up to 14 days.

The summary of the creep and shrinkage predictions can be seen in Figure 5-7. Due to the variety of values, the models predicting the least and greatest creep and shrinkage are indicated. The entire data set can be seen in Table D-1 in Appendix D.

Table 5-7: Least and Greatest Creep and Shrinkage Predictions at Erection

		Creep Coefficient		Shrinkage Strain (Magnitude)	
		The Least	**The Greatest**	**The Least**	**The Greatest**
High-Strength	SCC[(1)]	ACI 209	MC 2010	MC 2010& AASHTO LRFD	ACI 209
	SCC[(2)]	MC 2010 & AASHTO LRFD	ACI 209	AASHTO LRFD	ACI 209
	VC[(1)]	ACI 209	MC 2010	MC 2010& AASHTO LRFD	ACI 209
Moderate-Strength	SCC	ACI 209	AASHTO LRFD	MC 2010	AASHTO LRFD
	VC	ACI 209	MC 2010	MC 2010	AASHTO LRFD

[(1)]28-day strengths of the high-strength girders in Projects 1 and 3 range from 9670 to 11050 psi.
[(2)]28-day strengths of the high-strength girders in Project 2 are13160 and 13580 psi.

The high-strength girders in Projects 1 and 3 attained a compressive strength of about 2000 psi less than the girders in Project 2. It influences the creep and shrinkage predictions. Further, the predictions for the high-strength girders with SCC and VC do not differ from each other in Projects 1 and 3. However, the moderate-strength VC and SCC girders have inconsistency probably due to the unusual air content (11%) in Project 4.

Moreover, excluded shrinkage up to the benchmark reading is -57 microstrains at the most for MC 2010. It affects the strain predictions in Projects 1 and 3. The shrinkage readings may have been more accurate if benchmark readings were taken immediately after cast of fresh concrete. Autogenous shrinkage starts to develop prior to cast of fresh concrete.

The larger the creep coefficient is estimated, the greater the curvature and camber *growth* is predicted at midspan. Similarly, the less the shrinkage strain is predicted, the less the bottom-flange strain *growth* is predicted. Therefore, a model with the least creep coefficient (or shrinkage strain) becomes the most accurate model for the overpredicted curvatures and cambers (or overpredicted bottom-flange strains). Indeed, ACI 209 predicts the most accurate curvature and camber *growth* for the overpredicted high-strength girders in Projects 1 and 3. Similarly, AASHTO LRFD and MC 2010 estimate bottom-flange shrinkage strains more accurately for them.

5.7.5 Suggestions for Selecting a Material Prediction Model

In this section, the suggestions are made according to the fractional errors of the *growth* predictions as provided in Table 5-8. The high-strength T-Beams are not included in the analysis because they were only analyzed up to 14 days. Strain *growth* depends on shrinkage and creep, yet curvature and camber *growth* depend largely on creep.

Table 5-8: Fractional Errors at Erection

		Strain Growth			Curvature Growth			Camber Growth		
		AASHTO LRFD	ACI 209	MC 2010	AASHTO LRFD	ACI 209	MC 2010	AASHTO LRFD	ACI 209	MC 2010
High-Strength	SCC[(1)]	0.78	0.96	0.84	0.19	0.14	0.25	0.84	0.75	0.97
	SCC[(2)]	0.76	1.49	0.91	0.31	0.24	0.32	0.51	0.64	0.47
	VC[(1)]	0.69	0.76	0.75	0.17	0.18	0.19	0.41	0.38	0.50
Moderate-Strength	SCC	0.31	0.07	0.15	0.26	0.56	0.40	0.58	0.35	0.55
	VC	0.35	0.27	0.12	0.32	0.70	0.35	0.22	0.51	0.46
T-Beams (Accelerated)		N/A	N/A	N/A	N/A	N/A	N/A	0.55	0.44	0.60
T-Beams (Non-Acc.)		N/A	N/A	N/A	N/A	N/A	N/A	0.91	0.40	0.60

[(1)]28-day strengths of the high-strength girders in Projects 1 and 3 range from 9670 to 11050 psi.

[(2)]28-day strengths of the high-strength girders in Project 2 are 13160 and 13580 psi.

The moderate-strength girders are predicted more accurately than the high-strength girders with an exception of the curvature *growth*. AASHTO LRFD 2014 predicts creep more accurately with the accelerated curing properties in T-Beams, and the ACI 209 creep predictions are somewhat similar for both accelerated and non-accelerated curing properties.

ACI 209 gives the best creep estimation for the high-strength girders in Projects 1 and 3 based on the curvature and camber *growth*. For the high-strength girders in Project 2, the creep is predicted most accurately by ACI 209 based on the curvature *growth*.

The creep predictions for the VC moderate-strength girders are obtained most accurately by AASHTO LRFD based on the curvature and camber *growth*. For the SCC moderate-strength girders, AASHTO LRFD gives the most accurate creep predictions based on curvature *growth.*

Moreover, AASHTO LRFD predicts strain *growth* with the greatest accuracy in Projects 1 and 3 unlike curvature and camber *growth* (i.e., creep). It shows that AASHTO LRFD predicts shrinkage deformations most accurately. Based on this reasoning, AASHTO LRFD also estimates shrinkage most accurately for the high-strength SCC girders in Project 2.

fib MC 2010 estimates shrinkage with the greatest accuracy for the moderate-strength VC girders. ACI 209 reveals the best shrinkage predictions for the moderate-strength SCC girders.

In Table 5-9, the summary of AASHTO LRFD and AASHTO LRFD +20 are provided. AASHTO LRFD +20 includes the 20% increase in the shrinkage strain. AASHTO LRFD estimates the bottom-flange strain *growth* more accurately, but the curvature and camber *growth* less accurately. Project 1 is the only project checked for this increase.

Table 5-9: Comparison of AASHTO LRFD models

		Fractional Errors at Erection					
		Strain Growth		**Curvature Growth**		**Camber Growth**	
		AASHTO LRFD		AASHTO LRFD		AASHTO LRFD	
		Standard	+20	Standard	+20	Standard	+20
Project 1	SCC	0.78	0.92	0.19	0.16	0.84	0.81
	VC	0.76	0.94	0.17	0.17	0.51	0.44

Last but not least, Keske (2014) suggested the prediction adjustments for each prediction model tabulated in Table 5-9. They are recommended especially for predicting the time-dependent deformations in prestressed girders produced in Alabama. Equation 5-3 shows the calculation of the best-fit adjusted prediction of the creep coefficient or shrinkage strain, $Y_{Adjusted}$ (Keske 2014).

Table 5-10: Recommended Creep and Shrinkage Prediction Adjustments Factors, A_{AL} (Adapted from Keske [2014])

Material	Prediction Type	Reference		
		AASHTO LRFD	ACI 209	MC 2010
SCC	Creep	1.2	1.1	1.2
	Shrinkage	1.0	0.8	0.8
VC	Creep	1.1	1.0	1.0
	Shrinkage	0.8	0.7	0.6

Note: 1.0 = no change recommended

$$Y_{Adjusted} = A_{AL} \times Y_{Predicted} \qquad \textit{Equation 5-3}$$

where, $Y_{Predicted}$ = predicted creep coefficient or shrinkage strain

A_{AL} = the prediction adjustment

Chapter 6 Summary and Conclusions

6.1 Summary

Predicting time-dependent deflections in prestressed concrete girders is important to avoid additional costs related to misaligned deck forms or excessive deck concrete quantity. Underestimating camber may result in adjusting the design of deck at the time of construction; on the other hand, overestimating camber may result in a bridge sagging under superimposed dead load. In order to estimate time-dependent deflections, camber prediction software was developed with the time-step approach.

The first version of the camber software was created by Schrantz (2008) and revised by Johnson (2012). Within the scope of this thesis research, the source code of the application was updated and expanded to add recent material prediction models and new user-friendly features.

The new version includes one two-point concrete modulus of elasticity (MOE) model based on measured MOE (two-point MOE model) and three strength-based MOE models: AASHTO LRFD, ACI 209R-92, and *fib* Model Code (MC) 2010. The existing creep and shrinkage models were updated to include these three prediction models. Also, new version can save input and output data as a spreadsheet and import input variables from a spreadsheet, which allows users to collect data in fairly short time.

Experimental data were obtained from four previous prestressed girder projects: the Hillabee Creek Bridge Project, the AASHTO Type I Project, the HPC Project, and the T-Beam

Project—they are referenced as Projects 1, 2, 3, and 4, respectively. The girders were produced either with vibrated concrete (VC) or with self-consolidating concrete (SCC).

The collected data comprise camber and strain measurements of nineteen BT-54 girders, fourteen BT-72 girders and six Type I girders. The camber data of twelve 15-inch-deep T-Beams were also included in the analyses. The actual 28-day compressive strength of the girders ranges from 6300 to 13,600 psi.

Time-dependent responses such as strain, curvature, and camber were predicted with various creep and shrinkage models but same two-point MOE model. In order to evaluate the accuracy of the models, they were compared with the recorded responses of fifty-one girders.

6.2 Conclusions

The following conclusions were drawn for the initial predictions of bottom-flange strain, midspan curvature, and midspan camber:

- Initial bottom-flange strain predictions can be influenced by autogenous shrinkage depending on construction practice. In fact, autogenous shrinkage up to the benchmark reading was predicted as much as -57×10^{-6} in./in. with MC 2010.
- For the high-strength girders, the bottom-flange strains are mostly underpredicted at transfer, while the midspan curvatures and cambers are generally overpredicted.
- For the moderate-strength girders, the initial bottom-flange strains, midspan curvatures, and cambers are underpredicted on average.

The following conclusions were drawn for the *growth* predictions of bottom-flange strain, midspan curvature, and midspan cambers:

- For the high-strength girders, the bottom-flange strain *growth* and the camber *growth* are mostly overpredicted; however, the midspan curvature *growth* includes both over- and underpredictions.
- For the moderate-strength girders, the bottom-flange strain *growth* and the camber *growth* consist of over- and underestimations, and the midspan curvature *growth* is frequently underpredicted.
- The larger the creep coefficient is estimated, the greater the curvature and camber *growth* are predicted at midspan for AASHTO LRFD, ACI 209, and MC 2010 within the same girder group. Similarly, the greater the shrinkage strain is predicted, the greater the bottom-flange strain *growth* is predicted.
- The creep coefficients for SCC and VC are estimated very close to each other by AASHTO LRFD, ACI 209, and MC 2010.
- The AASHTO LRFD and MC 2010 shrinkage predictions do not reflect a sharp difference for SCC and VC. However, the ACI 209 shrinkage predictions for SCC are greater (in magnitude) than VC since the ACI 209 shrinkage prediction model is a function of slump.
- The curvature *growth* of BT-54 is overpredicted on average, but the curvature *growth* of BT-72 is underpredicted on average despite the same amount of predicted creep coefficients.
- For the high-strength girders, curvature *growth* is estimated more accurately than strain and camber *growth*. Camber *growth* is estimated with a greater accuracy than strain *growth*.

- For the high-strength girders with SCC and VC, ACI 209 gives the best creep estimation based on curvature *growth.*
- For the high-strength girders with SCC and VC, AASHTO LRFD gives the best shrinkage predictions based on bottom-flange strain *growth*.
- For the moderate-strength girders with SCC and VC, AASHTO LRFD gives the most accurate creep predictions based on curvature *growth*.
- Based on bottom-flange strain *growth*, the most accurate shrinkage predictions are obtained for the moderate-strength girders with SCC by ACI 209 and with VC by MC 2010.
- AASHTO LRFD predicts creep more accurately when employing the accelerated curing time, and the ACI 209 creep predictions are somewhat similar regardless of the accelerated and non-accelerated curing time.
- AASHTO LRFD estimates the bottom-flange strain *growth* much more accurately than AASHTO LRFD with 20% increase in the shrinkage strain due to the curing (accelerated) duration but the curvature and camber growth a little bit less accurately.

6.3 Recommendations for Future Study

The following recommendations are offered for the future study:

- The relationships for expected concrete strength and MOE suggested by Hofrichter (2014) can be implemented in the camber software. The relationship for expected concrete strength at transfer is explained in Equation 2-5 in Section 2.3.2. The modified MOE functions are provided in Equations 2-6 and 2-7 in Section 2.3.3.
- The creep and shrinkage adjustment factors recommended by Keske (2014) should be used to predict the responses such as strains, curvatures, and cambers. The adjustment factors are given in Table 5-10 in Section 5.7.5.
- The camber software should be edited to reveal the predictions at user-defined times; therefore, comparison of predictions and recorded responses can be quicker.
- The camber software should be modified in a way to employ different creep and shrinkage models at the same time. This modification can decrease the duration of multiple analyses.
- The *fib* MC 2010 coefficients, which depend on aggregate and cement type, are based on the European construction practice. Equivalent coefficients for US construction practice should be investigated further.
- The existing output VS forms developed by Schrantz (2012) should be changed in a way to provide results in data tables; thus, a user is able to copy and paste additional output data not included in an exported spreadsheet.

References

AASHTO. 2012. *AASHTO LRFD Bridge Design Specifications*. 6th ed. Washington, DC: American Association of State Highway and Transportation Officials (AASHTO).

AASHTO. 2014. *AASHTO LRFD Bridge Design Specifications*. 7th ed. Washington, DC: American Association of State Highway and Transportation Officials (AASHTO).

ACI 209. 1992. Prediction of Creep, Shrinkage, and Temperature Effects in Concrete Structures (ACI 209R-92). (Reapproved 1997). Farmington Hills, MI: American Concrete Institute.

ACI 209. 2008. Guide for Modeling and Calculating Shrinkage and Creep in Hardened Concrete (ACI 209.2R-08). Farmington Hills, MI: American Concrete Institute.

ACI 363. 1992. State-of-the-Art Report on High-Strength Concrete (ACI 363R-92). Farmington Hills, MI: American Concrete Institute.

ACI 435. 1995. Control of Deflection in Concrete Structures (ACI 435R). (Reapproved 2000). Farmington Hills, Michigan: American Concrete Institute, 435R-21 – R435-25.

ASTM C39. 2010. Standard Test Method for Compressive Strength of Cylindrical Concrete Specimens. *ASTM International*. West Conshohocken, PA.

ASTM C150. 2012. Standard Specification for Portland Cement. *ASTM International*. West Conshohocken, PA.

ASTM C219. 2013. Standard Terminology Relating to Hydraulic Cement. *ASTM International*. West Conshohocken, PA.

ASTM C469. 2010. Standard Test Method for Static Modulus of Elasticity and Poisson's Ratio of Concrete in Compression. *ASTM International*. West Conshohocken, PA.

BS EN 197-1. 2011. Cement, Composition, Specifications and Conformity Criteria for Common Cements. London, England: British Standard Institution (BSI).

Boehm, K. 2008. Structural Performance of Self-Consolidating Concrete in AASHTO Type I Prestressed Girders. M.S. Thesis, Auburn University.

fib. 2010. *Model Code for Concrete Structures 2010*. Lausanne, Switzerland: International Federation for Structural Concrete.

Dekking, F.M., C. Kraaikamp, H.P. Lopuhaä, and L.E. Meester. 2005. *A Modern Introduction to Probability and Statistics: Understanding Why and How,* pp. 285-298. Springer-Verlag, NY.

Geokon. 2010. Model 4200/4202/4210 Vibrating Wire Strain Gage Instruction Manual. Rev J, 04/07.

Glover, J.M. and J.M. Stallings. 2000. High-Performance Bridge Concrete. *TE-036 Report, ALDOT Research Project 930-373*. Montgomery, AL: Alabama Department of Transportation.

Hofrichter, A. 2014. Compressive Strength and Modulus of Elasticity Relationships for Alabama Prestressed Concrete Bridge Girders. M.S. Thesis, Auburn University.

Johnson, B.R. 2012. Time-Dependent Deformations in Precast, Prestressed Bridge Girders. M.S. Thesis, Auburn University.

Keske, S.D. 2014. Use of Self-Consolidating Concrete in Precast, Prestressed Girders. PhD Dissertation, Auburn University.

Levy, K.R. 2007. Bond Behavior of Prestressed Reinforcement in Beams Constructed with Self-Consolidating Concrete. M.S. Thesis, Auburn University.

Martin, I. 1971. Effects of Environmental Conditions on Thermal Variations and Shrinkage of Concrete Structures in the United States. In *Proceedings of Symposium on Designing for the Effect of Creep, Shrinkage, and Temperature in Concrete Structures*, SP-27, pp. 279-300. Farmington Hills, MI: American Concrete Institute.

Magura, D.D., M.A. Sozen, and C.P. Siess. 1962. A Study of Stress Relaxation in Prestressing Reinforcement. *Civil Engineering Studies, Structural Research Series No. 237*. Urbana, IL: University of Illinois.

Naaman, A.E. 2004. *Prestressed Concrete Analysis and Design: Fundamentals,* 2nd ed. Techno Press 3000, Ann Arbor, MI.

O'Neill C.R. and French C.E. 2012. Validation of Prestressed Concrete I-Beam Deflection and Camber Estimates. *MNDOT Research Project 2012-16.* St. Paul, MN: Minnesota Department of Transportation.

PCI. 2010. *PCI Design Handbook,*7th ed. Chicago, IL: Precast/Prestressed Concrete Institute (PCI).

Stallings, J.M., R.W. Barnes, and S. Eskildsen. 2003. Camber and Prestress Losses in Alabama HPC Bridge Girders. *PCI Journal* 48 (5): 90–104.

Stallings, J.M. and S. Eskildsen. 2001. Camber and Prestress Losses in High Performance Concrete Bridge Girders. *ALDOT Research Project 930-373.* Montgomery, AL: Alabama Department of Transportation.

Stephens, R. 2012. *Visual Basic® 2012: Programmer's Reference*. John Wiley and Sons, Inc., Indianapolis, IN.

Schrantz, C.E. 2012. Development of a User-Guided Program for Predicting Time-Dependent Deformations in Prestressed Bridge Girders. M.S. Thesis, Auburn University.

Tadros, M.K., N. Al-Omaishi, S.J. Seguirant, and J.T. Gallt. 2003. *NCHRP Report 496: Prestress Losses in Pretensioned High-Strength Concrete Bridge Girders*. National Cooperative Highway Research Program (NCHRP). Washington, DC: Transportation Research Board.

Appendices

Appendix for Chapter 2

Appendix I: Cement Types

Appendices for Chapter 3

Appendix A: Notation

Appendix J: Feature of Exporting to and Importing from a Spreadsheet File

Appendix K Camber Prediction Software—User-Guided Input Forms

Appendices for Chapter 4

Appendix B: Project 1

Appendix C: Project 2

Appendix D: Project 3

Appendix E: Project 4

Appendix F: Camber Prediction Software—Input Variables

Appendices for Chapter 5

Appendix G: Measured and Predicted Data

Appendix H: Fractional Errors

Appendix A Notation

A_c	area of concrete
$A_{p,k}$	total area of strands in a prestressing steel layer
$A_{s,k}$	total area of steel bars in a reinforcing steel layer
A_{tr}	area of transformed cross section
$A_{tr,ini}$	area of transformed cross section at time of initial prestress
E_c	modulus of elasticity of concrete (time-dependent)
E_{ci}	modulus of elasticity of concrete at time of initial prestress
E_p	modulus of elasticity of prestressing steel
I_{tr}	transformed moment of inertia
$I_{tr,ini}$	transformed moment of inertia at time of initial prestress
i	time interval
j	cross section
k	layer of prestressing/reinforcing steel
M_g	moment due to self-weight only
$M_{0,ini}$	moment due to effective prestress force immediately after transfer
$N_{0,ini}$	effective prestress force immediately after transfer
n_p	modular ratio with respect to prestressing steel
n_s	modular ratio with respect to reinforcing steel

y	distance from the centroid of transformed section (positive = downward)
y_p	distance from a prestressing steel layer to the centroid of transformed section
y_s	distance from a reinforcing steel layer to the centroid of transformed section
$y_{p,k}$	distance from each prestressing steel layer to the centroid of transformed section
$y_{s,k}$	distance from each reinforcing steel layer to the centroid of transformed section
$\Delta f_{p,R,k}$	incremental change in prestress in each layer
$\Delta\varepsilon_{cen,cr}$	incremental unrestrained creep strain in concrete at centroid of transformed section
$\Delta\varepsilon_{c,sh}$	incremental unrestrained shrinkage strain in concrete at centroid of transformed section
$\Delta\varepsilon_{cen}$	incremental strain at the centroid of the transformed section
$\Delta\phi_{c,cr}$	incremental curvature due to unrestrained creep
$\Delta\phi$	incremental curvature
$\Delta\varepsilon_c$	total strain on a concrete section for each cross section (j) in each time interval (i)
$\Delta\varepsilon_s$	total strain on each steel layer for each cross section (j) in each time interval (i)
$\Delta\varepsilon_p$	total strain on each prestress strand for each cross section (j) in each time interval (i)
Δf_c	incremental stress on a concrete section
Δf_s	incremental stress on a reinforcing steel layer
Δf_p	incremental stress on a prestressing steel layer

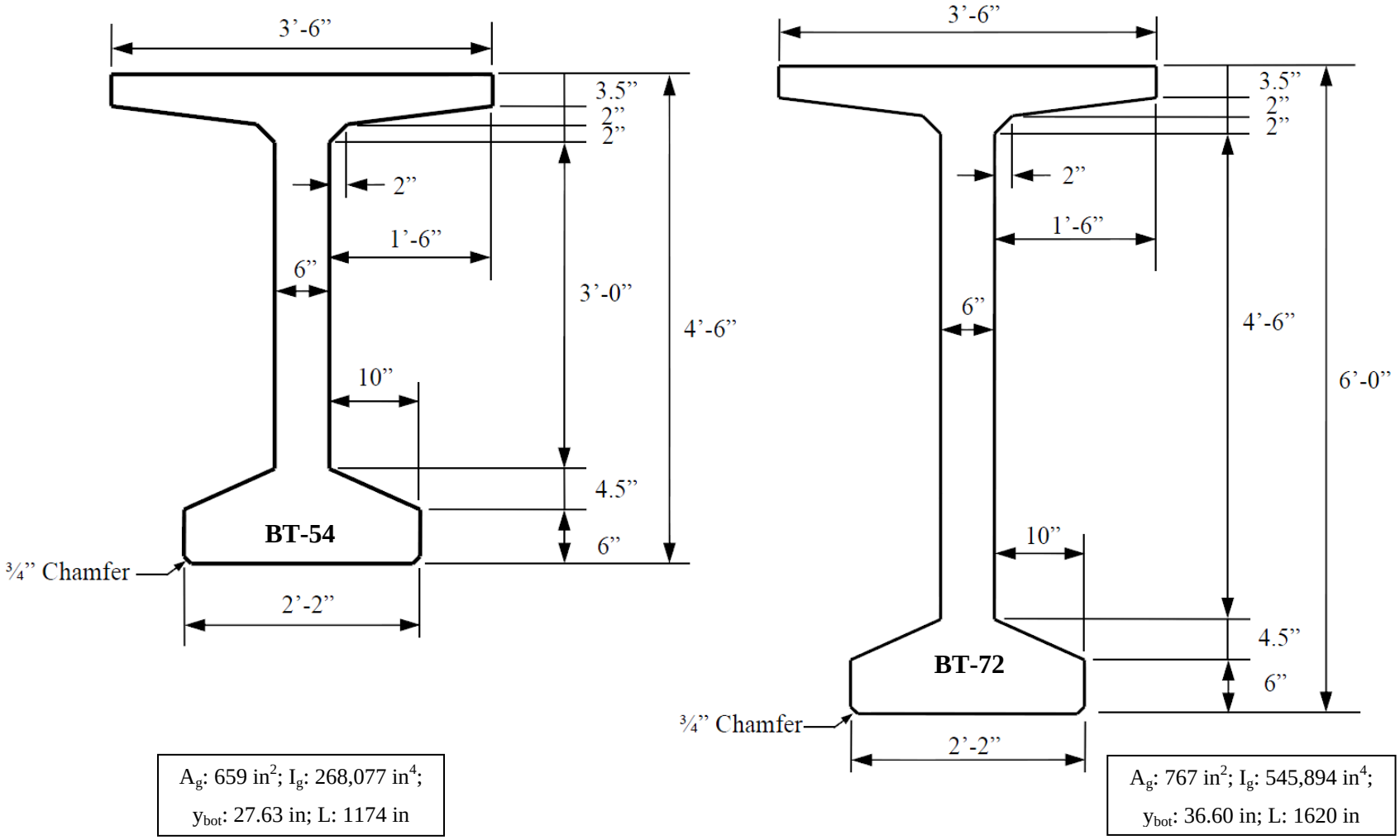

Figure B-1: Cross Section of BT-54 and BT-72 Girder (Adapted from Johnson [2012])

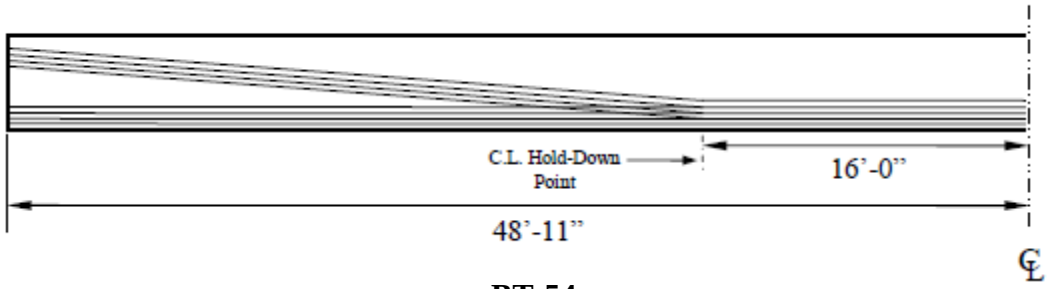

BT-54

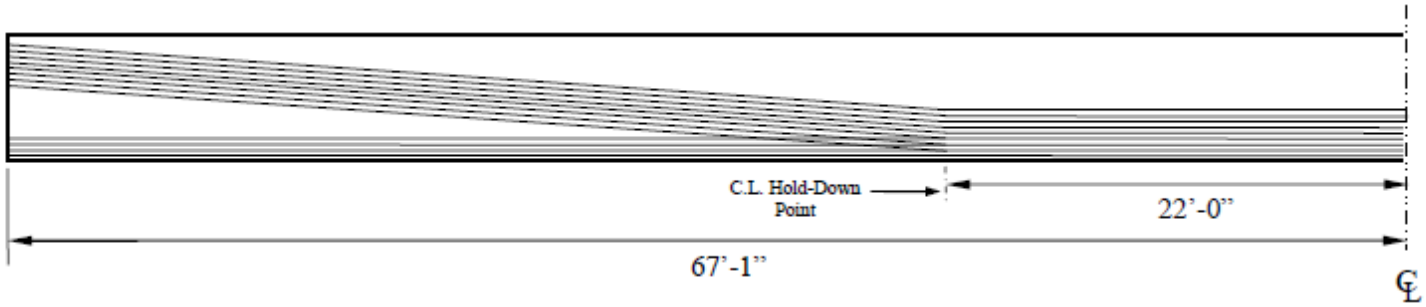

BT-72

Figure B-2: Profile and Hold-Down of Draped Strands for the BT-54 and BT-72 Girders (Johnson 2012)

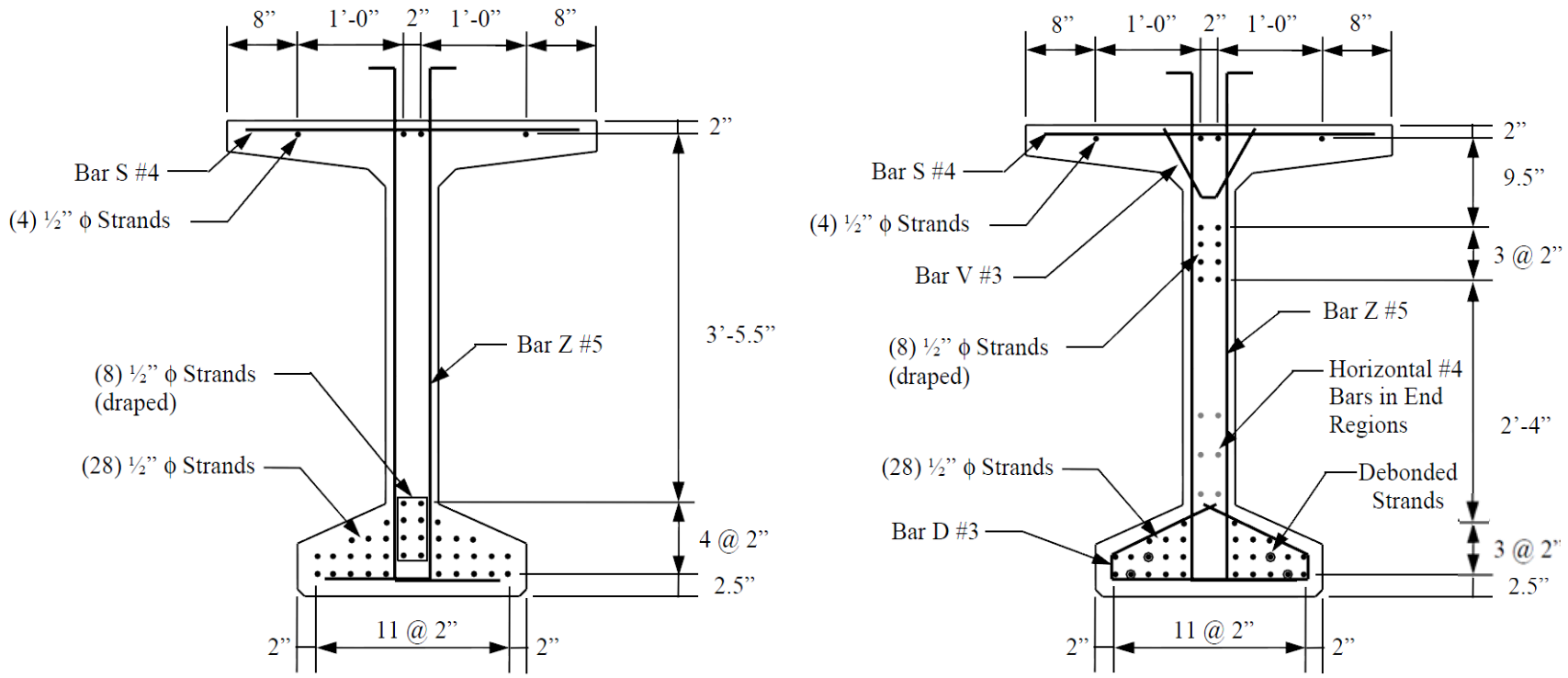

BT-54 at Midspan **BT-54 at Girder End**

Figure B-3: Mild Steel and Strand Arrangement for BT-54 Girder at Midspan and End (Adapted from Johnson [2012])

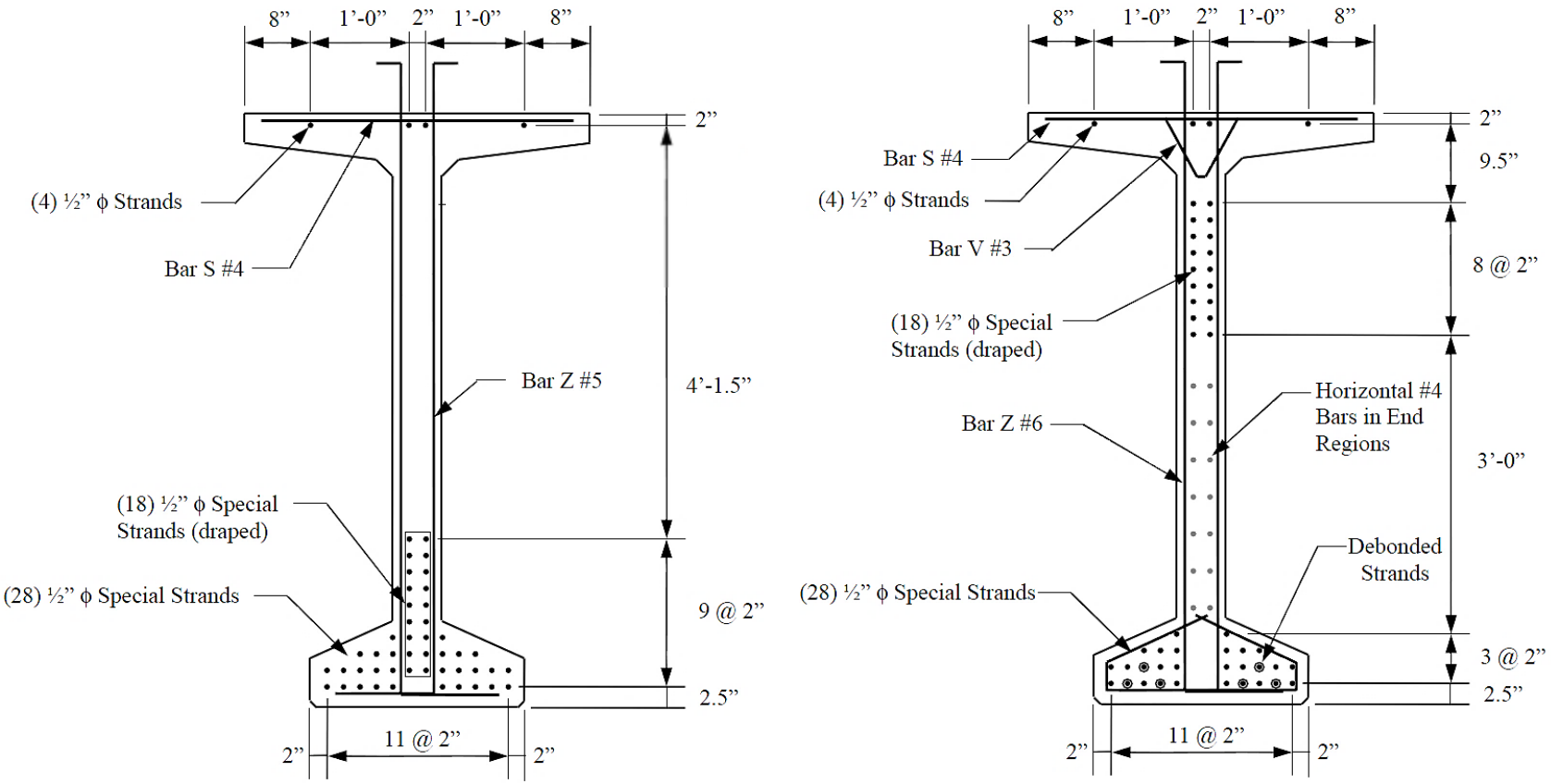

BT-72 at Midspan **BT-72 at Girder End**

Figure B-4: Mild Steel and Strand Arrangement for BT-72 Girder at Midspan and End (Adapted from Johnson [2012])

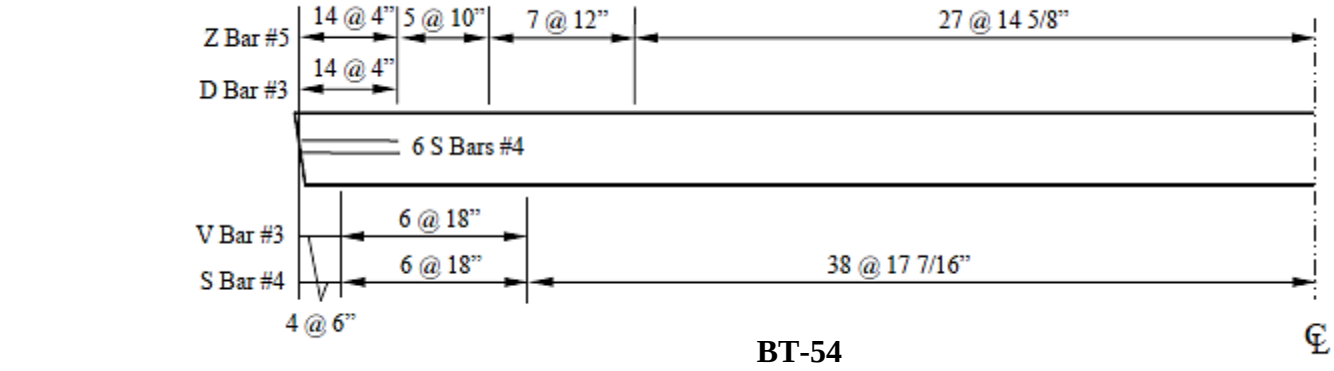

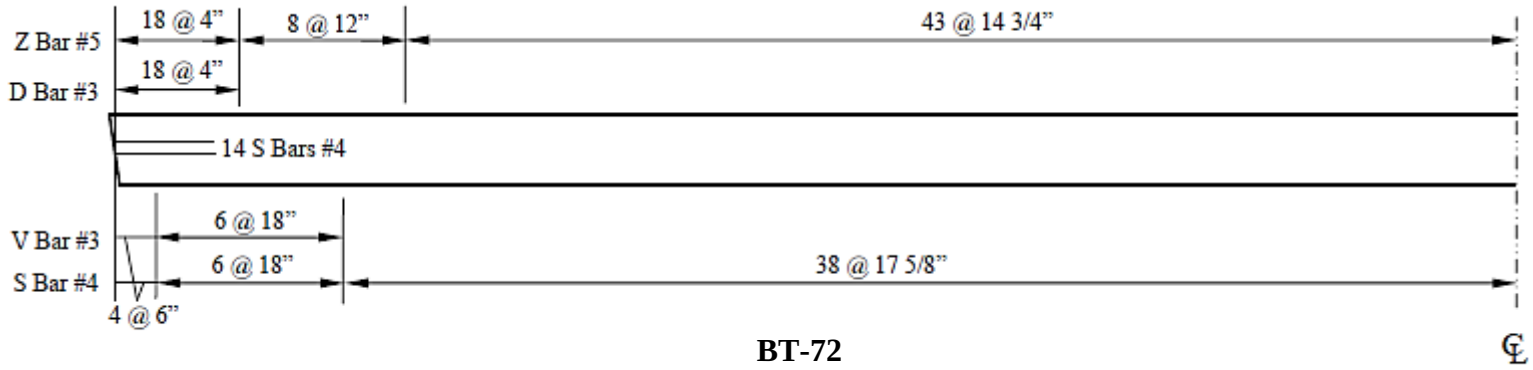

Figure B-5: Mild Steel Spacing in BT-54 and BT-72 Girder (Johnson 2012)

Table B-1: Fresh Concrete Properties (Johnson 2012)

Casting Group	Sample No.	Unit Weight (lb/ft^3)	Slump (in.)	Slump Flow (in.)	Air (%)	T50 (sec.)	VSI
A	1	149.1	-	28.0	3.3	-	1.5
	2	-	-	27.5	4.4	-	1.0
	3	-	-	26.0	4.5	-	1.0
B	1	152.3	9.00	-	3.9	-	-
	2	153.2	10.00	-	4.0	-	-
	3	-	8.75	-	4.0	-	-
C	1	-	-	27.0	2.6	7	1.0
	2	-	-	26.0	3.0	6	1.0
	3	-	-	27.0	4.6	8	1.0
D	1	-	8.50	-	4.2	-	-
	2	-	9.00	-	4.5	-	-
	3	-	8.75	-	4.4	-	-
E (SCC)	1	-	-	26.0	5.5	7	1.5
	2	-	-	26.0	4.2	8	1.5
E (CVC)	1	-	9.00	-	4.5	-	-
	2	-	8.75	-	3.9	-	-
F	1	150.1	-	25.0	3.7	10	0.0
	2	-	-	23.0	4.5	10	0.0
	3	-	-	24.0	3.8	11	0.0
G	1	-	8.50	-	4.0	-	-
	2	-	9.00	-	4.3	-	-
	3	-	8.75	-	3.5	-	-
H	1	-	-	26.0	3.3	8	1.0
	2	-	-	26.0	4.3	9	0.0
	3	-	-	23.0	4.8	14	0.0
I	1	-	9.00	-	3.1	-	-
	2	-	9.00	-	2.5	-	-
	3	-	9.25	-	3.1	-	-
J	1	149.8	-	22.5	4.2	9	1.0
	2	-	-	24.0	3.7	10	1.0
	3	-	-	22.0	3.8	15	1.0
K	1	153.4	8.50	-	3.6	-	-
	2	-	9.00	-	3.1	-	-
	3	-	9.00	-	3.5	-	-
L (SCC)	1	148.1	-	26.0	3.8	7	1.0
	2	-	-	28.0	3.7	5	1.5
L (CVC)	1	153.3	9.00	-	2.2	-	-
	2	-	8.25	-	3.2	-	-

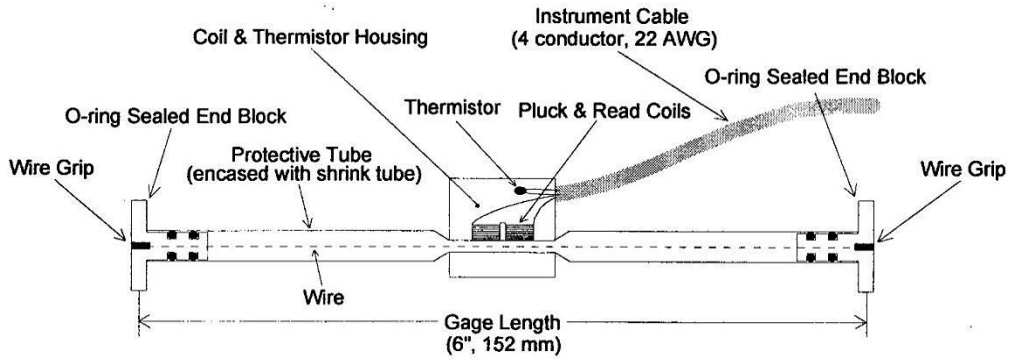

Figure B-6: Drawing of VCE-4200 Vibrating Wire Strain Gauge (Geokon 2010)

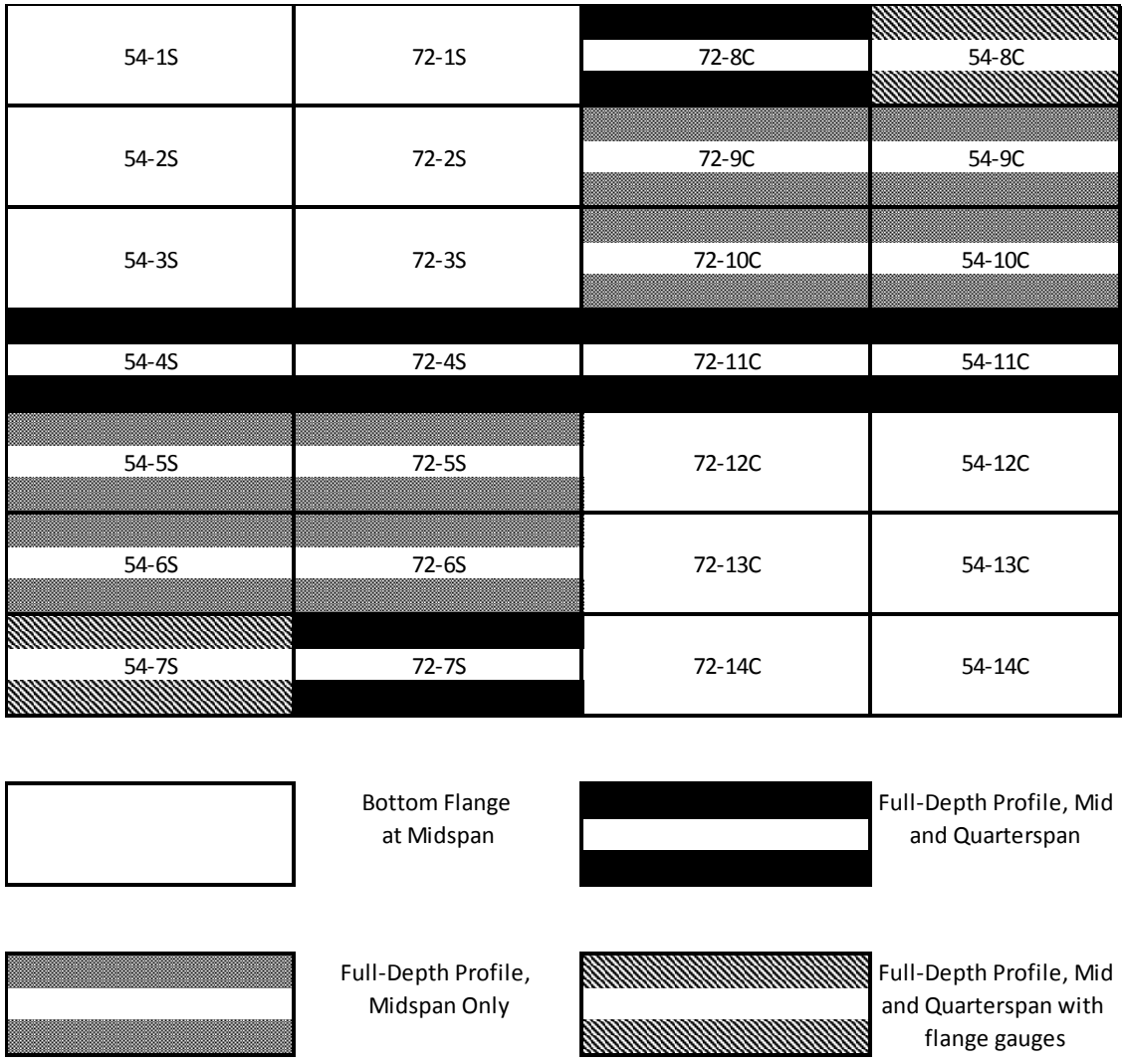

Figure B-7: Summary of the Instrumented VWSGs (Johnson 2012)

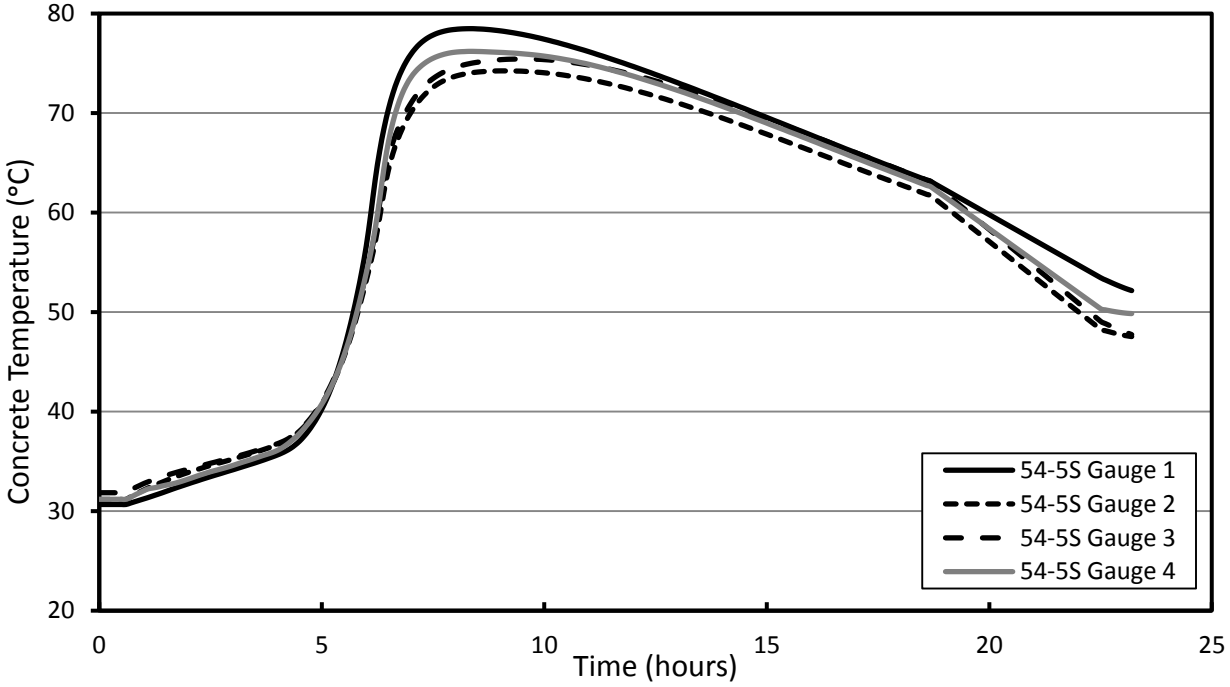

Figure B-8: Early-Age Concrete Temperatures for Casting Group A

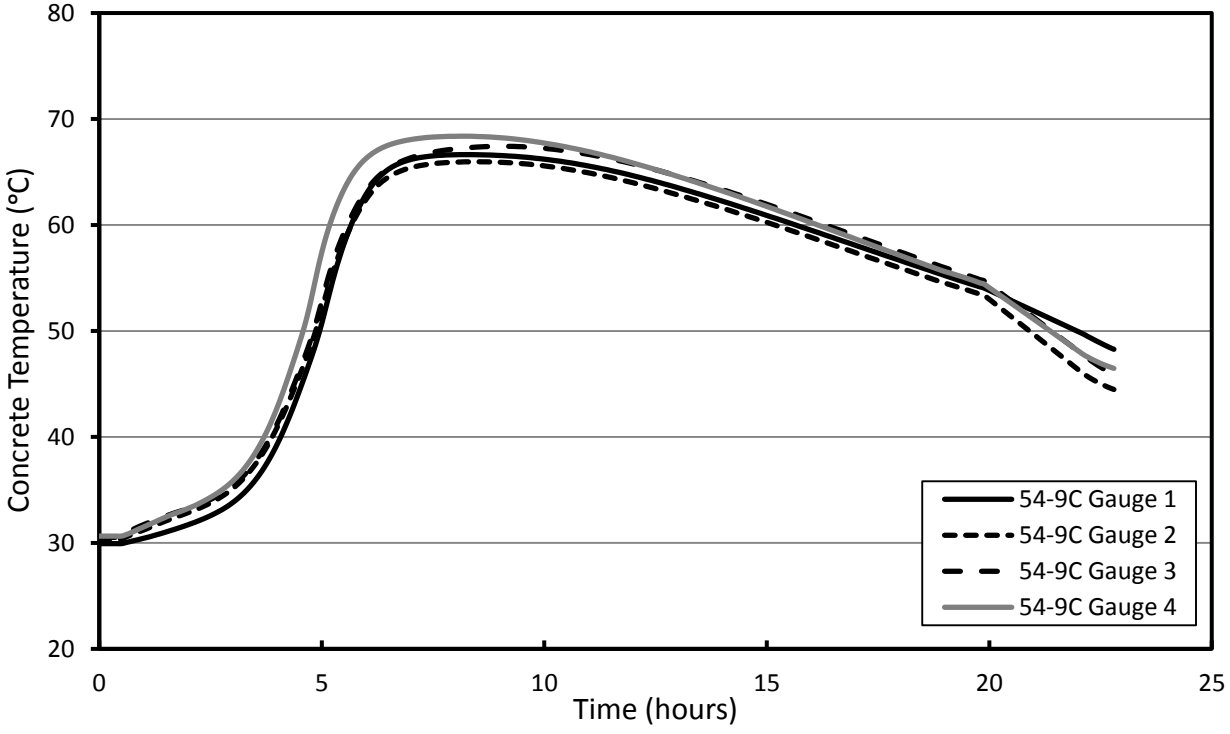

Figure B-9: Early-Age Concrete Temperatures for Casting Group B

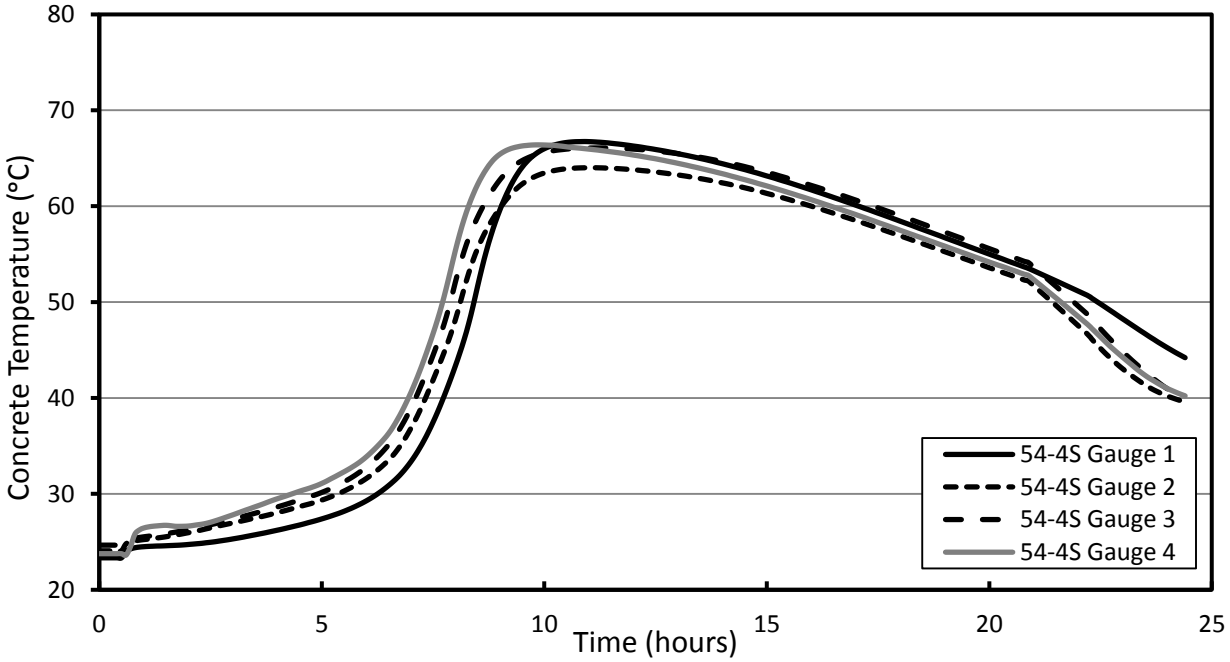

Figure B-10: Early-Age Concrete Temperatures for Casting Group C

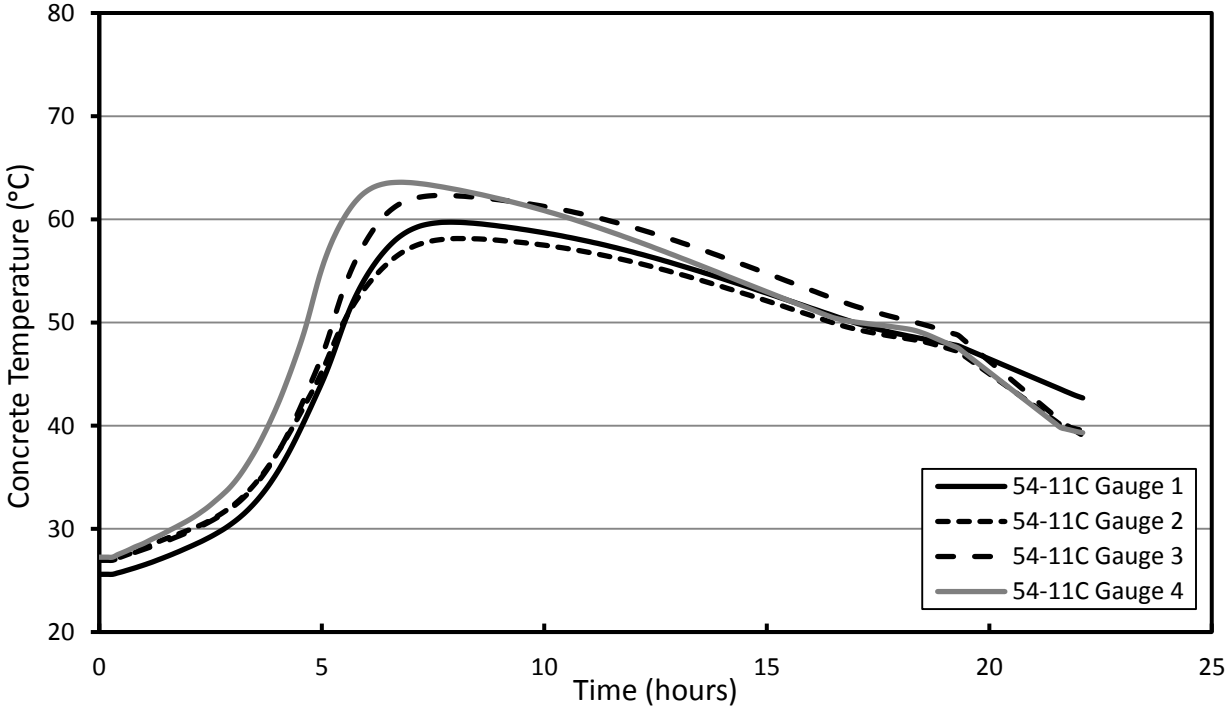

Figure B-11: Early-Age Concrete Temperatures for Casting Group D

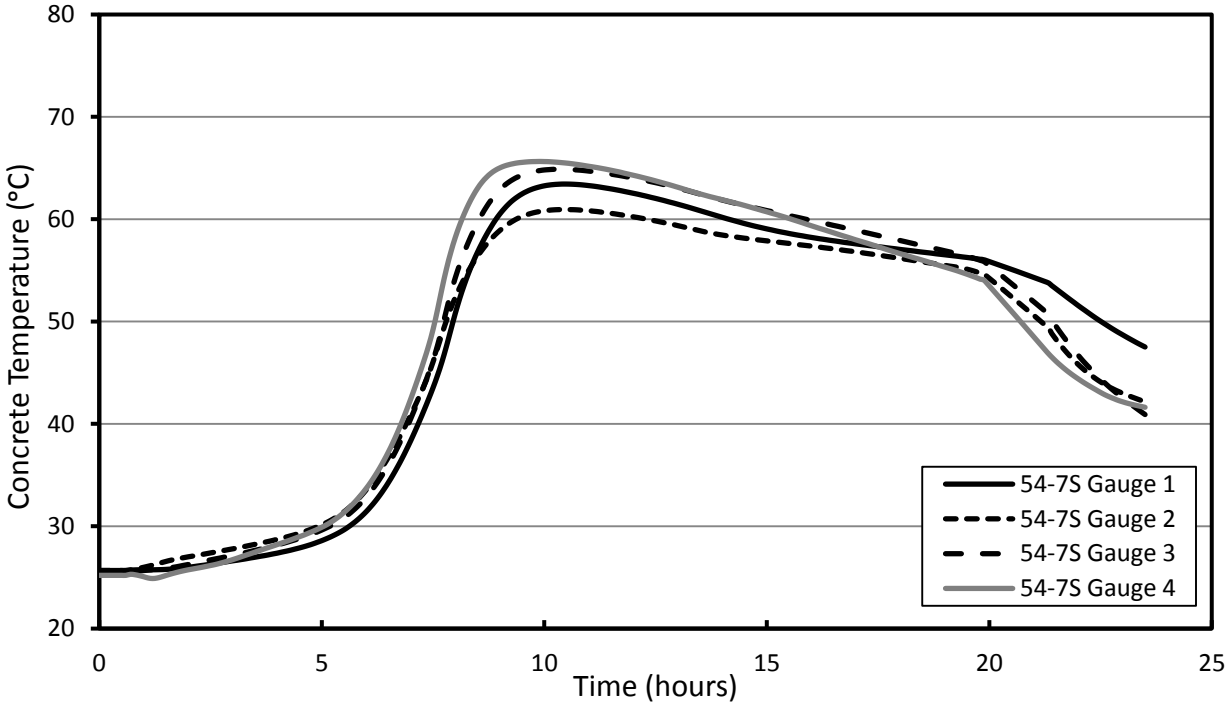

Figure B-12: Early-Age Concrete Temperatures for Casting Group E (SCC)

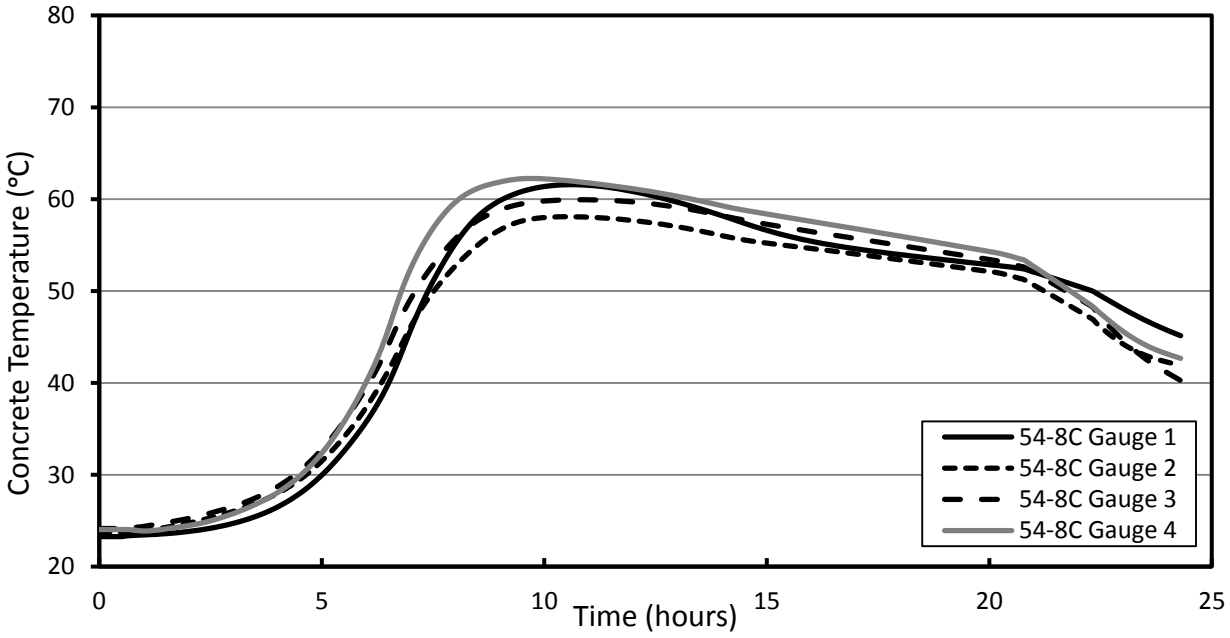

Figure B-13: Early-Age Concrete Temperatures for Casting Group E (VC)

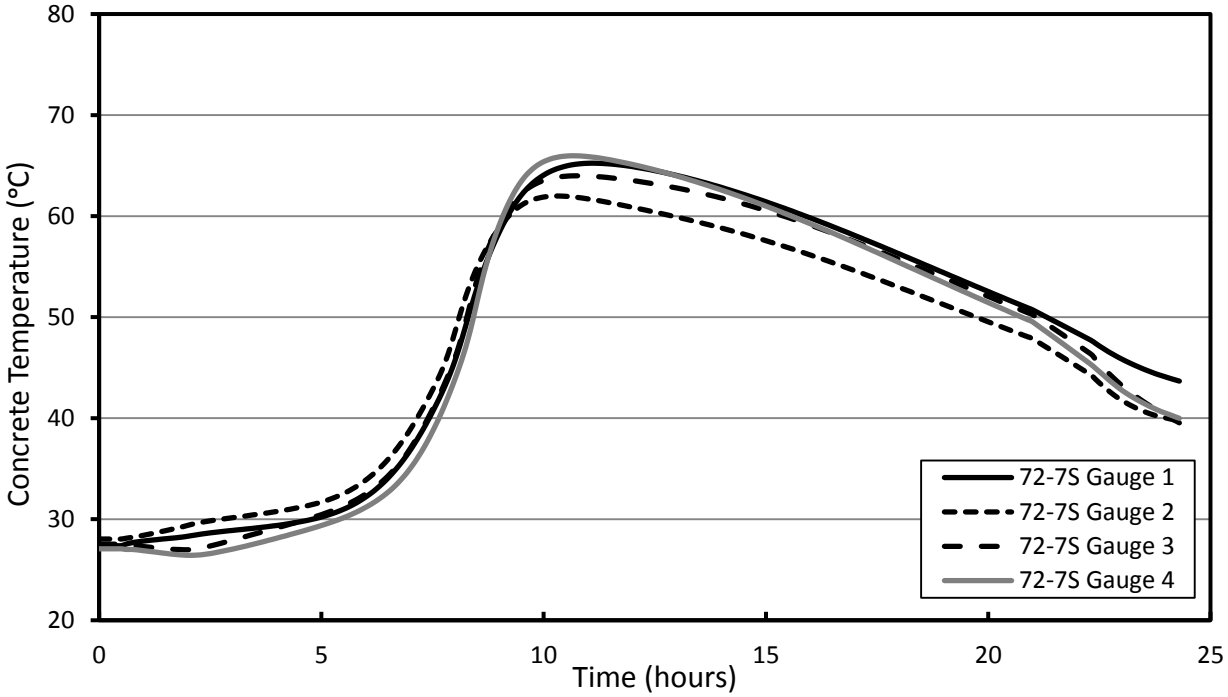

Figure B-14: Early-Age Concrete Temperatures for Casting Group F

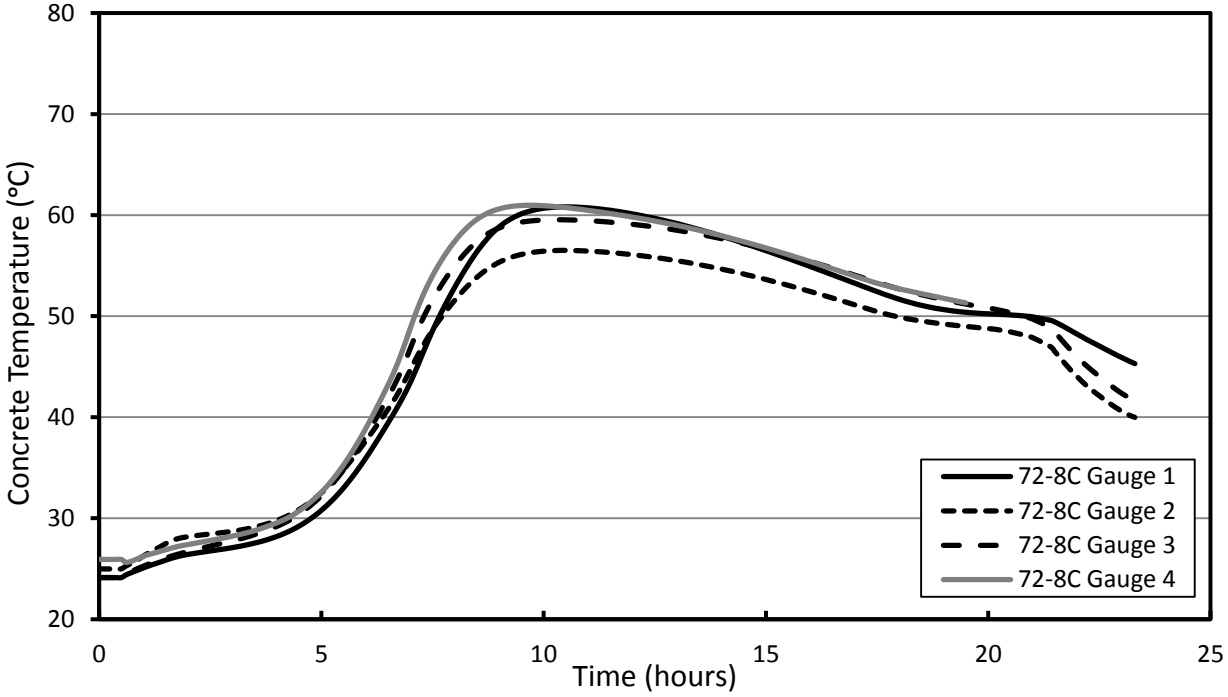

Figure B-15: Early-Age Concrete Temperatures for Casting Group G

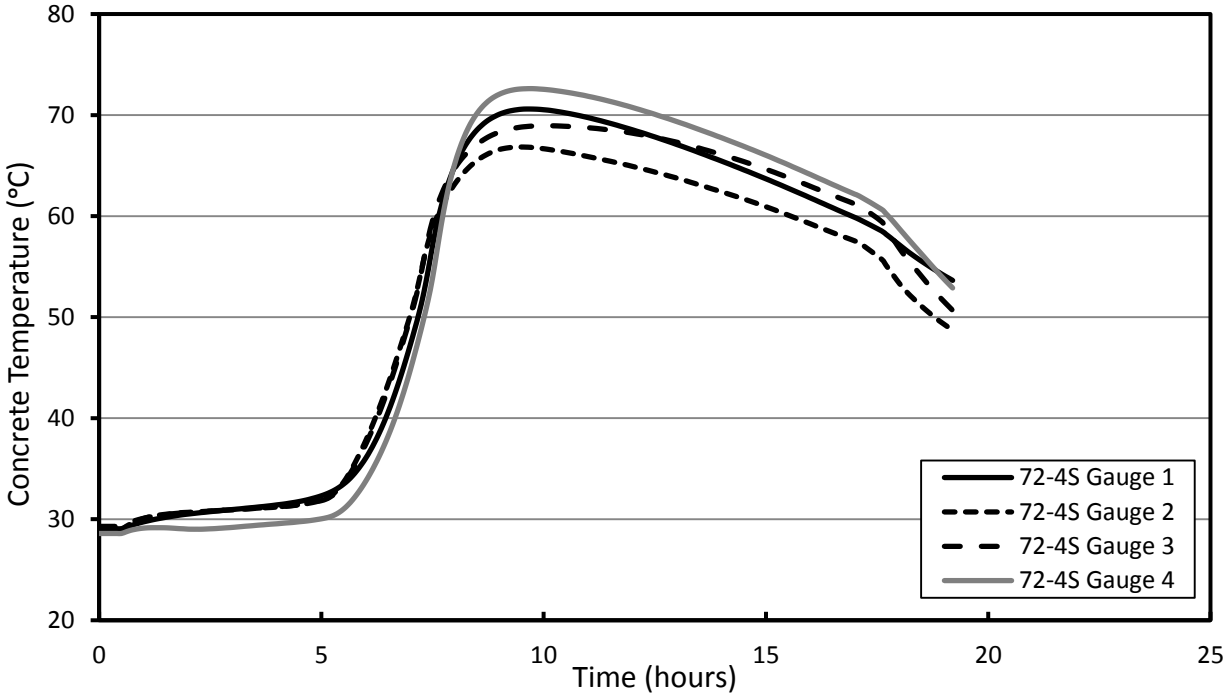

Figure B-16: Early-Age Concrete Temperatures for Casting Group H

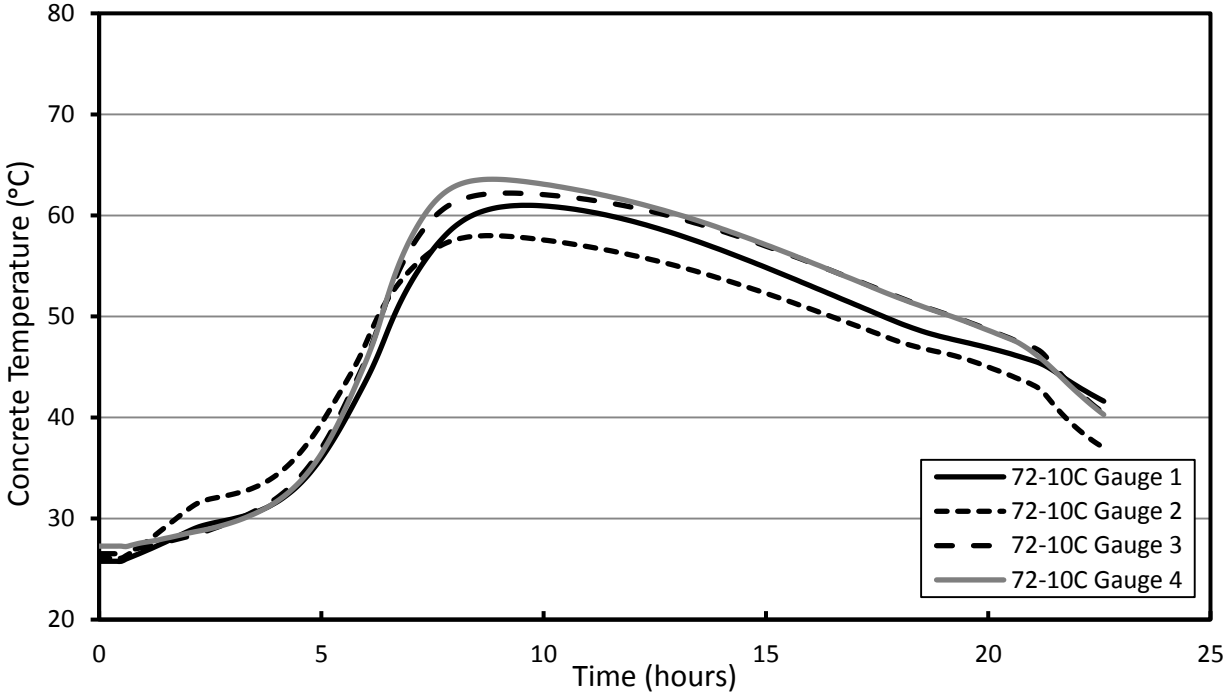

Figure B-17: Early-Age Concrete Temperatures for Casting Group I

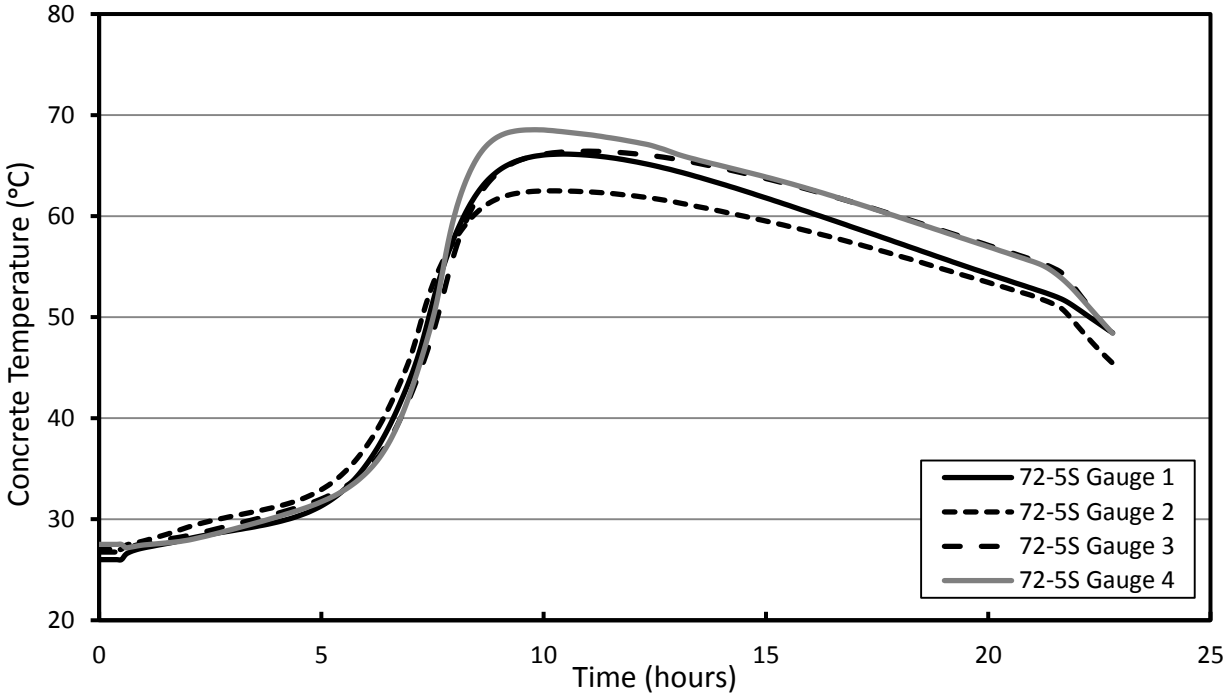

Figure B-18: Early-Age Concrete Temperatures for Casting Group J

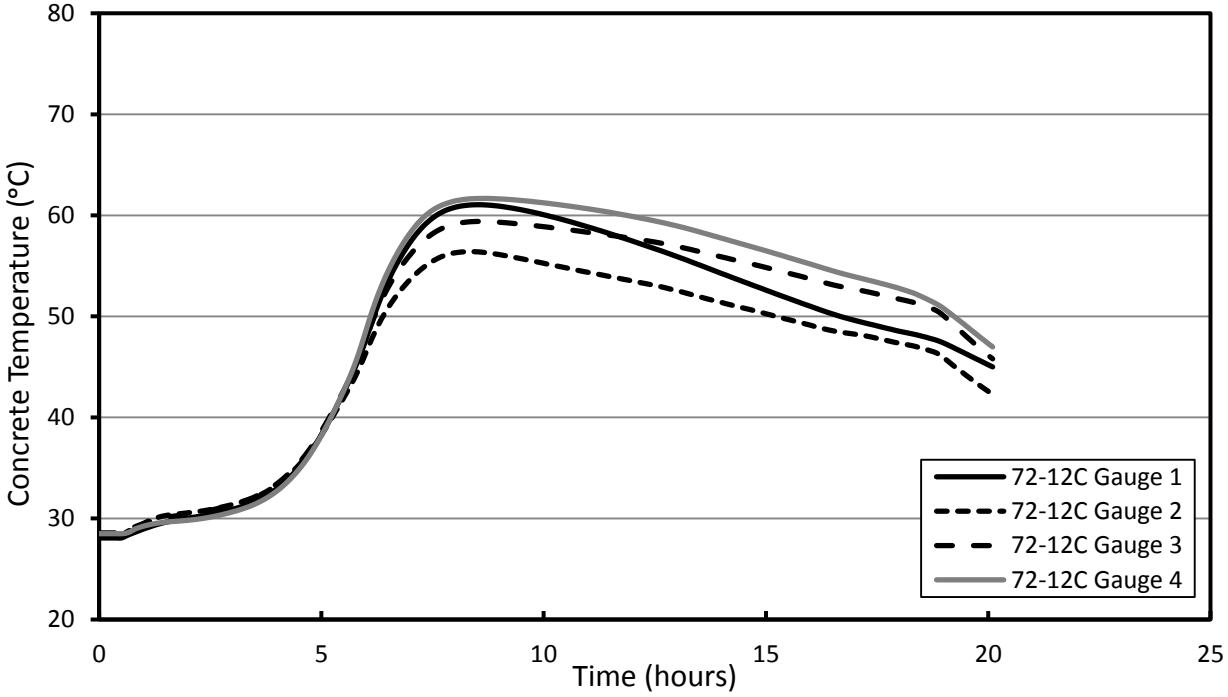

Figure B-19: Early-Age Concrete Temperatures for Casting Group K

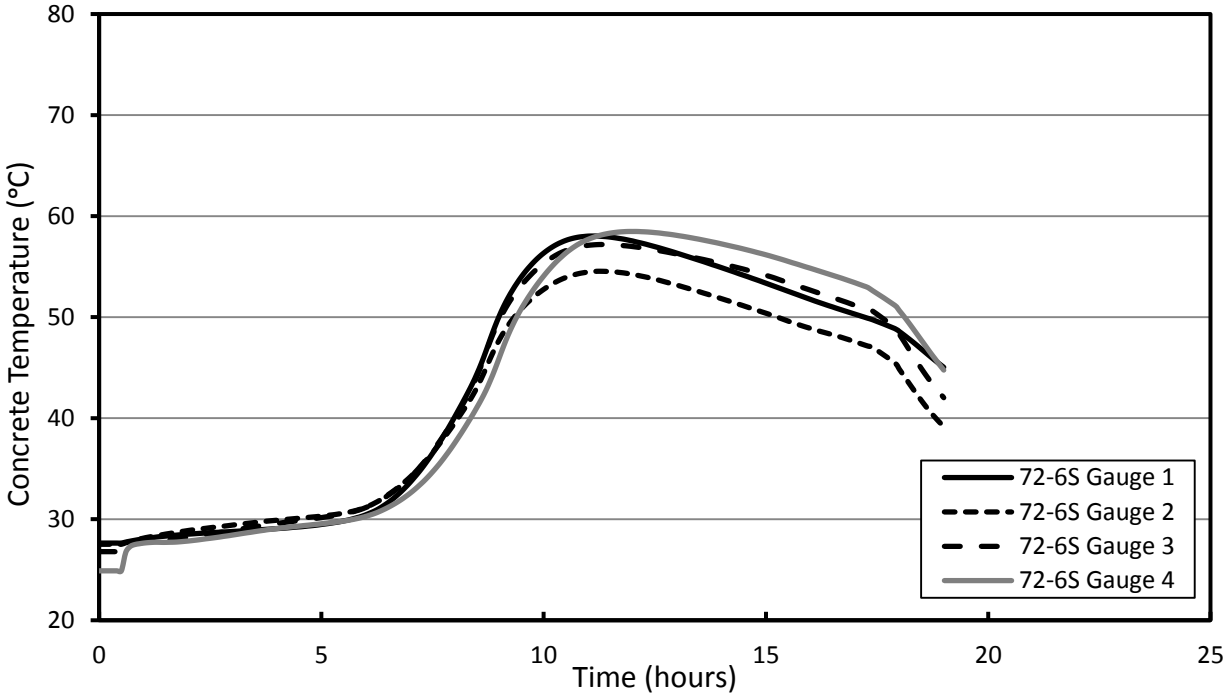

Figure B-20: Early-Age Concrete Temperatures for Casting Group E (SCC)

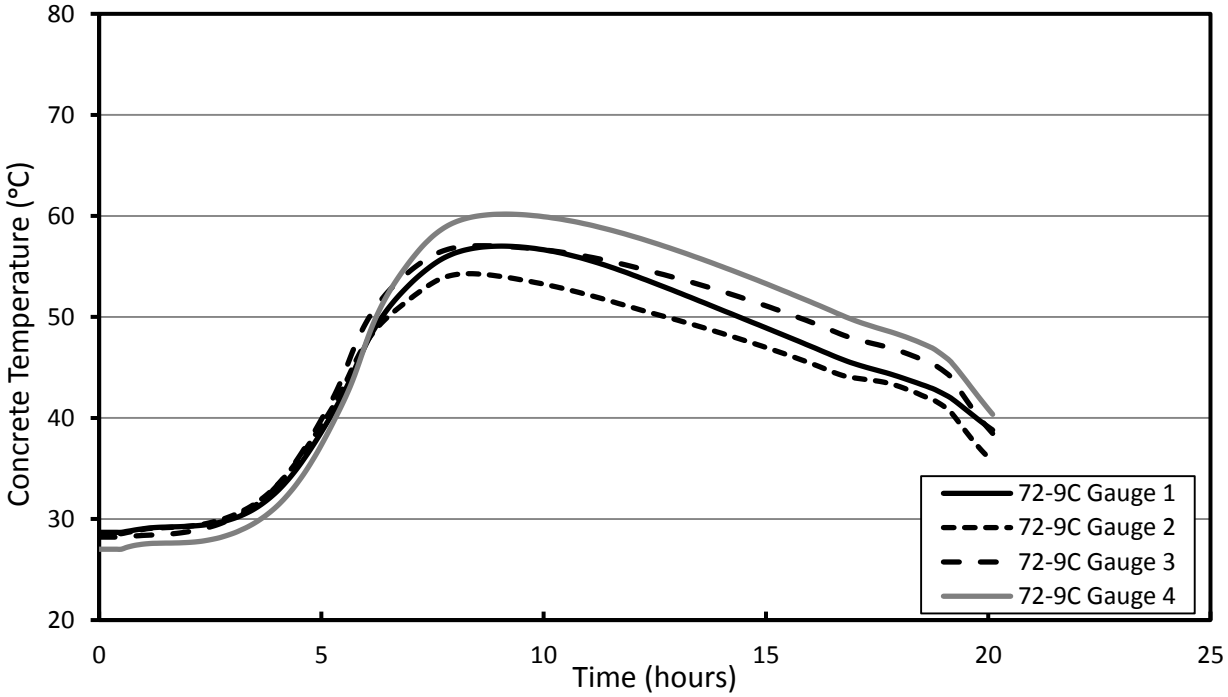

Figure B-21: Early-Age Concrete Temperatures for Casting Group E (VC)

Appendix C Project 2

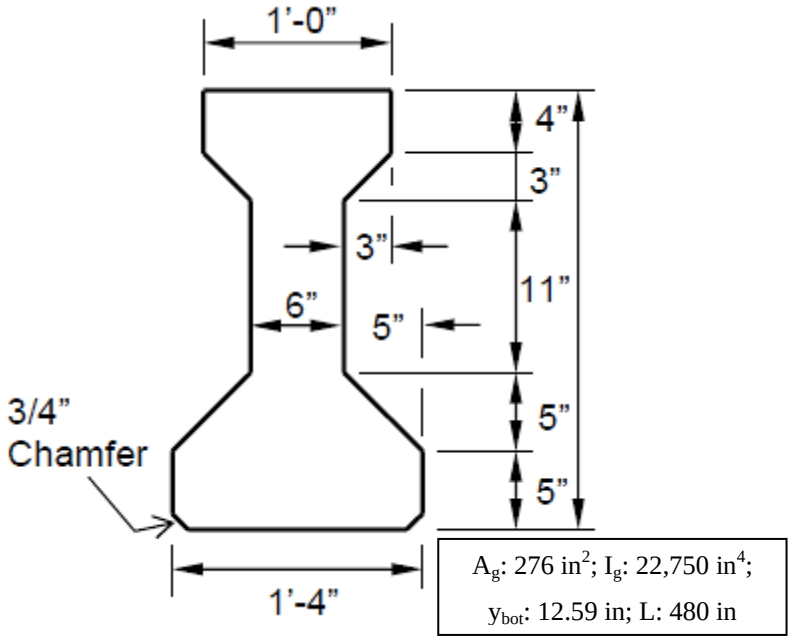

Figure C-1: Cross Section of AASHTO Type I Girder (Adapted from Boehm [2008])

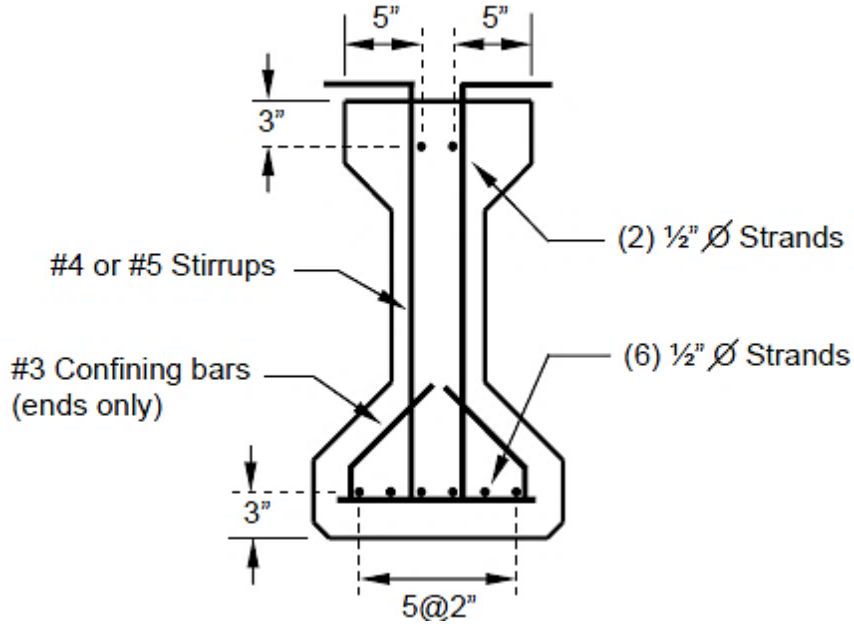

Figure C-2: Mild Steel and Strand Arrangement for AASHTO Type I Girder at Midspan and Girder End (Boehm 2008)

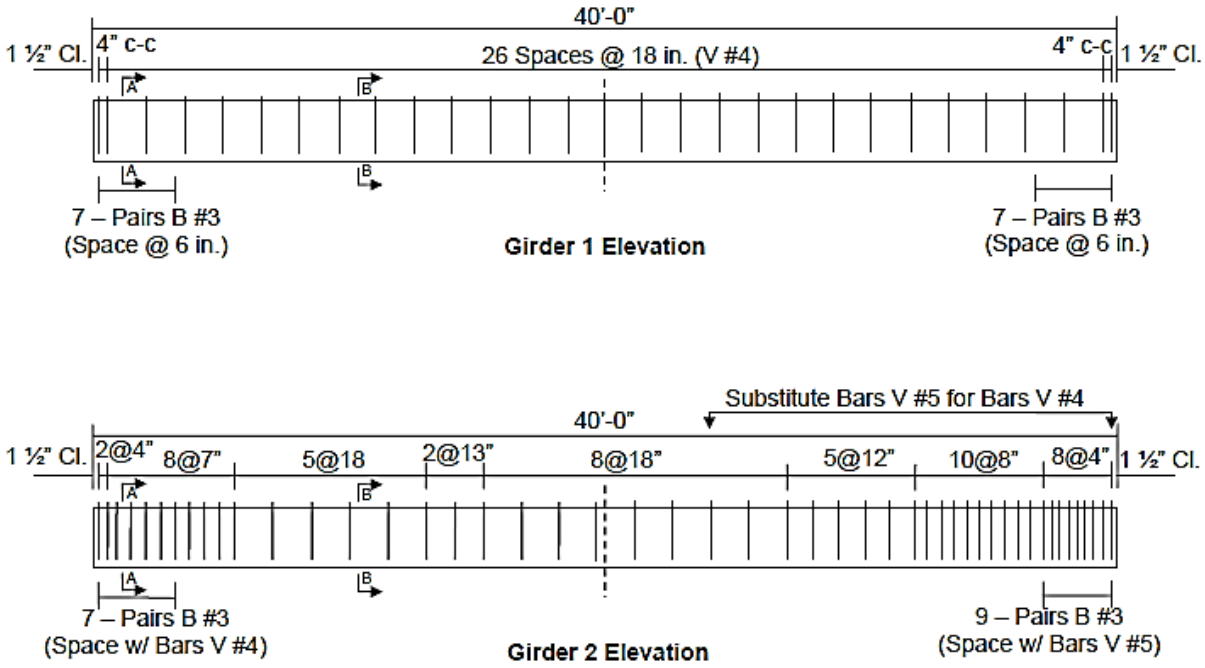

Figure C-3: Mild Steel Spacing in AASHTO Type I Girder (Boehm 2008)

Table C-1: Summary of Fresh Concrete Properties (Boehm 2008)

FRESH PROPERTIES	MIXTURES					
	STD-M		SCC-MS		SCC-HS	
	-1	-2	-1	-2	-1	-2
Slump Flow (in.)	6.75	6.5	26.25	27.75	28	28.25
Unit Weight (lb/ft^3)	Unknown	Unknown	148.5	150.3	153.6	153.2
Air (%)	3.4	3	3.8	1.8	1.5	1.5
VSI	—	—	1.5	1	1	1
T-50 (sec.)	—	—	4.5	3.1	Unknown	5
J-ring (in.)	—	—	26.25	28.6	28	26.25
L-Box (H_1/H_2)	—	—	0.67	0.86	0.8	Unknown

Table C-2: Summary of Hardened Concrete Property Testing Results (Boehm 2008)

HARDENED PROPERTIES		MIXTURES											
		STD-M-1		STD-M-2		SCC-MS-1		SCC-MS-2		SCC-HS-1		SCC-HS-2	
Compressive Strength		f'_c (psi)	E_c (ksi)	f'_c (psi)	E_c (ksi)	f'_c (psi)	E_c (ksi)	f'_c (psi)	E_c (ksi)	f'_c (psi)	E_c (ksi)	f'_c (psi)	E_c (ksi)
Air Cured	Transfer	4990	6050	4860	5550	5110	5200	4500	4950	10190	6750	10720	7150
	7	5790	5900	5740	6050	7110	6100	7210	5850	11710	7350	—	—
	28	6330	6350	6120	5800	8390	6450	8530	6350	12200	7500	12030	7550
	91	6610	6050	6370	6050	8840	5900	9110	6200	12340	7900	—	—
	Post-Test	6720	6150	6540	5800	8850	5850	9160	5900	13080	7100	12810	7200
Match Cured	Transfer	4780	5700	—	—	5540	5250	—	—	10430	7000	—	—
ASTM 6x12	28	6600	6750	7200	7300	9780	7400	9790	7500	13160	8600	13580	8300
CIP Deck (Post-Test)	West End	5720	4950	5370	5350	5480	5350	5080	5300	3720	4100	4820	4550
	East End	5630	5000	5410	5150	5270	5400	5210	5150	3800	3900	4680	4450
Modulus of Rupture		f_r (psi)		f_r (psi)		f_r (psi)		f_r (psi)		f_r (psi)		f_r (psi)	
Air-Cured	Post-Test	900		—	—	840		—	—	940		—	—
ASTM	Post-Test	1110		—	—	1420		—	—	1980		—	—

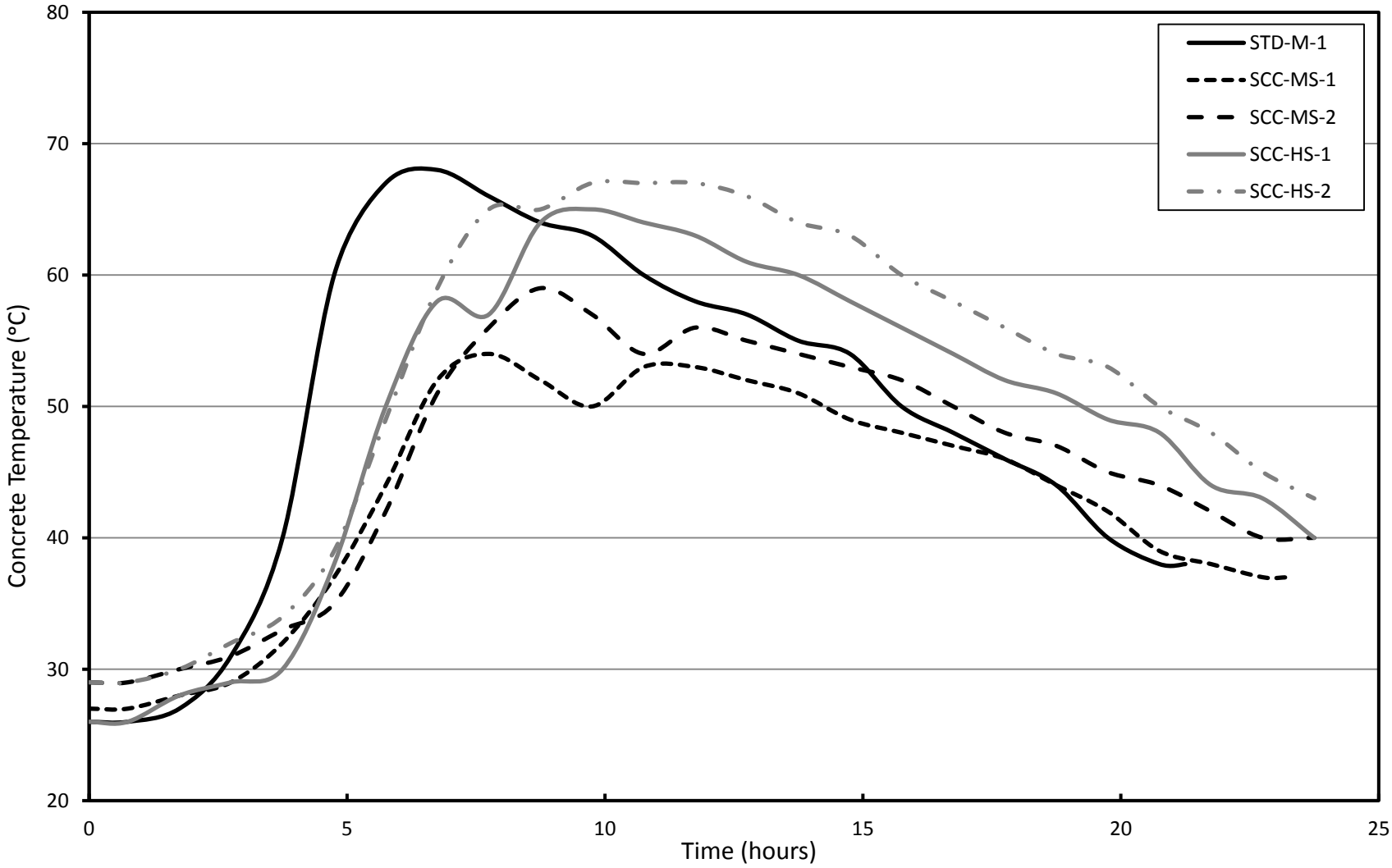

Figure C-4: Early-Age Concrete Temperatures for the AASHTO Type I Girders

Appendix D Project 3

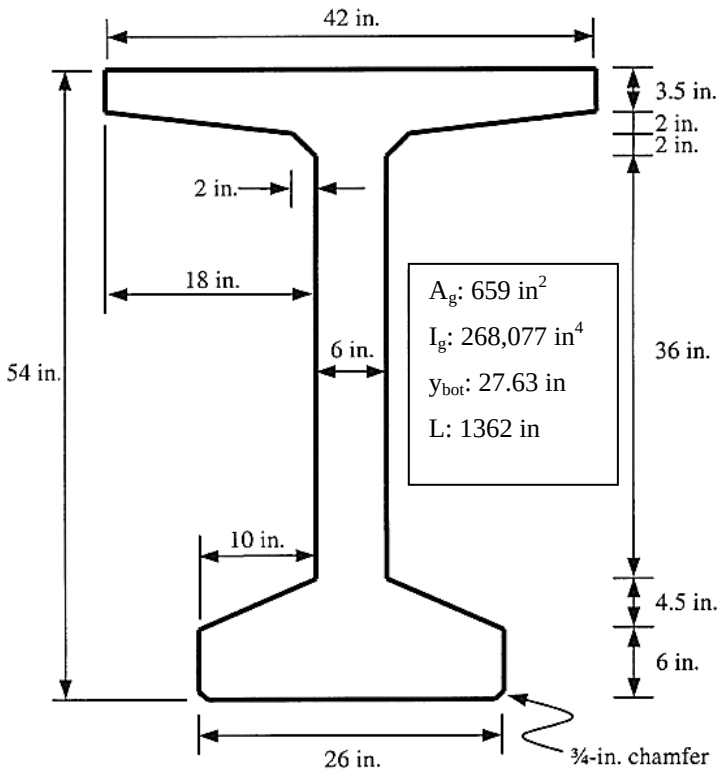

Figure D-1: Cross Section of the HPC BT-54 Girders (Stallings et al. 2003)

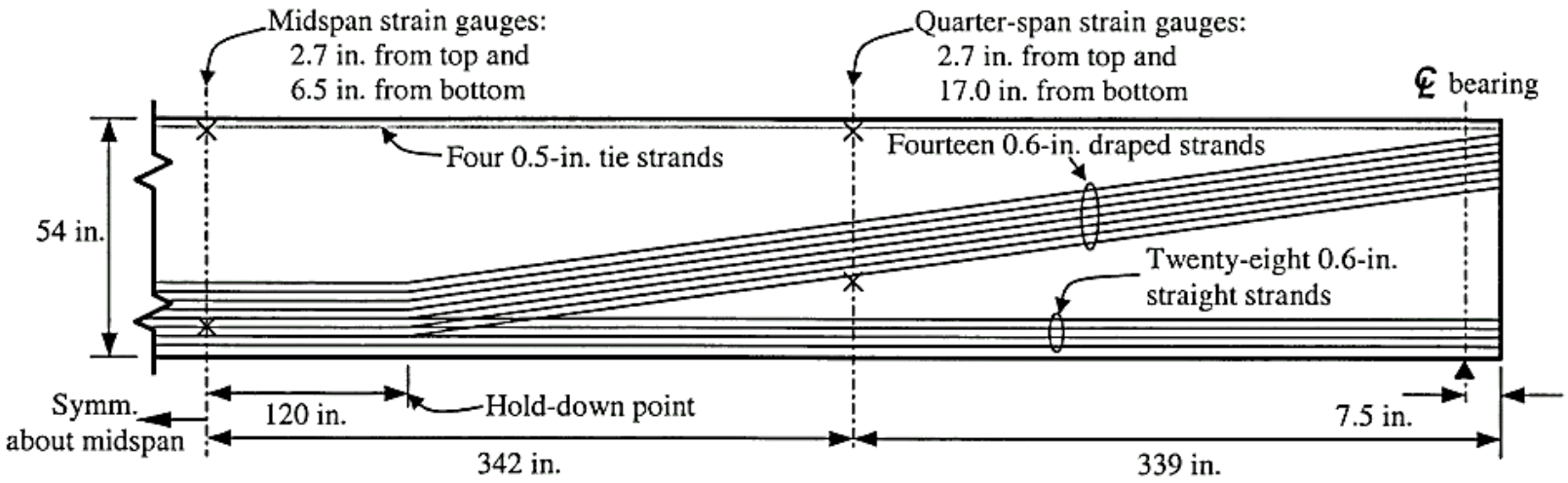

Figure D-2: Profile and Hold-Down of Draped Strands for the HPC BT-54 Girders (Stallings et al. 2003)

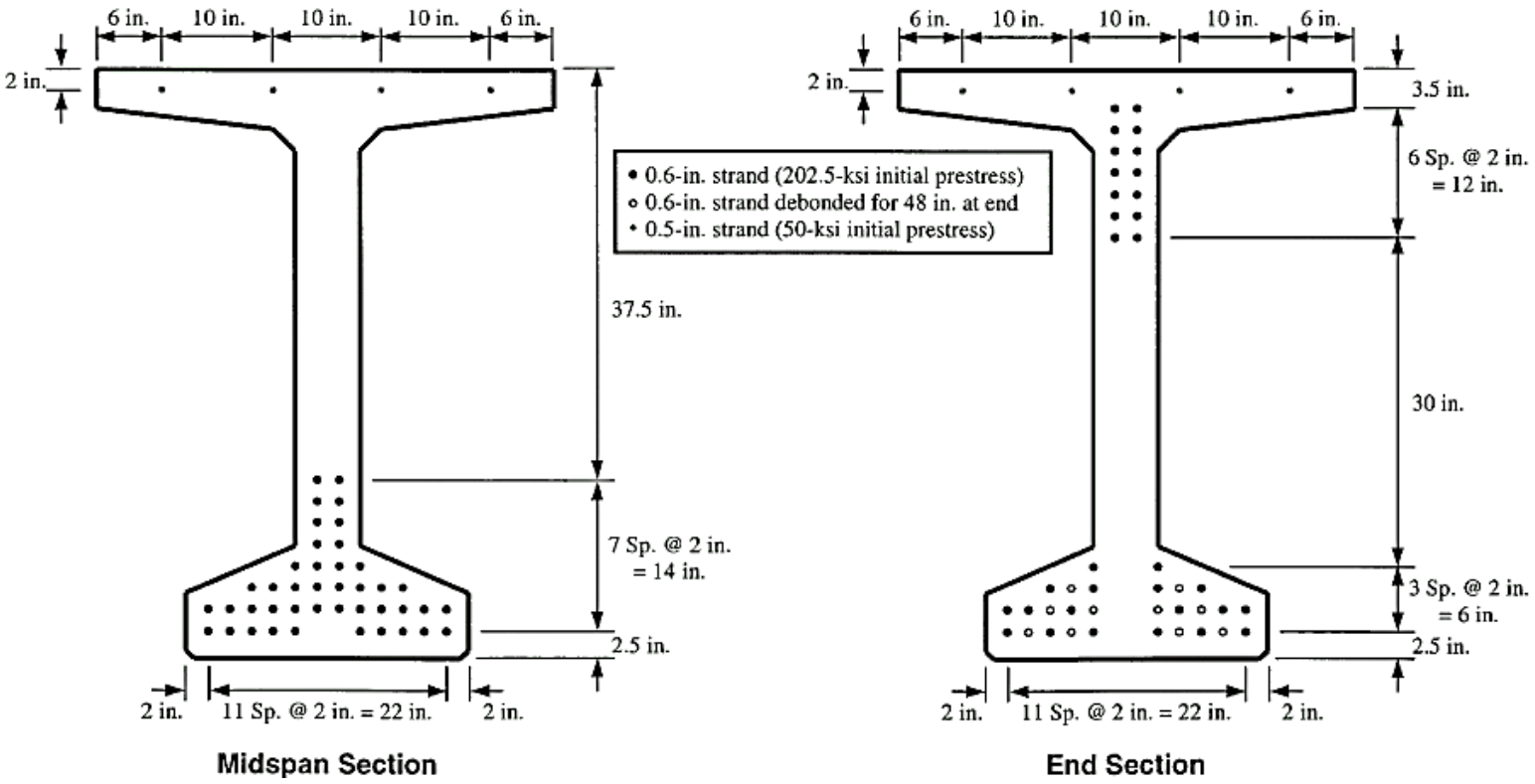

Figure D-3: Mild Steel and Strand Arrangement at Midspan and Girder Ends (Stallings et al. 2003)

Table D-1: HPC BT54—Compressive Strength Test Results (Glover and Stallings 2000)

Pour Number[3]	Release Time	Compressive Strength (psi)[2]			
		Release	28-Day	56-Day	Core[4]
1	24 hrs	8080	9890	10110	9730
2	42 hrs	8080	8440	9610	8200
3	19 hrs	8240	10240	10720	-
4	22 hrs	8080	9750	9470	9450
5	20.5 hrs	8300	10060	10360	-
6	22 hrs	8120	9210	8440	9720
7	5 days	8160	8540	8600	8950
8	21.5 hrs	8830	10000	10180	-
9	20.5 hrs	8040	9710	9550	8450
10	19.5 hrs	8480	9830	9670	10030
11	20 hrs	8080	10030	9710	-
12	45 hrs	8360	8950	8620	9530
13	21 hrs	9130	10820	10320	-
14	21 hrs	8680	10250	8980	-
15	19 hrs	9370	11060	11320	-
16	20 hrs	8340	10260	10540	-
17	20 hrs	9450	10900	11380	-
18	22 hrs	9810	10660	11600	-

1. Refer to Appendix A.5 for individual cylinder test results.
2. Average of 2 – 4 x 8 in. Sure Cure™ cylinders tested on sulfur caps.
3. No. 67 limestone used in pours 1 through 12, No. 7 limestone used in pours 13 through 18.
4. Core testing was conducted if the required 28-day strength was not achieved. 4 cores were cut according to AASHTO T 24. Core strengths were based on the best 3 out of 4 cores tested dry on sulfur caps without the AASHTO (L/D) ratio reduction factor applied.

Table D-2: HPC BT54—Modulus of Elasticity Test Results (Glover and Stallings 2000)

Pour Number	Curing Method[2]	Modulus of Elasticity (psi)[1]			
		Release	7-Day	28-Day	56-Day
1	(1)	5,900,000	6,600,000	6,000,000	5,900,000
3	(1)	-	-	-	6,000,000
4	(1)	-	-	-	4,300,000
4	(3)	-	-	-	6,150,000
5	(1)	-	-	-	4,400,000
6	(1)	-	-	-	5,350,000
8	(1)	-	-	5,600,000	5,600,000
9	(2)	5,400,000	5,600,000	5,450,000	5,900,000
10	(1)	-	-	5,300,000	5,400,000
10	(3)	-	-	5,500,000	5,050,000
13	(1)	-	-	5,200,000	6,000,000
14	(1)	-	-	-	5,800,000
15	(1)	5,250,000	-	5,800,000	5,300,000
16	(1)	-	-	6,300,000	5,800,000
17	(1)	5,300,000	-	7,100,000	7,000,000
18	(1)	-	-	6,500,000	6,900,000

1. Results are for one cylinder test performed at Auburn University.
2. (1) - 4 x 8 in. Sure Cure™ cylinders cured on the casting yard.
   (2) - 4 x 8 in. Sure Cure™ cylinders cured indoors.
   (3) - 4 x 8 in. standard plastic molded cylinders cured under the tarp and cured on the casting yard.

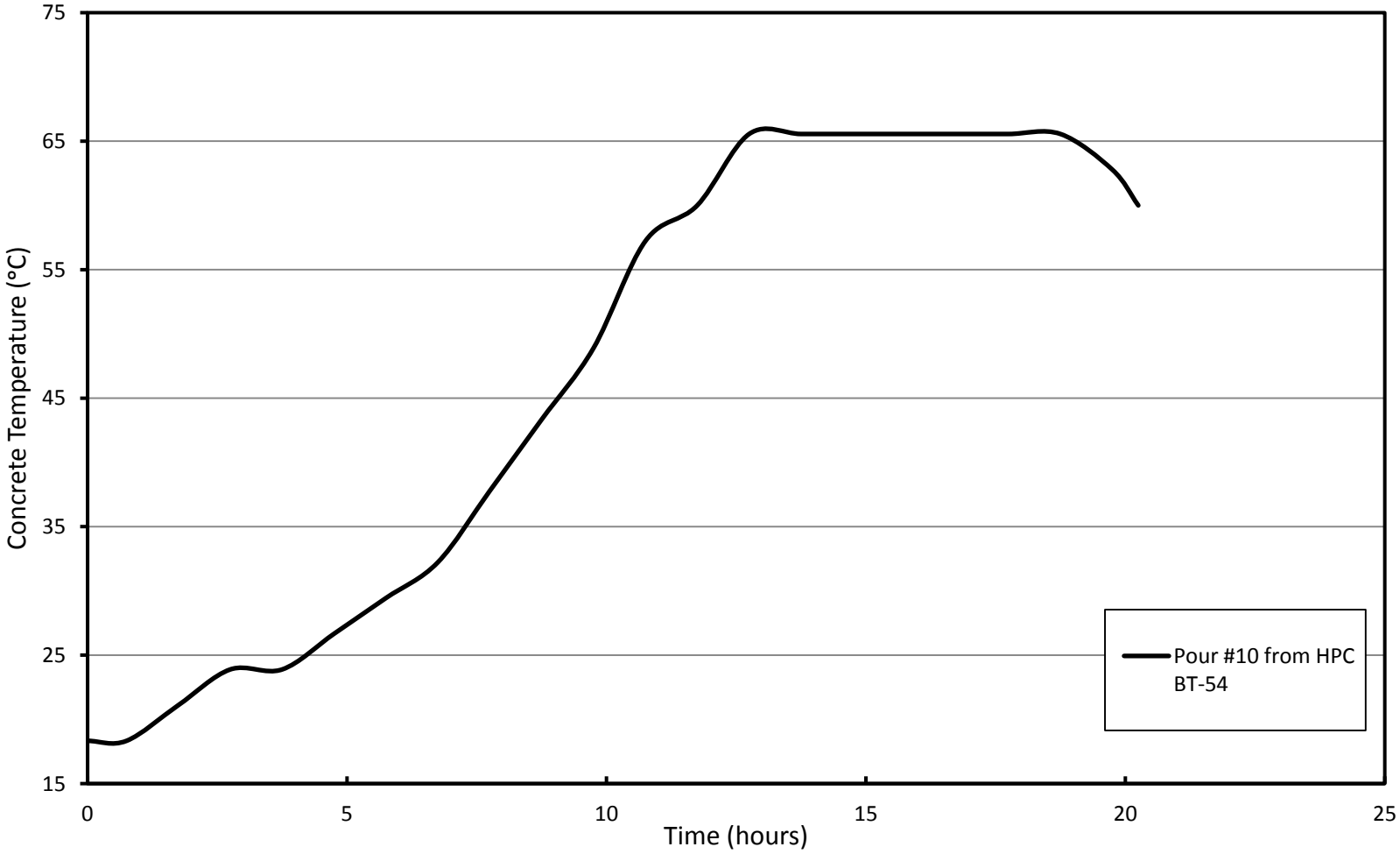

Figure D-4: Representative Early-Age Concrete Temperature for the HPC BT-54 Girders

Appendix E Project 4

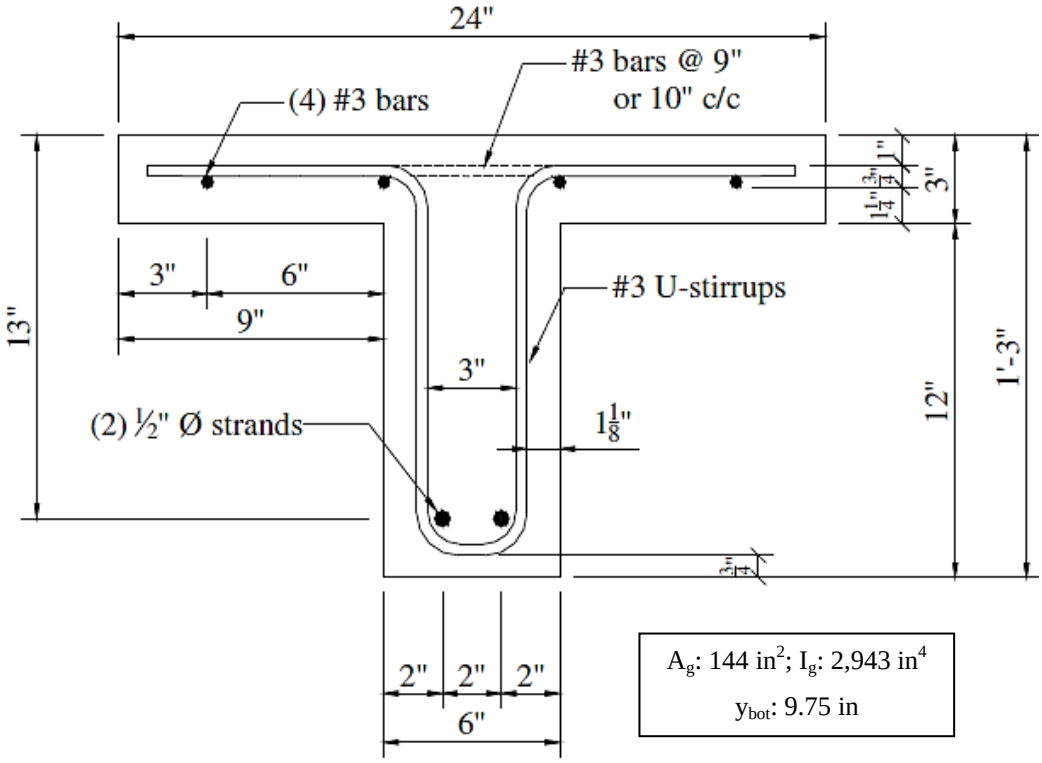

Figure E-1: Cross Section and Steel Arrangement of T-Beams (Levy 2007)

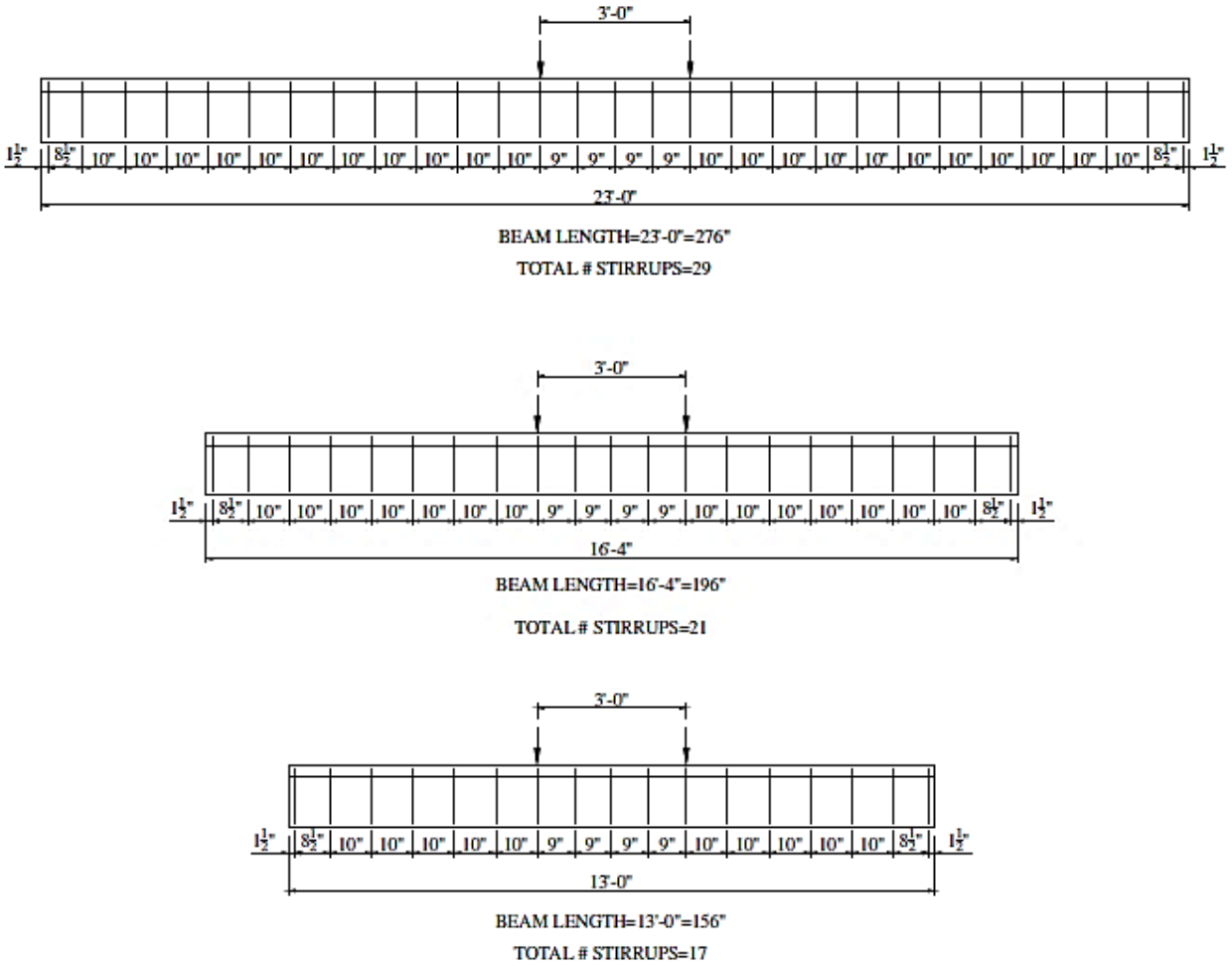

Figure E-2: T-Beams—Stirrup Spacing for "A", "B", and "C" Specimens (Levy 2007)

Table E-1: Summary of Fresh Concrete Properties (Levy 2007)

FRESH PROPERTIES	MIXTURES			
	STD-M	SCC-MA	SCC-MS	SCC-HS
Slump Flow (in.)	9.5	29	28.5	26
Unit Weight (lb/ft^3)	142.2	151.8	148.4	155.2
Air (%)	11.0	2.0	5.0	3.0
VSI	-	1.0	1.0	1.0
T-50 (sec.)	-	2.47	1.54	3.75
J-ring (Difference in in.)	-	1.5	2	2.5
L-Box (H_2/H_1)	-	0.84	0.92	0.63
Temperature (°F)	82	62	89	95

Table E-2: Summary of Hardened Concrete Property Testing Results (Levy 2007)

PROPERTY	MIXTURES			
	STD-M	SCC-MA	SCC-MS	SCC-HS
f'_{ci} (psi)	5000	5500	5300	9990
E_{ci}(ksi)	4900	4900	4950	6050
$f'_{c,28(ASTM)}$ (psi)	5990	8840	9640	13150
$f'_{c,28(AC)}$ (psi)	6320	8540	9170	13380
$E_{c,28(AC)}$ (ksi)	5150	5400	6950	7050
$f_{ct,28(AC)}$ (psi)	560	760	840	830

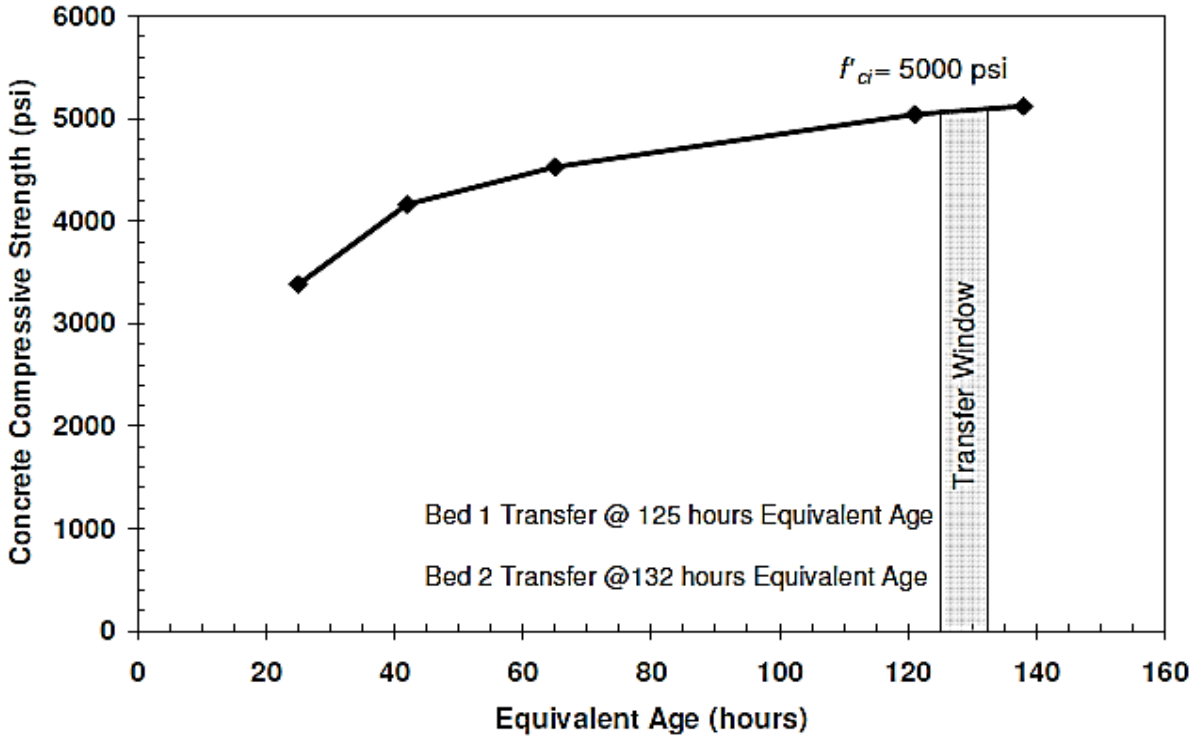

Figure E-3: Strength-Maturity Relationship Curve for STD-M (Levy 2007)

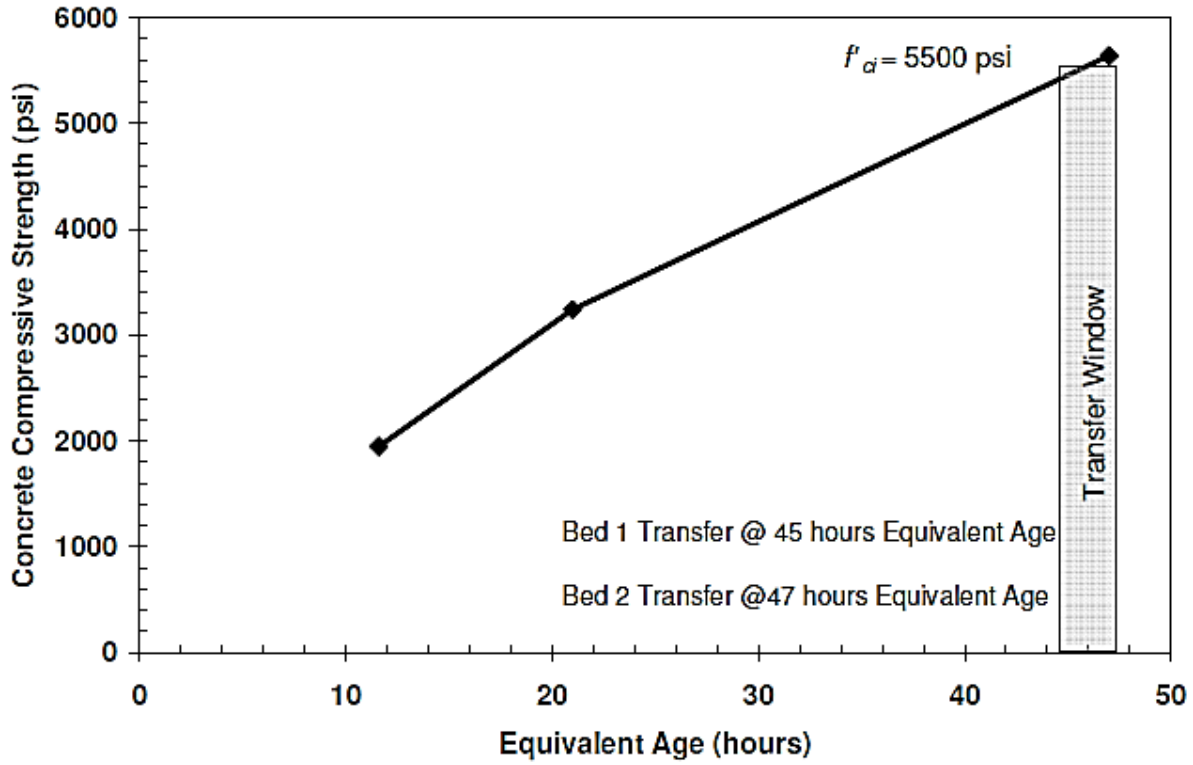

Figure E-4: Strength-Maturity Relationship Curve for SCC-MA (Levy 2007)

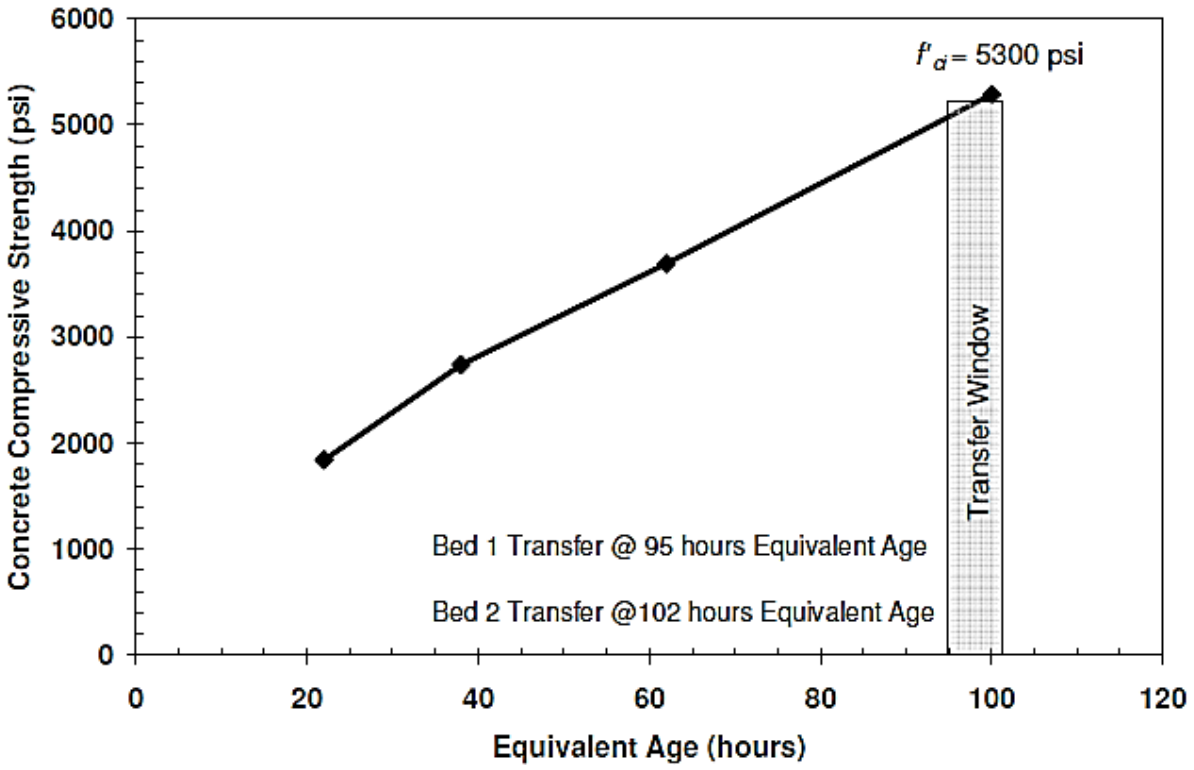

Figure E-5: Strength-Maturity Relationship Curve for SCC-MS (Levy 2007)

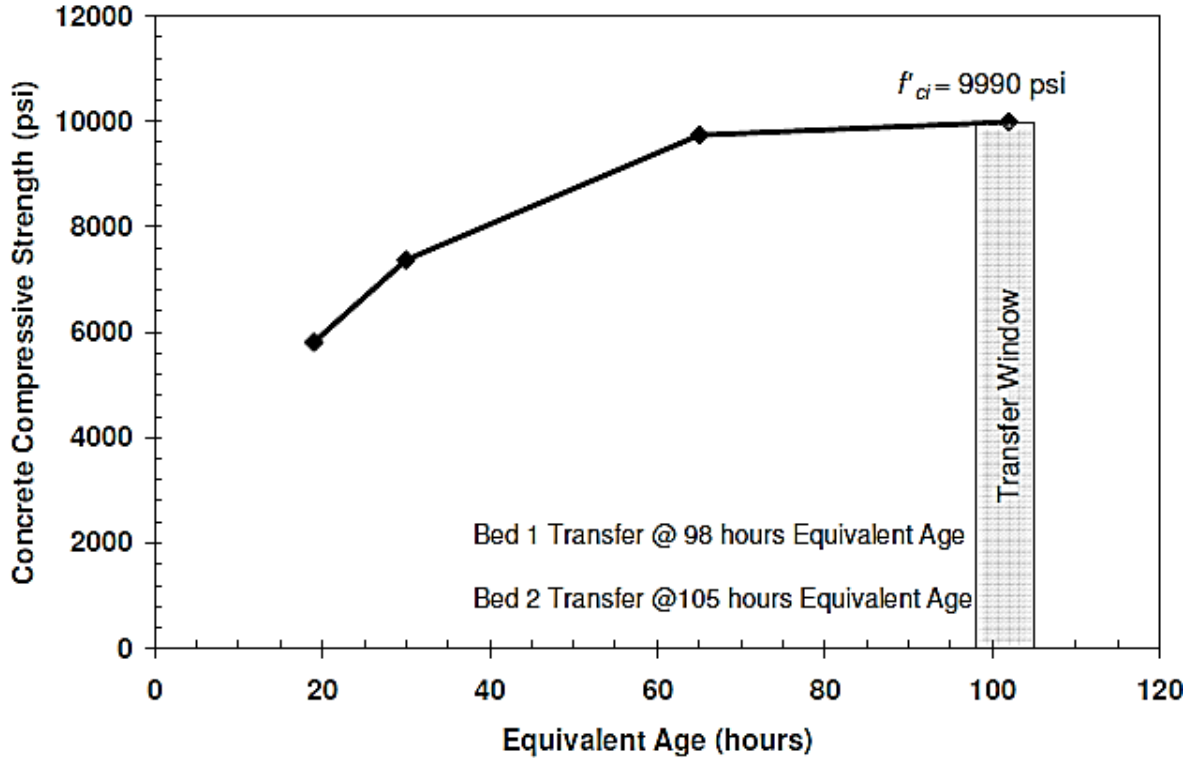

Figure E-6: Strength-Maturity Relationship Curve for SCC-HS (Levy 2007)

Appendix F Camber Prediction Software—Input Parameters

Table F-1: (1/4) AASHTO Type I and T-Beams—Property and Event Summary (Adapted from Schrantz [2012])

		Gross Cross-Sectional Properties							Hardened Concrete Properties			
	Beam ID	**A_g (in^2)**	**I_g (in^4)**	**y_b (in.)**	**h (in.)**	**L (in.)**	**V/S (in.)**	**Notional Size (in.)**	**f'_{ci} (psi)**	**E_{ci} (ksi)**	**$f'_{c,28}$ (psi)**	**$E_{c,28}$ (ksi)**
AASHTO Type I (Project 2)	STD-M-1	276	22750	12.59	28	480	3.07	6.57	4780	5700	6600	6750
	STD-M-2	276	22750	12.59	28	480	3.07	6.57	4780	5700	7200	7300
	SCC-MS-1	276	22750	12.59	28	480	3.07	6.57	5540	5250	9780	7400
	SCC-MS-2	276	22750	12.59	28	480	3.07	6.57	5540	5250	9790	7500
	SCC-HS-1	276	22750	12.59	28	480	3.07	6.57	10430	7000	13160	8600
	SCC-HS-2	276	22750	12.59	28	480	3.07	6.57	10430	7000	13580	8300
T-Beams (Project 4)	STD-M-A	144	2943	9.75	15	276	1.85	4.24	5000	4900	6320	5150
	STD-M-B	144	2943	9.75	15	196	1.85	4.24	5000	4900	6320	5150
	STD-M-C	144	2943	9.75	15	156	1.85	4.24	5000	4900	6320	5150
	STD-M-D	144	2943	9.75	15	116	1.85	4.24	5000	4900	6320	5150
	SCC-MA-A	144	2943	9.75	15	276	1.85	4.24	5500	4900	8540	5400
	SCC-MA-B	144	2943	9.75	15	196	1.85	4.24	5500	4900	8540	5400
	SCC-MA-C	144	2943	9.75	15	156	1.85	4.24	5500	4900	8540	5400
	SCC-MA-D	144	2943	9.75	15	116	1.85	4.24	5500	4900	8540	5400
	SCC-MS-A	144	2943	9.75	15	276	1.85	4.24	5300	4950	9170	6950
	SCC-MS-B	144	2943	9.75	15	196	1.85	4.24	5300	4950	9170	6950
	SCC-MS-C	144	2943	9.75	15	156	1.85	4.24	5300	4950	9170	6950
	SCC-MS-D	144	2943	9.75	15	116	1.85	4.24	5300	4950	9170	6950
	SCC-HS-A	144	2943	9.75	15	276	1.85	4.24	9990	6050	13380	7050
	SCC-HS-B	144	2943	9.75	15	196	1.85	4.24	9990	6050	13380	7050
	SCC-HS-C	144	2943	9.75	15	156	1.85	4.24	9990	6050	13380	7050
	SCC-HS-D	144	2943	9.75	15	116	1.85	4.24	9990	6050	13380	7050

Table F-1: (2/4) AASHTO Type I and T-Beams—Property and Event Summary (Adapted from Schrantz [2012])

		Fresh Properties				Mix		Cement		Ambient				
	Beam ID	Air (%)	Adj. Slump (in.)	Actual Slump (in.)	w_c (pcf)	Coarse Aggregate	FA (%)	Type	Content (pcy)	RH (%)	E_p (ksi)	f_{pu} (ksi)	f_{pv} (ksi)	E_s (ksi)
AASHTO Type I (Project 2)	STD-M-1	3.4	1.0	6.8	148.0	#78 Limestone	35.3	III	640	75	28900	270	243	-
	STD-M-2	3.0	1.0	6.5	148.0		35.3	III	640	75	28900	270	243	-
	SCC-MS-1	3.8	0.0	26.3	148.5		45.0	III	790	75	28900	270	243	-
	SCC-MS-2	1.8	0.0	27.8	150.3		45.0	III	790	75	28900	270	243	-
	SCC-HS-1	1.5	0.0	28.0	153.6		44.2	III	929	75	28900	270	243	-
	SCC-HS-2	1.5	0.0	28.3	153.2		44.2	III	929	75	28900	270	243	-
T-Beams (Project 4)	STD-M-A	11.0	1.0	9.5	142.2	#78 Limestone	46.0	III	640	55	28900	270	243	29000
	STD-M-B	11.0	1.0	9.5	142.2		46.0	III	640	55	28900	270	243	29000
	STD-M-C	11.0	1.0	9.5	142.2		46.0	III	640	55	28900	270	243	29000
	STD-M-D	11.0	1.0	9.5	142.2		46.0	III	640	55	28900	270	243	29000
	SCC-MA-A	2.0	0.0	29.0	151.8		46.0	III	750	55	28900	270	243	29000
	SCC-MA-B	2.0	0.0	29.0	151.8		46.0	III	750	55	28900	270	243	29000
	SCC-MA-C	2.0	0.0	29.0	151.8		46.0	III	750	55	28900	270	243	29000
	SCC-MA-D	2.0	0.0	29.0	151.8		46.0	III	750	55	28900	270	243	29000
	SCC-MS-A	5.0	0.0	28.5	148.4		46.0	III	750	55	28900	270	243	29000
	SCC-MS-B	5.0	0.0	28.5	148.4		46.0	III	750	55	28900	270	243	29000
	SCC-MS-C	5.0	0.0	28.5	148.4		46.0	III	750	55	28900	270	243	29000
	SCC-MS-D	5.0	0.0	28.5	148.4		46.0	III	750	55	28900	270	243	29000
	SCC-HS-A	3.0	0.0	26.0	155.2		46.0	III	929	55	28900	270	243	29000
	SCC-HS-B	3.0	0.0	26.0	155.2		46.0	III	929	55	28900	270	243	29000
	SCC-HS-C	3.0	0.0	26.0	155.2		46.0	III	929	55	28900	270	243	29000
	SCC-HS-D	3.0	0.0	26.0	155.2		46.0	III	929	55	28900	270	243	29000

Table F-1: (3/4) AASHTO Type I and T-Beams—Property and Event Summary (Adapted from Schrantz [2012])

		Time of Events					Analysis Intervals			
	Beam ID	Jacking (hrs)	Transfer (hrs)	Curing Type (M/S)	Eqv Adj Age (days)	Benchmark Reading (hrs)	Curing Length (hrs)	Number of CS	Max Time (days)	Number of TI
AASHTO Type I (Project 2)	STD-M-1	6	21	S	3.50	0.1	18	40	110	40
	STD-M-2	6	21	S	3.50	0.1	18	40	110	40
	SCC-MS-1	6	23	S	2.79	0.2	18	40	160	40
	SCC-MS-2	6	23	S	3.16	0.2	18	40	167	40
	SCC-HS-1	6	22	S	3.75	0.2	18	40	214	40
	SCC-HS-2	6	22	S	4.23	0.2	18	40	214	40
T-Beams (Project 4)	STD-M-A	96	72	S/M	5.42	6.0	66	40	120	40
	STD-M-B	96	72	S/M		6.0	66	40	120	40
	STD-M-C	96	72	S/M		6.0	66	40	120	40
	STD-M-D	96	72	S/M		6.0	66	40	120	40
	SCC-MA-A	24	30	S/M	1.92	6.0	24	40	201	40
	SCC-MA-B	24	30	S/M		6.0	24	40	201	40
	SCC-MA-C	24	30	S/M		6.0	24	40	201	40
	SCC-MA-D	24	30	S/M		6.0	24	40	201	40
	SCC-MS-A	96	72	S/M	4.08	6.0	66	40	120	40
	SCC-MS-B	96	72	S/M		6.0	66	40	120	40
	SCC-MS-C	96	72	S/M		6.0	66	40	120	40
	SCC-MS-D	96	72	S/M		6.0	66	40	120	40
	SCC-HS-A	192	30	S/M	4.25	6.0	24	40	120	40
	SCC-HS-B	192	30	S/M		6.0	24	40	120	40
	SCC-HS-C	192	30	S/M		6.0	24	40	120	40
	SCC-HS-D	192	30	S/M		6.0	24	40	120	40

Table F-1: (4/4) AASHTO Type I and T-Beams—Property and Event Summary (Adapted from Schrantz [2012])

		Prestressing Steel Layout									Reinforcing Steel Layout			
	Beam ID	Layer Group	Group Type	# of Strands	Strand Type	Nominal Diameter (in.)	Jacking Stress (ksi)	Distance at Midspan (in.) (from bot.)	Detail Length (in.)	Distance at Girder Ends (in.) (from bot.)	Steel Layer	# of Bars	Bar Size	Distance from Bottom (in.)
AASHTO Type I (Project 2)	STD-M-1	1	Fully Bonded, Straight	6	Low-relaxation	1/2" Oversized (0.164 in^2)	202.5	3	0	3	-	-	-	-
	STD-M-2													
	SCC-MS-1													
	SCC-MS-2	2	Fully Bonded, Straight	2	Low-relaxation	1/2" Oversized (0.164 in^2)	30.5	25	0	25				
	SCC-HS-1													
	SCC-HS-2													
T-Beams (Project 4)	STD-M-A	1	Fully Bonded, Straight	2	Low-relaxation	1/2" Oversized (0.164 in^2)	212.4	2	0	2	1	4	#3	13.25
	STD-M-B						205.0							
	STD-M-C						205.0							
	STD-M-D						212.4							
	SCC-MA-A						202.2							
	SCC-MA-B						198.0							
	SCC-MA-C						198.0							
	SCC-MA-D						202.2							
	SCC-MS-A						214.5							
	SCC-MS-B						210.3							
	SCC-MS-C						210.3							
	SCC-MS-D						214.5							
	SCC-HS-A						213.7							
	SCC-HS-B						213.7							
	SCC-HS-C						213.7							
	SCC-HS-D						213.7							

Table F-2: (1/5) The Hillabee Creek Bridge Project and HPC BT-54—Property and Event Summary

				Gross Cross-Sectional Properties							Hardened Concrete Properties			
		Casting ID	Girder ID	A_g (in^2)	I_g (in^4)	y_b (in)	h (in)	L (in)	V/S (in)	Notional Size (in.)	f'_{ci} (psi)	E_{ci} (ksi)	$f'_{c,28}$ (psi)	$E_{c,28}$ (ksi)
The Hillabee Creek Bridge Project (Project 1)	BT-54	A(SCC)	54-2S, 54-5S, 54-6S	659	268077	27.63	54	1174	3.01	6.02	9010	6200	10240	6400
		B(CVC)	54-9C, 54-10C, 54-13C	659	268077	27.63	54	1174	3.01	6.02	8790	7100	10590	7400
		C(SCC)	54-1S, 54-3S, 54-4S	659	268077	27.63	54	1174	3.01	6.02	8680	6300	10800	6600
		D(CVC)	54-11C, 54-12C, 54-14C	659	268077	27.63	54	1174	3.01	6.02	7860	6700	9670	6900
		E(SCC)	54-7S	659	268077	27.63	54	1174	3.01	6.02	7940	6100	10180	6200
		E(CVC)	54-8C	659	268077	27.63	54	1174	3.01	6.02	8760	6400	10360	6800
	BT-72	F(SCC)	72-1S, 72-7S	767	545894	36.60	72	1620	3.01	6.02	8120	5800	10490	6300
		G(CVC)	72-8C, 72-14C	767	545894	36.60	72	1620	3.01	6.02	8290	6700	10770	7000
		H(SCC)	72-3S, 72-4S	767	545894	36.60	72	1620	3.01	6.02	7860	5900	10770	6400
		I(CVC)	72-10C, 72-13C	767	545894	36.60	72	1620	3.01	6.02	8770	7100	10850	7300
		J(SCC)	72-2S, 72-5S	767	545894	36.60	72	1620	3.01	6.02	8220	5800	10550	6400
		K(CVC)	72-11C, 72-12C	767	545894	36.60	72	1620	3.01	6.02	8320	6800	11050	7700
		L(SCC)	72-6S	767	545894	36.60	72	1620	3.01	6.02	6930	5700	10070	6000
		L(CVC)	72-9C	767	545894	36.60	72	1620	3.01	6.02	7710	6600	10510	6900
HPC (Pr. 3) BT-54		BT-1 thru 5		659	268077	27.63	54	1362	3.01	6.02	8540	5740	9920	5740

Table F-2: (2/5) The Hillabee Creek Bridge Project and HPC BT-54—Property and Event Summary

			Fresh Properties				Mix			Cement		Ambient				
	Casting ID	Girder ID	Air (%)	Adj. Slump (in.)	Actual Slump (in.)	w_c (pcf)	Coarse Aggregate		FA (%)	Type	Content (pcy)	RH (%)	E_p (ksi)	f_{pu} (ksi)	f_{py} (ksi)	E_s (ksi)
The Hillabee Creek Bridge Project (Project 1) BT-54	A(SCC)	54-2S, 54-5S, 54-6S	4.1	0.0	27.17	149.1	#78	Limestone	48	III	892	70	28600	270	243	-
	B(CVC)	54-9C, 54-10C, 54-13C	4.0	0.5	9.25	152.8	#67		38	III	820	70	28600	270	243	-
	C(SCC)	54-1S, 54-3S, 54-4S	3.4	0.0	26.67	150.0	#78		48	III	892	70	28600	270	243	-
	D(CVC)	54-11C, 54-12C, 54-14C	4.5	0.5	8.75	150.0	#67		38	III	820	70	28600	270	243	-
	E(SCC)	54-7S	4.9	0.0	26.00	150.0	#78		48	III	892	70	28600	270	243	-
	E(CVC)	54-8C	4.2	0.5	8.88	150.0	#67		38	III	820	70	28600	270	243	-
BT-72	F(SCC)	72-1S, 72-7S	4.0	0.0	24.00	150.1	#78	Limestone	47	III	895	70	28900	270	243	-
	G(CVC)	72-8C, 72-14C	3.9	0.5	8.75	150.0	#67		38	III	833	70	28900	270	243	-
	H(SCC)	72-3S, 72-4S	4.1	0.0	25.00	150.0	#78		47	III	895	70	28900	270	243	-
	I(CVC)	72-10C, 72-13C	2.9	0.5	9.08	150.0	#67		38	III	833	70	28900	270	243	-
	J(SCC)	72-2S, 72-5S	3.9	0.0	22.83	149.8	#78		47	III	895	70	28900	270	243	-
	K(CVC)	72-11C, 72-12C	3.4	0.5	8.83	153.4	#67		38	III	833	70	28900	270	243	-
	L(SCC)	72-6S	3.8	0.0	27.00	148.1	#78		47	III	895	70	28900	270	243	-
	L(CVC)	72-9C	2.7	0.5	8.75	153.3	#67		38	III	833	70	28900	270	243	-
HPC (Pr. 3) BT-54	BT-1 thru 5		4.2	0.5	8.00	149.7	#67 or #7		37	III	904	70	27500	270	243	-

Table F-2: (3/5) The Hillabee Creek Bridge Project and HPC BT-54—Property and Event Summary

				Time of Events					Analysis Intervals			
	Casting ID	Girder ID	Jacking (hrs)	Transfer (hrs)	Curing Type (M/S)	Eqv Adj Age (days)	Benchmark Reading (hrs)	Curing Length (hrs)	Number of CS	Max Time (days)	Number of TI
The Hillabee Creek Bridge Project (Project 1) BT-54	A(SCC)	54-2S, 54-5S, 54-6S	26.0	22.5	S	5.35	1.2	12	40	219	40
	B(CVC)	54-9C, 54-10C, 54-13C	23.8	22.8	S	4.38	0.8	12	40	217	40
	C(SCC)	54-1S, 54-3S, 54-4S	99.5	23.2	S	3.89	0.9	12	40	212	40
	D(CVC)	54-11C, 54-12C, 54-14C	26.8	22.0	S	3.33	0.8	12	40	211	40
	E(SCC)	54-7S	24.5	23.4	S	3.64	0.9	12	40	205	40
	E(CVC)	54-8C	23.7	24.2	S	3.58	0.9	12	40	205	40
The Hillabee Creek Bridge Project (Project 1) BT-72	F(SCC)	72-1S, 72-7S	23.6	23.7	S	3.62	0.6	14	40	196	40
	G(CVC)	72-8C, 72-14C	72.7	22.3	S	3.29	1.0	12	40	192	40
	H(SCC)	72-3S, 72-4S	23.7	18.9	S	3.55	0.5	12	40	191	40
	I(CVC)	72-10C, 72-13C	22.8	21.9	S	3.34	0.7	14	40	189	40
	J(SCC)	72-2S, 72-5S	73.5	22.2	S	3.89	0.2	16	40	185	40
	K(CVC)	72-11C, 72-12C	22.3	19.9	S	2.95	0.9	13	40	184	40
	L(SCC)	72-6S	48.8	18.5	S	2.32	0.7	12	40	182	40
	L(CVC)	72-9C	47.4	19.8	S	2.67	0.7	12	40	182	40
HPC (Pr. 3) BT-54	BT-1 thru 5		6.0	20.0	S	3.30	0.0	20	40	311	40

Table F-2: (4/5) The Hillabee Creek Bridge Project and HPC BT-54—Property and Event Summary

		Prestressing Steel Layout									Reinforcing Steel Layout
		Layer Group	Group Type	# of Strands	Strand Type	Nominal Diameter	Jacking Stress (ksi)	Distance at Midspan (in.) (from bot.)	Detail Length (in.)	Distance at Girder Ends (in.) (from bot.)	
The Hillabee Creek Bridge Project (Project 1)	BT-54	1	Fully Bonded, Straight	8	Low-relaxation	1/2" (0.153 in^2)	202.5	2.5	0	2.5	-
		2	Fully Bonded, Straight	8				4.5	0	4.5	-
		3	Fully Bonded, Straight	6				6.5	0	6.5	-
		4	Fully Bonded, Straight	2				8.5	0	8.5	-
		5	Debonded	2				2.5	120	2.5	-
		6	Debonded	2				4.5	120	4.5	-
		7	Draped	8				7.5	192	39.5	-
		8	Fully Bonded, Straight	4			32.7	52.0	0	52.0	-
	BT-72	1	Fully Bonded, Straight	6	Low-relaxation	1/2" Oversized (0.167 in^2)	202.5	2.5	0	2.5	-
		2	Debonded	4				2.5	120	2.5	-
		3	Fully Bonded, Straight	8				4.5	0	4.5	-
		4	Debonded	2				4.5	120	4.5	-
		5	Fully Bonded, Straight	6				6.5	0	6.5	-
		6	Fully Bonded, Straight	2				8.5	0	8.5	-
		7	Draped	8				17.5	258	57.5	-
		8	Draped	10				8.5	270	48.5	-
		9	Fully Bonded, Straight	4		1/2" (0.153 in^2)	32.7	70.0	0	70.0	-

Table F-2: (5/5) The Hillabee Creek Bridge Project and HPC BT-54—Property and Event Summary

	Prestressing Steel Layout									Reinforcing Steel Layout
	Layer Group	Group Type	# of Strands	Strand Type	Nominal Diameter	Jacking Stress (ksi)	Distance at Midspan (in.) (from bot.)	Detail Length (in.)	Distance at Girder Ends (in.) (from bot.)	
HPC BT-54 (Project 3)	1	Fully Bonded, Straight	6	Low-relaxation	0.6 " (0.217 in^2)	202.5	2.5	0	2.5	-
	2	Debonded	4				2.5	48	2.5	-
	3	Fully Bonded, Straight	6				4.5	0	4.5	-
	4	Debonded	4				4.5	48	4.5	-
	5	Fully Bonded, Straight	4				6.5	0	6.5	-
	6	Debonded	2				6.5	48	6.5	-
	7	Fully Bonded, Straight	2				8.5	0	8.5	-
	8	Draped	2				4.5	120	38.5	-
	9	Draped	2				6.5	120	40.5	-
	10	Draped	2				8.5	120	42.5	-
	11	Draped	2				10.5	120	44.5	-
	12	Draped	2				12.5	120	46.5	-
	13	Draped	2				14.5	120	48.5	-
	14	Draped	2				16.5	120	50.5	-
	15	Fully Bonded, Straight	4		1/2" (0.153 in^2)	50.0	52	0	0	-

Appendix G Measured and Predicted Data

Table G-1: (1/2) Predicted Total Creep Coefficient and Shrinkage Strain

Casting Group		Time After Transfer (days)	Total Creep Coefficient			Total Shrinkage Strain			Shrinkage Strain Prior to the Benchmark Reading		
			AASHTO LRFD	ACI 209	MC 2010	AASHTO LRFD	ACI 209	MC 2010	AASHTO LRFD	ACI 209	MC 2010
The Hillabee Creek Bridge Project	A	219	0.909	0.898	1.001	-229	-330	-245	-5	-3	-54
	B	217	0.924	0.911	0.991	-232	-281	-246	-5	-3	-52
	C	217	0.930	0.896	0.987	-235	-327	-248	-5	-3	-50
	D	211	1.006	0.906	1.093	-253	-280	-254	-4	-2	-43
	E(SCC)	205	0.988	0.888	1.032	-250	-327	-247	-5	-3	-47
	E(VC)	205	0.914	1.018	1.018	-231	-277	-246	-6	-3	-48
	F	196	0.964	0.879	0.998	-244	-317	-243	-4	-3	-47
	G	192	0.954	0.891	0.981	-240	-275	-242	-5	-2	-47
	H	191	1.011	0.875	0.973	-251	-317	-241	-3	-2	-47
	I	189	0.915	0.889	0.970	-230	-272	-242	-4	-2	-46
	J	185	0.956	0.870	0.974	-242	-314	-239	-3	-2	-47
	K	184	0.959	0.884	0.962	-239	-272	-242	-3	-2	-43
	L(SCC)	182	1.106	0.867	1.062	-274	-313	-248	-3	-2	-36
	L(VC)	182	1.013	0.883	1.010	-252	-269	-244	-3	-2	-41
AASHTO Type I	STD-M-1	110	1.220	0.784	1.194	-300	-199	-190	0	0	-26
	STD-M-2	110	1.220	0.784	1.111	-300	-198	-189	0	0	-28
	SCC-MS-1	160	1.185	0.802	0.964	-295	-263	-216	0	0	-35
	SCC-MS-2	167	1.195	0.809	0.961	-297	-262	-216	0	0	-38
	SCC-HS-1	214	0.777	0.844	0.785	-192	-286	-224	0	0	-53
	SCC-HS-2	214	0.777	0.844	0.756	-192	-286	-221	0	0	-57

Table G-1: (2/2) Predicted Total Creep Coefficient and Shrinkage Strain

Casting Group		Time After Transfer (days)	Total Creep Coefficient			Total Shrinkage Strain			Shrinkage Strain Prior to the Benchmark Reading		
			AASHTO LRFD	ACI 209	MC 2010	AASHTO LRFD	ACI 209	MC 2010	AASHTO LRFD	ACI 209	MC 2010
HPC BT-54 Girders		180	0.940	0.883	1.043	-236	-276	-285	0	0	0
T-Beams	STD-M-A	90	1.292	1.549	1.576	-409	-354	-346	0	0	0
	STD-M-B	90									
	STD-M-C	90									
	SCC-MA-A	200	1.615	1.270	1.576	-460	-414	-405	0	0	0
	SCC-MA-B	200									
	SCC-MA-C	200									
	SCC-MS-A	56	1.047	0.856	1.008	-332	-273	-272	0	0	0
	SCC-MS-B	56									
	SCC-MS-C	56									
	SCC-HS-A	14	0.423	0.558	0.476	-121	-105	-159	0	0	0
	SCC-HS-B	14									
	SCC-HS-C	14									

Table G-2: (1/4) Measured vs. Predicted Strains (με) at Gauge 1

Casting Group		Girder ID	Temp. Corr. Meas. Strains			Prediction Models			
			Initial	56-day	Erection		Initial	56-day	Erection
The Hillabee Creek Bridge Project—BT-54	A	54-2S	-419	-610	-680	AASHTO LRFD	-427	-827	-943
		54-5S	-467	-735	-754	ACI 209	-427	-845	-1033
		54-6S	-437	-630	-703	*fib* MC 2010	-429	-811	-991
	B	54-9C	-405	-650	-674	AASHTO LRFD	-374	-755	-869
		54-10C	-419	-620	-651	ACI 209	-374	-745	-911
		54-13C	-437	-705	-731	*fib* MC 2010	-376	-734	-904
	C	54-1S	-437	-665	-725	AASHTO LRFD	-417	-821	-943
		54-3S	-440	-645	-709	ACI 209	-417	-831	-1017
		54-4S	-405	-650	-716	*fib* MC 2010	-420	-800	-975
	D	54-11C	-467	-715	-770	AASHTO LRFD	-396	-811	-949
		54-12C	-468	-720	-764	ACI 209	-396	-778	-944
		54-14C	--	--	--	*fib* MC 2010	-399	-797	-979
	E (SCC)	54-7S	-451	-715	-780	AASHTO LRFD	-432	-858	-996
						ACI 209	-432	-852	-1035
						fib MC 2010	-435	-835	-1011
	E (VC)	54-8C	-440	-660	-719	AASHTO LRFD	-412	-809	-926
						ACI 209	-412	-829	-1003
						fib MC 2010	-414	-803	-975

Table G-2: (2/4) Measured vs. Predicted Strains (με) at Gauge 1

Casting Group		Girder ID	Temp. Corr. Meas. Strains			Prediction Models			
			Initial	56-day	Erection		Initial	56-day	Erection
The Hillabee Creek Bridge Project—BT-72	F	72-1S	-495	-820	-939	AASHTO LRFD	-491	-934	-1071
		72-7S	-517	-800	-932	ACI 209	-491	-927	-1107
						MC 2010	-494	-911	-1084
	G	72-8C	-452	-700	-807	AASHTO LRFD	-426	-838	-961
		72-14C	-458	-730	-839	ACI 209	-425	-816	-974
						MC 2010	-428	-815	-974
	H	72-3S	-502	-710	-863	AASHTO LRFD	-484	-940	-1082
		72-4S	-473	-660	-793	ACI 209	-484	-1008	-1094
						MC 2010	-486	-896	-1063
	I	72-10C	-472	-690	-799	AASHTO LRFD	-405	-799	-908
		72-13C	-489	-740	-859	ACI 209	-405	-786	-939
						MC 2010	-409	-784	-938
	J	72-2S	-466	-670	-831	AASHTO LRFD	-489	-934	-1064
		72-5S	-469	-665	-803	ACI 209	-489	-926	-1099
						MC 2010	-492	-907	-1071
	K	72-11C	-469	-685	-794	AASHTO LRFD	-422	-838	-959
		72-12C	-460	-665	-765	ACI 209	-422	-812	-966
						MC 2010	-425	-811	-965
	L (SCC)	72-6S	-503	-765	-884	AASHTO LRFD	-500	-995	-1160
						ACI 209	-500	-939	-1110
						MC 2010	-503	-953	-1125
	L (VC)	72-9C	-445	-650	-746	AASHTO LRFD	-432	-867	-1001
						ACI 209	-432	-823	-976
						MC 2010	-435	-838	-995

Table G-2: (3/4) Measured vs. Predicted Strains (με) at Gauge 1

Girder ID		Temp. Corr. Meas. Strains				Prediction Models				
		Initial	56-day	110-day	Erection		Initial	56-day	110-day	Erection
AASHTO Type I Girders	STD-M-1	-250	-585	-641	--	AASHTO LRFD	-201	-601	-706	--
						ACI 209	-201	-465	-533	--
						fib MC 2010	-203	-515	-593	--
	STD-M-2	-262	-625	-687	--	AASHTO LRFD	-201	-602	-707	--
						ACI 209	-201	-465	-533	--
						fib MC 2010	-203	-503	-578	--
	SCC-MS-1	-227	-540	-600	-626	AASHTO LRFD	-217	-593	-686	-728
						ACI 209	-217	-511	-587	-626
						fib MC 2010	-221	-499	-566	-606
	SCC-MS-2	-217	-520	--	--	AASHTO LRFD	-215	-590	--	--
						ACI 209	-216	-507	--	--
						fib MC 2010	-220	-494	--	--
	SCC-HS-1	-164	-340	-370	-369	AASHTO LRFD	-165	-409	-444	-465
						ACI 209	-164	-433	-507	-567
						fib MC 2010	-169	-388	-441	-495
	SCC-HS-2	-169	-340	-365	-357	AASHTO LRFD	-162	-405	-440	-461
						ACI 209	-162	-430	-503	-563
						fib MC 2010	-167	-379	-431	-484

Table G-2: (4/4) Measured vs. Predicted Strains (με) at Gauge 1

Girder ID		Measured Cambers			Prediction Models			
		1-day	56-day	180-day		1-day	56-day	180-day
HPC BT-54	Girder 1	-910	-1110	-1355	AASHTO LRFD	-766	-1280	-1428
	Girder 2	-943	-1170	-1480	ACI 209	-806	-1251	-1435
	Girder 3	-866	-1110	-1430	*fib* MC 2010	-920	-1322	-1520
	Girder 4	-869	-1130	-1440				
	Girder 5	-806	-1015	-1285				

Table G-3: (1/4) Measured vs. Predicted Midspan Curvatures (x10^{-6}/in.)

	Casting Group	Girder ID	Temp. Corr. Meas. Strains			Prediction Models			
			Initial	56 day	Erection		Initial	56 day	Erection
The Hillabee Creek Bridge Project—BT-54 (Using Gauges 1&4)	A	54-2S	--	--	--	AASHTO LRFD	-7.70	-11.27	-12.23
		54-5S	-7.43	-12.10	-12.12	ACI 209	-7.70	-11.09	-12.09
		54-6S	-6.81	-9.95	-10.57	*fib* MC 2010	-7.70	-11.60	-12.85
	B	54-9C	-5.69	-9.70	-9.55	AASHTO LRFD	-6.70	-9.93	-10.83
		54-10C	-6.29	-9.40	-9.73	ACI 209	-6.70	-9.85	-10.81
		54-13C	--	--	--	*fib* MC 2010	-6.69	-10.16	-11.27
	C	54-1S	--	--	--	AASHTO LRFD	-7.50	-11.06	-12.06
		54-3S	--	--	--	ACI 209	-7.50	-10.85	-11.83
		54-4S	-6.31	-9.65	-10.19	*fib* MC 2010	-7.50	-11.28	-12.48
	D	54-11C	-7.46	-11.55	-12.11	AASHTO LRFD	-7.15	-10.76	-11.87
		54-12C	--	--	--	ACI 209	-7.15	-10.47	-11.46
		54-14C	--	--	--	*fib* MC 2010	-7.15	-11.20	-12.47
	E (SCC)	54-7S	-7.07	-10.35	-10.77	AASHTO LRFD	-7.78	-11.54	-12.66
						ACI 209	-7.78	-11.17	-12.12
						fib MC 2010	-7.78	-11.84	-13.08
	E (VC)	54-8C	-6.96	-10.40	-11.01	AASHTO LRFD	-7.38	-10.84	-11.79
						ACI 209	-7.38	-11.24	-12.37
						fib MC 2010	-7.38	-11.25	-12.45

Table G-3: (2/4) Measured vs. Predicted Midspan Curvatures (x10^{-6}/in.)

Casting Group		Girder ID	Temp. Corr. Meas. Strains			Prediction Models			
			Initial	56-day	Erection		Initial	56-day	Erection
The Hillabee Creek Bridge Project—BT-72 (Using Gauges 1&4)	F	72-1S	-5.18	-7.50	-8.11	AASHTO '05(+)	-5.85	-8.23	-8.88
		72-7S				ACI 209	-5.85	-8.03	-8.57
						fib MC 2010	-5.84	-8.42	-9.14
	G	72-8C	-3.97	-7.40	-6.74	AASHTO '05(+)	-5.02	-7.15	-7.71
		72-14C				ACI 209	-5.02	-7.06	-7.58
						fib MC 2010	-5.01	-7.30	-7.92
	H	72-3S				AASHTO '05(+)	-5.77	-8.25	-8.93
		72-4S	-3.31	-6.15	-6.15	ACI 209	-5.77	-8.74	-8.47
						fib MC 2010	-5.77	-8.28	-8.96
	I	72-10C	-4.71	-7.40	-7.63	AASHTO '05(+)	-4.81	-6.83	-7.33
		72-13C				ACI 209	-4.81	-6.79	-7.29
						fib MC 2010	-4.80	-7.00	-7.60
	J	72-2S				AASHTO '05(+)	-5.82	-8.22	-8.85
		72-5S	-4.31	-7.40	-7.31	ACI 209	-5.82	-8.02	-8.55
						fib MC 2010	-5.81	-8.37	-9.06
	K	72-11C				AASHTO '05(+)	-4.98	-7.18	-7.75
		72-12C	-5.05	-9.25	-9.27	ACI 209	-4.98	-7.05	-7.58
						fib MC 2010	-4.98	-7.25	-7.87
	L (SCC)	72-6S	-4.77	-8.30	-8.31	AASHTO '05(+)	-6.00	-8.70	-9.48
						ACI 209	-6.00	-8.22	-8.74
						fib MC 2010	-6.00	-8.83	-9.57
	L (VC)	72-9C	-4.40	-7.60	-7.54	AASHTO '05(+)	-5.09	-7.33	-7.95
						ACI 209	-5.09	-7.14	-7.64
						fib MC 2010	-5.09	-7.48	-8.10

Table G-3: (3/4) Measured vs. Predicted Midspan Curvatures (x10^{-6}/in.)

Girder ID		Measured Strains				Prediction Models				
		Initial	56-day	110-day	Erection		Initial	56-day	110-day	Erection
AASHTO Type I Girders	STD-M-1	-10.40	-21.10	-20.81	--	AASHTO LRFD	-7.79	-13.96	-15.53	--
						ACI 209	-7.79	-12.08	-12.83	--
						MC 2010	-7.78	-14.39	-15.58	--
	STD-M-2	-10.91	-20.20	-20.48	--	AASHTO LRFD	-7.79	-14.01	-15.59	--
						ACI 209	-7.79	-12.11	-12.87	--
						MC 2010	-7.78	-13.95	-15.06	--
	SCC-MS-1	-8.68	-16.90	-18.95	-19.98	AASHTO LRFD	-8.39	-14.46	-15.91	-16.56
						ACI 209	-8.39	-12.77	-13.53	-13.93
						MC 2010	-8.39	-13.64	-14.59	-15.14
	SCC-MS-2	-7.27	-13.45	--	--	AASHTO LRFD	-8.33	-14.34	--	--
						ACI 209	-8.33	-12.66	--	--
						MC 2010	-8.32	-13.46	--	--
	SCC-HS-1	-5.29	-8.75	-9.85	-10.92	AASHTO LRFD	-6.24	-9.55	-10.02	-10.30
						ACI 209	-6.24	-9.51	-10.08	-10.59
						MC 2010	-6.23	-9.24	-9.78	-10.32
	SCC-HS-2	-5.55	-8.20	-8.95	-10.24	AASHTO LRFD	-6.25	-9.56	-10.02	-10.30
						ACI 209	-6.25	-9.52	-10.09	-10.59
						MC 2010	-6.24	-9.14	-9.66	-10.18

Table G-3: (4/4) Measured vs. Predicted Curvatures (x10^{-6}/in.)

Girder ID		Temp. Corr. Meas. Cambers			Prediction Models			
		1-day	56-day	180-day		1-day	56-day	180-day
HPC BT-54	Girder 1	-15.24	-18.70	-21.05	AASHTO LRFD	-13.9	-19.2	-20.6
	Girder 2	-17.57	-21.10	-23.85	ACI 209	-14.6	-18.8	-20.1
	Girder 3	-15.25	-19.00	-21.95	*fib* MC 2010	-15.6	-19.7	-21.3
	Girder 4	-15.14	-18.70	-20.30				
	Girder 5	--	--	--				

Table G-4: (1/6) Measured vs. Predicted Midspan Cambers (in.)

Casting Group		Girder ID	Temp. Corr. Meas. Cambers			Prediction Models			
			Initial	56-day			Initial	56-day	
The Hillabee Creek Bridge Project—BT-54	A	54-2S	1.37	1.91	2.05	AASHTO LRFD	1.37	2.05	2.23
		54-5S	1.10	1.26	1.35	ACI 209	1.37	2.00	2.19
		54-6S	1.49	1.91	1.91	*fib* MC 2010	1.37	2.09	2.32
	B	54-9C	0.99	1.64	1.68	AASHTO LRFD	1.20	1.81	1.98
		54-10C	0.92	1.32	1.24	ACI 209	1.20	1.78	1.96
		54-13C	0.96	1.77	1.71	*fib* MC 2010	1.20	1.84	2.04
	C	54-1S	0.92	1.52	1.57	AASHTO LRFD	1.34	2.01	2.20
		54-3S	1.04	1.39	1.48	ACI 209	1.34	1.96	2.15
		54-4S	0.71	1.46	1.61	*fib* MC 2010	1.34	2.04	2.26
	D	54-11C	1.09	1.73	1.88	AASHTO LRFD	1.28	1.96	2.17
		54-12C	1.21	1.78	1.94	ACI 209	1.28	1.89	2.07
		54-14C	1.06	1.69	1.77	*fib* MC 2010	1.28	2.02	2.26
	E (SCC)	54-7S	0.97	1.72	1.80	AASHTO LRFD	1.39	2.10	2.32
						ACI 209	1.39	2.02	2.20
						fib MC 2010	1.39	2.14	2.37
	E (VC)	54-8C	0.94	1.54	1.60	AASHTO LRFD	1.32	1.97	2.16
						ACI 209	1.32	2.03	2.25
						fib MC 2010	1.32	2.03	2.26

Table G-4: (2/6) Measured vs. Predicted Midspan Cambers (in.)

Casting Group		Girder ID	Temp. Corr. Meas. Cambers			Prediction Models			
			Initial	56-day	Erection		Initial	56-day	Erection
The Hillabee Creek Bridge Project—BT-72	F	72-1S	1.52	2.50	2.55	AASHTO LRFD	1.94	2.81	3.05
		72-7S	1.43	2.15	2.17	ACI 209	1.94	2.71	2.92
						MC 2010	1.94	2.84	3.11
	G	72-8C	1.38	2.15	2.09	AASHTO LRFD	1.67	2.44	2.66
		72-14C	1.35	2.16	2.15	ACI 209	1.67	2.39	2.58
						MC 2010	1.67	2.47	2.70
	H	72-3S	1.67	2.47	2.50	AASHTO LRFD	1.92	2.81	3.07
		72-4S	1.42	2.31	2.22	ACI 209	1.92	2.95	2.88
						MC 2010	1.91	2.79	3.04
	I	72-10C	1.24	2.09	2.09	AASHTO LRFD	1.60	2.33	2.52
		72-13C	1.14	2.11	2.00	ACI 209	1.60	2.29	2.48
						MC 2010	1.60	2.37	2.58
	J	72-2S	1.17	2.29	2.31	AASHTO LRFD	1.93	2.81	3.04
		72-5S	1.17	2.20	2.14	ACI 209	1.93	2.71	2.90
						MC 2010	1.93	2.83	3.08
	K	72-11C	1.53	2.43	2.37	AASHTO LRFD	1.66	2.45	2.67
		72-12C	1.37	2.45	2.45	ACI 209	1.66	2.38	2.58
						MC 2010	1.66	2.45	2.68
	L (SCC)	72-6S	1.59	2.76	2.72	AASHTO LRFD	1.99	2.97	3.27
						ACI 209	1.99	2.77	2.96
						MC 2010	1.99	2.98	3.25
	L (VC)	72-9C	1.23	2.41	2.28	AASHTO LRFD	1.69	2.51	2.74
						ACI 209	1.69	2.42	2.60
						MC 2010	1.69	2.53	2.76

Table G-4: (3/6) Measured vs. Predicted Midspan Cambers (in.)

Girder ID		Temp. Corr. Meas. Cambers				Prediction Models				
		Initial	56-day	110-day	Erection		Initial	56-day	110-day	Erection
AASHTO Type I Girders	STD-M-1	0.31	0.58	0.59	--	AASHTO LRFD	0.25	0.45	0.50	--
						ACI 209	0.25	0.39	0.41	--
						fib MC 2010	0.25	0.46	0.50	--
	STD-M-2	0.23	0.45	0.47	--	AASHTO LRFD	0.25	0.45	0.50	--
						ACI 209	0.25	0.39	0.41	--
						fib MC 2010	0.25	0.45	0.49	--
	SCC-MS-1	0.26	0.44	0.47	0.48	AASHTO LRFD	0.27	0.47	0.51	0.54
						ACI 209	0.27	0.41	0.44	0.45
						fib MC 2010	0.27	0.44	0.47	0.49
	SCC-MS-2	0.21	0.36	0.39	0.41	AASHTO LRFD	0.27	0.46	0.51	0.53
						ACI 209	0.27	0.41	0.43	0.45
						fib MC 2010	0.27	0.43	0.47	0.48
	SCC-HS-1	0.17	0.23	0.25	0.29	AASHTO LRFD	0.20	0.31	0.32	0.33
						ACI 209	0.20	0.31	0.33	0.34
						fib MC 2010	0.20	0.30	0.32	0.34
	SCC-HS-2	0.12	0.16	0.18	0.21	AASHTO LRFD	0.20	0.31	0.32	0.33
						ACI 209	0.20	0.31	0.33	0.34
						fib MC 2010	0.20	0.30	0.31	0.33

Table G-4: (4/6) Measured vs. Predicted Midspan Cambers (in.)

Girder ID		Measured Cambers			Prediction Models			
		Transfer	56-day	180-day		Transfer	56-day	180-day
HPC BT-54	Girder 1	2.90	3.89	4.18	AASHTO LRFD	2.85	4.07	4.38
	Girder 2	3.53	4.91	4.67	ACI 209	2.85	3.98	4.27
	Girder 3	2.78	3.89	4.05	*fib* MC 2010	2.83	4.17	4.52
	Girder 4	2.63	4.02	4.08				
	Girder 5	2.63	3.96	4.19				

Table G-4: (5/6) Measured vs. Predicted Midspan Cambers (in.)

Girder ID		Measured Cambers					Prediction Models					
		Initial	14-day	56-day	90-day	200-day		Initial	14-day	56-day	90-day	200-day
T-Beams (Accelerated Curing)	STD-M-A	0.34	0.46	0.57	0.59	--	AASHTO LRFD	0.27	0.38	0.51	0.56	--
							ACI 209	0.27	0.47	0.58	0.62	--
							MC 2010	0.27	0.49	0.59	0.63	--
	STD-M-B	0.20	0.24	0.33	0.33	--	AASHTO LRFD	0.15	0.22	0.29	0.31	--
							ACI 209	0.15	0.26	0.33	0.35	--
							MC 2010	0.15	0.28	0.33	0.35	--
	STD-M-C	0.10	0.14	0.16	0.18	--	AASHTO LRFD	0.10	0.14	0.19	0.21	--
							ACI 209	0.10	0.17	0.22	0.23	--
							MC 2010	0.10	0.18	0.22	0.23	--
	SCC-MA-A	0.30	0.45	0.50	0.52	0.54	AASHTO LRFD	0.27	0.39	0.52	0.57	0.62
							ACI 209	0.27	0.41	0.48	0.51	0.55
							MC 2010	0.27	0.45	0.53	0.57	0.62
	SCC-MA-B	0.16	0.26	0.29	0.30	0.31	AASHTO LRFD	0.15	0.22	0.30	0.32	0.35
							ACI 209	0.15	0.23	0.27	0.29	0.31
							MC 2010	0.15	0.26	0.30	0.32	0.35
	SCC-MA-C	0.08	0.15	0.17	0.17	0.20	AASHTO LRFD	0.10	0.14	0.20	0.21	0.23
							ACI 209	0.10	0.15	0.18	0.19	0.21
							MC 2010	0.10	0.17	0.20	0.21	0.23

Table G-4: (6/6) Measured vs. Predicted Midspan Cambers (in.)

Girder ID		Measured Cambers					Prediction Models					
		Initial	14-day	56-day	90-day	200-day		Initial	14-day	56-day	90-day	200-day
T-Beams (Accelerated Curing)	SCC-MS-A	0.29	0.41	0.42	--	--	AASHTO LRFD	0.27	0.37	0.50	--	--
							ACI 209	0.27	0.39	0.47	--	--
							MC 2010	0.27	0.43	0.50	--	--
	SCC-MS-B	0.17	0.24	0.24	--	--	AASHTO LRFD	0.15	0.21	0.28	--	--
							ACI 209	0.15	0.22	0.26	--	--
							MC 2010	0.15	0.24	0.28	--	--
	SCC-MS-C	0.10	0.14	0.15	--	--	AASHTO LRFD	0.10	0.14	0.18	--	--
							ACI 209	0.10	0.14	0.17	--	--
							MC 2010	0.10	0.16	0.18	--	--
	SCC-HS-A	0.24	0.31	--	--	--	AASHTO LRFD	0.22	0.30	--	--	--
							ACI 209	0.22	0.33	--	--	--
							MC 2010	0.22	0.31	--	--	--
	SCC-HS-B	0.16	0.20	--	--	--	AASHTO LRFD	0.12	0.17	--	--	--
							ACI 209	0.12	0.19	--	--	--
							MC 2010	0.12	0.18	--	--	--
	SCC-HS-C	0.07	0.10	--	--	--	AASHTO LRFD	0.08	0.11	--	--	--
							ACI 209	0.08	0.12	--	--	--
							MC 2010	0.08	0.12	--	--	--

Appendix H Fractional Errors

Table H-1: Bottom-Flange Strain—Unbiased Estimates of the Standard Deviation

Casting Type		Age		Bottom-Flange Strains (Fractional Error)				
				# of Data	AASHTO LRFD		ACI 209	MC 2010
					Standard	+20		
The Hillabee Creek Bridge Project	**BT-54 SCC** (Gage at 6.20")	At transfer		7	0.05	0.05	0.05	0.05
		Growth from transfer	To 56-day	7	0.91	1.06	0.97	0.81
			To erection	7	0.92	1.08	1.21	1.05
	BT-54 VC (Gage at 6.20")	At transfer		7	0.13	0.13	0.13	0.13
		Growth from transfer	To 56-day	7	0.75	0.90	0.71	0.67
			To erection	7	0.96	1.13	1.10	1.09
	BT-72 SCC (Gage at 8.80")	At transfer		7	0.04	0.04	0.04	0.04
		Growth from transfer	To 56-day	7	1.14	1.29	1.24	0.96
			To erection	7	0.69	0.81	0.73	0.65
	BT-72 VC (Gage at 8.80")	At transfer		7	0.11	0.11	0.11	0.11
		Growth from transfer	To 56-day	7	0.90	1.05	0.78	0.77
			To erection	7	0.66	0.80	0.68	0.68
					AASHTO LRFD		**ACI 209**	**MC 2010**
AASHTO Type I Girders	**STD – M (VC)** (Gage at 3.25")	At transfer		2	0.31		0.31	0.29
		Growth from transfer	To 56-day	2	0.22		0.34	0.19
			To erection	2	0.35		0.27	0.12
	SCC - MS (Gage at 3.25")	At transfer		2	0.04		0.04	0.03
		Growth from transfer	To 56-day	2	0.31		0.07	0.15
			To 110-day	0	N/A		N/A	N/A
			To erection	0	N/A		N/A	N/A
	SCC - HS (One at 3.00", other at 3.38")	At transfer		2	0.04		0.04	0.03
		Growth from transfer	To 56-day	2	0.57		0.77	0.34
			To 110-day	2	0.55		0.99	0.48
			To erection	2	0.76		1.49	0.91
HPC	**BT-54 - VC** (Gage at 6.50 in)	At 1 day		5	0.15		0.11	0.08
		Growth from 1 day	To 56-day	5	1.45		1.10	0.89
			To 180-day	5	0.35		0.28	0.23

Table H-2: Midspan Curvature—Unbiased Estimate of the Standard Deviation

	Casting Type	Age		Midspan Curvature (Fractional Error)				
				# of Data	AASHTO LRFD		ACI 209	MC 2010
					Standard	+20		
The Hillabee Creek Bridge Project	BT-54 SCC	At transfer		4	0.15	0.15	0.15	0.15
		Growth from transfer	To 56-day	4	0.19	0.18	0.17	0.23
			To erection	4	0.27	0.24	0.16	0.37
	BT-54 VC	At transfer		4	0.11	0.11	0.11	0.11
		Growth from transfer	To 56-day	4	0.12	0.13	0.18	0.13
			To erection	4	0.16	0.13	0.18	0.28
	BT-72 SCC	At transfer		4	0.50	0.50	0.50	0.50
		Growth from transfer	To 56-day	4	0.18	0.20	0.28	0.18
			To erection	4	0.10	0.07	0.15	0.11
	BT-72 VC	At transfer		4	0.18	0.18	0.18	0.18
		Growth from transfer	To 56-day	4	0.40	0.42	0.45	0.37
			To erection	4	0.20	0.22	0.26	0.19
					AASHTO LRFD		ACI 209	MC 2010
AASHTO Type I Girders	STD-M (VC)	At transfer		2	0.38		0.38	0.38
		Growth from transfer	To 56-day	2	0.57		0.83	0.55
			To erection	2	0.32		0.70	0.35
	SCC - MS	At transfer		2	0.15		0.15	0.15
		Growth from transfer	To 56-day	2	0.26		0.56	0.40
			To 110-day	0	N/A		N/A	N/A
			To erection	0	N/A		N/A	N/A
	SCC - HS	At transfer		2	0.22		0.22	0.22
		Growth from transfer	To 56-day	2	0.25		0.24	0.16
			To 110-day	2	0.20		0.20	0.22
			To erection	2	0.31		0.24	0.32
HPC	BT-54 VC	At 1 day		4	0.15		0.10	0.07
		Growth from 1-day	To 56-day	4	0.56		0.20	0.15
			To 180-day	4	0.20		0.14	0.12

Table H-3: (1/2) Camber—Unbiased Estimate of the Standard Deviation

Casting Type		Age		Midspan Camber (Fractional Error)				
				# of Data	AASHTO LRFD		ACI 209	MC 2010
					Standard	+20		
The Hillabee Creek Bridge Project	BT-54 SCC	At transfer		7	0.48	0.48	0.48	0.47
		Growth from transfer	To 56-day	7	1.40	1.36	1.27	1.53
			To erection	7	1.19	1.15	1.09	1.39
	BT-54 VC	At transfer		7	0.27	0.27	0.27	0.27
		Growth from transfer	To 56-day	7	0.26	0.25	0.24	0.32
			To erection	7	0.65	0.62	0.62	0.77
	BT-72 SCC	At transfer		7	0.46	0.46	0.46	0.46
		Growth from transfer	To 56-day	7	0.17	0.17	0.27	0.17
			To erection	7	0.33	0.30	0.19	0.34
	BT-72 VC	At transfer		7	0.30	0.30	0.30	0.30
		Growth from transfer	To 56-day	7	0.21	0.22	0.27	0.19
			To erection	7	0.21	0.19	0.16	0.26
					AASHTO LRFD		ACI 209	MC 2010
AASHTO Type I Girders	STD – M (VC)	At transfer		2	0.20		0.20	0.20
		Growth from transfer	To 56-day	2	0.28		0.61	0.23
			To erection	2	0.13		0.53	0.11
	SCC - MS	At transfer		2	0.28		0.28	0.28
		Growth from transfer	To 56-day	2	0.32		0.21	0.11
			To 110-day	2	0.39		0.21	0.10
			To erection	2	0.41		0.18	0.09
	SCC - HS	At transfer		2	0.68		0.68	0.68
		Growth from transfer	To 56-day	2	2.02		1.98	1.63
			To 110-day	2	1.26		1.31	1.04
			To erection	2	0.51		0.64	0.47

Table H-3: (2/2) Camber—Unbiased Estimate of the Standard Deviation

Casting Type		Age		Midspan Camber (Fractional Error)			
				# of Data	AASHTO LRFD	ACI 209	*fib* MC 2010
HPC	BT-54 VC	At 1 day		5	0.11	0.11	0.11
		Growth from transfer	To 56-day	5	0.19	0.16	0.30
			To 180-day	5	0.32	0.23	0.49
T-Beams	STD - M (Acc.)	At transfer		3	0.21	0.21	0.21
		Growth from transfer	To 14-day	3	0.29	1.34	1.63
			To 56-day	3	0.47	0.86	0.90
			To 90-day	3	0.30	0.62	0.65
	STD - M (Non-Acc.)	At transfer		3	0.21	0.21	0.21
		Growth from transfer	To 14-day	3	0.60	1.27	1.63
			To 56-day	3	0.82	0.81	0.90
			To 90-day	3	0.65	0.56	0.65
	SCC - MA (Acc.)	At transfer		3	0.22	0.22	0.22
		Growth from transfer	To 14-day	3	0.41	0.28	0.22
			To 56-day	3	0.24	0.11	0.31
			To 90-day	3	0.32	0.11	0.33
			To 200-day	3	0.41	0.17	0.40
	SCC - MA (Non-Acc.)	At transfer		3	0.22	0.22	0.22
		Growth from transfer	To 14-day	3	0.23	0.37	0.22
			To 56-day	3	0.58	0.17	0.31
			To 90-day	3	0.69	0.16	0.33
			To 200-day	3	0.78	0.18	0.40
	SCC - MS (Acc.)	At transfer		3	0.12	0.12	0.12
		Growth from transfer	To 14-day	3	0.16	0.05	0.38
			To 56-day	3	0.97	0.62	0.94
	SCC - MS (Non-Acc.)	At transfer		3	0.12	0.12	0.12
		Growth from transfer	To 14-day	3	0.12	0.05	0.38
			To 56-day	3	1.51	0.56	0.94
	SCC - HS (Acc.)	At transfer		3	0.24	0.24	0.24
		Growth from transfer	To 14-day	3	0.21	0.63	0.34
	SCC - HS (Non Acc.)	At transfer		3	0.24	0.24	0.24
		Growth from transfer	To 14-day	3	0.56	0.43	0.34

Appendix I Cement Types

I.1 Overview

The purpose of this section is to present the available cement types in line with the governing European and U.S. standards. Cement type is a key factor to determine the concrete properties and the time-dependent deflections. In fact, the European and U.S. material prediction models such as stiffness, creep and shrinkage are based on cement type.

In the following sections, two cement types are introduced, namely, the British implementation of European Standard (BS EN) 197-1:2011 and the American Society of Testing and Materials (ASTM) C150/C150M-12. Some of the physical and chemical properties of various cement types are also presented.

The European and ASTM standards differ from each other in terms of the cement classifications, the requirements, and the material testing methods. Further, these standards do not offer direct equivalence.

I.2 European Cement Types

The European Standard, EN 197-1 (2011), gives the specifications of the cement types including the proportions of the constituents, the requirements of their mechanical, physical, chemical and durability properties. British implementation of EN 197-1 is called as the British Standard and identical to other European Standards (BS EN 197-1 2011).

EN 197-1 (2011) defines the cement as “a hydraulic binder, i.e., a finely grounded inorganic material which, when mixed with water, forms a paste which sets and hardens by

means of hydration reaction and processes and which, after hardening, retains its strength and stability even under water".

Cement types satisfying the requirements of EN 197-1 are named as CEM. They are divided into five main groups as listed below.

- CEM I : Portland cement
- CEM II : Portland-composite cement
- CEM III : Blast furnace cement
- CEM IV : Pozzolanic cement
- CEM V : Composite cement

Mechanical and physical requirements of three standard strength classes are provided in Table I-1. Strength classes of these cement types are further divided into three categories based on their early compressive strengths. Letter 'L' indicates a class with low early strength. On the other hand, letter 'N' is used for ordinary early strength; while, letter 'R' is used for high early strength. Compressive strength is determined in conformity with EN 196-1. Initial setting time and soundness (expansion) are tested in accordance to EN 196-3 (BS EN 197-1 2011).

Table I-1: Mechanical and Physical Requirements (Adapted from BS EN 197-1 [2011])

Strength Class	Early strength				Standard strength				Initial Setting Time	Soundness	
	2D		7D		28 days						
	MPa	psi	MPa	psi	MPa	psi	MPa	psi	minutes	mm	in
32,5 L [(1)]	–		≥12.0	≥1740	≥32.5	≥4710	≤52.5	≤6160	≥75	≤10	≤0.39
32,5N	–		≥16.0	≥2320							
32,5R	≥10.0	≥1450	–								
42,5 L [(1)]	–		≥16.0	≥2320	≥42.5	≥6160	≤62.5	≤7610	≥60		
42,5N	≥10.0	≥1450	–								
42,5R	≥20.0	≥2900	–								
52,5 L [(1)]	≥10.0	≥1450	–		≥52.5	≥7610	–	–	≥45		
52,5N	≥20.0	≥2900	–								
52,5R	≥30.0	≥4350	–								

Note: The values in the US customary units may not be exact equivalents. Three significant figures are used while converting them.
[(1)] Strength class is only defined for CEM III cements

Chemical properties of common twenty-seven cement types are tabulated in Table I-2. Loss on ignition, insoluble residue, sulfate content, and chloride content are determined according to EN 196-2. However, the pozzolanicity test is carried out in conformity with EN 196-5. More explanations about the main constituents can be found in EN 197-1 (2011).

The representation of the cement types is required to follow the similar designation with the examples presented below.

- Example 1: Portland cement, conforming to EN 197-1, of strength class 32.5 with ordinary early strength should be designated by :

  Portland cement EN 197-1 – CEM I 32,5 N
- Example 2: Portland-slag cement, conforming to EN 197-1, containing between 6% and 20% by mass of blast-furnace slag (S) and of strength class 42.5 with high early strength should be designated by :

  Portland-slag cement EN 197-1 – CEM II/A-S 42,5 R
- Example 3: Portland-fly ash cement, conforming to EN 197-1, containing between 6% and 20% by mass of siliceous fly ash (V) by mass and of strength class 52.5 with high early strength should be designated by :

  Portland-slag cement EN 197-1 – CEM II/A-V 52,5 R

Table I-2: Chemical Properties of Common Cements in EN 197-1:2011 (Adapted from BS EN 197-1 [2011])

Main types	Notation of the 27 products (types of common cement)		Composition [percentage by mass (1)]										
			Main constituents										Minor additional constituents
			Clinker	Blast-furnace slag	Silica fume	Pozzolana		Fly ash		Burnt shale	Limestone		
						natural	natural calcined	siliceous	calcareous				
			K	S	D (2)	P	Q	V	W	T	L	LL	
CEM I	Portland cement	CEM I	95 to 100	–	–	–	–	–	–	–	–	–	0 to 5
CEM II	Portland-slag cement	CEM II/A-S	80 to 94	6 to 20	–	–	–	–	–	–	–	–	0 to 5
		CEM II/B-S	65 to 79	21 to 35	–	–	–	–	–	–	–	–	0 to 5
	Portland-silica fume cement	CEM II/A-D	90 to 94	–	6 to 10	–	–	–	–	–	–	–	0 to 5
	Portland-pozzolana cement	CEM II/A-P	80 to 94	–	–	6 to 20	–	–	–	–	–	–	0 to 5
		CEM II/B-P	65 to 79	–	–	21 to 35	–	–	–	–	–	–	0 to 5
		CEM II/A-Q	80 to 94	–	–	–	6 to 20	–	–	–	–	–	0 to 5
		CEM II/B-Q	65 to 79	–	–	–	21 to 35	–	–	–	–	–	0 to 5
	Portland-fly ash cement	CEM II/A-V	80 to 94	–	–	–	–	6 to 20	–	–	–	–	0 to 5
		CEM II/B-V	65 to 79	–	–	–	–	21 to 35	–	–	–	–	0 to 5
		CEM II/A-W	80 to 94	–	–	–	–	–	6 to 20	–	–	–	0 to 5
		CEM II/B-W	65 to 79	–	–	–	–	–	21 to 35	–	–	–	0 to 5
	Portland-burnt shale cement	CEM II/A-T	80 to 94	–	–	–	–	–	–	6 to 20	–	–	0 to 5
		CEM II/B-T	65 to 79	–	–	–	–	–	–	21 to 35	–	–	0 to 5
	Portland-limestone cement	CEM II/A-L	80 to 94	–	–	–	–	–	–	–	6 to 20	–	0 to 5
		CEM II/B-L	65 to 79	–	–	–	–	–	–	–	21 to 35	–	0 to 5
		CEM II/A-LL	80 to 94	–	–	–	–	–	–	–	–	6 to 20	0 to 5
		CEM II/B-LL	65 to 79	–	–	–	–	–	–	–	–	21 to 35	0 to 5
	Portland-composite cement (3)	CEM II/A-M	80 to 88	< ——— 12 to 20 ——— >									0 to 5
		CEM II/B-M	65 to 79	< ——— 21 to 35 ——— >									0 to 5

Table I-2: (Continued) Chemical Properties of Common Cements in EN 197-1:2011 (Adapted from BS EN 197-1 [2011])

Main types	Notation of the 27 products (types of common cement)		Composition [percentage by mass [1]]										
			Main constituents										Minor additional constituents
			Clinker	Blast-furnace slag	Silica fume	Pozzolana		Fly ash		Burnt shale	Limestone		
						natural	natural calcined	siliceous	calcareous				
			K	S	D [2]	P	Q	V	W	T	L	LL	
CEM III	Blastfurnace cement	CEM III/A	35 to 64	36 to 65	–	–	–	–	–	–	–	–	0 to 5
		CEM III/B	20 to 34	66 to 80	–	–	–	–	–	–	–	–	0 to 5
		CEM III/C	5 to 19	81 to 95	–	–	–	–	–	–	–	–	0 to 5
CEM IV	Pozzolanic cement [3]	CEM IV/A	65 to 89	–	< ——— 11 to 35 ——— >					–	–	–	0 to 5
		CEM IV/B	45 to 64	–	< ——— 36 to 55 ——— >					–	–	–	0 to 5
CEM V	Pozzolanic cement [3]	CEM V/A	40 to 64	18 to 30	–	< ——— 18 to 30 ——— >			–	–	–	–	0 to 5
		CEM V/B	20 to 38	31 to 49	–	< ——— 31 to 49 ——— >			–	–	–	–	0 to 5

[1] The values in the table refer to the sum of the main and minor additional constituents.

[2] The proportion of silica fume is limited to 10 %.

[3] In Portland-composite cements CEM II/A-M and CEM II/B-M, in pozzolanic cements CEM IV/A and CEM IV/B and in composite cements CEM V/A and CEM V/B the main constituents other than clinker shall be declared by designation of the cement

I.3 ASTM Portland Cement Types

ASTM Standard C219 (2013) defines cementitious material as “an inorganic material or a mixture of inorganic materials that sets and develops strength by chemical reaction with water by formation of hydrates and that is capable of doing so underwater”. Likewise, portland cement is defined as “a hydraulic cement produced by pulverizing clinker, consisting essentially of crystalline hydraulic calcium silicates, and usually containing one or more of the following: water, calcium sulfate, up to 5 % limestone, and processing additions”.

Moreover, ASTM Standard C150 (2012) explains the specifications of the ten portland cement types. It also covers the allowable ingredients, the requirements of chemical compositions, physical properties, testing methods. Ten types of portland cement in ASTM C150 are listed below.

- Type I : General use cement which does not satisfy the special properties for any other type
- Type IA : Air-entraining cement having the similar uses with Type I
- Type II : General use cement with moderate sulfate resistance
- Type IIA : Air-entraining cement having the similar uses with Type II
- Type II(MH) : General use cement with moderate heat of hydration and moderate sulfate resistance
- Type II(MH)A : Air-entraining cement having the similar uses with Type II(MH)
- Type III : High early strength cement
- Type IIIA : Air-entraining cement having the similar uses with Type III
- Type IV : Low heat of hydration cement
- Type V : High sulfate resistance cement

The physical requirements of ten portland cement types are tabulated in Table I-3. Five different physical and mechanical properties can be seen and each property is determined by using a different test method. Strength tests are carried out according to the Test Method C109/C109M. Time of setting is determined by Gillmore Needles as described in the Test Method C266. Autoclave expansion is determined in accordance with the Test Method C151; on the other hand, air content of mortar is determined in compliance with the Test Method C185. Finally, fineness is determined by an air permeability test according to the Test Method C204 (ASTM Standard C150 2012).

In Table I-4, the chemical requirements can be seen. The testing methods are also noted in this table. For the purpose of delivery in packages, the cement should follow a certain set of rules. The label “Portland Cement”, the type of cement, the name and brand of the manufacturer and the mass of the cement in the package are required to be printed on each package. Also, the words “air-entraining” should be marked for the related cement type. (ASTM Standard C150 2012)

Table I-3: Standard Physical Requirements (Adapted from ASTM Standard C150/C150M [2012])

Cement Type	Compressive Strength[1]								Time of setting[2]	Autoclave Expansion	Air content of mortar [3]		Fineness (specific surface)	
	1D		3D		7D		28 days							
	MPa	psi	MPa	psi	MPa	psi	MPa	psi	minutes	%	volume,%		m^2/kg	
I	–		≥12.0	≥1740	≥19.0	≥2760	–		≥45 ≤375	≤0.80	–	≤12	≥260	–
IA	–		≥10.0	≥1450	≥16.0	≥2320	–				≥16	≤22	≥260	–
II	–		≥10.0	≥1450	≥17.0	≥2470	–				–	≤12	≥260	–
IIA	–		≥8.0	≥1160	≥14.0	≥2030	–				≥16	≤22	≥260	–
II(MH)	–		≥10.0[5]	≥1450[5]	≥17.0[5]	≥2470	–				–	≤12	≥260	≤430[4]
II(MH)A	–		≥8.0[5]	≥1160[5]	≥14.0[5]	≥2030	–				≥16	≤22	≥260	≤430[4]
III	≥12.0	≥1740	≥24.0	≥3480	–		–				–	≤12	–	
IIIA	≥10.0	≥1450	≥19.0	≥2760	–		–				≥16	≤22	–	
IV	–		–		≥7.0	≥1020	≥17.0	≥2470			–	≤12	≥260	≤430
V	–		≥8.0	≥1160	≥15.0	≥2180	≥21.0	≥3050			–	≤12	≥260	–

[1] The strength at any specified test age shall be not less than that attained at any previous specified age.

[2] The time of setting is that described as initial setting time in Vicat test in C191.

[3] Compliance with the requirements of this specification does not necessarily ensure that the desired air content will be obtained in concrete.

[4] Maximum fineness limits do not apply if the sum of C3S + 4.75C3A is less than or equal to 90.

[5] When the optional heat of hydration at 7 days is specified as ≤290 kJ/kg for these cement types.

Table I-4: Standard Composition Requirements (Adapted from ASTM Standard C150/C150M [2012])

Cement Type	I and IA	II and IIA	II(MH) and II(MH)A	III and IIIA	IV	V	Applicable Test Method
Aluminum oxide (Al_2O_3), %	–	≤6.0	≤6.0	–	–	–	C114
Ferric oxide (Fe_2O_3), %	–	≤6.0 (1)	≤6.0 (1), (2)	–	≤6.5	–	C114
Magnesium oxide (MgO), %	≤6.0	≤6.0	≤6.0	≤6.0	≤6.0	≤6.0	C114
Sulfur trioxide (SO_3), (3) , %							C114
When (C_3A), (4), is 8 % or less	≤3.0	≤3.0	≤3.0	≤3.5	≤2.3	≤2.3	
When (C_3A), (4), is more than 8 %	≤3.5	X (5)	X (5)	≤4.5	X (5)	X (5)	
Loss on ignition, %	≤3.0	≤3.0	≤3.0	≤3.0	≤2.5	≤3.0	C114
Insoluble residue, %	≤0.75	≤0.75	≤0.75	≤0.75	≤0.75	≤0.75	C114
Tricalcium silicate (C_3S),(4), %	–	–	–	–	≤35 (2)	–	Calculated according to Annex A1 of ASTM Standard C150/C150M -12
Dicalcium silicate (C_2S), (4), %	–	–	–	–	≥40 (2)	–	
Tricalcium aluminate (C_3A),(4), %	–	≤8	≤8	≤15	≤7 (2)	≤5 (1)	
Sum of $C_3S + 4.75C_3AG$, (6), %	–	–	≤100 (2), (7)	–	–	–	
Tetracalcium aluminoferrite plus twice the tricalcium aluminate ($C_4AF + 2(C_3A)$), or solid solution ($C_4AF + C_2F$), as applicable, %	–	–	–	–	–	≤25 (1)	

(1) The limit does not apply when the sulfate resistance limit in Table 4 of ASTM Standard C150/C150M -12 is specified

(2) The limit does not apply when the heat of hydration in Table 4 of ASTM Standard C150/C150M -12 is specified

(3) It is permitted to exceed the values in the table for SO_3 content as stated in Table 1 of ASTM Standard C150/C150M -12

(4) It is required to calculate according to the Annex A1 of ASTM Standard C150/C150M -12.

(5) These limits are not applicable.

(6) The limit is consistent with a Test Method C186 7-day heat of hydration limit of 335 kJ/kg (80 cal/g).

(7) Additionally, 7-day heat of hydration testing by Test Method C186 is required to be done at least once every six months. Such testing shall not be used for acceptance or rejection of the cement, but results shall be reported for informational purposes.

Appendix J Feature of Exporting to and Importing from a Spreadsheet File

J.1 Fundamental Logic

The computer software is now able to import input values from a spreadsheet file and to export data to a spreadsheet. The source code of the software is entirely rearranged to enable data transmission between the software and a Microsoft Excel (2010) spreadsheet file. The Excel file extensions, "*.xls" and "*.xlsx", are used. Figure J-1 explains the developed fundamental logic to enable the data transfer between a spreadsheet file and Visual Basic (VB) software. It also demonstrates the required objects and the relationship between them.

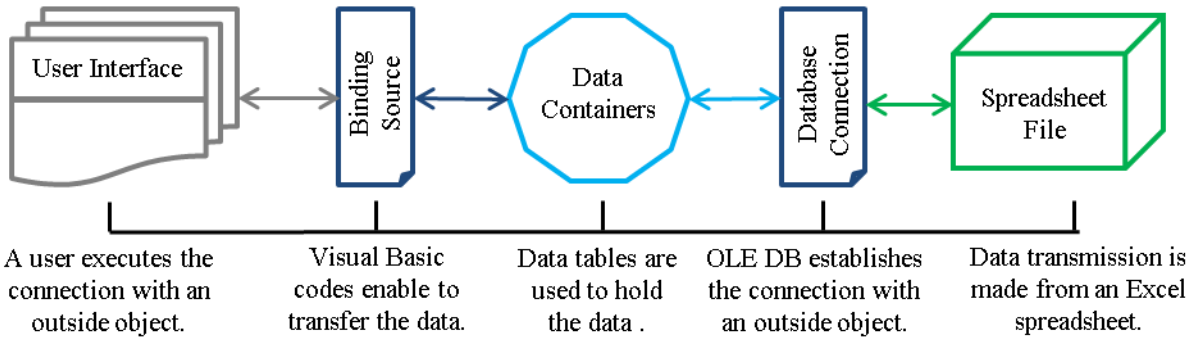

Figure J-1: Required Visual Basic Objects to Transmit Data

The user interface is the user-controlled area; i.e., windows forms. A user needs to proceed along several forms and enter each of the required variables such as concrete properties or time of prestressing events.

Clicking the specified button, then, initiates the communication, and each user-input data (or output data) begins to occupy a specific cell of a data table. Storing the data in data tables

makes the programming much easier and more efficient. This connection is provided by a lengthy block of the VB coding explained in the coming subsection.

Following the data transmission to a data table, the database connection is used to establish the interaction between the VB software and the Excel spreadsheet. It is important to note that both of these environments are alien to each other by default and they require special components to recognize each other.

For this specific case, components of Microsoft Object Linking and Embedding, Database (OLE DB), are utilized. OLE DB is an application programming interface (API) facilitating to access data which is stored in a variety of sources. Nonetheless, these sources have to be compatible with the OLE DB provider. Some types of the sources can be Microsoft Access databases or Microsoft Excel spreadsheets. Besides, the API supplies a group of Component Object Model (COM) -based interfaces. COM is used to implement objects created in different environments (Stephens 2012).

A successful attempt can provide the communication with the software and an Excel spreadsheet; as a result, a user will be able to load the data as a spreadsheet file and save them as a spreadsheet file.

J.2 Implementation of Fundamental Logic in Computer Software

Spreadsheet type is chosen to be compatible with Microsoft Excel (2010). Also, a Microsoft Access Database (2010) file is connected to the software as the database object. The logic for data transmission is mapped in Figure J-2.

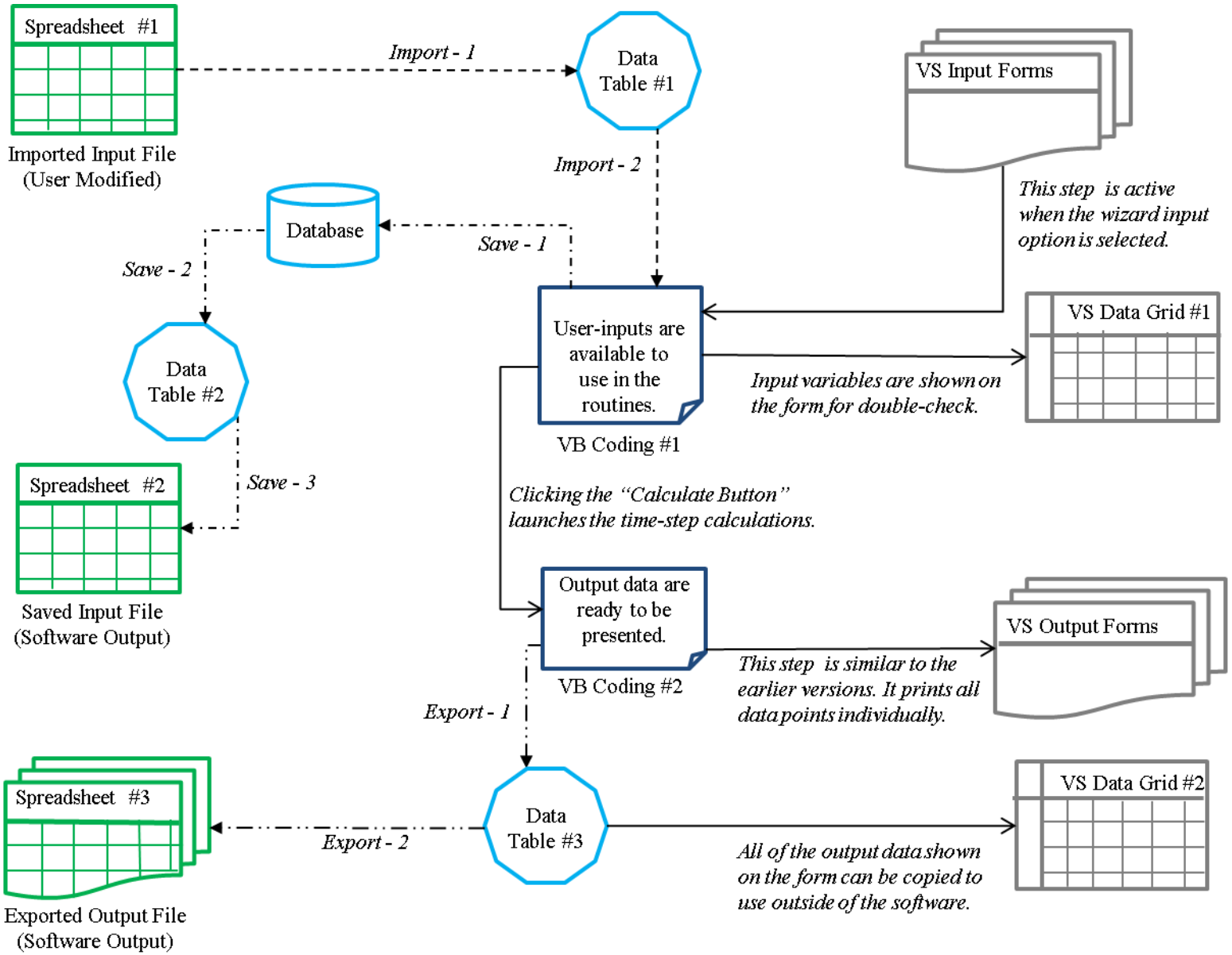

Figure J-2: Mapping of Data Transmission From/To a Spreadsheet File

The objects placed on the right hand side of the figure are the windows forms visible to users. Visual Studio (VS) Input and Output Forms were existed in the previous versions; whereas, VS Data Grid #1 and #2 are created in the new version in order to allow users to navigate data easily and copy them out. The time-step calculations are carried out between VB Coding #1 and #2 as explained in Section 3.2.1.

The Import 1 and 2 paths portray the process for importing the input data. The procedure to save the input data is depicted with the Save 1, 2 and 3 paths. Exporting output data is illustrated with the Export 1 and 2 paths. They are discussed further in the following subsections.

The component "System.Data.OleDb" is imported in the beginning of the code editor in order to provide the parameters for the connection between the VB software and the Microsoft products. The reference called "Microsoft.Office.Interop.Excel" is also added in the computer software to allow interoperability with the COM object (OLE DB).

The Excel files need to be organized in a certain way before imported. First, the column names such as "C01" and "C02" have to be printed in the first row. Second, each input variable has to occupy the predetermined cell. For instance, total cross-sectional area of the girder, Ag, has to be inputted in the cell located on the 5^{th} row and the column "C02". Third, the sheet name has to be "Sheet1". The style and format of the text are not important as long as the first three conditions are satisfied. However, merging the cells of the spreadsheet file may not be allowed. The computer software exports the data occupying the similar cells for importing purposes. As a result of that, a sample input Excel file can be obtained after the first input attempt with the wizard option.

J.3.1 Importing Input Variables from a Spreadsheet File (Import 1 and 2)

The path Import 1 represents how an Excel spreadsheet file is connected to a Data Table object. The partial coding block can be seen in Figure J-3. The connection is provided with an OleDbConnection object. The OleDbDataAdapter object is used to access the data and return them as commanded. Structured Query language (SQL) is used in the software as a programming language for the database management.

```
connection = New OleDbConnection("Provider=Microsoft.ACE.OLEDB.12.0;Data Source="
& Path & ";Extended Properties=Excel 12.0")

'The line above defines the type of source that will be used in the connection.
Path is the location of the user-selected Excel file.

connection.Open()

   command.Connection = connection
'command is defined as an OleDbConnection object.

   command.CommandType = CommandType.Text
'CommandType is defined in a certain way to make it understand the SQL query
below.

   command.CommandText = ("SELECT * from [Sheet1$]")
'It is a SQL query commanding to select all of data from the Sheet #1.

   dapter.SelectCommand = command
'dapter is a OleDbDataAdapter object and it will transfer data from a connection
to a DataTable.

   dapter.Fill(va)
'va is a DataTable object and it is filled by the dapter in accordance with the
defined SQL query.

connection.Close()
connection = Nothing
```

Figure J-3: The Path Import 1

The path Import 2 shows the established binding process. A variable is picked up from a cell of data table and saved as an internal variable. It is repeated for each variable. The illustration of the code block can be seen in Figure J-4.

```
NumberCS = CInt(datainput.Rows(32)(4))
'NumberCS is one of the input variables and datainput is the DataTable filled
with the data from the Excel spreadsheet. (note that it is referred as "va" in
the earlier block.) In this case, NumberCS is equated to the integer value placed
on the 32nd row and 4th column.

MaxTime = CInt(datainput.Rows(33)(4))

TimeIntervals = CInt(datainput.Rows(34)(4))

NumberLayerGroups = CInt(datainput.Rows(35)(4))

'These steps are repeated for all of the input variables.
```

Figure J-4: The Path Import 2

It is important to note that the variables are corresponded with a predetermined cell, and this necessitates providing input variables in an organized fashion. First, the column names such as "C01" and "C02" have to be printed in the first row. Second, each input variable has to occupy the predetermined cell. Third, the sheet name has to be "Sheet1". The style and format of the text are not important. A sample input Excel file can be obtained after the first input attempt with the wizard option. A template input spreadsheet can be seen in Figure J-5.

	A	B	C	D	E	F	G	H	I	J	K	L	M	N	O	P	Q
1	C01	C02	C03	C04	C05	C06	C07	C08	C09	C10	C11	C12	C13	C14	C15		
2	**FORM1-ProjectName**			**FORM13 Reinforcing Steel Layout**				**FORM6-12 Prestressing Steel Layout**									
3	L(VC)-BT72			Es(ksi)	29000			GT_array	nps_array	ST_array	Ap_array(in^2	fpj_array(ksi)	yp_mid_array(in)	DL_array(in)	yp_end_array(in)		
4	**FORM3**			NumberSteelLayers	0		1	0	6	0	0.167	202.5	2.5	0	2.5		
5	Ag(in^2)	767		nrs_array	Ar_array(in^2	yr_array(in)	2	1	4	0	0.167	202.5	2.5	120	2.5		
6	Ig(in^4)	545894	1	0	0	0	3	0	8	0	0.167	202.5	4.5	0	4.5		
7	yb(in)	36.6	2	0	0	0	4	1	2	0	0.167	202.5	4.5	120	4.5		
8	h(in)	72	3	0	0	0	5	0	6	0	0.167	202.5	6.5	0	6.5		
9	L(in)	1620	4	0	0	0	6	0	2	0	0.167	202.5	8.5	0	8.5		
10	**FORM4**		5	0	0	0	7	2	8	0	0.167	202.5	17.5	258	57.5		
11	fci_actual(psi)-CrSh:AASHT	7710		**FORM14a**			8	2	10	0	0.167	202.5	8.5	270	48.5		
12	*fc28_actual(psi)-CrSh:AAS*	10510		Model_CrSh	0		9	0	4	0	0.153	32.7	70	0	70		
13	wc(pcf)	153.3		(3,4)fcm_fib_CrSh	10510		10	0	0	0	0	0	0	0	0		
14	**FORM4b**			(3,4)h_fib_CrSh	6.02		11	0	0	0	0	0	0	0	0		
15	MOEModel	0		(3,4)CementType_fib_C	0		12	0	0	0	0	0	0	0	0		
16	StrengthType	0		(4)odDensity_fib_CrSh	153.3		13	0	0	0	0	0	0	0	0		
17	(0)Eci_supp(ksi)	6600		(4)StrengthLW_fib_CrS	10510		14	0	0	0	0	0	0	0	0		
18	(0)Ec28_supp(ksi)	6900		*(0,1,2,3,4)TransferTime*	19.83		15	0	0	0	0	0	0	0	0		
19	(1,2)K1_MOE_AA	1		*(0,1,2,3,4)RH(%)*	70		16	0	0	0	0	0	0	0	0		
20	*(1,2,3,4,5,6,7)fci_MOE(psi)*	7710		(2)Slump(in)	0.5		17	0	0	0	0	0	0	0	0		
21	*(1,2,3,4,5,6,7)fc28_MOE(psi*	10510		(2)CementContent(pcy)	833		18	0	0	0	0	0	0	0	0		
22	*(1,2,3,4,7)wc_MOE(pcf)*	153.3		(2)AirContent(%)	2.7		19	0	0	0	0	0	0	0	0		
23	(1)CementTypeACI	1		*(0,1,2)fc(ksi)*	3.01		20	0	0	0	0	0	0	0	0		
24	(1,3)CuringType	1		(2)FA(%)	38		21	0	0	0	0	0	0	0	0		
25	*(3,4)K1_MOE_NC*	1		**FORM15**			22	0	0	0	0	0	0	0	0		
26	*(3,4)K2_MOE_NC*	1		MaturityType	2		23	0	0	0	0	0	0	0	0		
27	*(3)CementTypeWchip*	1		(0,1,2)JackingTime(hrs)	47.42		24	0	0	0	0	0	0	0	0		
28	(5,7)CementTypefib	0		(0)CureTemp(Celcius)	0		25	0	0	0	0	0	0	0	0		
29	(5,6)AggregateTypefib	0		(1)EqvAge(days)	2.67		26	0	0	0	0	0	0	0	0		
30	**FORM5**			CureType	1		27	0	0	0	0	0	0	0	0		
31	Ep(ksi)	28600		(00)MoistPeriod**(days)**	0		28	0	0	0	0	0	0	0	0		
32	fpu(ksi)	270		(01)SteamPeriod**(days**	0.5		29	0	0	0	0	0	0	0	0		
33	fpy(ksi)	243		**FORM16_a2**			30	0	0	0	0	0	0	0	0		
34	**FORM16_a1**			NumberCS	40												
35	NumberStrainGages	4		MaxTime(days)	182												
36		y_strainloc(in)		TimeIntervals	40												
37	1	8.8		NumberLayerGroups	9												
38	2	24															
39	3	51															
40	4	70															
41	5	0															
42	6	0															
43																	

Figure J-5: Template Input Spreadsheet

J.3.2 Saving Input Variables as Spreadsheet File (Save 1, 2, and 3)

The VB software and the Access database file are linked with each other for the path Save 1. The database file is used as a template explaining each input variable. Figure J-6 demonstrates the part of the coding for the path Save 1 — transferring input data to the Access database table. All of the paths are demonstrated in Figure J-2.

```
UpdateDataBaseLogic(CObj(NumberCS), 34, "C05")

'UpdateDataBaseLogic is a subroutine enabling the connection with the Access
Database file. Once the connection is established, it changes the value of a
specified cell. In this case, the cell on the 34th row and the column “C05” is
changed with the value of “NumberCS”.

UpdateDataBaseLogic(CObj(MaxTime), 35, "C05")

UpdateDataBaseLogic(CObj(TimeIntervals), 36, "C05")

UpdateDataBaseLogic(CObj(NumberLayerGroups), 37, "C05")

'Some examples are shown here and it is repeated for all of the input variables.
“CObj” converts a variable type to an Object type.
```

Figure J-6: The Path Save 1

The subroutine, “UpdateDataBaseLogic”, is used to insert an internal variable into a cell of the Access database table. The programming for this subroutine can be found in Figure J-7.

```
Public Sub UpdateDataBaseLogic(ByRef variablename As Object, ByRef IDnumber As
Integer, ByRef IDcol As String)

'UpdateDataBaseLogic is a subroutine and it needs an object, an integer value and a
string value to proceed the subroutine.

Try
'Try catches any exceptions so that the application stops execution.
   If Microsoft.VisualBasic.Right(Application.StartupPath, 1) = "\" Then
'Checking if the path has a backslash in the end of the string
   StringCon = "Provider=Microsoft.ACE.OLEDB.12.0;Data Source=" &
Application.StartupPath & "dbexport.accdb;Persist Security Info=False;"
   Else
   StringCon = "Provider=Microsoft.ACE.OLEDB.12.0;Data Source=" &
Application.StartupPath & "\dbexport.accdb;Persist Security Info=False;"
   End If
'The lines above define the type of source that will be used in the connection.
Data source is chosen to be the connected inner database file. In this case, it is
a Microsoft Access Database file and named as “dbexport.accdb”.

connection.Open()

   command.Connection = connection
'command is defined as an OleDbConnection object.

   command.CommandType = CommandType.Text
'CommandType is defined in a way to make it understand the SQL query below.

   command.CommandText = "UPDATE InputVariables SET " & IDcol & "= @C WHERE ID =
@ID"

'It is a SQL query commanding to update the cell on the column “IDcol” and the row
“ID”.  The table “InputVariables” can be considered as one of the worksheet file of
the Access Database. This table will include all of the input variables.

   command.Parameters.AddWithValue("@C", variablename)

   command.Parameters.AddWithValue("@ID", IDnumber)

'The lines above make the value of “variablename” become equal to the cell
specified with the row “IDnumber” and the column “IDcol”.
   command.ExecuteNonQuery()
Catch
   MsgBox(ErrorToString)
'Message box is shown when an exception is encountered.
Finally
   connection.Close()
   connection = Nothing
End Try
End Sub
```

Figure J-7: Subroutine for Communicating with Access Database

The path Save 2 shows how the data is transferred from an Access database file to a data table object. The block of the developed coding can be found in Figure J-8. It employs similar OLE DB objects instructed in the path Import 1.

```
If Microsoft.VisualBasic.Right(Application.StartupPath, 1) = "\" Then

'Checking whether the path has a backslash in the end of the string or not.
   StringCon = "Provider=Microsoft.ACE.OLEDB.12.0;Data Source=" &
Application.StartupPath & "dbexport.accdb;Persist Security Info=False;"
Else
   StringCon = "Provider=Microsoft.ACE.OLEDB.12.0;Data Source=" &
Application.StartupPath & "\dbexport.accdb;Persist Security Info=False;"
End If
 'The lines above define the type of source that will be used in the connection.
Data source is chosen to be the connected inner database file. In this case, it is
a Microsoft Access Database file and named as “dbexport.accdb”.
connection.Open()

   command.Connection = connection
'command is defined as an OleDbConnection object.

   command.CommandType = CommandType.Text
'CommandType is defined in a way to make it understand the SQL query below.

   command.CommandText = ("SELECT * from InputVariables")
'It is a SQL query commanding to select all of the data from the table
“InputVariables”. It can be considered to be one of the worksheet file of the
Access Database. This table includes all of the input variables.
   dapter.SelectCommand = command
'dapter is a OleDbDataAdapter object and it will transfer data from a connection
to a DataTable.
   dapter.Fill(datainput)
'datainput is a Data Table object and it is filled by the dapter in accordance
with the defined SQL query.
connection.Close()
```

Figure J-8: The Path Save 2

Exporting the input data from the data table to an Excel spreadsheet file is illustrated with the path Save 3. First, an Excel spreadsheet file is created including a book and a sheet. Second, the values stored in Data Table are transmitted to the worksheet one at a time. The developed coding can be seen in Figure J-9.

```
oApp = New Microsoft.Office.Interop.Excel.Application
oBook = oApp.Workbooks.Add(oValue)
oSheet = oBook.Worksheets("Sheet1")

'The lines above create a new Excel file consisting of a new book and a new sheet.

For Each row As DataRow In datainput.Rows
   oCol = 1
      For Each col As DataColumn In datainput.Columns
         If col.ColumnName <> "ID" Then

            oSheet.Cells(oRow, oCol - 1) = row(oCol - 1)
'The values stored in each cell of “datainput” are transferred to the Excel
worksheet by using the two ‘for’ loops since “datainput” holds rows and columns.
         End If
      oCol += 1'increment
      Next
   oRow += 1'increment
Next
.........
'The dots above represent the hidden coding lines figure since it uses the similar
idea of the earlier ‘for’ loops. It transfers the column names of “datainput” into
the spreadsheet file.

oSheet.SaveAs(PathSave)
oBook.Close()
oApp.Quit()

'The lines above save the worksheet file and quit the Excel file.

releaseobject(oApp)
releaseobject(oBook)
releaseobject(oSheet)

'The lines above release all of the Excel objects by using the code:
System.Runtime.InteropServices.Marshal.ReleaseComObject(obj)
```

Figure J-9: The Path Save 3

J.3.3 Exporting Results as a Spreadsheet File (Export 1 and 2)

The path Export 1 demonstrates the data transmission from the output data to a data table. Part of the coding can be seen in Figure J-10. First, the columns are defined in the data table. Second, the rows are inserted in an order. Understanding this path can be very useful to modify the exported spreadsheet file in the future. New arrays and variables can be added by using the reserved names given in Figure 3.4.2 and 3.4.3.

```
table2.Columns.Add("Variable Name", GetType(String))

table2.Columns.Add("Value", GetType(Object))

table2.Columns.Add("Explanations", GetType(String))

'Three columns are defined with the data types in the Table2.

table2.Rows.Add("", 1, "") 'A row is added for formatting purposes

table2.Rows.Add("Initial Camber(in)", Initial_Camber_Calculation, "At Midspan”

table2.Rows.Add("", 2, "")

table2.Rows.Add("MOE Model=", MOEModel.ToString, "")

table2.Rows.Add("Creep and Shrinkage Model=", Model_CrSh.ToString, "")

table2.Rows.Add("", 3, "")

table2.Rows.Add("Ec_initial(ksi)", Ec_initial, "")

table2.Rows.Add("Ec28(ksi)", Ec28, "")

table2.Rows.Add("Ec_max(ksi)", Econ_array(TimeIntervals), "t=tmax," &
MaxTime.ToString)

table2.Rows.Add("", 4, "")
```

Figure J-10: The Path Export 1

The path Export 2 represents the connection from a data table to an Excel spreadsheet. It is similar to the Save 3 path and shown in Figure J-11. The screenshot of the exported Excel file can be seen in Figures J-12 and J-13.

```
oApp = New Microsoft.Office.Interop.Excel.Application
oApp.SheetsInNewWorkbook = 2 'Number of sheets created
oBook = oApp.Workbooks.Add(oValue)
oApp.DisplayAlerts = True ' alerts are on

'The lines above create a new Excel file consisting of a new book and a new
sheet.

'TABLE1
oSheet1 = oBook.Worksheets(1) 'creating an excel sheet

Dim oRow As Integer = 2
Dim oCol As Integer = 1

For Each col As DataColumn In table1.Columns
'creating a column for excel to loop through datatable

   oSheet1.Cells(1, oCol) = col.ColumnName
'assigning value to each cell , specify row and column

   oCol += 1 'increment
Next

For Each row As DataRow In table1.Rows
   oCol = 1
      For Each col As DataColumn In table1.Columns
      oSheet1.Cells(oRow, oCol) = row(oCol - 1)
'Assigning the value of each field to selected sheet cell.
      oCol += 1'increment
      Next
   oRow += 1'increment
Next

'TABLE2
oSheet2 = oBook.Worksheets(2) 'creating an excel sheet
oRow = 2
oCol = 1

For Each col As DataColumn In table2.Columns
'creating a column for excel to loop through datatable
```

➔Cont'd

```
 ➔Cont'd
  oSheet2.Cells(1, oCol) = col.ColumnName
'assigning value to each cell , specify row and column

   oCol += 1 'increment
Next

For Each row As DataRow In table2.Rows
   oCol = 1
      For Each col As DataColumn In table2.Columns

oSheet2.Cells(oRow, oCol) = row(oCol - 1)
'Assigning the value of each field to selected sheet cell.
      oCol += 1'increment
      Next
   oRow += 1'increment
Next

oApp.DisplayAlerts = False

'msgbox will not appear to ask user whether to create a new sheet or not

PathSave = SaveDialog.FileName
oSheet1.SaveAs(PathSave)
oSheet2.SaveAs(PathSave)oBook.Close()
oApp.Quit()

'The lines above save the worksheet file and quit the Excel file.

releaseobject(oApp)
releaseobject(oBook)
releaseobject(oSheet1)
releaseobject(oSheet2)

'The lines above release all of the Excel objects by using the code:
System.Runtime.InteropServices.Marshal.ReleaseComObject(obj)
```

Figure J-11: The Path Export 2

	A	B	C	D	E	F	G	H	I	J	K	L	M	N
1	Time After Transfer (days)	Age of Concrete (days)	Strength of Concrete(psi)	Modulus of Elasticity(ksi)	Total Camber at Midspan(in)	Total Curvature (1/in)*10^-6	Total Strain (*10^-6) at StrainGage Loc1 =6in	Total Strain (*10^-6) at StrainGage Loc2 =19.5in	Total Strain (*10^-6) at StrainGage Loc3 =37.5in	Total Strain (*10^-6) at StrainGage Loc4 =52in	Incremental Creep Coefficient	Incremental Unrestrained Shrinkage Strain(*10^-6)	Equivalent Effective Prestress at Midspan(ksi)	
2	0	0.966667	0	6300	1.339589	-7.499682397	-417.2667104	-316.0210035	-181.026728	-72.281342	0	-0.443217516	185.7916107	
3	0.58149	1.548159	0	6375.978027	1.361720681	-7.61984802	-431.3537502	-328.4857958	-191.328552	-80.8407567	0.02258252	-6.717065389	185.3443909	
4	0.86355	1.830217	0	6399.129395	1.372089744	-7.676135283	-437.9645688	-334.3367134	-196.166307	-84.8623458	0.01060536	-3.156266075	185.1355743	
5	1.13539	2.102057	0	6416.930176	1.381874442	-7.729244317	-444.2061181	-339.8612898	-200.734925	-88.6608832	0.01001468	-2.981501439	184.9389496	
6	1.41441	2.381073	0	6431.96875	1.391709328	-7.78262347	-450.4837852	-345.418317	-205.331133	-92.4830892	0.01007453	-3.000328434	184.741684	
7	1.7083	2.674967	0	6445.219727	1.40184772	-7.837642443	-456.9593584	-351.1511313	-210.073602	-96.4277788	0.01039458	-3.096707132	184.5386658	
8	2.0222	2.988862	0	6457.177734	1.412432313	-7.895077033	-463.7251841	-357.1416019	-215.030246	-100.551631	0.01086355	-3.237572628	184.3270264	
9	2.36037	3.327038	0	6468.13623	1.423562169	-7.955464753	-470.8460765	-363.4472669	-220.248912	-104.894672	0.01143742	-3.409868214	184.1047363	
10	2.72691	3.693581	0	6478.286621	1.43531692	-8.019232155	-478.3738987	-370.1142268	-225.768075	-109.489207	0.01209563	-3.607528015	183.8702545	
11	3.12604	4.092703	0	6487.763672	1.447764158	-8.086744856	-486.353907	-377.1828196	-231.621423	-114.363625	0.01282776	-3.827483397	183.6222229	
12	3.56227	4.528938	0	6496.665527	1.460965514	-8.158334822	-494.8276328	-384.6900945	-237.840068	-119.544216	0.01362812	-4.068089311	183.3593597	
13	4.04063	5.0073	0	6505.068359	1.474978328	-8.234311281	-503.8344534	-392.6712088	-244.453608	-125.056104	0.01449342	-4.328432169	183.0805054	
14	4.56676	5.53343	0	6513.030273	1.489857793	-8.31496618	-513.4121748	-401.1600686	-251.490681	-130.923683	0.01542158	-4.607932169	182.7845764	
15	5.14708	6.113744	0	6520.600586	1.505655527	-8.400576917	-523.5974095	-410.189532	-258.979155	-137.170806	0.01641094	-4.906170489	182.4704895	
16	5.78894	6.755607	0	6527.817871	1.522420287	-8.491404515	-534.4254314	-419.7913513	-266.946096	-143.82074	0.01745972	-5.222678283	182.1371765	
17	6.50087	7.467533	0	6534.71582	1.540198326	-8.5876909	-545.9298845	-429.9959692	-275.417551	-150.896027	0.01856579	-5.556889846	181.7836456	
18	7.29276	8.259424	0	6541.321289	1.559031248	-8.68965526	-558.1423757	-440.8319655	-284.418202	-158.418188	0.01972615	-5.90799209	181.4090271	
19	8.1762	9.142868	0	6547.658203	1.578955054	-8.797485862	-571.0916594	-452.3255338	-293.970836	-166.407277	0.02093671	-6.274835414	181.0124359	
20	9.16483	10.1315	0	6553.748535	1.599999309	-8.91133368	-584.8028231	-464.4997243	-304.095767	-174.881396	0.02219206	-6.655897778	180.5931549	
21	10.2748	11.24145	0	6559.609863	1.622184277	-9.031305126	-599.2961233	-477.3734254	-314.809993	-183.856027	0.02348504	-7.049091892	180.1505737	
22	11.5253	12.49193	0	6565.258301	1.645522952	-9.157449313	-614.5859952	-490.960374	-326.126319	-193.343265	0.02480645	-7.451760212	179.6842804	
23	12.9393	13.90595	0	6570.70752	1.670012236	-9.289748959	-630.6794821	-505.2678171	-338.05237	-203.350966	0.02614493	-7.860566257	179.1940613	
24	14.5446	15.51125	0	6575.97168	1.695637345	-9.428105841	-647.574605	-520.2951143	-350.589224	-213.881649	0.0274863	-8.271315892	178.6799469	
25	16.3748	17.34149	0	6581.061523	1.722365737	-9.572332601	-665.2589072	-536.0323703	-363.730389	-224.931515	0.02881387	-8.679049643	178.1423035	
26	18.4712	19.43786	0	6585.986816	1.750144958	-9.722138202	-683.7076508	-552.4587468	-377.460237	-236.489199	0.03010786	-9.077792129	177.5817719	
27	20.8845	21.85114	0	6590.758301	1.778903127	-9.877113371	-702.8818945	-569.5408327	-391.75275	-248.534576	0.03134527	-9.460678484	176.999527	
28	23.6778	24.64447	0	6595.383789	1.808542728	-10.03672423	-722.7269816	-587.2311885	-406.570092	-261.037552	0.03250036	-9.81987705	176.3970184	

Sheet1 Sheet2

Figure J-12: Screenshot of Exported Output File—Sheet 1

	A	B	C	D	E
1	Variable Name	Value	Explanations		
2		1			
3	Initial Camber(in)	1.361307	At Midspan (considering prestressing steel relaxation loss and elastic shortening of concrete)		
4		2			
5	MOE Model=	Stiffness.Based.Model			
6	Creep and Shrinkage Model=	AASHTO05			
7		3			
8	Ec_initial(ksi)	6300			
9	Ec28(ksi)	6600			
10	Ec_max(ksi)	6645.108	t=tmax,217		
11		4			
12	Aps_midspan(in^2)	5.508	Total area of fully stressed (fpj>100ksi) prestressing strands at midspan		
13	ep_midspan_ini(in)	21.89746	Equivalent initial eccentricity of fully stressed (fpj>100ksi) prestressing strands at midspan		
14	fpe_midspan_ini(ksi)	202.5	Equivalent initial effective prestress of fully stressed (fpj>100ksi) prestressing strands at midspan		
15		5			
16	Aps_support(in^2)	4.896	Total area of fully stressed (fpj>100ksi) prestressing strands at supports		
17	ep_support_ini(in)	13.9687	Equivalent initial eccentricity of fully stressed (fpj>100ksi) prestressing strands at supports		
18	fpe_support_ini(ksi)	202.5	Equivalent initial effective prestress of fully stressed (fpj>100ksi) prestressing strands at supports		
19		6			
20	Tot.Cr.Coef.	0.93049	Total Creep Coefficient		
21	Tot.Unr.Shr.Str.(*10^-6)	-281.482	Total Unrestrained Shrinkage Strain At Midspan(*10^-6)		
22	Shr. Str. At Benchmark Reading(*10^-6)	-5.16245	Shrinkage strain at the benchmark (zero) reading which is 0.9 (hrs) before the prestress transfer(*10^-6)		
23		7			
24	ytr_initial(in)	27.06413	Distance to Centroid from Bottom Fiber(At Midspan,Transformed Prop.,Initial)(ytr)(in)		
25	Atr_initial(in^2)	680.6628	Area of Transformed Section(At Midspan,Transformed Prop.,Initial)(Atr)(in^2)		
26	Itr_initial(in^4)	279065.9	Moment of Inertia of Transformed Section(At Midspan,Transformed Prop.,Initial)(Itr)(in^4)		
27		8			
28	ytr(in)	27.1007	Distance to Centroid from Bottom Fiber(At Midspan,Transformed Prop., Final)(ytr)(in)		
29	Atr(in^2)	679.22	Area of Transformed Section(At Midspan,Transformed Prop.,Final)(Atr)(in^2)		
30	Itr(in^4)	278347.1	Moment of Inertia of Transformed Section(At Midspan,Transformed Prop.,Final)(Itr)(in^4)		
31					
32					

Sheet1 Sheet2

Figure J-13: Screenshot of Exported Output File—Sheet 2

Appendix K Camber Prediction Software—User-Guided Input Forms

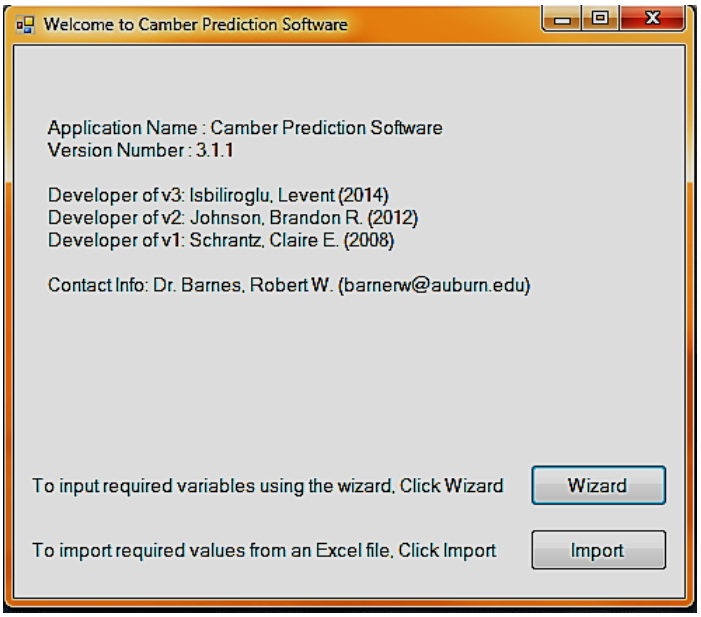

Figure K-1: Form 0—Welcome

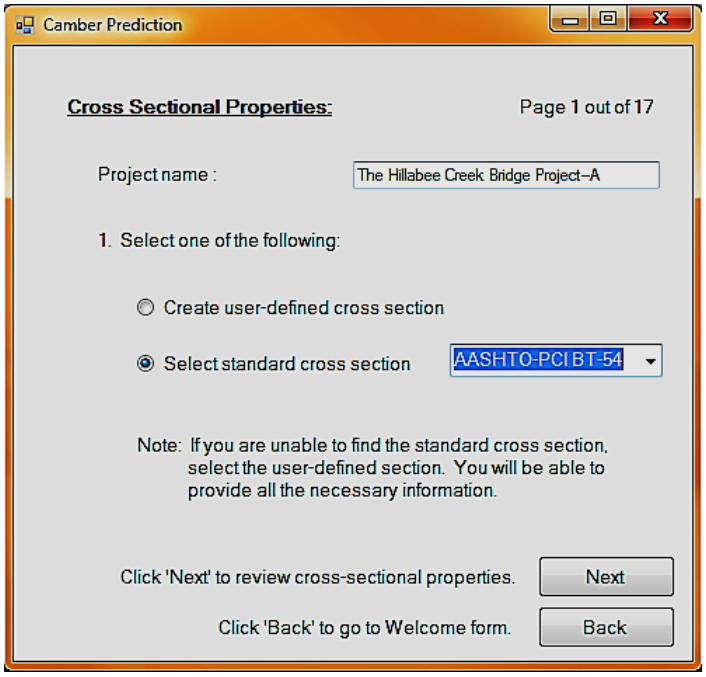

Figure K-2: Form 1—Project Name

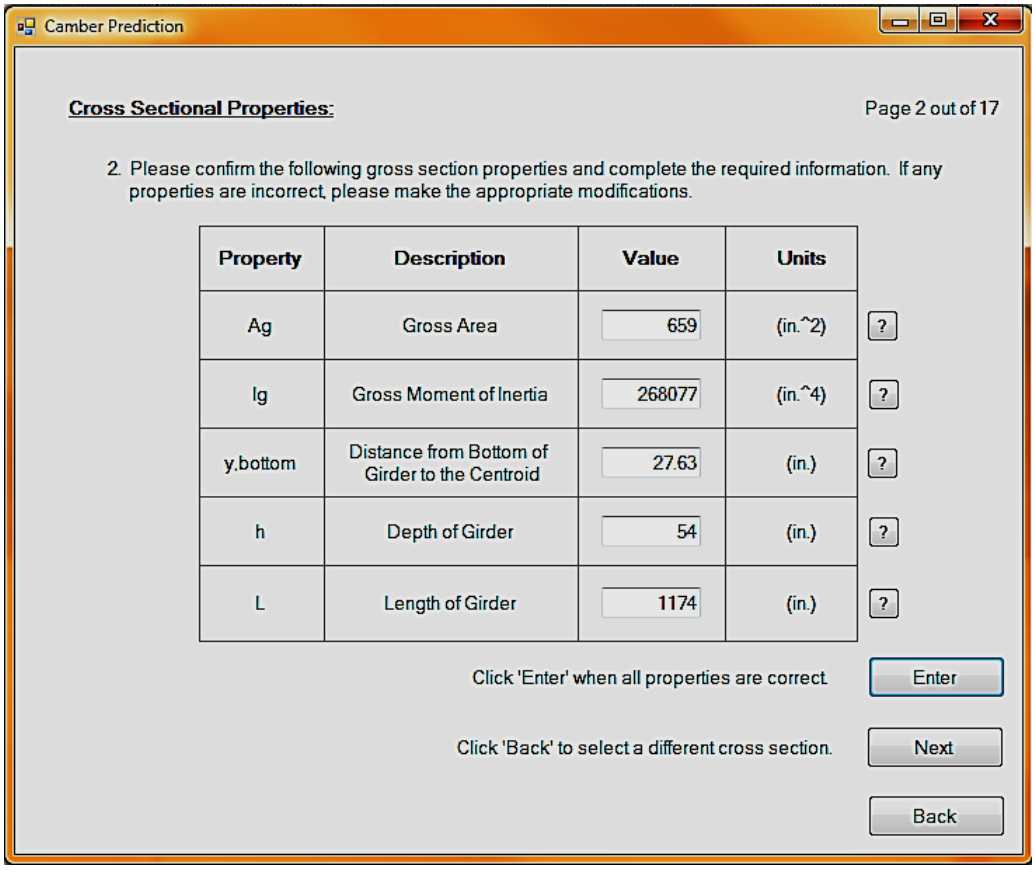

Figure K-3: Form 2—Cross-sectional Properties

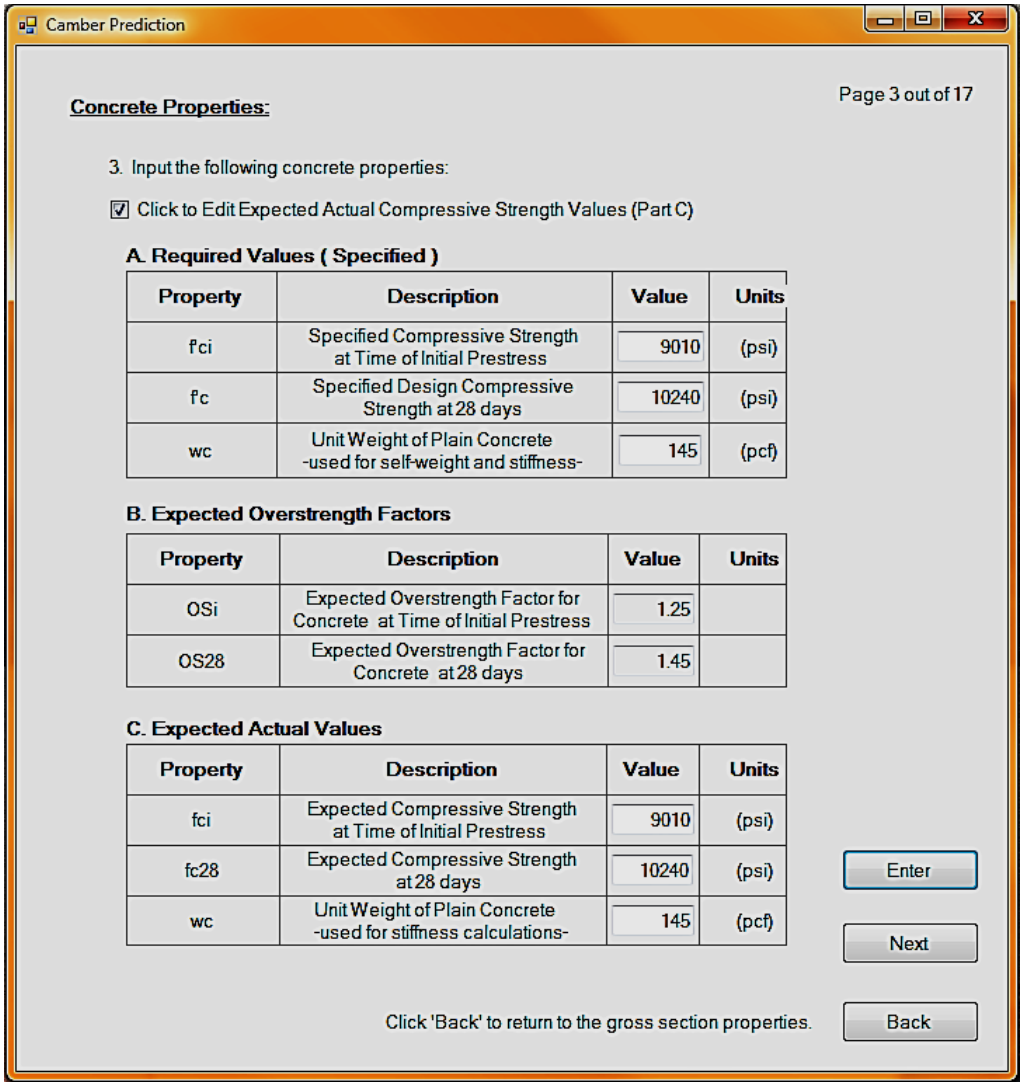

Figure K-4: Form 3—Hardened Concrete Properties

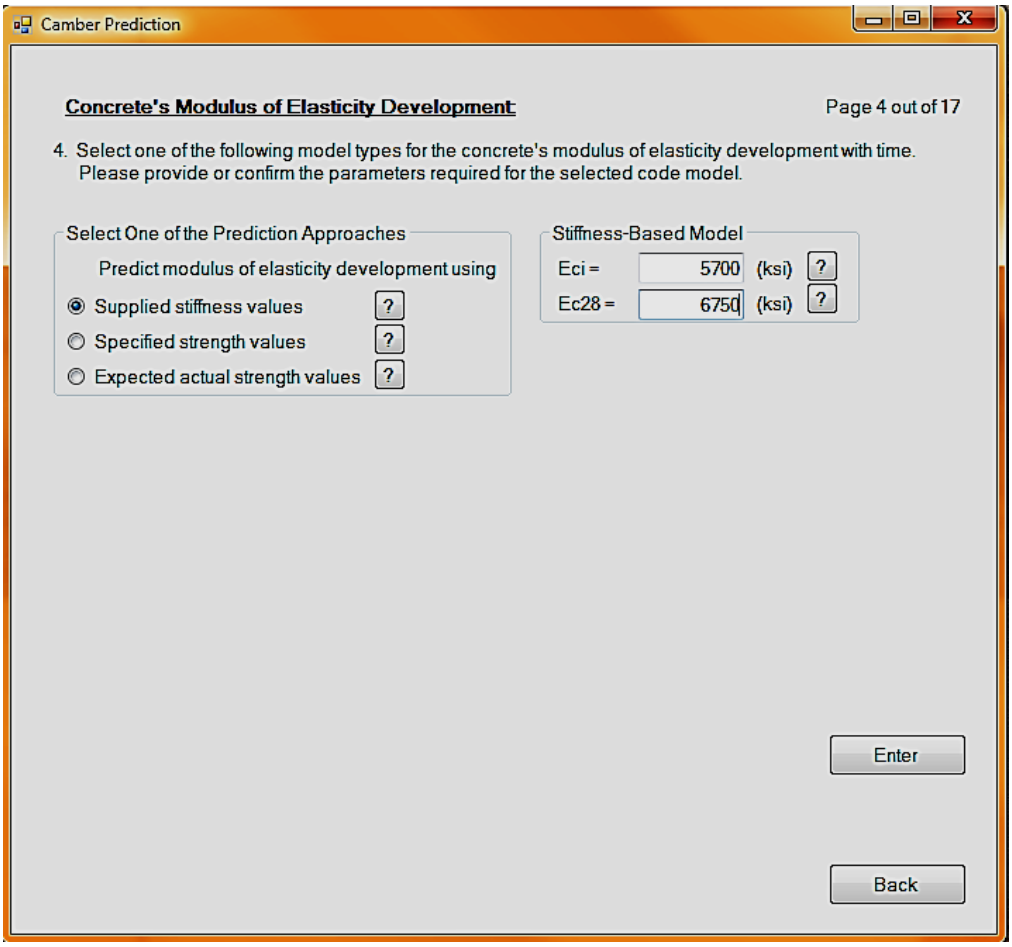

Figure K-5: Form 4—Two-Point MOE Model

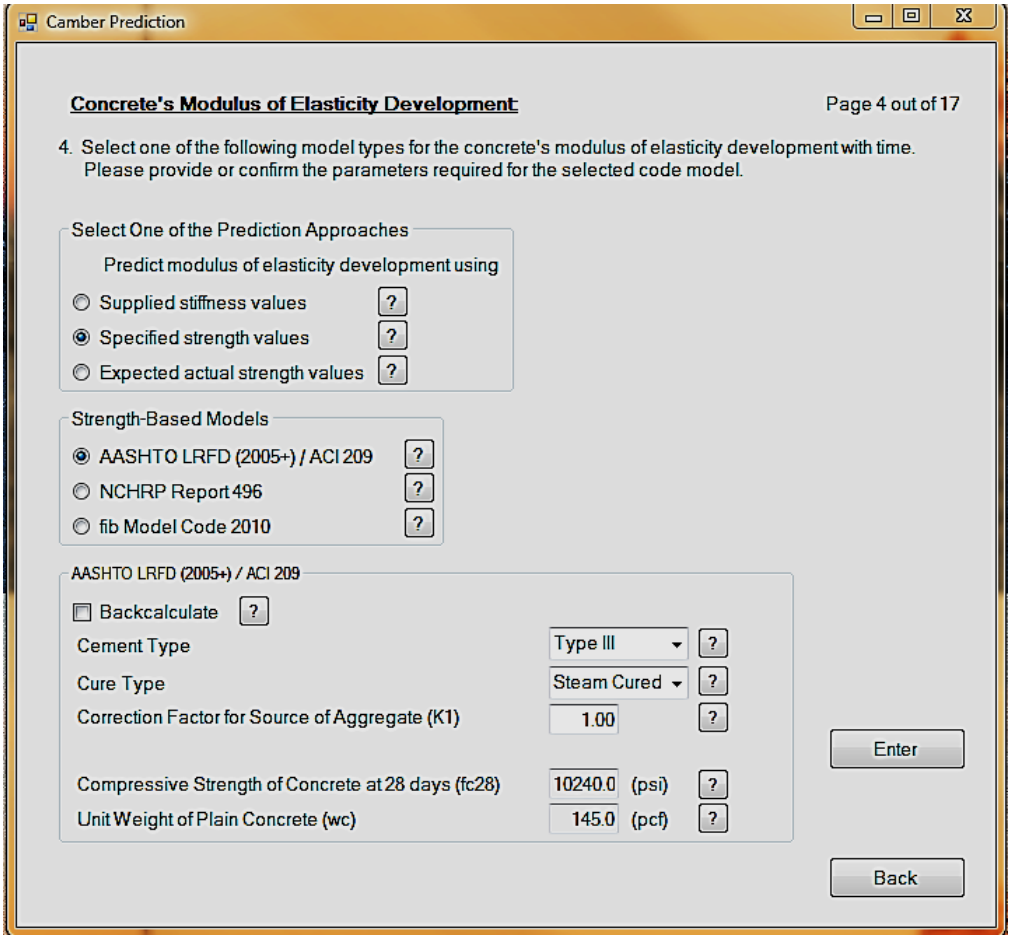

Figure K-6: Form 4—ACI 209 MOE Model

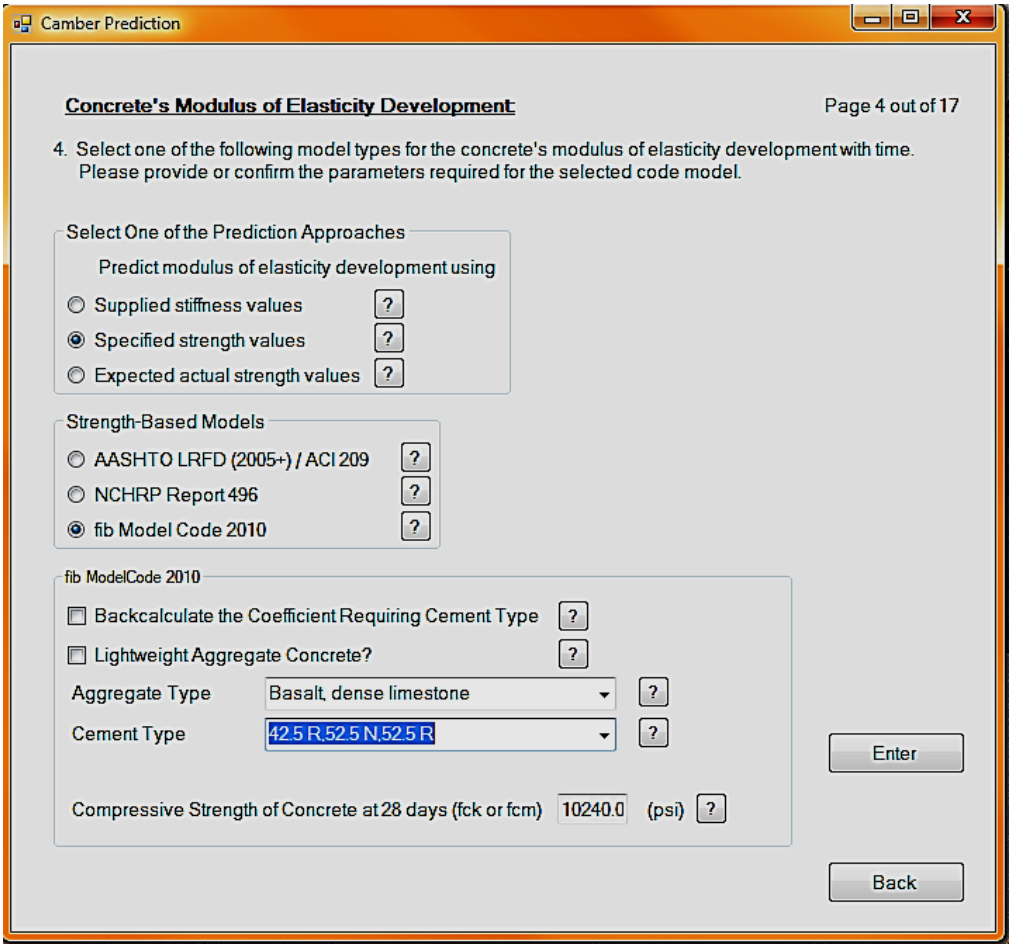

Figure K-7: Form 4—MC 2010 MOE Model

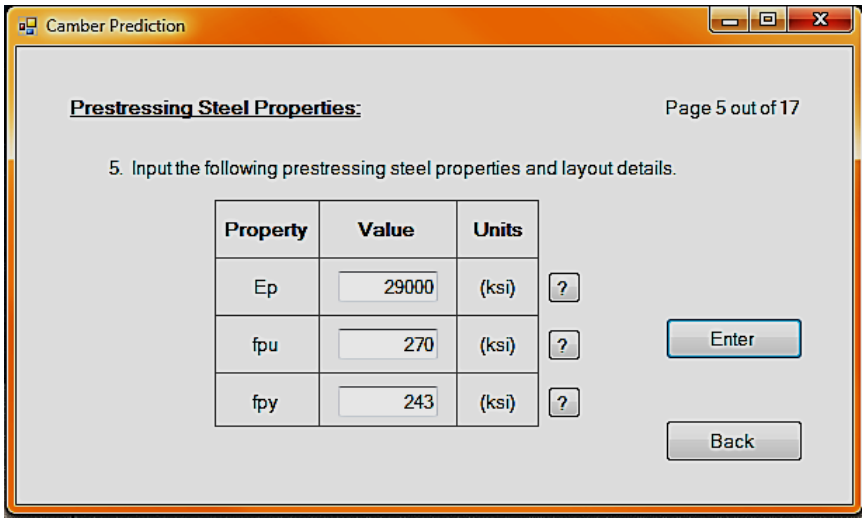

Figure K-8: Form 5—Prestressing Steel Properties

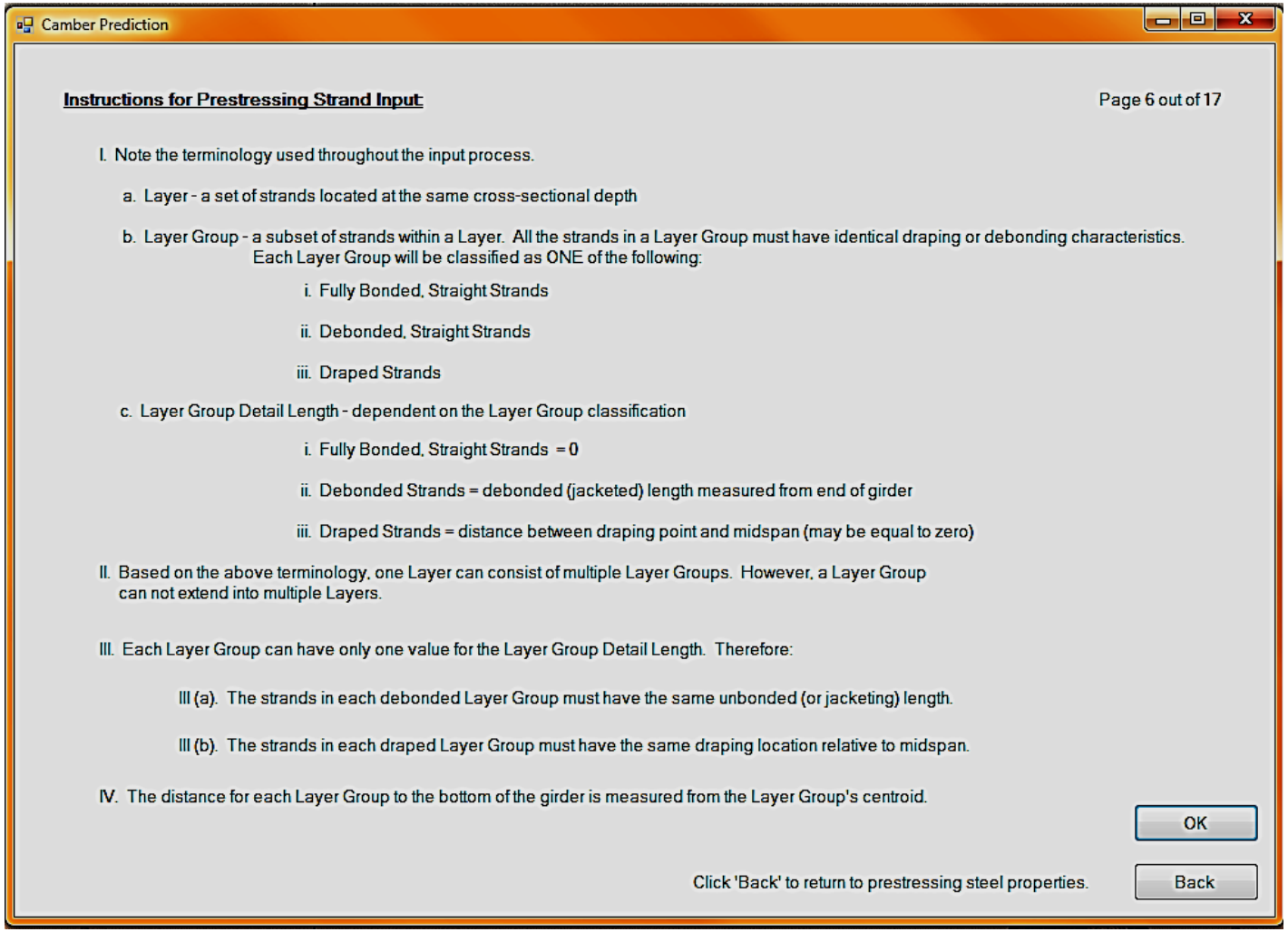

Figure K-9: Form 6—Instructions for Prestressing Steel Layout

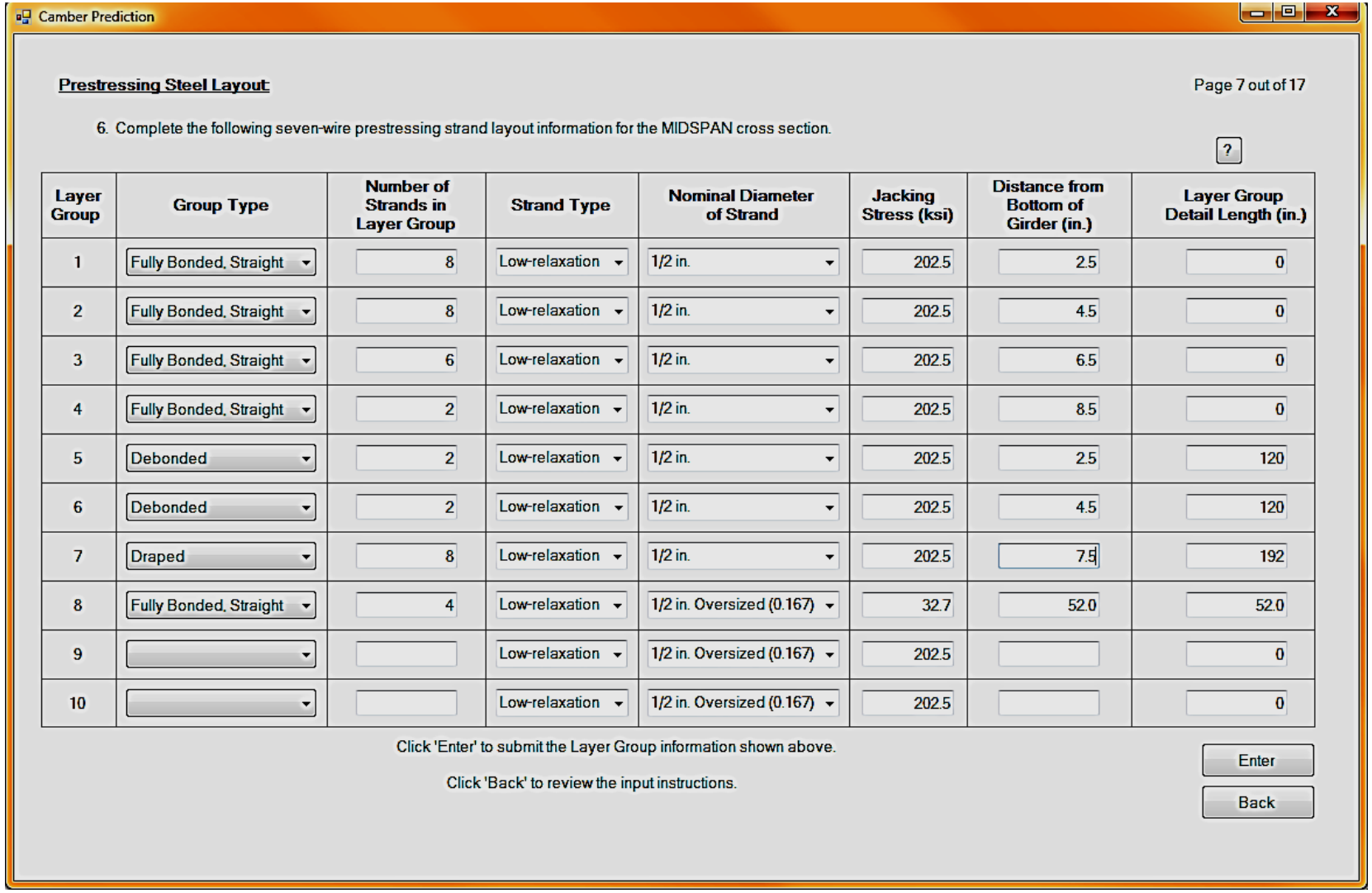

Figure K-10: Forms 7, 8, and 9—Prestressing Steel Layout

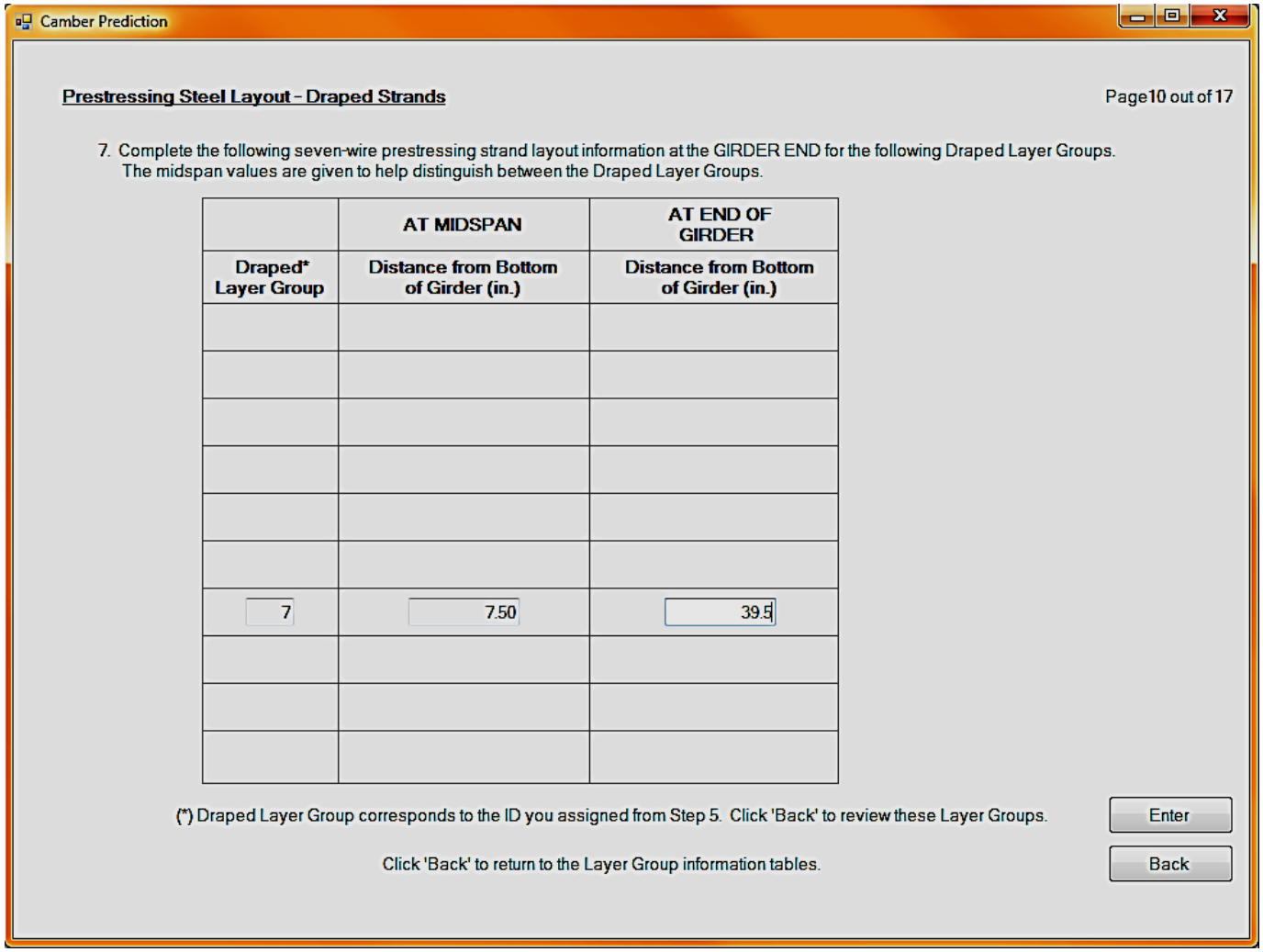

Figure K-11: Forms 10, 11, and 12—Draped Strands

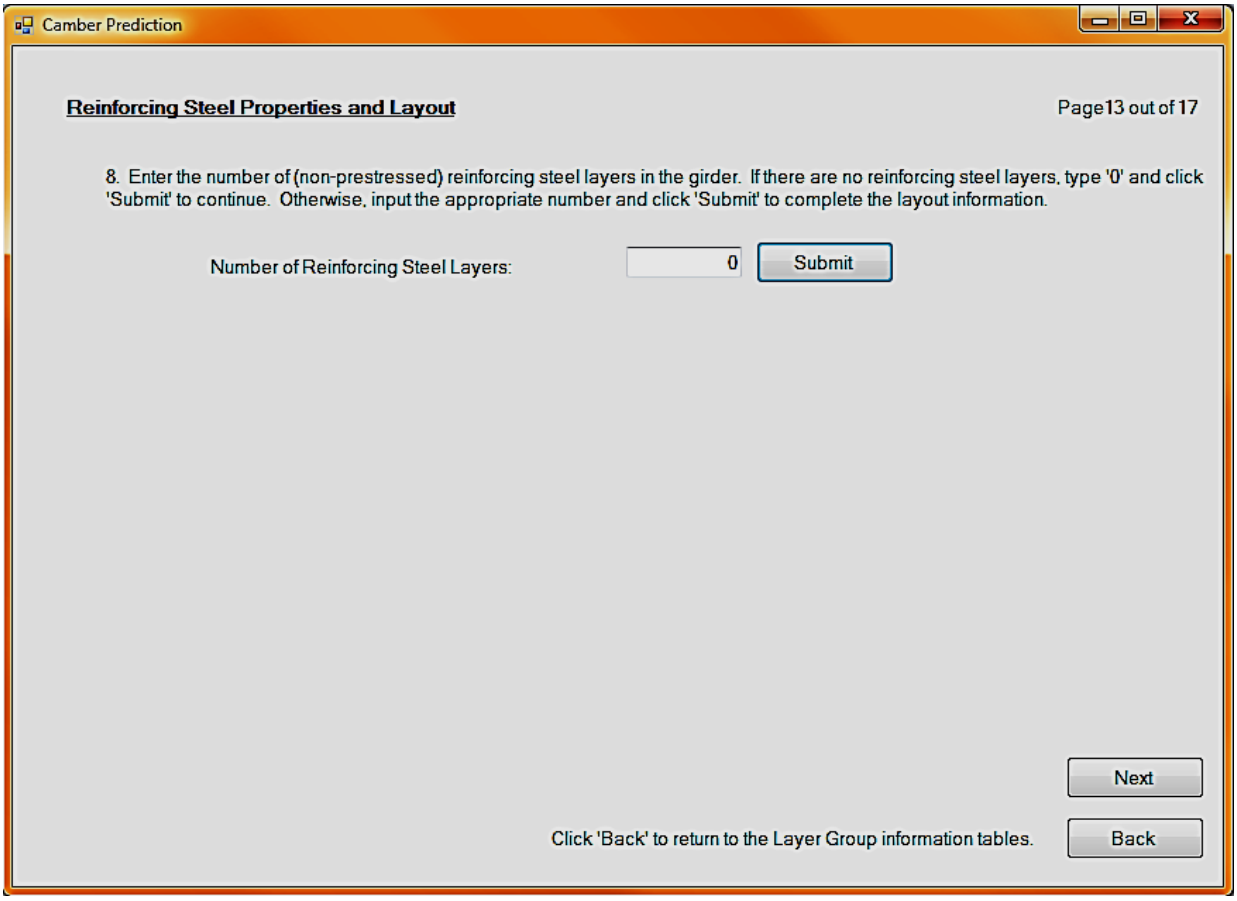

Figure K-12: Form 13—Reinforcing Steel Layout and Properties

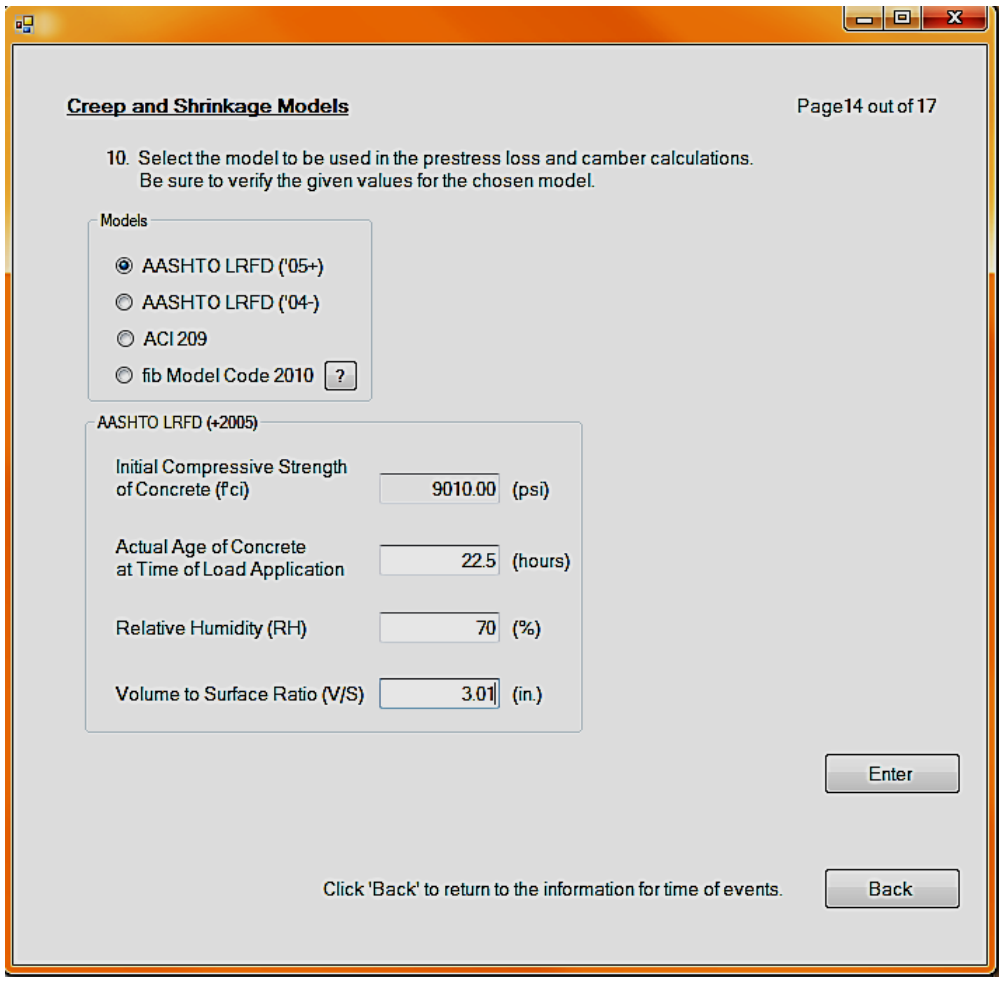

Figure K-13: Form 14—AASHTO LRFD Creep and Shrinkage Model

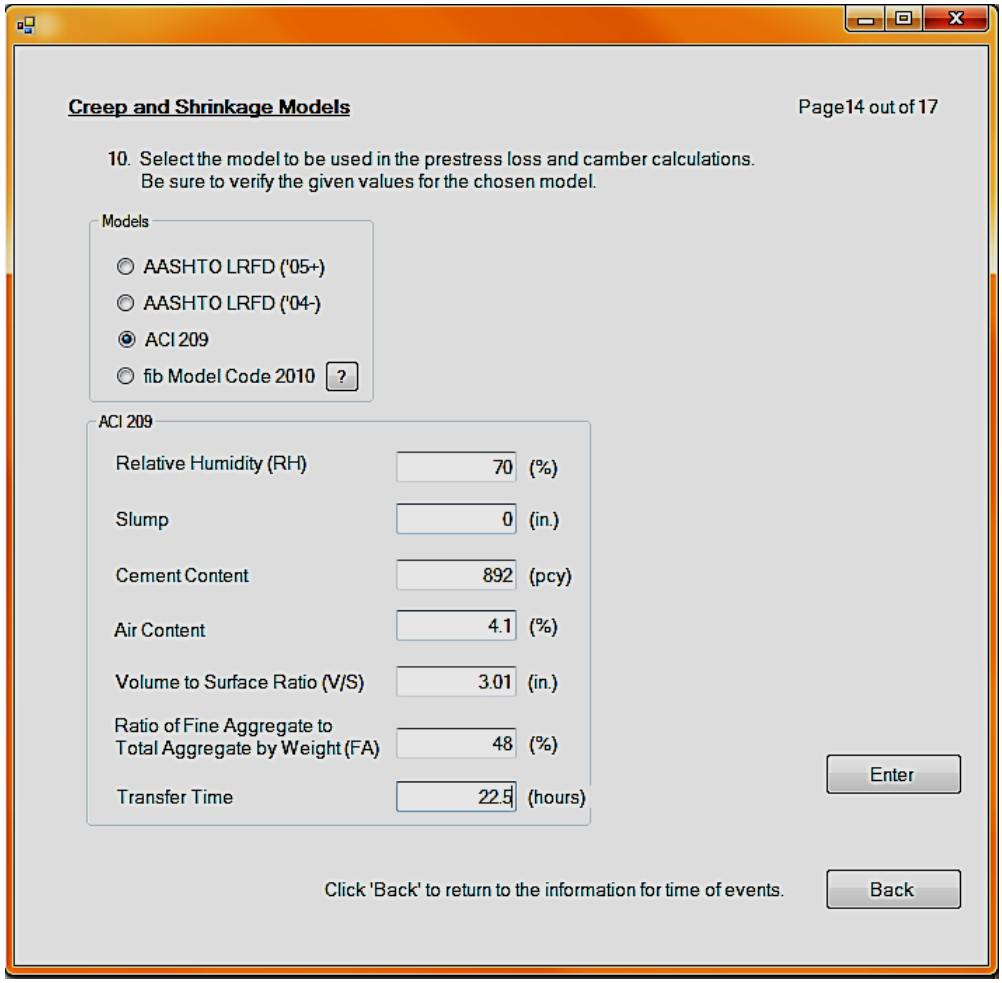

Figure K-14: Form 14—ACI 209 Creep and Shrinkage Model

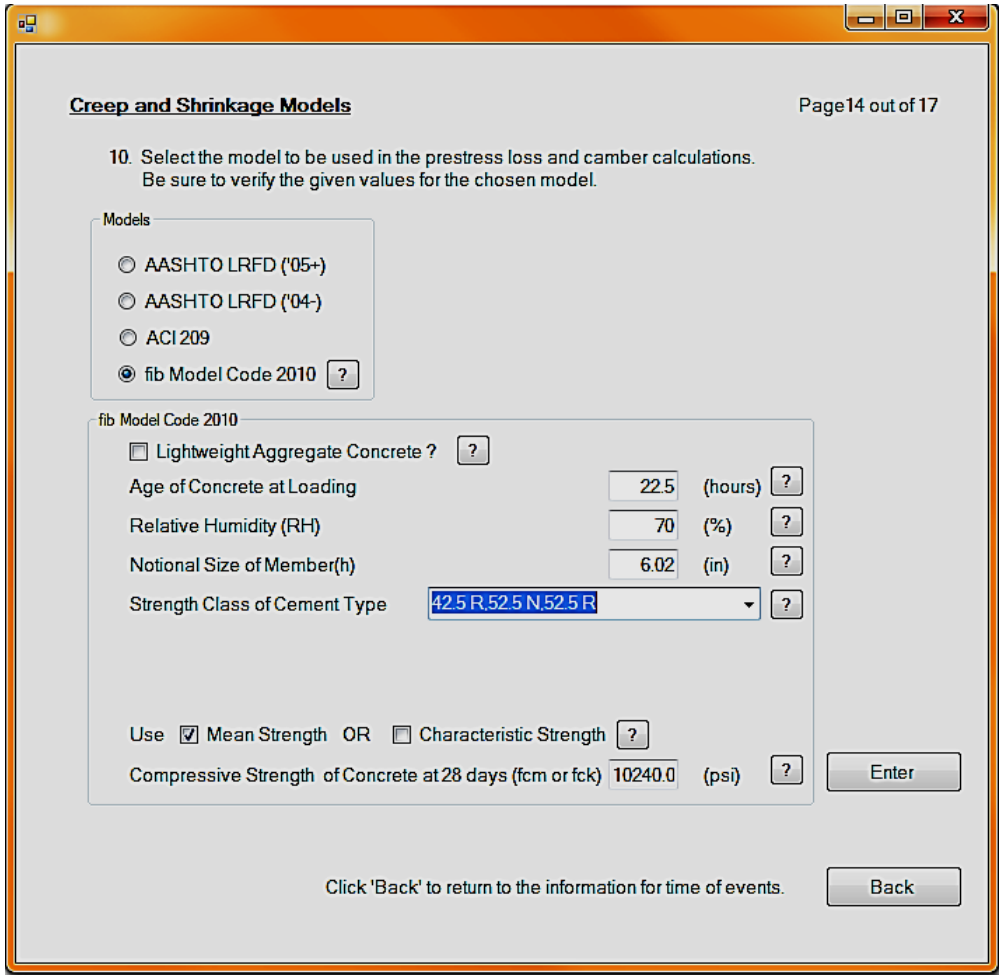

Figure K-15: Form 14—MC 2010 Creep and Shrinkage Model

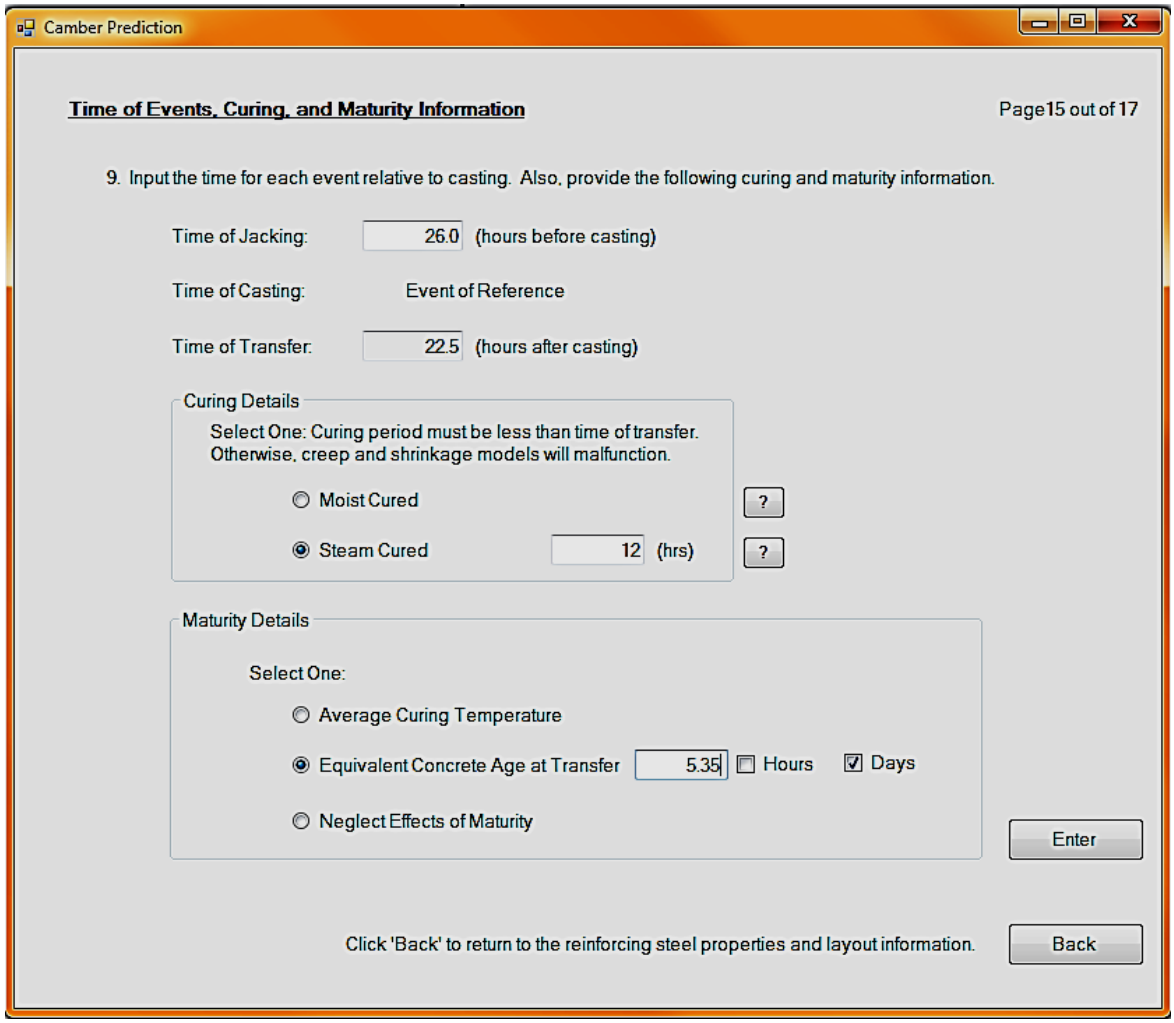

Figure K-16: Form 15—Time of Events

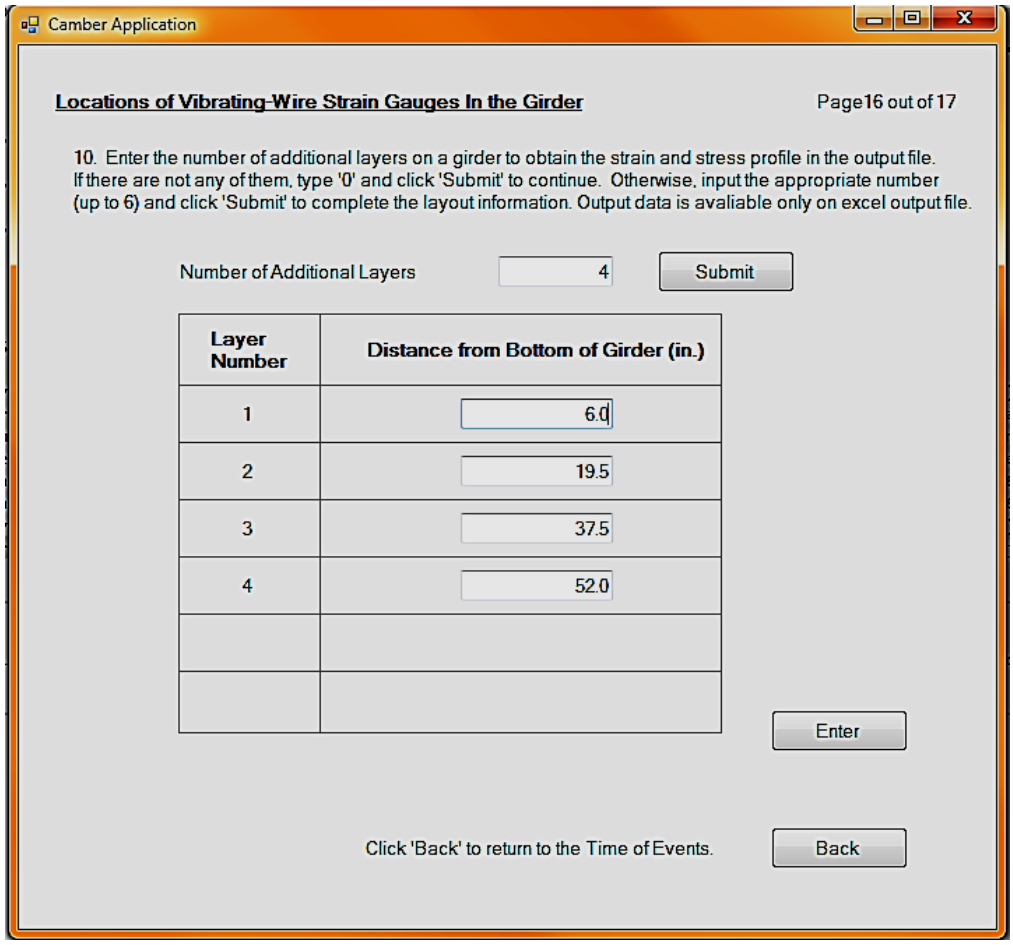

Figure K-17: Form 16—Additional Layers Revealing Strain

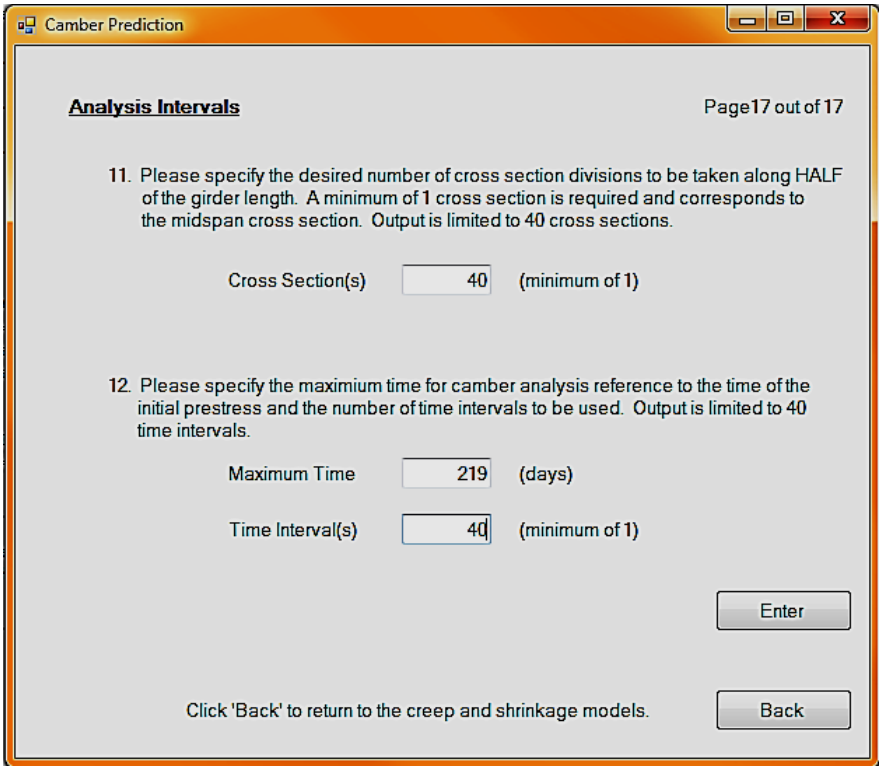

Figure K-18: Form 17—Analysis Intervals

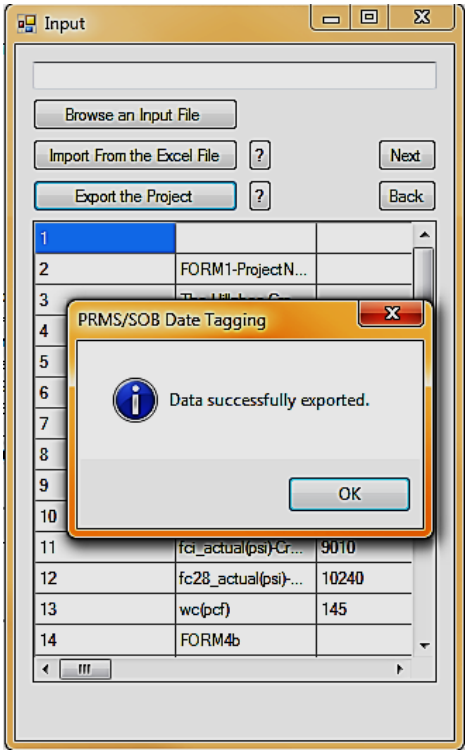

Figure K-19: Form 18—Input Variables: Import and Export

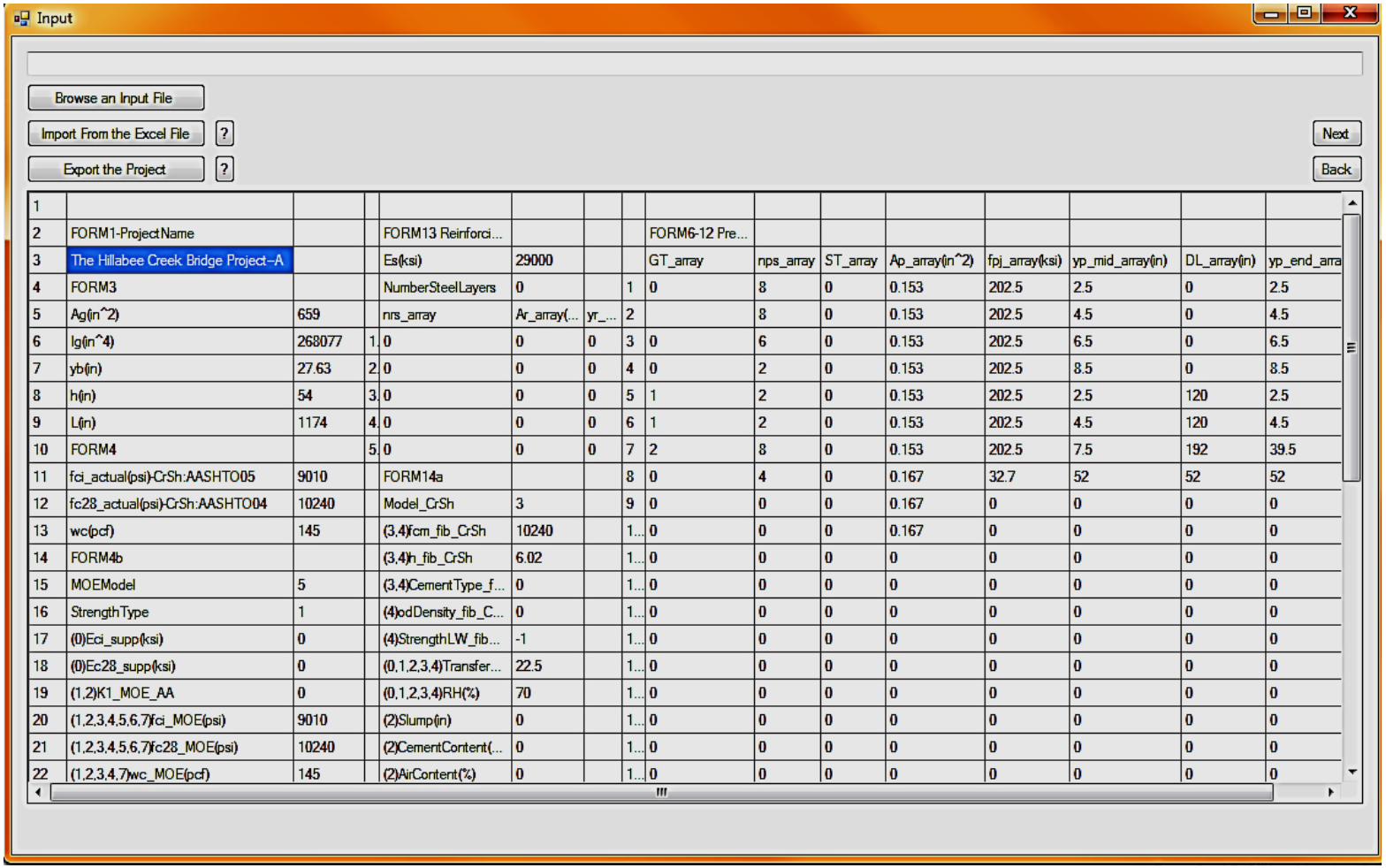

1															
2	FORM1-ProjectName			FORM13 Reinforci...				FORM6-12 Pre...							
3	The Hillabee Creek Bridge Project–A			Es(ksi)	29000			GT_array	nps_array	ST_array	Ap_array(in^2)	fpj_array(ksi)	yp_mid_array(in)	DL_array(in)	yp_end_arra
4	FORM3			NumberSteelLayers	0		1	0	8	0	0.153	202.5	2.5	0	2.5
5	Ag(in^2)	659		nrs_array	Ar_array(...	yr_...	2		8	0	0.153	202.5	4.5	0	4.5
6	Ig(in^4)	268077	1.	0	0	0	3	0	6	0	0.153	202.5	6.5	0	6.5
7	yb(in)	27.63	2.	0	0	0	4	0	2	0	0.153	202.5	8.5	0	8.5
8	h(in)	54	3.	0	0	0	5	1	2	0	0.153	202.5	2.5	120	2.5
9	L(in)	1174	4.	0	0	0	6	1	2	0	0.153	202.5	4.5	120	4.5
10	FORM4		5.	0	0	0	7	2	8	0	0.153	202.5	7.5	192	39.5
11	fci_actual(psi)-CrSh:AASHTO05	9010		FORM14a			8	0	4	0	0.167	32.7	52	52	52
12	fc28_actual(psi)-CrSh:AASHTO04	10240		Model_CrSh	3		9	0	0	0	0.167	0	0	0	0
13	wc(pcf)	145		(3,4)fcm_fib_CrSh	10240		1...	0	0	0	0.167	0	0	0	0
14	FORM4b			(3,4)h_fib_CrSh	6.02		1...	0	0	0	0	0	0	0	0
15	MOEModel	5		(3,4)CementType_f...	0		1...	0	0	0	0	0	0	0	0
16	StrengthType	1		(4)odDensity_fib_C...	0		1...	0	0	0	0	0	0	0	0
17	(0)Eci_supp(ksi)	0		(4)StrengthLW_fib...	-1		1...	0	0	0	0	0	0	0	0
18	(0)Ec28_supp(ksi)	0		(0,1,2,3,4)Transfer...	22.5		1...	0	0	0	0	0	0	0	0
19	(1,2)K1_MOE_AA	0		(0,1,2,3,4)RH(%)	70		1...	0	0	0	0	0	0	0	0
20	(1,2,3,4,5,6,7)fci_MOE(psi)	9010		(2)Slump(in)	0		1...	0	0	0	0	0	0	0	0
21	(1,2,3,4,5,6,7)fc28_MOE(psi)	10240		(2)CementContent(...	0		1...	0	0	0	0	0	0	0	0
22	(1,2,3,4,7)wc_MOE(pcf)	145		(2)AirContent(%)	0		1...	0	0	0	0	0	0	0	0

Figure K-20: Form 18—Input Variables: Data Table

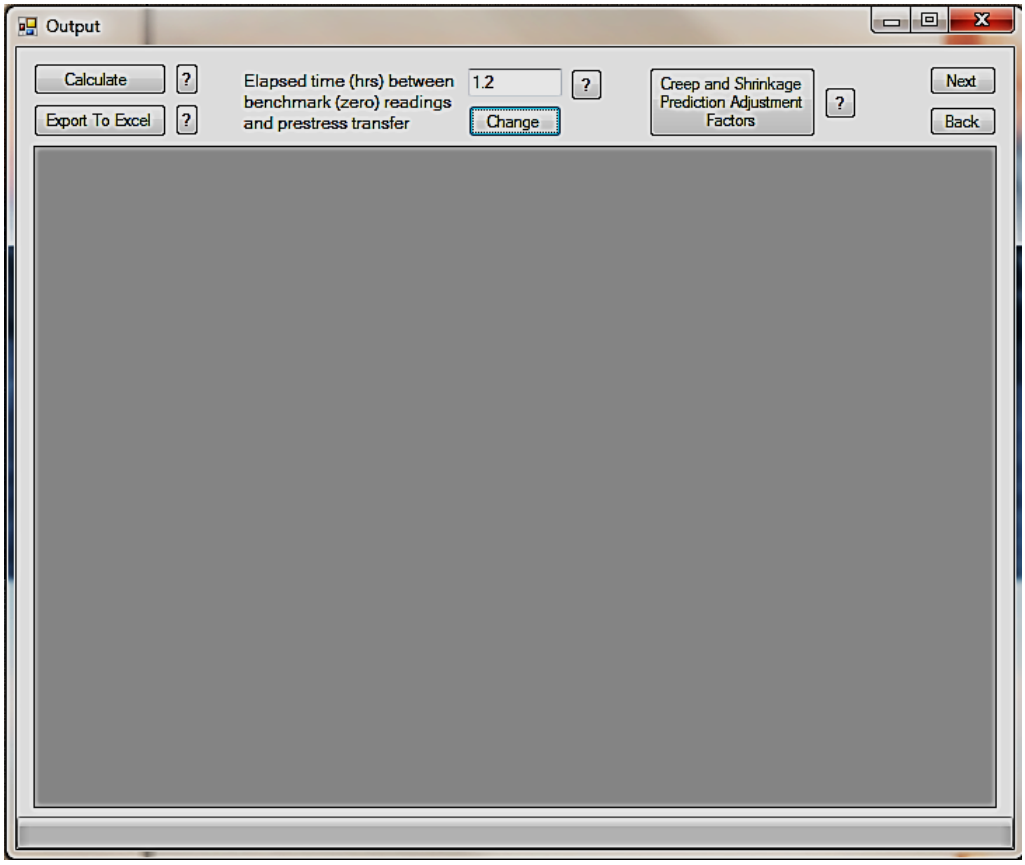

Figure K-21: Form 19—Output Variables: Benchmark Reading

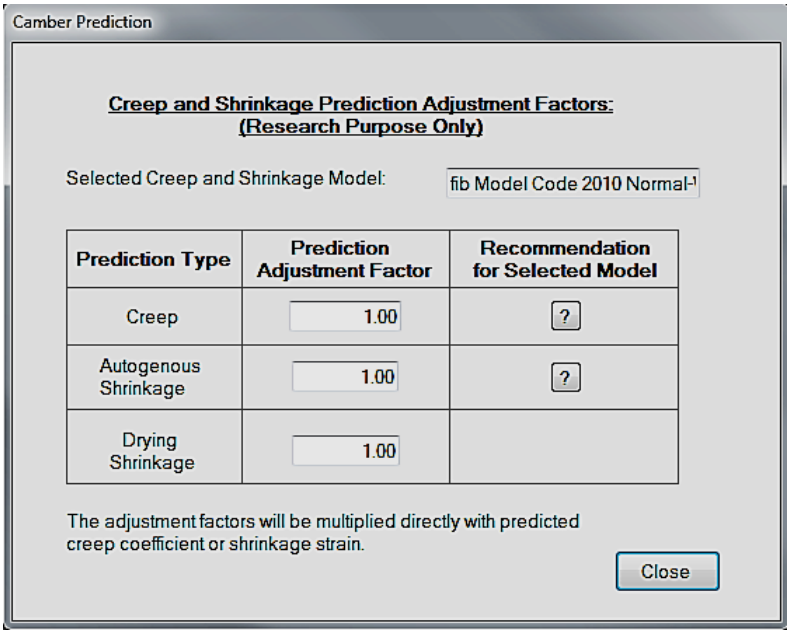

Figure K-22: Form 19—Output Variables: Creep and Shrinkage Adjustment Factors

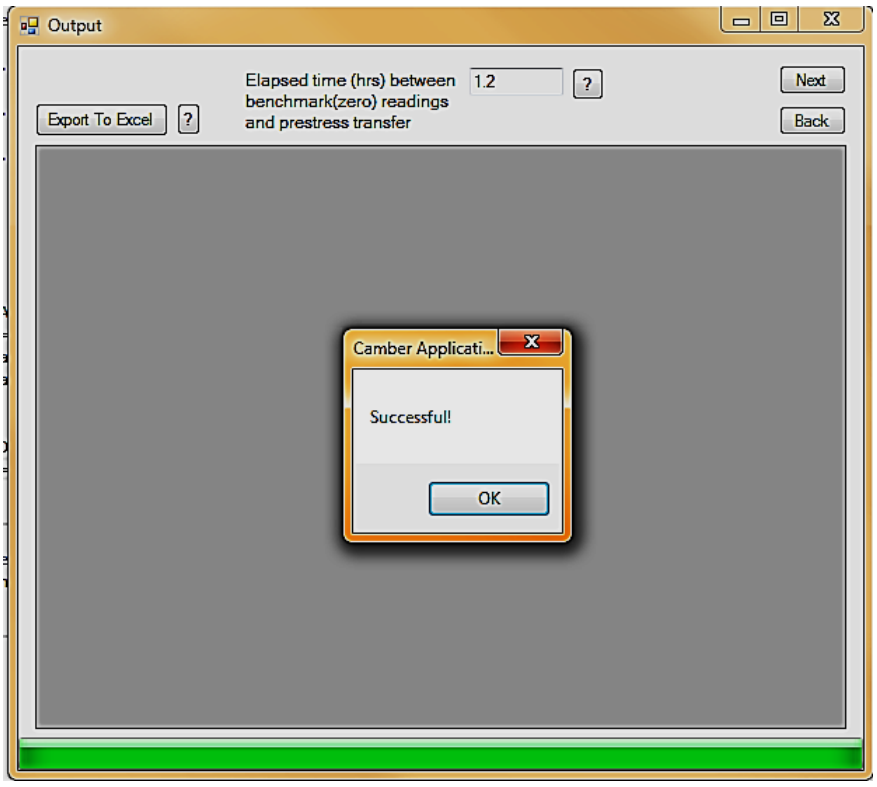

Figure K-23: Form 19—Output Variables: Calculate Button

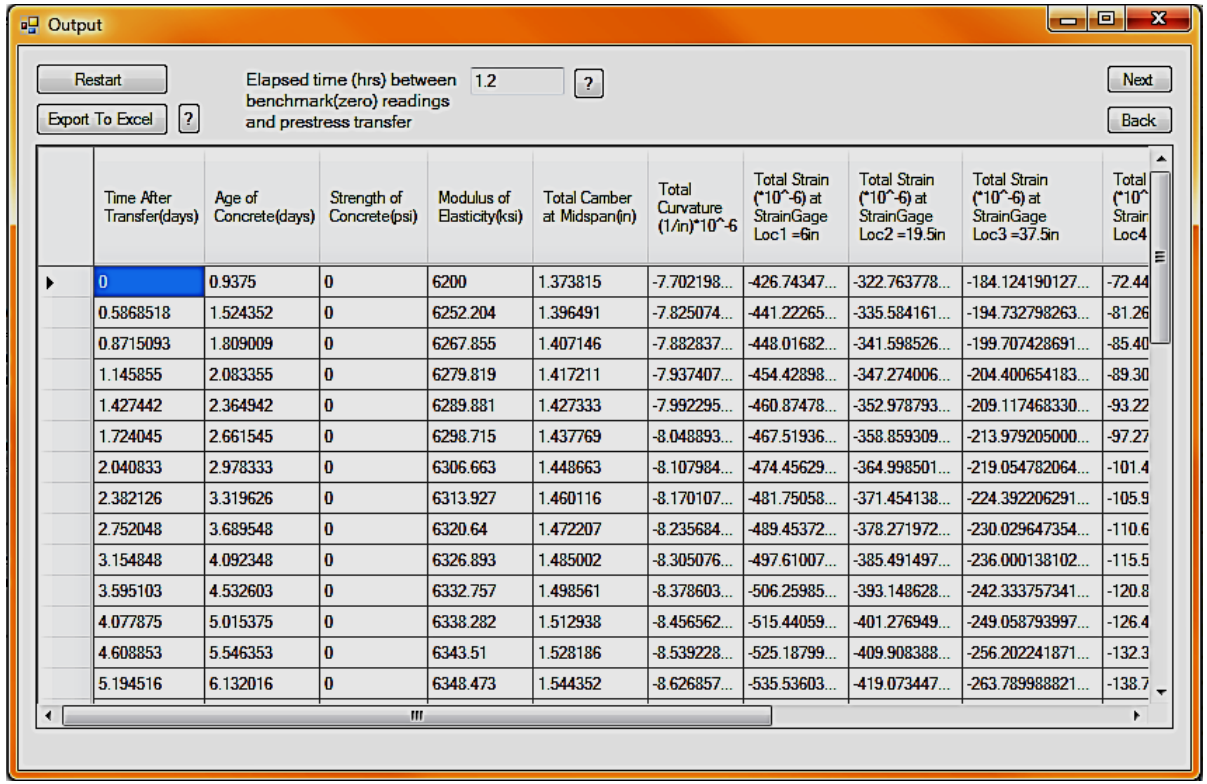

Figure K-24: Form 19—Output Variables: Export